Characterization of effector proteins involved in the early *Chlamydia pneumoniae* infection

Inaugural dissertation

For the attainment of the title of doctor
in the Faculty of Mathematics and Natural Sciences at the
Heinrich-Heine-University Düsseldorf

presented by

Corinna Ursula Braun
from Überlingen (Germany)

Düsseldorf, March, 2019

from the Institute of Functional Microbial Genomics
at the Heinrich-Heine-University Düsseldorf

Published by permission of the
Faculty of Mathematics and Natural Science at
the Heinrich-Heine-University Düsseldorf

Supervisor: Prof. Dr. Johannes H. Hegemann

Co-supervisor: Prof. Dr. Thomas Klein

Date of the oral examination: 21.05.2019

Content

Abbreviations

°C	Celsius degree
%	Percentage
aa	Amino acid
AB	Aberrant body
bp	base pair
C.	*Chlamydia*
cm^2	Square centimeter
cOMC	*Chlamydia* outer membrane complex
DOPC	Phosphatidylcholine
DOPS	Phosphatidylserine
E.	*Escherichia coli*
EB	Elementary body
EE	Early endosome
EEA1	Early endosome antigen 1
EGFR	Epidermal growth factor receptor
et al	"*et alia*", and others
Fig.	Figure
FITC	NHS-Fluorescin
FCS	Fetal bovines serum
g	grams
GAGs	Glycosaminoglycans
GAP	GTPase accelerating protein
GDF	GDP dissociation factor
GDI	GDP dissociation inhibitor
GDP	Guanosine diphosphate
GEF	Guanine exchange factor
GST	Glutathione-S-Transferase
GTP	Guanosine triphosphate
GUV	Giant unilammelar vesicle
h	Hours
HBSS	Hanks buffered salt solution
His	Histidine-tag
hMW	High Molecular Weight
hpi	Hours post infection
IM	Inner membrane
Inc	Inclusion membrane protein
kDa	Kilo Dalton
l	Liter

LPS	Lipopolysaccharide
Mb	Mega base pairs
mg	Milligram
min	Minutes
min pi	minutes post infection
ml	Milliliter
mM	Millimolar
MOI	Multiplicity of infection
MOMP	Major outer membrane protein
MW	Molecular Weight
OM	Outer membrane
ON	Over night
OmcB	Outer membrane protein B
P	Pellet
PAGE	Polyacrylamide gel electrophoresis
PBS	phosphate buffered saline
PFA	Paraformaldehyde
PC	Phosphatidylcholine
Pmp	Polymorphic membrane protein
PS	Phosphatidylserine
PtdIns	Phosphatidylinositides
r	Recombinant
RB	Reticulate body
RILP	Rab-interacting lysosomal protein
RT	Room temperature
S	Supernatant
s	Seconds
SDS	Sodium dodecyl sulphate
S. cerevisiae	*Saccharomyces cerevisiae*
SNP	Single nucleotide polymorphism
S. pombe	*Schizosaccharomyces pombe*
T3SS	Type III secretion system
TarP	Translocated actin recruiting phosphoprotein
µg	Microgram
µl	Microliter
μm^2	Square micrometer
WGA	Wheat germ agglutinin

Summary

Chlamydia pneumoniae (*C. pneumoniae*) is one of the two major species of the *Chlamydiaceae* family that infects humans. *C. pneumoniae* causes infections in the upper and lower respiratory tract and is linked to a number of chronic diseases. The adhesion of the *Chlamydiae* to the human cell is the first essential step of the infection followed by the internalization and the establishment of a membrane-bound intracellular niche, termed the inclusion. *Chlamydiae* secrete effector proteins via the type III secretion system, whose purpose it is to facilitate the internalization, replication, survival and release of the bacteria from the host cell. One of the best-characterized secreted effector proteins is the *C. trachomatis* **t**ranslocated **a**ctin **r**ecruiting phospho**p**rotein (TarP), which recruits and polymerizes actin at the entry site of the infectious chlamydial cell to support the internalization process. However, bacterial and human proteins involved in these early phases of the infection are ill-defined.

In the first part of this thesis, the *C. pneumoniae* TarP ortholog, CPn0572, was investigated. TarP orthologs from different species are quite diverse in their amino acid (aa) sequence but they share important domains, like the G-actin binding domain (ABD) or a proline-rich domain (PRD). In this work, early infection studies show that, upon bacterial invasion, CPn0572 is secreted into the host cell and associates with actin patches via the ABD conserved in TarP proteins. Ectopic expression of various GFP-CPn0572 deletion variants in human cells, as well as in *Saccharomyces cerevisiae* and *Schizosaccharomyces pombe*, revealed that association of CPn0572 to actin is not only mediated by the ABD. The C-terminus of CPn0572 without ABD binds to F-actin *in vitro* and associates with actin cables in human epithelial cells when ectopically expressed. Strikingly, the same assays revealed a possible inhibitory effect of the N-Terminus on the ABD. Furthermore, over bioinformatic and immunofluorescence microscopy a vinculin binding sequence (VBS) could be identified. Finally, *in vitro* actin filament binding assay showed that CPn0572 might have a stabilizing effect on actin, as it seems to displace cofilin from F-actin structures.

In the second part of this thesis, a new *C. pneumoniae*-specific cluster of 13 genes (termed *cee1-13*) was characterized. A bioinformatic screen identified the hypothetical protein Cee1, because of a localized 27.9 % identity to the human Rab36 GTPase. Rab GTPases together with phosphoinositides (PtdIns) are key regulators of vesicular transport and membrane identity. The Cee cluster proteins share a 32.6 % overall identity and harbor up to two different domains of unknown function (DUF), DUF575 and DUF562. Moreover, in all proteins harboring a DUF domain, Ras-specific G1, G3- and G5 box motifs could be identified which are involved in guanine-triphosphate binding. In ectopic expression studies

all DUF575 containing proteins show vesicle-like structures in human cells. Interestingly, Cee1 shows a G1 box motif-dependent association with early endosomes, endogenous, endocytosed EGFR and recycling-specific Rab11 and Rab14 proteins. Finally, during a *C. pneumoniae* infection specific antibodies against Cee1 and Cee4 detected both endogenous proteins associated with adhering EBs as early as 5 min post infection. Interestingly, recombinant Cee1 and Cee4 bind to membranes and interact with phosphatidylserine and PtdIns(4)P. These data suggest that the cluster proteins are effector proteins with a possible function as molecular mimic of Rab proteins during the early *C. pneumoniae* infection phase.

1. Introduction

The *Chlamydiae* phylum is comprised of obligate intracellular, Gram-negative bacteria, which are responsible for a variety of infections in humans and animals. Even though different hosts are infected, all *Chlamydiae* species share a unique biphasic life cycle, which consists of two morphological forms: the metabolic inactive but infectious elementary body (EB) and the intracellular metabolic active reticulate body (RB).

1.1 Taxonomy

Due to their unique life cycle and phylogenetic analysis *Chlamydia* are classified in the genus *Chlamydia* in the family *Chlamydiaceae* of the order *Chlamydiales*. By comparative analysis of ribosomal RNA (rRNA) 16S and 23S, the order *Chlamydiales* was divided in four families: *Chlamdiaceae, Parachlamydiacea, Waddilaceae* and *Simikaniaceae* (Everett, Bush, and Andersen 1999) (Fig1). Based on differential clustering of the 16S rRNA in the same analysis two genera in the *Chlamydiaceae* family were identified: *Chlamydia*, with the species, *C. trachomatis*, *C. suis* and *C. muridarum* and the family *Chlamydophila* with the species, *C. pneumoniae*, *C. psittaci*, *C. pecorum*, *C. caviae*, *C. abortus* and *C. felis* (Everett, Bush, and Andersen 1999). The community had different opinions about the proposal of the two genera and lacked a cohesive taxonomy. In 2009 a new extensive analysis by complete genome sequencing was performed, which provided new understanding in the evolutionary history of *Chlamydiaceae* and it was proposed to reunite *Chlamydia* and *Chlamydophila* in one genus "*Chlamydia*" (Stephens et al. 2009). This change was officially adopted in 2010 (Greub 2010). In recent years a novel method to estimate evolutionary and phenotypic distance of two strains was introduced by using the percentage of conserved proteins (POCP), which confirmed the recommended genus classification of the family *Chlamydiaceae* (Fig1) (Pannekoek et al. 2016).

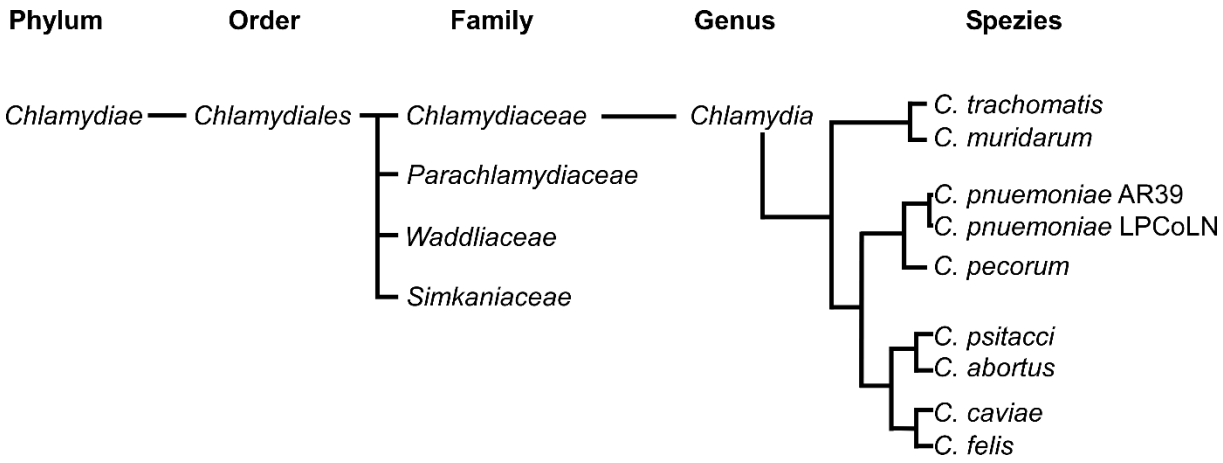

Fig1: Taxonomy of the order *Chlamydiales*.
Schematic representation of the families included in the order *Chlamydiales* and the species belonging to the genus *Chlamydia*. Length of line is not representative of phylogenetic distances. (modified after (Pillonel et al. 2015)[5]).

1.2 Genomics of the *Chlamydiaceae*

For a long time, it was not possible to genetically manipulate *Chlamydia*, but since 2011 a protocol to transform *C. trachomatis* and very recently in September 2018 a technique to transform *C. pneumoniae* was published (Wang et al. 2011; Shima et al. 2018). Before, sequencing genomes was an important tool to analyze *Chlamydia*. The first sequenced genome of the family *Chlamydiaceae* was from a *C. trachomatis* isolate in 1998 (Stephens et al. 1998). Since then, more isolates of *C. trachomatis*, 18 clinical isolates of *C. pneumoniae*, the animal isolate from the koala LPCoLN and even genomes of different *Chlamydia* species have been sequenced, like *C. pecorum*, *C. psittaci* or *C. gallinacean* (Jeffrey et al. 2010; Weinmaier et al. 2015; Mojica et al. 2011; Voigt, Schofl, and Saluz 2012; Holzer et al. 2016).
Even though the individual *Chlamydia* species share a unique biphasic life cycle and conserved genes, significant genetic diversity can be found (Clarke 2011). *Chlamydia* species show a tendency to delete non-essential DNA and have one of the smallest prokaryotic genomes. An obvious difference among species can be observed in the size of the genomes of, *C. trachomatis* and *C. pneumoniae*. *C. trachomatis* has, with a genome of 1.04 Mb coding for 887 proteins, a coding content of approximately 90 %, and *C. pneumoniae* has a 1.23 Mb genome, coding for 1029 proteins (Andersson 1999; NCBI cited Dec 2018). Further comparisons of these two genomes revealed 214 protein-coding sequences in *C. pneumoniae* not found in *C. trachomatis*, among them an expansion of a family of 21 sequence variant outer membrane proteins (Kalman et al. 1999). Furthermore, genetic diversity can be found in genes coding for proteins that mediate the interaction with the host, like the number and size of the family of polymorphic membrane proteins (*pmps*),

type III secreted effector proteins and genes located in the region called the plasticity zone, a region which is characterized by high levels of polymorphisms and displays the major dissimilarities in gene content and sequence among *Chlamydiaceae* (Van Lent et al. 2016; Grimwood and Stephens 1999; Voigt, Schofl, and Saluz 2012; Nunes and Gomes 2014). All these proteins are likely chlamydial factors involved in virulence, host-pathogen relationships, host specificity and show a high genetic difference among *Chlamydia* species (Voigt, Schofl, and Saluz 2012; Mitchell et al. 2010). Comparative studies of the human *C. pneumoniae* strains and the koala *C. pneumoniae* strain showed that the koala isolate encodes the largest number of full-length *pmps*, whereas the human isolates carry several truncated *pmps* (Myers et al. 2009; Mitchell et al. 2010). Together with the broad host range of *C. pneumoniae*, with strains being found in horses, koalas and amphibians and based on these genomic and phylogenetic analysis of conserved genes of the koala *C. pneumoniae* LPCoLN isolate and human isolates, it was proposed that humans were originally infected zoonotically by animal isolates (Myers et al. 2009). Even though no transmission of *C. pneumoniae* from animals to human has been reported up to date, the hypothesis of a zoonotic origin of human *Chlamydia* is further supported by cases of *C. abortus* and *C. psittaci* being transferred from animals to humans (Pospischil et al. 2002; Beeckman and Vanrompay 2009).

1.3 The human pathogen *C. pneumoniae*

C. pneumoniae is, next to *C trachomatis* the second most important human pathogen in the genus *Chlamydia*. The infection occurs via inhalation of infected aerosols and is often asymptomatic. *C. pneumoniae* causes infections in the upper respiratory tract, causing mild symptoms like pharyngitis and sinusitis; and the lower respiratory tract, causing bronchitis and pneumonia (Hahn, Dodge, and Golubjatnikov 1991). Furthermore, *C. pneumoniae* accounts for 6 to 10 % of community acquired pneumonia (Peeling and Brunham 1996). In serological studies, it was estimated that the antibody prevalence of *C. pneumoniae* at the age between 60 and 70 years is between 70-80 % (Blasi 2009). Next to acute infections, *C. pneumoniae* is associated with chronic diseases like asthma, atherosclerosis and Alzheimer disease (Grayston et al. 1993; Belland et al. 2004; Gerard et al. 2006). Moreover, in a meta-analysis from 2010, *C. pneumoniae* was found in association with lung cancer (Zhan et al. 2011). Even though it was possible to induce lung cancer in rats through a *C. pneumoniae* infection, the connection between infection and cancer is thus far not clear (Chu et al. 2012).

1.4 The *Chlamydia* life cycle

C. pneumoniae, like all *Chlamydia*, undergoes a life cycle in which two functionally and morphologically distinct cell types are recognized: the smaller extracellular and infectious EB (0,3 µm) and the larger intracellular metabolically active RB (1 µm) (Chi, Kuo, and Grayston 1987; Miyashita, Kanamoto, and Matsumoto 1993). Even though the stages of the life cycle are shared by all *Chlamydia*, the amount of time to complete the life cycle differs between species. For instance, *C. trachomatis* completes its cycle in 48 h, while *C. pneumoniae* needs 72 – 96 h (Wolf, Fischer, and Hackstadt 2000). For the purpose of this work, all further reference to life cycle times refer to that of *C. pneumoniae*.

The first step of the infection is the adhesion of the EB to the human cell with the help of chlamydial adhesins, followed by the internalization. (Proteins involved in that process are described in more detail in 1.4.1) (Fig2). After the initial contact of the EB to the host cell, effector proteins become secreted into the host cell through the type III secretion system of the bacteria, like the *C. pneumoniae* TarP ortholog CPn0572, which recruits and polymerizes actin and promotes bacterial entry (1.5.4). Once internalized the EB stays in a membrane-bound endosome, called the inclusion during the rest of the developmental cycle (Wolf, Fischer, and Hackstadt 2000). The inclusion is transported to the perinuclear region of the host cell two hours after entry, along the microtubule cytoskeleton of the host cell in a dynein dependent manner. So far a dynein dependent transport could only be observed for *C. trachomatis* and not *C. pneumoniae*, which indicates differences in cytoskeletal organization induced by these two *Chlamydia* species (Clausen et al. 1997; Grieshaber, Grieshaber, and Hackstadt 2003). During the transport to the microtubule organizing center (MTOC) the inclusion acquires different Rab GTPases, important regulators in membrane identity and vesicle transport, in a species-specific manner. At the perinuclear region the inclusion stays close to the Golgi apparatus and acquires nutrients, such as sterols, sphingolipids and cholesterol, by fusing with a subset of host vesicles. During the infection cycle, the chlamydial inclusion evades endolysosomal pathway and instead acquires a subset of exocytic vesicle markers (Valdivia 2008; Saka and Valdivia 2010; Scidmore, Fischer, and Hackstadt 2003). Furthermore, to enhance access to nutrients, *Chlamydia* hijack ARF GTPases to reposition the Golgi complex around the inclusion. The inclusion is furthermore surrounded by an F-actin cage and posttranslational modified microtubules to maintain the integrity of the inclusion (Wesolowski et al. 2017; Kumar and Valdivia 2008).

After 12 h p. i. (hpi) the EBs differentiate to the metabolically active RBs, which in the next 36 h keep dividing and replicating (Fig2) (Wolf, Fischer, and Hackstadt 2000). Under some circumstances the developmental cycle can be reversible arrested. For example, under environmental stress, like nutrient deprivation, exposure to antibiotics or interferon gamma,

RBs transition to aberrantly enlarged non-dividing persistent forms, the aberrant body (AB). Once the stress is relieved, the persistent form turns back into active RBs (Elwell, Mirrashidi, and Engel 2016; Beatty, Byrne, and Morrison 1993). 48 hpi. the infection cycle becomes asynchronous as RBs start to re-differentiate into EBs (Fig2). During this asynchronous stage, typical EBs with the right size and displaying a condensed nucleoid are observed, as well as intermediate forms and RBs (Wolf, Fischer, and Hackstadt 2000). After 72 hpi. the EBs are released. This can happen via lysis of the host cell or via extrusion. Released EBs can then start a new infection round (Wolf, Fischer, and Hackstadt 2000). For the process of extrusion septins and the recruitment or stabilization of the actin cage around the inclusion seems important (Volceanov et al. 2014).

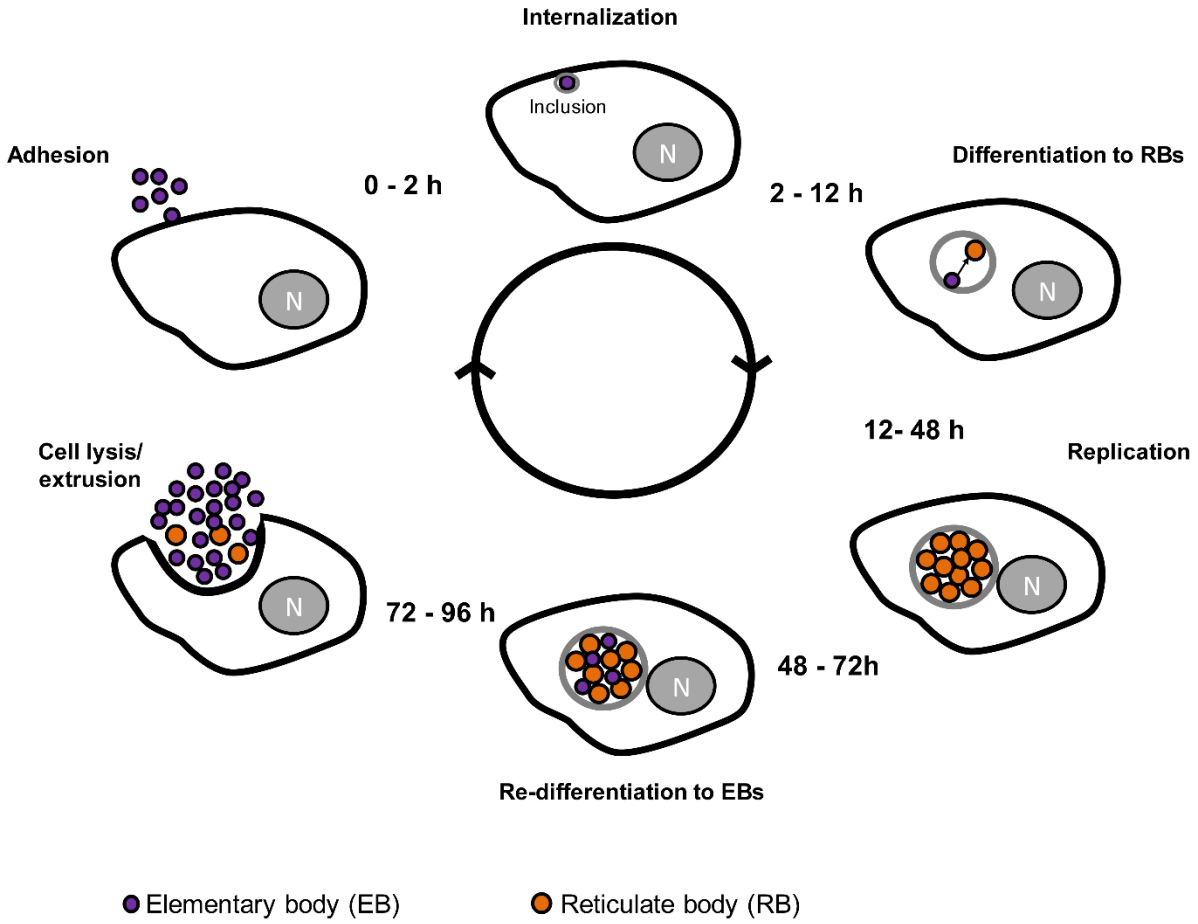

Fig2: The chlamydial life cycle.

Schematic representation of the unique biphasic life cycle of *Chlamydia*. The times in hours (h) are representative for a *C. pneumoniae* infection (Wolf, Fischer, and Hackstadt 2000).

1.4.1 Adhesion and internalization

The adhesion of the EBs to the human cell is the first essential step of the infection followed by internalization and establishment of the inclusion. First contact of the EB to the host cell occurs by binding of the conserved adhesin OmcB to heparan sulfate-like proteoglycans (GAGs) (Moelleken and Hegemann 2008). The binding occurs over basic amino acids located in one of two XBBXBX (X hydrophobic; B basic amino acid) heparin-binding motifs. Further neutralization studies with anti-heparan sulfate antibodies showed that *C. pneumoniae* OmcB interacts with domains of heparan sulfate with diverse O-sulfations (Moelleken and Hegemann 2008; Fechtner et al. 2013). As it is assumed that binding of OmcB to GAGs is weak and reversible, more adhesins for a stable contact of EBs to the human cells are needed. More proteins with adhesive capacity are describe, even though not all are conclusively identified as part of the adhesion process or completely understood. Adhesins are typically located on the surface of the bacterium, show adhesive capacities and inhibit a *Chlamydia* infection after incubation of host cells with recombinant protein by saturating the host receptors. One adhesin candidate is the chlamydial lipopolysaccharide (LPS), which is a major surface component of all Gram-negative bacteria. In studies, addition of *C. trachomatis* LPS or LPS antibodies result in a reduction of the infection, which suggests a role in chlamydia infectivity (Fadel and Eley 2008). Another candidate that shows characteristic of an adhesin is the chlamydial protein GroEL1. It was found to localize on the surface of EBs, is able to adhere to human epithelia cells and pre-incubation of host cells with recombinant protein leads to a significant reduction of a subsequent *C. pneumoniae* infection (Wuppermann et al. 2008). In recent studies, CPn0473, a new *C. pneumoniae* specific adhesin was identified (Fechtner, Galle, and Hegemann 2016). CPn0473 is expressed late in the infection cycle, which usually means the protein is needed early during the infection and can be found on the surface of the EB. Adhesion studies showed that the protein has the capacity to bind to human epithelial cells. Interestingly, pre-incubation with the recombinant protein did not lead to a reduction of the subsequent *C. pneumoniae* infection. Instead the internalization of EBs was boosted in a dose-dependent manner (Fechtner, Galle, and Hegemann 2016; Galle 2017). Up to date no human interaction partner could be identified for CPn0473, but it could be shown that the protein preferably binds to negatively charged lipids, such as phosphatidylserine (PS) and lipid raft domains (Galle 2017; Fechtner, Galle, and Hegemann 2016). Moreover, binding of CPn0473 to the human cell leads to externalization of PS from the inner leaflet of the plasma membrane to the outer leaflet, which could increase the curvature of the membrane around the EB and lead to the re-localization of membrane associated human proteins such as, Rac proteins. These data

suggest that CPn0473 not only has a function during the adhesion, but also during the internalization of the EB (Galle 2017).

Another group of adhesins are the polymorphic membrane proteins (Pmps). During genome sequencing it was revealed that all *Chlamydia* harbor members of the Pmp family. Interestingly, all members of the Pmp family are quite heterogeneous in their amino acid sequence and size (Grimwood and Stephens 1999). In *C. trachomatis* nine members have been identified and 21 members in *C. pneumoniae*, which have been divided in six phylogenetic subgroups (Grimwood and Stephens 1999). All *pmps* are transcribed, but not all *C. pneumoniae pmps* are translated, due to frameshift mutations *pmp3/4/5/12/17* are not translated (Grimwood, Olinger, and Stephens 2001). All Pmps share predicted type-V autotransporter characteristics, an N-terminal signal sequence, a passenger domain and a C-terminal β-barrel (Grimwood and Stephens 1999; Rockey, Lenart, and Stephens 2000). For Pmp6, Pmp20 and Pmp21 from *C. pneumoniae* adhesive capacity could be shown (Mölleken, Schmidt, and Hegemann 2010). A more detail analysis showed that the Pmps build homo and heteromeric complexes and that for adhesion at least two of the repetitive motifs, FxxN and GGA(I/L/V), are needed (Mölleken, Schmidt, and Hegemann 2010; Luczak et al. 2016). Up to date only the epidermal growth factor receptor (EGFR) as a human interaction partner of Pmp21 has been identified (Mölleken, Becker, and Hegemann 2013). Pmp21 binds to EGFR homodimers and activates the EGFR. Activation of the EGFR leads to recruitment of the adaptor protein Grb2 and the ubiquitin ligase c-Cbl. The binding of Grb2 to the activated EGFR induces the ERK1/2 signaling via Ras and Raf and recruits c-Cbl, which is involved in receptor endocytosis (Mölleken, Becker, and Hegemann 2013). Interestingly, the endocytosed EGFR stays associated with the early inclusion (Mölleken, Becker, and Hegemann 2013). Thus, binding of Pmp21 to the EGFR and the ensuing signal cascades are not only important for a stable adhesion, but also for the internalization and even for the establishment of the inclusion (further described in 1.4.2).

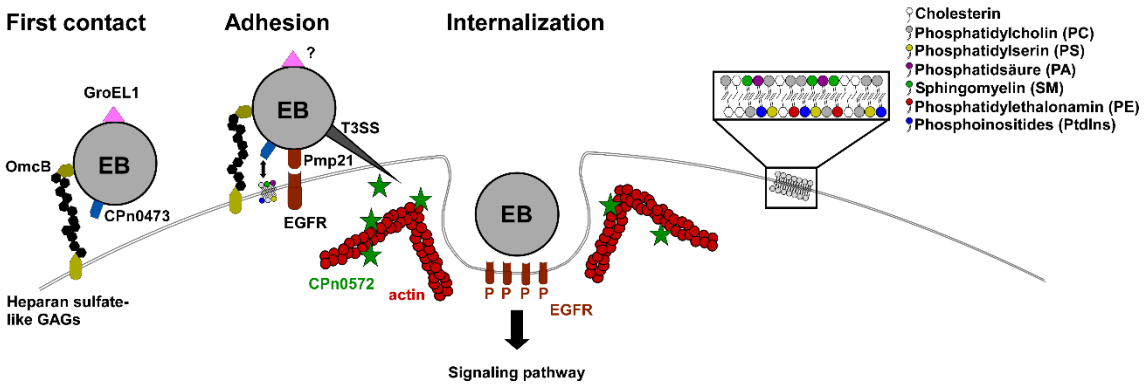

Fig3: Adhesion and internalization of *C. pneumoniae*.

The model shows that the adhesion of *C. pneumoniae* EBs takes place by binding of adhesins like OmcB, Pmp21, GroEL1 and CPn0473 to specific human proteins and receptors like the EGFR or lipids of the plasma membrane. Binding of Pmp21 to the EGFR leads to the activation of signaling pathways. After the stable contact, type III secreted proteins like CPn0572 are secreted into the host cell. CPn0572 polymerizes actin at the site of bacterial invasion and promotes internalization.

1.4.2 Establishing the inclusion

After adhesion and internalization, the next crucial step of the chlamydial life cycle is to modify the endosomal compartment, the inclusion. As it was described before, it was shown that Pmp21 of *C. pneumoniae* interacts and activates the human EGFR which stays associated with the inclusion membrane also in later stages of the infection. Typically, the activation of the EGFR either leads to the degradation of the receptor in the lysosomal pathway or it is recycled back to the plasma membrane (Madshus and Stang 2009). Thus, *Chlamydia* needs a way to avoid EGFR-induced degradation, be transported to the peri-Golgi region and avoid fusion with the lysosomes. One way to control the interactions of the inclusion could be mimicry. This could be achieved by the recruitment or exclusion of specific host proteins involved in regulation of vesicle trafficking in the host cell (Fields and Hackstadt 2002). Rab GTPases are essential regulators of intracellular trafficking and define compartment identity. Rab1, which is involved in endoplasmic reticulum (ER) to Golgi trafficking and Rab4 and Rab11, which function in receptor recycling, localize to the mature inclusion of *C. trachomatis*, *C. muridarum* and *C. pneumoniae* from 2 h post infection (hpi) (Rzomp et al. 2003). Further analysis showed that the recruitment of other Rab GTPases to the inclusion is species dependent. For example, Rab6 is only recruited by the *C. trachomatis* mature inclusion, but not by *C. pneumoniae* or *C. muridarum*, whereas the opposite was observed for Rab10 (Rzomp et al. 2003). Differences in chlamydial developmental cycle could explain the species-specific recruitment of Rab proteins to the mature chlamydial inclusion. Studies showed that the *C. trachomatis* inclusion recruits

recycling Rab11 as soon as one hour post infection (Rzomp et al. 2003). Recent work from 2017 gave a first insight in the chlamydia-specific vesicle-shaping events that occur during EB internalization between 0 and 60 min post infection. It was shown that the nascent chlamydial inclusion acquires early endosomal (EE) membrane identity and recruits Rab4, Rab5, late endosomal Rab7 and recycling Rab11 and Rab14 as early as 5 min post infection. Moreover, it was shown that Rab11 and Rab14 are sustained, whereas Rab7 and Rab4 disappear 30 min post infection (Molleken and Hegemann 2017).

Another important class of proteins involved in membrane identity, vesicle transport and endocytosis are phosphoinositides kinases and phosphatases, which represent good targets to hijack for pathogens (Jean and Kiger 2012).

Activation of the EGFR via ligand/*Chlamydia* leads to the activation of the class I phosphoinositide 3-kinase (PI3K). This kinase converts phosphatidylinositol 4,5-bisphosphate (PtdIns(4,5)P_2) located at in the inner leaflet of the plasma membrane, to phosphatidylinositol 3,4,5-triphosphate (PtdIns(3,4,5)P_3). This conversion triggers the Akt pathway and PtdIns(3,4,5)P_3 is transformed to phosphatidylinositol 3-phosphate (PtdIns(3)P), which is mostly localized to early endosomes (Molleken and Hegemann 2017). These steps of activation are essential for the *C. pneumoniae* inclusion. Moreover, it was shown that the activity of Akt and its downstream target the PIKfyve kinase, phosphorylate PtdIns(3)P to PtdIns(3,5)P. PtdIns(3,5)P is characteristic for a late endosomal membranes, and seems to be important for the release of Rab7 from the inclusion membrane and to avoid degradation (Molleken and Hegemann 2017). Up to date not much more is known about the proteins or PtdIns involved during the early stages of the inclusion (0 to 60 min).

As soon as 2 hpi the *Chlamydia* inclusion starts to recruit a Golgi complex localized phosphatidylinositol 5-phosphates, OCRL1, which binds to multiple Rabs. PtdIns(4)P, the product of OCRL1, also localized to the inclusion, which with Arf1 mediates the recruitment of PtdIns(4)P binding proteins to the Golgi (Moorhead et al. 2010).

Furthermore, *Chlamydia* species express a unique family of effector proteins, the inclusion membrane proteins (Incs). Incs are expressed early during the infection (2 hpi) and contribute in the modification of the inclusion (Fields and Hackstadt 2002). Even though all Incs share a predicted hydrophobic domain of approximately 40 amino acids, the primary sequence similarity is quite low (Fields and Hackstadt 2002). The *C. pneumoniae* Inc protein, CPn0585, was shown to interact with Rab1, Rab10 and Rab11, which suggest an involvement in recruiting Rab GTPases to the inclusion. This shows how *Chlamydia* seem to use host proteins and effector proteins to avoid fusion with lysosomes and establishes its own intracellular niche (Moore and Ouellette 2014; Cortes et al. 2007).

Despite important discoveries about the recruitment of host proteins and Inc proteins, not a lot is known about chlamydial proteins involved in the early infection, especially between

0ˆand 60 min post infection. One part of this work was to identify effector proteins involved in the early chlamydial infection.

1.5 The host actin cytoskeleton is used by pathogens for entry

The human cytoskeleton has many important functions, they render mechanical support of the cell, maintenance of cell shape, generating coordinated forces that enable the cell to move and it organizes and anchors cell organelles. Furthermore, it connects the cell physically and biochemically to the external environment. The cytoskeleton consists of three main polymers: actin filaments, microtubules and intermediate filaments. (Fletcher and Mullins 2010; Neil A. Campbell 2006). Especially, the actin cytoskeleton, being an important part of the cell cortex, seems to play an integral role in the internalization of extracellular particles, which includes pathogens. The next section describes the actin cytoskeleton and its dynamics, followed by a summary of known ways of how pathogens utilize the host actin cytoskeleton.

1.5.1 Structure and dynamics of the actin cytoskeleton

Actin was first discovered in 1942 as a water-soluble component of mouse muscle cells and is highly conserved in eukaryotic cells. Cellular actin exists in two different forms, the monomeric G-actin, which has a tendency to polymerize into the second form, the filamentous F-actin (Kabsch and Holmes 1995). G-actin consists of two domains, which are divided into four subdomains (Kabsch et al. 1990). Every G-actin molecule has a nucleotide (ATP or ADP) binding site in the cleft between the two domains and has a single high affinity and several low affinity sites for divalent cations, either Ca^{2+} or Mg^{2+}. An additional small cleft is important for actin-actin interaction within the actin filament and is known to be a target for actin-binding proteins (ABPs) (Dominguez 2004; Kabsch and Holmes 1995).

F-actin filaments are double helical, non-equilibrium polymers with a pointed end, which is the slow growing minus end and the barbed end, which is the fast growing plus end (Chen, Bernstein, and Bamburg 2000). At least four reversible steps of actin polymerization are known: First, activation, which is a conformational change induced by salts, second, nucleation, which is the formation of oligomers by association of monomers, third, elongation, during which the ATP bound monomers bind to both ends at different rates and fourth, annealing (Cooper and Pollard 1982). The first two steps are much slower than the other and responsible for the initial lag phase in pure actin monomer polymerization, especially *in vitro* as spontaneous nucleation is kinetically unfavorable. After incorporation of the ATP-monomer to the barbed end, ATP is hydrolyzed to ADP, which becomes depolymerized at

the pointed end. At a steady state concentration, were the G-actin assembly at the plus end equals the disassembly at the minus end, filament length and number is relatively stable, which is called treadmilling (Chen, Bernstein, and Bamburg 2000; Cooper and Pollard 1982). Actin polymerization *in vivo* can be 100-200 fold faster than *in vitro*, as the rapid turnover at both ends cannot be accomplished without ABPs. ABPs for example interact with actin monomers to enhance nucleotide exchange or cap filament ends to nucleate filament growth, which subsequently leads to a simultaneous growing and shrinking (Chen, Bernstein, and Bamburg 2000).

1.5.2 Role of actin binding proteins in modulating actin filament dynamics

ABPs play an essential role in actin polymerization and assembly. One example of ABPs are actin nucleators. The Arp2/3 complex was the first actin nucleator discovered. It consists of seven protein subunits, with two actin related proteins Arp2 and Arp3, proposed to form similar dimers as actin (Mullins, Heuser, and Pollard 1998; Pak, Flynn, and Bamburg 2008). Through binding to proteins in the Wiscott-Aldrich Syndrome protein family (WASP), which are activated by cdc42, the Arp2/3 complex is activated for actin nucleation. The Arp2/3 complex caps the pointed ends of F-actin and inhibits monomer addition and dissociation. This activity seems to stabilize actin filaments *in vivo*. Furthermore, it binds laterally along F-actin filaments and promotes branching of actin filaments and increasing the number of barbed ends for enhanced polymerization (Mullins, Heuser, and Pollard 1998; Chen, Bernstein, and Bamburg 2000; Pak, Flynn, and Bamburg 2008). A second group of actin nucleators are the formins. They follow the barbed end of F-actin filaments, stabilize actin dimers and bind to profilin-actin complexes, which in turn leads to an increase in monomer addition at the barbed end (Pak, Flynn, and Bamburg 2008).

Another group of actin binding proteins are proteins that sever actin filaments, like ADF/cofilin (Rafelski and Theriot 2004). Disassemble of actin filaments into monomers is important to reproduce a pool of G-actin. Cofilin can bind to G- and F-actin and shows a high affinity to ADP-bound monomers, which leads to an enhance dissociation of monomers at the pointed ends of actin filaments and leads to a faster recycling of monomeric actin (DesMarais et al. 2005; Rafelski and Theriot 2004). Additionally, cofilin has the ability to sever actin filaments and generating more barbed ends, and thus leads to more polymerization (DesMarais et al. 2005). Both processes seem to be rely in the ability of cofilin to bind to F-actin, which causes a twist in the filament, which in turn endorses the destabilization of actin-actin interaction and thus fragmentation of actin filaments. Moreover, cofilin is regulated by phosphorylation, the binding of PtdIns(4,5)P_2, signaling cascades and interaction with 14-3-3ζ (DesMarais et al. 2005).

Vinculin represents a different type of ABP. Vinculin can be divided in three domains, which bind to different other proteins, also actin: vinculin head, linker and vinculin tail. The vinculin head can bind to α-actinin, which is an ABP that cross links actin filaments and talin, among others. The linker between head and tail domain binds to Arp2/3 and the tail domain is the one binding to actin and paxillin. Vinculin is together with paxillin and FAK a component of the focal adhesion and plays a role in cell-cell and cell-matrix adhesion (Bays and DeMali 2017).

1.5.3 Effector proteins of pathogens that manipulate the host actin cytoskeleton

Many pathogens exploit the host actin cytoskeleton during different stages of their developmental cycle. This might take place during entry into the host cell or later on when bacteria use the actin cytoskeleton to move inside the host cytosol.

Two general mechanisms of bacterial entry can be described according to the type of morphological changes that occur in the host cell: the “zipper” and “trigger” mechanism. During the zipper mechanism a bacterial protein interacts with a host receptor, which is usually involved in cell adhesion or activation of the actin cytoskeleton. One example for a “zipper” mechanism are the surface located proteins internalin A (InlA) and internalin B (InlB) of *Listeria monocytogenes*. The human interaction partner of InlA is the extracellular region of E-cadherin, which is responsible for cell-cell adhesion, whereas the cytoplasmic domain interacts with catenins, which interact with the actin cytoskeleton which in turn leads to the actin remodeling through InlA binding (Dramsi and Cossart 1998; Cossart, Pizarro-Cerda, and Lecuit 2003). In contrast to InlA, InlB binds to three different receptors. The first identified receptor was gC1qR, which is a receptor for C1q the first component of the complement cascade. The second receptor is the tyrosine kinase receptor Met, which is recruited to the bacterial entry site and binding of InlB induces actin dependent membrane ruffling and stimulates tyrosine phosphorylation and activation of PI-3-kinase and Rho GTPases. The last identified receptor are glycosaminoglycans (GAGs). Due to the presence of GAGs, the InlB dependent activation of Met is significantly increased (Cossart, Pizarro-Cerda, and Lecuit 2003).

The trigger mechanism means a pathogen secretes effector proteins into the host cell, which activate actin remodeling and signaling cascades, resulting in membrane ruffles and uptake of the bacterium (Cossart, Pizarro-Cerda, and Lecuit 2003). An example for entry over the “trigger” mechanism is *Salmonella*, by secreting six effector proteins that can manipulate actin dynamics during *Salmonella* invasion (Cain, Hayward, and Koronakis 2008). SopE and SopB together activate Cdc42 and Rac-1 thus triggering actin polymerization and nucleation.

On the other hand, SipC and SipA bind actin directly. Furthermore, SipC directly nucleates actin and is essential for the entry of *Salmonella*, whereas SipA enhances the uptake efficiency and suppresses F-actin de-polymerization by inhibiting cofilin (McGhie, Hayward, and Koronakis 2004; Hayward and Koronakis 1999).
Also at the entry site of *Chlamydia* actin rearrangement was observed, which is in part due to the *Chlamydia* TarP protein. TarP is another example for a secreted effector protein that recruits and modulates actin, which is described in more detail in the next paragraph.

1.5.4 The TarP orthologs of *Chlamydia*

TarP (**t**ranslocated **a**ctin **r**ecruiting phospho**p**rotein) is a type III secreted effector protein, which binds and polymerizes actin and was shown to play a critical role in chlamydial invasion. Members of the *C. trachomatis* TarP protein family could be identified in all sequenced *Chlamydia* species (Clifton et al. 2004; Clifton et al. 2005). Proteins of this family share conserved domains, but the amino acid sequence identity is quite divergent between 40 % and 94 % by comparison of *C. trachomatis* L2 TarP to other TarP orthologs (Clifton et al. 2005). All studied TarP proteins, also the *C. pneumoniae* ortholog CPn0572, have a proline-rich domain (PRD), which was shown to promote TarP oligomerization and is required for TarP-dependent actin polymerization (Jewett et al. 2006) (Fig4). Furthermore, in sequence analysis it was shown that all examined TarP orthologs of different strains of *Chlamydiae* (*C. trachomatis* L2, *C. trachomatis* D, *C. trachomatis* A, *C. muridarum*, *C. pneumoniae* CPn0572 and *C. caviae*) harbor at least one actin-binding domain (ABD), some up to four, which are predicted to form a helical secondary structure (Fig4). This finding is interesting as the overall protein sequence of these orthologs is quite divergent (Jewett et al. 2006; Jewett et al. 2010). *In vitro* pull down assays showed that every tested TarP ortholog harbors at least one functional actin binding domain and actin polymerization assays showed that all TarP orthologs harboring an ABD and PRD, are able to polymerize actin (Jewett et al. 2010). Even without the PRD, TarP orthologs with more than one functional ABD were able to nucleate actin, which suggest unique mechanisms of actin nucleation for different TarP orthologs (Jewett et al. 2010). By obstructing the ABD of the *C. trachomatis* L2 ABD, by pre-loading an anti-ABD antibody, the host cells become more resistant to EB invasion (Jewett et al. 2010). In 2016, after it became possible to transform *C. trachomatis*, invasion assays with *C. trachomatis* transformants expressing dominant negative forms of TarP, were performed. The first *in vivo* evidence of the important role of TarP during a *C. trachomatis* infection, came with the expression of a version of TarP without the ABD, which showed a significant reduction in host cell invasion compared to wild type. (Parrett et al. 2016). Further studies of the *C. trachomatis* L2 TarP revealed two additional F-actin

binding domains (FAB) in the C-terminus, next to the one ABD (Jiwani et al. 2013) (Fig4). It was shown that the previously described ABD binds monomeric and filamentous actin, whereas the new identified FABs preferentially associates with F-actin (Jiwani et al. 2013). Even though the TarP orthologs share common characteristics required for actin binding and polymerization, the N-terminus differs. Only the *C. trachomatis* L2 TarP harbors an N-terminal tyrosine-rich domain, which is phosphorylated at the site of entry, which leads to binding of Rac GEFs and activation of Rac GTPases (Clifton et al. 2004; Carabeo et al. 2004). Compared to the cooperation with the Arp2/3 complex, to increase concentration of branched actin, which seems independent of the phosphorylation status of the protein (Jiwani et al. 2012). Moreover, the TarP orthologs of *C. trachomatis*, *C. abortus*, *C. felis*, *C. caviae* and *C. muridarum* recruit the focal adhesion kinase (FAK) by mimicking the LD2 motif of the FAK binding partner paxillin (Thwaites et al. 2014). Up to date a vinculin binding sequence (VBS) could only be identified in *C. trachomatis*, *C. abortus*, *C. felis*, *C. caviae* and *C. muridarum*, but not in the *C. pneumoniae* CPn0572 (Thwaites et al. 2015) (Fig4). In *C. caviae* it was shown that vinculin is recruited to the EB internalization site and is required for the invasion (Thwaites et al. 2015). The depletion of vinculin does not lead to a complete loss of invasion, which is most likely related to other pathways, like the FAK-dependent pathway (Thwaites et al. 2015; Thwaites et al. 2014).

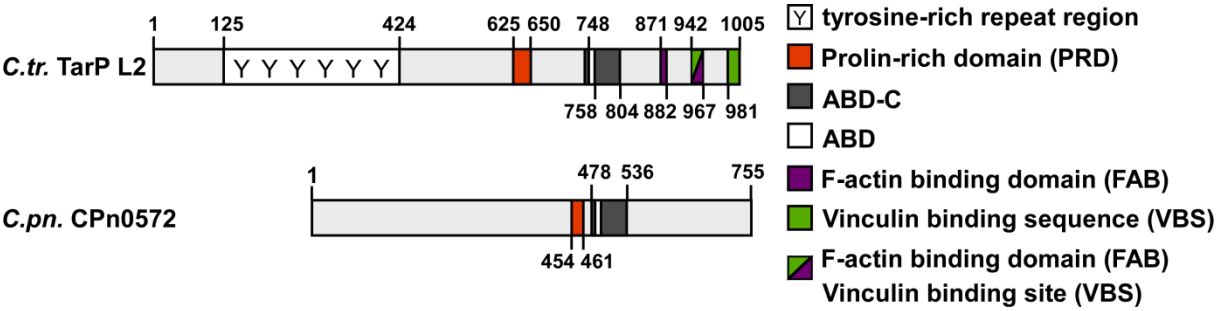

Fig4: Comparison of *C. trachomatis* TarP and *C. pneumoniae* CPn0572.
Schematic representation of *C. trachomatis* L2 TarP and the *C. pneumoniae* ortholog CPn0572 with all up to date identified domains (modified from (Braun et al. 2019).

1.6 Rab GTPases and phosphoinositides are used by pathogens to favor their intracellular survival

Eukaryotic cells separate their enzymatic reactions in membrane-enclosed compartments and require a vesicle-mediated transport mechanism between the compartments, endocytosed vesicles and internalized receptors. Rab GTPases (Rabs) and phosphoinositides (PtdIns) are two important players in membrane identity and regulation of vesicle formation, trafficking and transport (Langemeyer, Frohlich, and Ungermann 2018; Hutagalung and Novick 2011). Especially Rabs and their effectors, but also PtdIns have

become a target for bacterial effector proteins to evade the host defenses by hijacking Rabs involved in endocytic pathways. The next paragraph describes Rabs and PtdIns in more detail, followed by a summarization of bacterial effectors hijacking these players (Hutagalung and Novick 2011).

1.6.1 Rab GTPases

The Ras superfamily of small guanosine triphosphatases (GTPases) consists of 150 human members and is divided into five groups: Ras; Rho; Ran, Arf and Rabs. The Rabs are with more than 60 human and 11 yeast members the biggest group of Ras proteins. They are highly conserved among eukaryotic cells and play an important role in vesicle transport and membrane identity (Wennerberg, Rossman, and Der 2005; Brumell and Scidmore 2007). Rabs regulate membrane trafficking by cycling between a GDP (inactive) or GTP (active) bound state and specific domains play an important role in this function (Fig5). Conserved regions in all members of the Ras family have been identified: GDP/GTP-binding motif elements (G1-G5) that recognize the purine base, three phosphate/magnesium binding motifs (PM1-PM3) and a hypervariable tail (Wennerberg, Rossman, and Der 2005; Pereira-Leal and Seabra 2000; Pan et al. 2006; Pylypenko et al. 2018). An additional characteristic of Rabs is a C-terminal CAAX box that usually contains two cysteine where geranylgeranyl tails are attached over which Rab proteins can be integrated into target membranes (Hutagalung and Novick 2011). The previously described conserved domains play an essential role in this cycle and the different states of the Rab. Bound GTP leads to constraining interactions between the PM motifs, which stabilizes the Switch 1 and Switch 2 regions and keeps the protein in its active form. By hydrolysis of GTP to GDP and the release of Pi the Switches become destabilized, which leads to the inactive GDP-bound conformation change (Pylypenko et al. 2018). This switch mechanism and the strong binding of GTP or GDP at the catalytic side of Rabs is important for their essential function as the active from can be recognized by effector proteins and is a timer for specific activity at the membrane and thus controls how long their effectors stay bound (Pylypenko et al. 2018). Moreover, Rab specific sequences were identified, called RabF1 to RabF5, which can be important for recognition of effector proteins (Pylypenko et al. 2018; Pereira-Leal and Seabra 2000).

To control the precise localization and activity of Rabs, cellular partners are needed, which in most cases bind in a nucleotide-dependent manner. New synthesized Rabs, mostly in their GDP-bound state bind to a Rab escort protein (REP), which then presents them to a Rab gernalygeranyl transferase (RabGGT), which geranylgernaylates the Rab on the C-terminal cysteine (Pylypenko et al. 2018). The subsequent integration and targeting of a Rab protein into the appropriate membrane can be supported by a GDP dissociation inhibitor (GDI) or

dissociation factor (GDF). After integration of the GDP-bound (inactive) form a guanine exchange factor (GEF) converts it to a GTP-bound (active) form (Fig5). The GTP is then hydrolyzed to GDP by a GTPase accelerating protein (GAP) and the GDI, which binds to GDP-bound Rabs, extracts the Rab from the membrane. The Rab protein in its inactive GDP-bound state is then ready to be integrated again and start the cycle anew (Fig5) (Hutagalung and Novick 2011; Pylypenko et al. 2018).

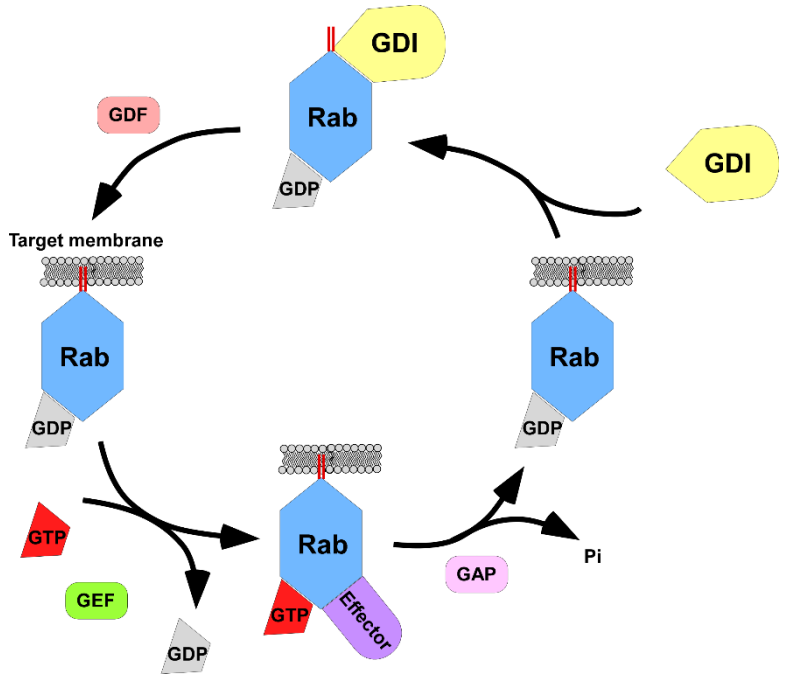

Fig5: The Rab switch and cycle.

The inactive GDP-bound Rab protein is recruited and incorporated into its target membrane over its prenyl tails (red lines). A guanine nucleotide exchange factor (GEF) exchanges the GDP to GTP, which in turn activates the Rab protein. This activated Rab protein is then interacting with effectors, which play a role in the membrane traffic of the respective Rab protein. Afterwards, the GTPase activating protein (GAP) catalyzes the hydrolysis of GTP to GDP. Over a guanine nucleotide dissociation inhibitor (GDI) the Rab is removed from the membrane and is ready for the next cycle. The incorporation of the GDP bound Rab is mediated by a GDI dissociation factor (GDF).

As there are a multitude and diversity of Rabs it is quite interesting how the G-domain has evolved so that common partners like GDI can bind, but at the same time being different enough in their sequence that allows specific recognition of regulators, like GAPs and GEFs and effectors. Generally, effectors are defined as proteins which interact preferentially with the GTP-bound state of their respective Rab. There are a variety of effector proteins as Rabs play important roles in membrane identity, but also trafficking and tethering of vesicles to their target compartment, leading to membrane fusion. Rab 5 for example plays a role in the early endocytic pathway and the effector EEA1 mediates the tethering/docking of early endosomes. EEA1 possess a FYVE domain that binds to PtdIns(3)P, which is enriched on early endosomes (EE). Another effector of Rab5 is the PI3-OH kinase Vps34 and is with PI(4) And PI(5)-phosphatases important for the enrichment of PtdIns(3)P on EEs.

Recruitment of effectors with different function is important. For example, is the function of Vps34 absent, recruitment of EEA1 is prevented, thus the fusion of EEs is blocked (Zerial and McBride 2001; Hutagalung and Novick 2011). Other effectors are important for vesicle transport and interact with the host cytoskeleton, like Rab11 family interacting protein 2 (Rab11-FIP2), which interacts with myosin Vb to regulate plasma membrane recycling (Hutagalung and Novick 2011).
Rab proteins and their effector proteins play this central role in membrane trafficking, so it is not surprising that intracellular pathogens evolved mechanisms to manipulate and exploit Rab function to evade degradation, which will be describe in more detail in paragraph 1.6.3.

1.6.2 Phosphoinositides

Next to Rab proteins another important player in membrane identity and trafficking are phosphoinositides (PtdIns) (Jean and Kiger 2012). Furthermore, PtdIns have an important role in controlling the activity of transporters, the immune cell function and chemotaxis (Balla 2013).
PtdIns are phosphorylated derivates of phosphatidylinositol. They consist of a *myo*-inositol ring that is linked to a diacylgylcerol (DG) backbone and a “chair” like conformation with six –OH groups (Balla 2013). Through different experimental approaches, like transfection of fusion PtdIns with fluorescent proteins, it was shown that different PtdIns mark different membranes. For example, PtdIns(4)P is mostly localized at the Golgi, PtdIns(4,5)P_2 and PtdIns(3,4,5)P_3 at the plasma membrane and PtdIns(3)P at EEs. More detailed studies showed that different PtdIns can be found not only at their signature membrane, like PtdIns(4)P and PtdIns(3)P can also be found at the plasma membrane (Schink, Tan, and Stenmark 2016). In general, PtdIns are able to regulate membrane dynamics in direct and indirect ways, like recruitment of GEFs, GAPs, cytoskeleton-binding proteins or signaling proteins, like phosphatases or kinases. Moreover, PtdIns can generate second messengers, control ion channels, by interacting with channel proteins and recruit coat proteins, lipid-modifying proteins and membrane-shaping proteins, thus directly control membrane dynamics (Schink, Tan, and Stenmark 2016).
Endocytotic processes, like phagocytosis, micropinocytosis and clathrin-mediated receptor endocytosis, are tightly controlled by different PtdIns. PtdIns(4,5)P_2-binding proteins, like sorting nexin 9 (SNX9) play an important role during clathrin-mediated endocytosis, which is a membrane binding protein. After the clathrin-coated vesicle leaves the plasma membrane, PtdIns(4,5)P_2 is dephosphorylated to PtdIns(4)P. Other PtdIns, like PtdIns(3)P have a function during endosome maturation and dynamics. The accumulation of PtdIns(3)P at EEs is mostly due to the phosphorylation of phosphoinositols by PI3K-II and PI3K-III. To bind to

PtdIns(3)P, many proteins involved in endosome positioning or endosome maturation contain a PX or FYVE domain. The latest described processes also show a connection between the function of PtdIns and Rab proteins. Vesicle from the plasma membrane are as described before coated with Rab5. GTP-bound Rab5 recruits the PI3K-III complex and thus synthesis of PtdIns(3)P, which results in recruitment of other effectors. These other effectors lead to the displacement of Rab5 to Rab7 and thus to the switch between early and late endosomes (Schink, Tan, and Stenmark 2016). Moreover, PtdIns also play a role in autophagy, cell division and epithelial cell polarity. Such a variety of functions and the close connection to Rab proteins made PtdIns another target for pathogens to manipulate to their advantage, which is described in more detail in the following paragraph.

1.6.3 Rab GTPases and PtdIns are manipulated by pathogens

Intracellular pathogens have evolved highly efficient mechanisms to subvert host immune system and engage host organelles to establish their unique intracellular niche and gain increased access to host nutrients. Phagosomal maturation through endosomal fusion is an important step to eliminate invading microbes by macrophages. In this process Rab5 and EEA1 play a crucial role. Thus, Rabs and PtdIns are host proteins that are hijacked or mimicked by effector proteins of intracellular pathogens to subvert trafficking mechanisms and establish their intracellular niche.

Legionella pneumophila, which resides in the *Legionella*-containing vacuole (LCV) after internalization, uses type IV secreted effectors proteins to manipulate membrane trafficking, as the LCV does not follow the classical phagocytic maturation route. One such effector is VipD, which binds to Rab5, preventing interaction with its effectors and catalyzes the removal of PtdIns(3)P from endosomal membranes and rendering them fusion incompetent (Gaspar and Machner 2014; Spano and Galan 2018). Another effector of *Legionella* to aid in the evasion of the endocytic/phagocytic pathway by depletion of PtdIns(3)P might be the phosphatase SidP, which hydrolyzes PtdIns(3)P *in vitro* (Pizarro-Cerda, Kuhbacher, and Cossart 2015).

Salmonella secretes the effector SopB, which has a phosphatidylinositide phosphatase activity which modulates the phosphoinositide composition of the *Salmonella*-containing vacuole (SCV) and recruits Rab5. Furthermore, SopB hydrolyzes PtdIns(4,5)P_2, which leads to a reduction of membrane tension through removal of actin and associated proteins (Pizarro-Cerda, Kuhbacher, and Cossart 2015). *Salmonella* replicates in an intracellular compartment that acquires features of a lysosome, like an acidic pH. Thus, recruiting Rab7, its effector Rab-interacting lysosomal protein (RILP) and lysosomal glycoproteins like LAMP-1 are essential for *Salmonella* replication in epithelial cell. (Spano and Galan 2018).

As described before also *Chlamydia* recruit Rab proteins. It was shown that Inc proteins like the *C. trachomatis* CT229 which interacts with Rab4-GTP and the *C. pneumoniae* CPn0585 which binds Rab1, Rab10 and Rab11, are able to interact with Rabs. This interaction between host Rabs and the chlamydial inclusion might facilitate the transport and interaction with intracellular structures, like Rab11 as a recycling endosomal Rab (Damiani, Gambarte Tudela, and Capmany 2014). Recent studies could show that the early *Chlamydia* inclusion also acquires Rabs, like recycling Rab11, Rab14, late endosomal Rab 7 and an early membrane identity (Molleken and Hegemann 2017). Rab11, Rab14 are sustained and Rab7 disappears, which allows *C. pneumoniae* to hide in a recycling endosome vesicle and consequentially evading lysosomal degradation (Molleken and Hegemann 2017).

1.7 Objectives of this thesis

After the adhesion of the *Chlamydia* EB to the human cell the next essential steps of the infection are the internalization and establishment of the inclusion. However, the processes and players involved are not all known and fully understood yet. The aim of this work was to analyze the *C. pneumoniae* TarP ortholog CPn0572 and a novel *C. pneumoniae* specific gene cluster of potential effector proteins.

The first part of this work (manuscript I and II) focused on analyzing CPn0572 and its influence on the human actin cytoskeleton. The host actin cytoskeleton plays an important role during the internalization of *Chlamydia* EBs and as CPn0572 is the *C. pneumoniae* TarP ortholog it should be investigated if CPn0572 has nucleating, polymerization and stabilizing effects on actin. Using yeast model organisms as well as biochemical assays and immunofluorescence microscopy in human cells, the significance of CPn0572 and possible actin binding domains should be analyzed.

The second part of this work (manuscript III, unpublished data 2.3) focused on characterizing a newly identified protein cluster of thirteen *C. pneumoniae* effector protein candidates (GiD_A_04840-04720, termed Cee1-Cee13). The proteins of this cluster are hypothetical and were identified in a bioinformatic screen because of a local identity to a human RabGTPase, which are known to be involved in vesicle transport and membrane identity. Thus, ectopic and co-expression studies with endosomal marker, like recycling specific Rab11 and PtdIns(3)P, both present at the early inclusion, should be performed to investigate a possible presence of the cluster proteins during the early *C. pneumoniae* infection. Furthermore, the localization and time of expression of the endogenous proteins during chlamydial infection should be analyzed. Moreover, with adhesion and biochemical assays the ability to bind to the human plasma membrane and different phospholipids/phosphoinositides and with that different membrane compartments, should be

investigated. Finally, a possible effect of the cluster proteins on the chlamydial infection and relevance for *C. pneumoniae* infection should be characterized.

2. Results

The first essential step of the *C. pneumoniae* infection is the adhesion, during which adhesins, bind to receptors or lipids on the human plasma membrane. Afterwards the pathogen gets internalized. During the internalization processes *Chlamydia* secretes, via the type III secretion system, effector proteins into the host cell to facilitate entry. One such effector protein is TarP, which recruits and polymerized actin at the entry site. Next, the establishment of the intracellular niche, the inclusion, needs to be established to guarantee survival inside the host cell and subsequently completion of the chlamydial life cycle. The proteins and processes involved are up to date poorly understood.

The purpose of this thesis was to investigate the *C. pneumoniae* TarP ortholog CPn0572, its effect on the host actin cytoskeleton and function during the *C. pneumoniae* infection (investigated in manuscript I and manuscript II). Furthermore, a cluster of thirteen chlamydial effector proteins and their possible involvement in early phase of the infection was to be investigated (results shown in manuscript III and unpublished data in chapter 2.3).

2.1 Summaries of the manuscripts

2.1.1 Summary manuscript I

The *Chlamydia pneumoniae* Tarp Ortholog CPn0572 Stabilizes Host F-Actin by Displacement of Cofilin (Zrieq, Braun, and Hegemann 2017).

The first essential step of the chlamydial infection is the adhesion, followed by the secretion of type III effector proteins, which influence host cell processes, and internalization of the pathogen. As described before, one example for such an effector protein is the *C. trachomatis* TarP. In this study the function of the *C. pneumoniae* TarP ortholog CPn0572 and its influence on the host actin cytoskeleton was investigated. It could be shown that CPn0572 does not only associate with actin patches in transfected human epithelial cells, as it was shown for TarP, but also with actin filaments. The model organism *Saccharomyces cerevisiae* (*S. cerevisiae*) was used to further analyze the role of CPn0572, in modulating the host actin cytoskeleton, as many processes and proteins are conserved among eukaryotes. As it was observed in human cells, also in *S. cerevisiae* the expression of CPn0572 lead to actin patches, reorganization of the actin cytoskeleton and additionally inhibited growth. Furthermore, a domain of unknown function (DUF), which contains the actin-binding domain (ABD), a domain shared by the *Chlamydia* TarP orthologs, was identified as seemingly required for the localization of CPn0572 to F-actin. In an *in vitro* assay it could be shown that

CPn0572 binds to F-actin and seemed to displace cofilin from F-actin structures. These results suggest a F-actin stabilizing role of CPn0572. In early infection studies it could also be shown that CPn0572 associated with actin patches and EBs at the site of entry as early as 15 min post infection (Zrieq, Braun, and Hegemann 2017).

2.1.2 Summary manuscript II

CPn0572, the *C. pneumoniae* ortholog of TarP, reorganizes the actin cytoskeleton via a newly identified F-actin binding domain and recruitment of vinculin (Braun et al. 2019)

The previous study has shown that in transfection analysis CPn0572 associates with F-actin via an actin binding domain, shared by the *Chlamydia* TarP family and expression inhibits *S. cerevisiae* growth. In this investigation, with the help of the fission yeast *Schizosaccharomyces pombe* (*S. pombe*) and immunofluorescence analysis of various CPn0572 GFP fusion variants in human epithelial cells, a second actin modulating domain in the C-terminal part of the protein could be identified. *In vitro* pull down assays showed that the C-terminus of CPn0572 ($CPn0573^{536-755}$) directly binds to F-actin, independent of the previously described ABD domain. Through further microscopic analysis in transfection studies of human epithelial cells, an association of CPn0572 to vinculin was observed. Bioinformatic studies revealed a vinculin binding sequence (VBS) in the second predicted α-helix of the C-terminus of CPn0572 (Braun et al. 2019).

2.1.3 Summary manuscript III

A novel set of Rab GTPase-related *Chlamydia* effector proteins involved in the early phase of infection (Braun, Hegemann, and Mölleken 2019, submitted)

After adhesion and internalization, the next essential step during the chlamydial infection is, establishing the intracellular niche, the inclusion. It is known that the adhesin Pmp21 binds and activates the human EGFR, which stays associated with the inclusion membrane. As activation of the EGFR usually either leads to the degradation of the receptor in the lysosomal pathway or recycling back to the plasma membrane, *Chlamydia* needs to somehow avoid these pathways to complete its life cycle. In this study a bioinformatic screen of all *C. pneumoniae* hypothetical proteins against the human and other intracellular pathogen genomes, identified a gene cluster (*GiD_A_04840-04720*) that encodes for early chlamydial effectors, one of which exhibits localized identity to the human RabGTPase 36. The proteins share an overall pairwise identity of 32.6 % and harbor either one or both domains of unknown function DUF575 and DUF562. Furthermore, in all proteins with a DUF domain Rab-specific G1, G3 and G5 box motifs were identified. In depth bioinformatic

analysis could show that the cluster is *C. pneumoniae* specific and could also be found in the ancestral koala strain LPCoLN. Single nucleotide polymorphism (SNPs) in individual genes were identified. The distribution of the SNPs within human strains is specific for respiratory and vascular strains, which could represent a possible adaptation to the host and/or tissue. Expression of GFP fusion proteins in human epithelial cells showed different localization phenotypes, most interesting the observed vesicle-like structures of cluster proteins harboring the DUF575. Co-transfection studies revealed an association of 04840 vesicle with the early endosomal marker PtdIns(3)P, the endogenous, endocytosed EGFR and recycling-specific Rab11 and Rab14 proteins, in an G1-box motif depending manner. Early and late infection studies with specific antibodies could show that 04840 and 04810 associate to adhering EBs and are most likely synthesized mid-/late during the infection cycle. Furthermore, it could be shown that individual proteins of the cluster bind to the plasma membrane of human cells, but do not impair a subsequent *C. pneumoniae* infection. An ability to bind to different phospholipids/phosphoinositides and with that a possible binding to different membranes could also be shown. Together this data suggests that the proteins of this cluster are involved in the early infection (Braun, Hegemann, and Mölleken 2019, submitted).

2.2 Manuscripts

2.2.1 Manuscript I

The *Chlamydia pneumoniae* Tarp Ortholog CPn0572 Stabilizes Host F-Actin by Displacement of Cofilin

Rafat Zrieq, **Corinna Braun** and Johannes H. Hegemann

Second author

Contribution: 5 %

Corinna Braun performed transfection experiments of HEp-2 and HEK293 cells expressing GFP-CPn0572 fusion proteins, which were analyzed *via* westernblot analysis and immunofluorescence microscopy. Additionally, did she generate figure S3B and was involved in the review and editing process.

Published in: Frontiers in Cellular and Infection Microbiology, December 2017, DOI: 10.3389/fcimb.2017.00511

Impact factor: 4.3 (2017)

frontiers in Cellular and Infection Microbiology

ORIGINAL RESEARCH
published: 12 December 2017
doi: 10.3389/fcimb.2017.00511

The *Chlamydia pneumoniae* Tarp Ortholog CPn0572 Stabilizes Host F-Actin by Displacement of Cofilin

Rafat Zrieq[1,2], *Corinna Braun*[2] *and Johannes H. Hegemann*[2]*

[1] Department of Clinical Laboratory Sciences, College of Applied Medical Sciences, University of Ha'il, Ha'il, Saudi Arabia,
[2] Funktionelle Genomforschung der Mikroorganismen, Heinrich-Heine Universität Düsseldorf, Düsseldorf, Germany

Pathogenic *Chlamydia* species force entry into human cells via specific adhesin-receptor interactions and subsequently secrete effector proteins into the host cytoplasm, which in turn modulate host-cell processes to promote infection. One such effector, the *C. trachomatis* Tarp factor, nucleates actin polymerization *in vitro*. Here we show that its *C. pneumoniae* ortholog, CPn0572, associates with actin patches upon bacterial invasion. GFP-CPn0572 ectopically expressed in yeast and human cells co-localizes with actin patches and distinctly aberrantly thickened and extended actin cables. A 59-aa DUF 1547 (DUF) domain, which overlaps with the minimal actin-binding and protein oligomerization fragment required for actin nucleation in other Tarp orthologs, is responsible for the aberrant actin phenotype in yeast. Interestingly, GFP-CPn0572 in human cells associated with and led to the formation of non-actin microfilaments. This phenotype is strongly enhanced in human cells expressing the GFP-tagged DUF deletion variant (GFP-ΔDUF). Finally ectopic CPn0572 expression in yeast and *in-vitro* actin filament binding assays, demonstrated that CPn0572 stabilizes pre-assembled F-actin by displacing and/or inhibiting binding of the actin-severing protein cofilin. Remarkably, the DUF domain suffices to displace cofilin from F actin. Thus, in addition to its actin-nucleating activities, the *C. pneumoniae* CPn0572 also stabilizes preformed host actin filaments.

Keywords: chlamydia, actin cytoskeleton, TARP, effector proteins, CPn0572, microbe-host cell interaction

OPEN ACCESS

Edited by:
Rey Carabeo,
Washington State University,
United States

Reviewed by:
Scott Grieshaber,
University of Idaho, United States
Luís Jaime Mota,
Faculdade de Ciências e Tecnologia
da Universidade Nova de Lisboa,
Portugal

***Correspondence:**
Johannes H. Hegemann
johannes.hegemann@hhu.de

Received: *12 August 2017*
Accepted: *27 November 2017*
Published: *12 December 2017*

Citation:
Zrieq R, Braun C and Hegemann JH (2017) The Chlamydia pneumoniae Tarp Ortholog CPn0572 Stabilizes Host F-Actin by Displacement of Cofilin. Front. Cell. Infect. Microbiol. 7:511. doi: 10.3389/fcimb.2017.00511

INTRODUCTION

Chlamydiae are Gram-negative intracellular pathogens that infect a variety of organisms and tissues, and are responsible for several serious respiratory, ocular and urogenital diseases (Schachter, 1999). All *Chlamydia* species have a biphasic developmental cycle, alternating between the infectious but metabolically inert elementary body (EB) and the non-infectious, metabolically active reticulate body (RB). RBs replicate within a parasitophorous vacuole, termed an inclusion (Schramm et al., 1996; Belland et al., 2004). Successful uptake of EBs is crucial for *Chlamydia* infection, but the underlying molecular mechanisms are not well-understood.

Generally, the ability of bacterial pathogens to enter host cells depends upon cross-talk between bacterial and host factors, beginning with direct engagement of receptors on the target cell by adhesins, and/or translocation of effector proteins into the host-cell cytosol. These processes usually result in a rearrangement of the host-cell cytoskeleton, which in turn promotes a reorganization

of the host plasma membrane architecture that facilitates bacterial uptake (Pizarro-Cerdá and Cossart, 2006). Initial attachment of the chlamydial EB is normally mediated by the interaction of the chlamydial surface protein OmcB with glycosaminoglycans (GAGs) on the host-cell surface, and is followed by more specific adhesin-receptor interactions (Hegemann and Moelleken, 2012). Thus, the *C. pneumoniae* adhesin/invasin Pmp21 binds directly to the human epidermal growth factor receptor (EGFR), activating signaling cascades that facilitate the uptake of *C. pneumoniae* EBs into their target cells (Mölleken et al., 2013). Moreover, the EB surface protein CPn0473 also mediates adhesion to human epithelial cells, and promotes EB uptake in a lipid-raft-dependent manner (Fechtner et al., 2016).

The *C. trachomatis* protein Tarp (translocated actin-recruiting phosphoprotein) is an early virulence effector protein implicated in host-cell invasion (Clifton et al., 2004; Lane et al., 2008; Jewett et al., 2010; Parrett et al., 2016). Tarp, which is assumed to be secreted by a Type-3 secretion system via Slc1 (SycE-like chaperone 1; CT043), is translocated into targeted cells within minutes of EB attachment, and associates with recruited actin at the site of bacterial attachment (Clifton et al., 2004; Brinkworth et al., 2011). This is accompanied by phosphorylation of several tyrosine residues near the N-terminus of Tarp by Src family tyrosine kinases and Ab1 kinase (Clifton et al., 2004; Jewett et al., 2008; Mehlitz et al., 2008). However, Tarp phosphorylation is not essential for chlamydia entry or actin recruitment. The protein most probably acts as a molecular scaffold to recruit host proteins that regulate actin dynamics and signaling events required for the early phase of chlamydial infection (Clifton et al., 2005; Jewett et al., 2008; Mehlitz et al., 2008; Thwaites et al., 2014).

Recruitment of actin to attached EBs early in the infection, in a pattern similar to that seen in *C. trachomatis*, has been observed for a number of chlamydial species (Clifton et al., 2005). However, although orthologs of the *C. trachomatis* Tarp gene are present in all sequenced *Chlamydia* species, they differ widely in amino acid sequence (displaying between 40 and 94% identity), domain structure and length (Clifton et al., 2005; Jewett et al., 2010; Jiwani et al., 2013), with the least conserved being the *C. pneumoniae* orthologs. For example, the *C. muridarum* and *C. pneumoniae* orthologs (but not the *C. caviae* ortholog) lack the tyrosine repeats (Clifton et al., 2005). In contrast, all Tarp orthologs harbor a protein oligomerization domain, and the actin-binding domains found in all examined chlamydial strains and species are able to nucleate actin polymerization *in vitro*. Interestingly, *C. pneumoniae* Tarp is the sole ortholog that has only a single actin-binding domain (Jewett et al., 2010). Recently, evidence was provided that the Tarp orthologs from serovars of *C. trachomatis* harbor two F-actin binding domains which seem to be absent from Tarp orthologs in other chlamydial species (Jiwani et al., 2013). Moreover, binding domains for the focal adhesion kinase (FAK) and for vinculin have been identified for Tarp proteins from various chlamydial species, but are not found in the *C. pneumoniae* ortholog (Thwaites et al., 2014, 2015).

To elucidate the functional consequences of these differences, we characterized CPn0572, the putative *C. pneumoniae* ortholog of Tarp. CPn0572 is secreted into the host-cell cytoplasm upon EB uptake and is associated with actin recruitment to the site of entry. Ectopically expressed CPn0572 stabilizes actin filaments (F-actin) both in yeast and in human HEK293T cells. Moreover, CPn0572 has the ability to generate or interact with other filamentous structures not associated with F-actin structures. Interestingly, detailed analysis revealed that CPn0572 blocks the disassembly of F-actin by displacing the F-actin destabilizing protein cofilin. Thus, in addition to the known function of Cpn0572 in nucleating F-actin, our findings provide evidence that the protein (like the prototypical Tarp from *C. trachomatis*) is a microbial F-actin-stabilizing protein. To our knowledge, this is the first bacterial effector protein that has been shown to directly modulate both actin nucleation/polymerization and depolymerization in host cells.

MATERIALS AND METHODS

Bacterial Strains, Eukaryotic Strains and Cell Lines, and Growth Conditions

Escherichia coli (*E. coli*) XL-1 (Stratagene) was used for plasmid amplification and BL21 (Stratagene) for protein expression. Transformed *E. coli* strains were cultured in LB medium containing the appropriate antibiotics. *C. pneumoniae* GiD and *C. trachomatis* L2 (434) were propagated in HEp-2 cells (ATCC No.: CCL-23) and purified as described previously (Jantos et al., 1997; Wuppermann et al., 2008). The *Saccharomyces cerevisiae* strain CEN.PK2 (*MATa/MATα ura3-52/ura3-52 trp1-289/trp1-289 leu2-3,112/leu2-3,112 his3-Δ1/his3-Δ1*) (EUROSCARF) was used for the homologous recombination cloning and the characterization of CPn0572 in yeast. The *aip1Δ* (*MATa his3Δ1 leu2Δ0 met15Δ0 ura3Δ0 YMR092c::kanMX4*) strain and the corresponding wt strain BY4741 (*MATa his3Δ1 leu2Δ0 met15Δ0 ura3Δ0*) (both from EUROSCARF) were used for cofilin (Cof1p) localization. Plasmid-bearing strains were grown on selective synthetic dextrose (SD) medium supplemented with 2% (wt/vol) glucose, raffinose or galactose (Sherman, 1991). HEK293T cells (ATCC No.: CRL-11268) were routinely cultured in IMDM medium (Invitrogen) supplemented with 10% (vol/vol) fetal calf serum (FCS; Invitrogen).

Comparison of Protein Sequences

The following Cpn0572 and Tarp protein were used (accession numbers are included):

C. pneumoniae Cpn0572 CWL029 NP_224768.1
C. trachomatis Tarp LGV-434 AAT47185.1
C. muridarum TC0741 AAF39550
C. caviae CCA00170 AAP04921

Levels of similarity and identity between Cpn0572 and Tarp were calculated by EMBOSS http://emboss.bioinformatics.nl/cgi-bin/emboss/needle. Multiple sequence alignments of DUF domains from CPn0572 and its chlamydial orthologs were performed using MultAlin: http://bioinfo.genotoul.fr/multalin/multalin.html. The prediction of α-helices in DUF was carried out with the helical wheel projection prediction program (http://rzlab.ucr.edu/scripts/wheel/wheel.cgi).

DNA Manipulations and Plasmid Construction

Plasmids were constructed either by homologous recombination in *S. cerevisiae* or by ligation as indicated. In general, the plasmids used to generate the plasmids required for this study are listed in Table S1. The bacterial DNA sequences were amplified from genomic DNA or pre-existing plasmids using the oligonucleotides listed in Table S2. For expression of $CPn0572_{6His}$ in *E. coli*, the pAC2 vector was cut at *Bgl*II and *Eco*RI sites and the coding sequence of *cpn0572* was integrated by homologous recombination in yeast. For expression of CPn0572 or its variants in mammalian cells, amplified DNA fragments were cloned into the pBYE vector (a modified pcDNA3.1/NT-GFP, see Table S1) at the *Acc*65I site. For yeast growth tests, the DNA coding sequences of *cpn0572* and its derivatives were cloned into the p426MET25 vector at the *Sma*I site (Mumberg et al., 1994). For localization studies in yeast *cpn0572* and its derivatives were also cloned into the pUG34 vector at the *Sma*I site via homologous recombination in yeast. Only the DNA fragment encoding GFP-C-terminal-ΔDUF was cloned into pUG34 by ligation. To do so, the DNA fragment was isolated from a p426MET25-GFP-C-terminal-ΔDUF vector by cleavage with *Spe*I and *Xho*I and cloned into the same sites in pUG34. To express GST fusion proteins in *E. coli*, *cpn0572* or the coding sequence for DUF or C-terminal-ΔDUF was amplified and integrated into the pKM36 vector at the *Sma*I site by homologous recombination. For expression of CPn0572 in the *aip1*Δ mutant strain and in wild type BY4741, the coding region of $cpn0572_{6His}$ was isolated from the p426MET25-cpn0572 vector using *Spe*I and *Xho*I, and integrated at the corresponding sites in p423GAL1 by ligation.

Host-Cell Transfections and Infection with *C. pneumoniae*

HEp-2 or HEK293T cells grown overnight on coverslips were transfected with 0.5–1 μg of the desired DNA plasmid using Turbofect (Thermo Scientific) as recommended by the manufacturer. Transfected cells were incubated in a CO_2 incubator at 37°C for the indicated time periods (16 to 24 h). Human HEp-2 cells expressing mCherry-actin were infected with *C. pneumoniae* by adding purified EBs (suspended in cold DMEM medium) to attached HEp-2 cells, followed by centrifugation at 2,800 rpm, 4°C for 20 min. The medium was replaced by pre-warmed fresh medium and the cells were shifted to 37°C for the time periods indicated in the Figure legends. Samples were then prepared for microscopy as described below.

Fluorescence Microscopy and Western Blots

Yeast F-actin was stained with 6.6 μM rhodamine-phalloidin (Molecular Probes). To visualize cofilin and $CPn0572_{6His}$, cells were fixed and indirectly immunostained as described previously (Pringle et al., 1991), using polyclonal chicken antibodies against cofilin (Okada et al., 2006) and a monoclonal mouse anti-His antibody (Novagen).

For indirect immunostaining infected or transfected human cells growing on glass coverslips were washed with 1x PBS, fixed in 3.7% (wt/vol) paraformaldehyde and permeabilized with 0.1% Triton X-100 (vol/vol). Permeabilized infected cells were then incubated with antibodies against *C. pneumoniae* MOMP (anti-MOMP antibody was kindly provided by G. Zhong, University of Texas Health Science Center, San Antonio, USA) to identify EBs and CPn0572 (anti-CPn0572 antibody was produced against the recombinant central domain of CPn0572 (aa S343 to A535) in rabbits by Eurogentec SA, Seraing, Belgium), and subsequently with labeled secondary antibodies. Staining of actin in human cells with rhodamine-phalloidin was performed as recommended by the manufacturer (Molecular Probes). Microscopy was carried out using either a spinning-disk confocal instrument or an Axiovert 200 microscope (Carl Zeiss).

For detection of GFP-tagged proteins from yeast on Western blots, a rabbit anti-GFP antibody (Molecular Probes) was employed, and for detection of proteins from human cells a mouse anti-GFP antibody (Thermo Scientific) was used.

Disruption of the Actin Cytoskeleton

Yeast cells in mid-log phase were exposed to either Latrunculin-A (Lat-A) diluted in DMSO or to the solvent DMSO alone (final concentration 2.5 μM). At various times after addition of the agent, cells were removed, fixed immediately, and stained with rhodamine-phalloidin. The actin cytoskeleton of transfected HEK293T cells was disrupted by adding cytochalasin D (CD; Sigma) to the medium (final concentration 10 μM) for 30 min at 37°C.

F-actin/Cofilin Co-sedimentation Assay

F-actin was assembled *in vitro* as recommended by the supplier (Cytoskeleton Inc.). Equimolar amounts (2 μM) of recombinant human cofilin (Cytoskeleton) and pre-assembled F-actin were then incubated at pH 6.8 in the presence or absence of recombinant GST-CPn0572 (2 μM). The assay was then performed as described by the manufacturer.

RESULTS

CPn0572 Is Secreted into HEp-2 Cells Early During Infection by *C. pneumoniae* and Associates with F-Actin

CPn0572 is currently annotated as a hypothetical *C. pneumoniae* protein. When we used a polyclonal antibody raised against the central region of the predicted ORF ($CPn0572^{S343-A535}$) to probe western blots bearing protein extracts obtained from purified *C. pneumoniae* EBs, the antiserum (but not the corresponding preimmune serum) recognized a band of 110–115 kDa, similar in size to the recombinant full-length protein produced in *E. coli* ($rCPn0572_{6His}$), indicating that CPn0572 is present in infectious EBs (**Figure 1A** and Figure S1).

To determine whether the protein is translocated into the host-cell cytoplasm, infected HEp-2 cells were fixed at various time points after exposure to *C. pneumoniae*, and analyzed by immunofluorescence microscopy. At time 0, we observed no significant signal with anti-CPn0572 (**Figure 1B**). After 15 min, some bacteria were found to lie close to, or to partially overlap CPn0572 signals, as has previously been shown for the *C.*

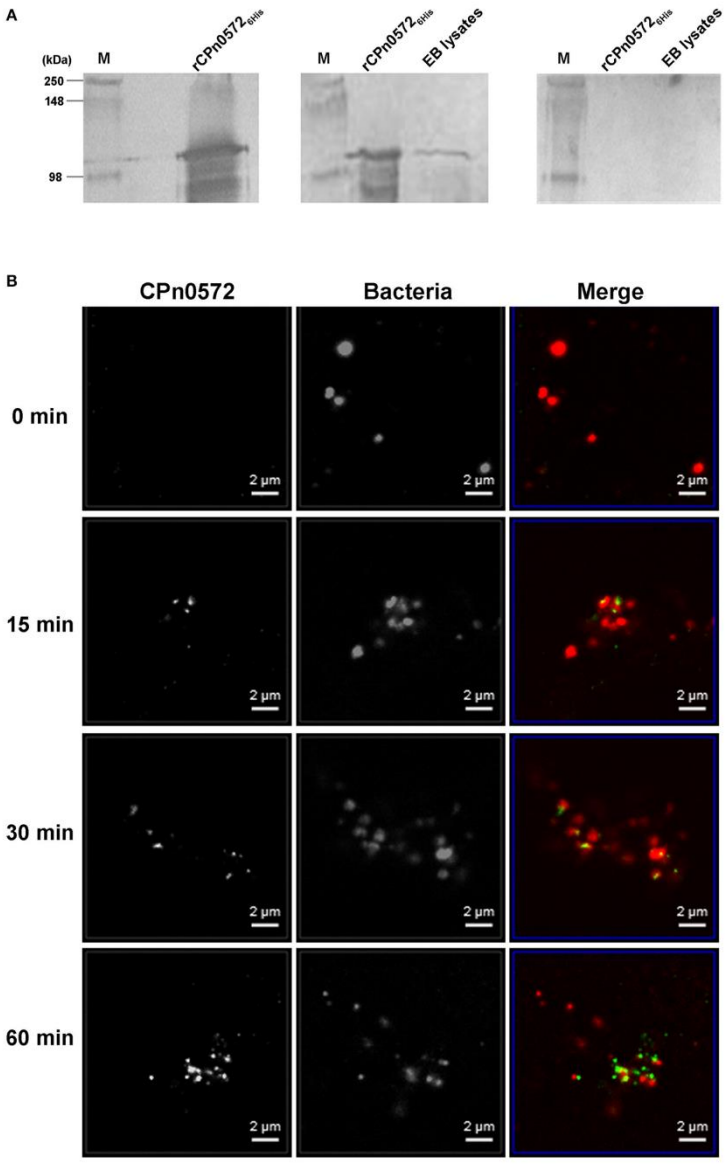

FIGURE 1 | *C. pneumoniae* EBs express CPn0572 and secreted CPn0572 associates with F-actin. **(A)** CPn0572 is present in EBs. $rCPn0572_{6His}$ protein and the endogenous protein expressed in *C. pneumoniae* EBs (EB lysates) were detected on immunoblots probed with a monoclonal anti-His antibody (left panel) and a polyclonal rabbit anti-CPn0572 antibody (middle panel), respectively. The blot shown on the right was probed with the corresponding preimmune serum. Full-scale images of the original blots are presented in Figure S1. **(B)** CPn0572 secretion increases over the first 60 min p.i.. Secretion of CPn0272 was investigated at 0, 15, 30, and 60 min after HEp-2 cells had been infected with purified *C. pneumoniae* EBs (MOI = 50). EBs and CPn0572 were detected using anti-MOMP and anti-CPn0572 antibodies, respectively.

trachomatis Tarp and other secreted chlamydial proteins (Clifton et al., 2004; Hower et al., 2009). These results suggest that secretion of CPn0572 from the EBs had begun prior to this point. After 30 min and 60 min of infection, CPn0572 was detected in association with almost every EB, and the intensity of the signal increased over time (**Figure 1B**). To investigate whether EBs induce accumulation of actin at sites of entry, and to determine if CPn0572 is associated with actin, HEp-2 cells expressing mCherry-actin were infected with *C. pneumoniae* EBs. Adherent EBs were found to lie close by or immediately adjacent to CPn0572 signals and actin patches as early as 15 min p.i. (**Figure 2A**). These results indicate that CPn0572 is secreted from EBs into HEp-2 cells and is found in the vicinity of patches of F-actin accumulation at sites of EB entry.

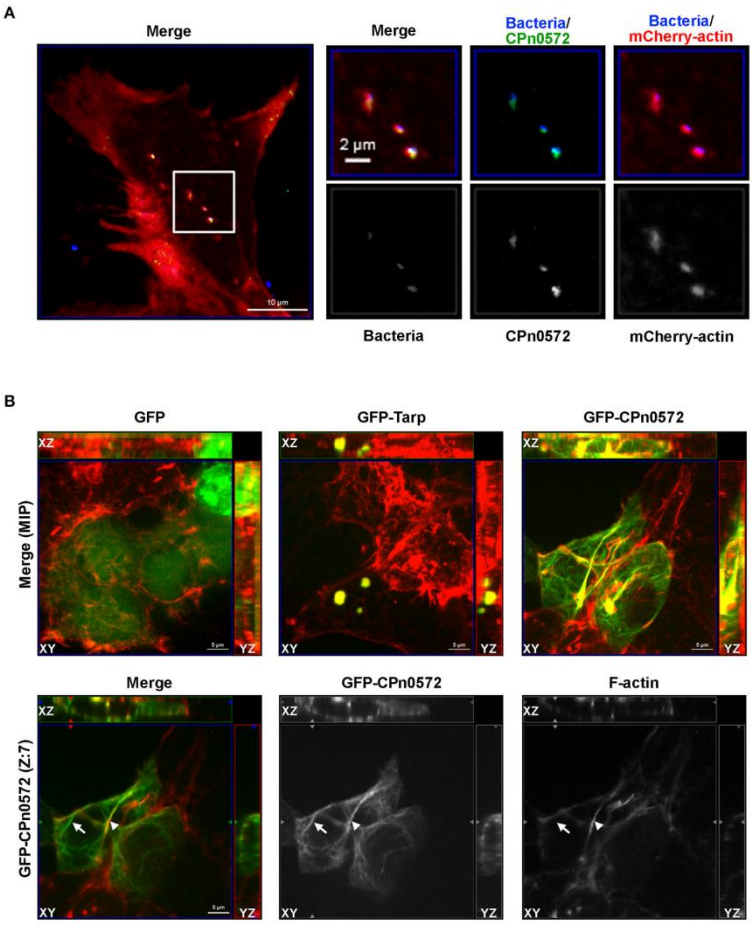

FIGURE 2 | CPn0572 is associated with the host actin cytoskeleton in infected and transfected human cells. **(A)** Secreted CPn0572 colocalizes with host actin early in infection. HEp-2 cells expressing mCherry-actin (red) were infected with purified *C. pneumoniae* EBs (blue, MOI = 5). Secreted CPn0572 (green) is associated with actin recruitment to sites of EB entry at 30 min post-infection. The overall distributibbon of F-actin (red) is depicted in the merged image on the left; the boxed area is shown in greater detail on the right. **(B)** The effect of *C. pneumoniae* GFP-CPn0572 on the actin cytoskeleton differs from that of *C. trachomatis* GFP-Tarp. Upper row: Transfected HEK293T cells stained for GFP, GFP-CPn0572 or GFP-Tarp (green) and F-actin (red). The images shown are maximum intensity projections (MIP) of z-stacks. Lower row: A single section (Z: 7) from the z-stack of GFP-CPn0572 depicted in the upper row is shown. Note that not all GFP-CPn0572 filaments (arrows) coincide with actin fibers (arrowheads).

Tarp and CPn0572 Show Different Patterns of Localization and Association with F-actin in Transfected HEK293T Cells

CPn0572 and its *C. trachomatis* ortholog Tarp show 22.9% sequence identity and 32.5% similarity; moreover, Tarp harbors an N-terminal extension of 276 amino acids (aa), while CPn0572 carries a unique 16-aa C-terminal extension. Interestingly, all Tarp orthologs harbor at least one copy of DUF, which overlaps with the minimal actin-binding and protein oligomerization region required for actin nucleation (Jewett et al., 2010). To determine whether CPn0572 expression in human cells results in an actin phenotype similar to that seen for the expression of *C. trachomatis* Tarp (Clifton et al., 2004; Jiwani et al., 2013), we expressed GFP, GFP-Tarp and GFP-CPn0572 in human HEK293T cells. In each cell expressing GFP-Tarp, the fusion protein was found exclusively in one or more discrete actin-containing structures (**Figure 2B**), similar to what has been described for HeLa cells expressing GFP-Tarp (Clifton et al., 2004; Jiwani et al., 2013). Interestingly, in all cells transfected with GFP-CPn0572, the fusion protein was detected not only in such actin-containing aggregates, but also in distinctly filamentous structures emanating from them (**Figure 2B**, merge, upper panel). Moreover, in more than 80% of the transfected cells, not all GFP-CPn0572-positive filaments were coincident with phalloidin-positive signals (**Figure 2B**; lower panel; compare the Cpn0572-positive fibers marked by an arrow and an arrowhead, respectively, and note the pair of Cpn0572-labeled non-actin filaments seen above the latter). As expected, GFP-CPn0572 expressed in human epithelial HEp-2 cells associated with actin aggregates and actin filaments but also formed fibers not associated with F-actin (Figure S2). These results suggest that CPn0572, like Tarp, associates with and alters the organization of the actin cytoskeleton independently of other chlamydial effectors. However, CPn0572 differs from Tarp in that it can also form fibers that apparently do not contain F-actin.

CPn0572 Inhibits Yeast Growth and DUF Mediates Disruption of F-Actin

Because many of the processes and proteins in host cells that are altered or otherwise subverted during bacterial infections are conserved among eukaryotes (Valdivia, 2004; Siggers and Lesser, 2008; Zrieq et al., 2015), we used the yeast *S. cerevisiae* as a model system to investigate the role of CPn0572 in modulating cytoskeletal organization in greater detail. First, we expressed $CPn0572_{6His}$ from an inducible promoter, and studied its effects on growth rate using serial-dilution patch tests. $CPn0572_{6His}$-expressing cells displayed a severe growth defect, implying that CPn0572 disrupts an essential process in yeast (**Figure 3A**). We therefore examined the actin cytoskeleton in cells expressing GFP-CPn0572, and found the fusion protein in one large structure which colocalized with F-actin (**Figure 3B**). Moreover, a few of these aggregates were found to be associated with small numbers of short actin cables.

Collectively, these findings demonstrate that CPn0572 severely perturbs the yeast actin cytoskeleton by transforming actin structures into aggregates, as it does in human cells expressing GFP-CPn0572. Expression of the *C. trachomatis* Tarp in yeast causes a similar phenotype (Sisko et al., 2006). These data confirm the utility of yeast as a model for further studies of the role of CPn0572 in remodeling the actin cytoskeleton.

The DUF domain (59 amino acids) is the most striking element common to CPn0572 and its orthologs in other *Chlamydia* species (**Figure 3C**). It is predicted to consist of three α-helices (**Figure 3D**) and it forms part of the shortest fragment of CPn0572 (101 amino acids) found to pull down actin *in vitro*, while it overlaps partially with the potential actin-binding domain (ABD) (Jewett et al., 2010). Therefore, we suspected that DUF might be linked to the actin phenotype. Indeed, yeast cells expressing either an N-terminal (M^1-A^{536}) or C-terminal (Q^{478}-K^{755}) segment of CPn0572 including DUF displayed a growth phenotype like that seen with the full-length CPn0572 (**Figure 4B**), while deletion of the DUF domain alone (Q^{478}-A^{536}, ΔDUF, **Figure 4A**) restored normal growth of yeast cells expressing this variant (**Figure 4B**). In contrast, expression of the DUF domain (**Figure 4A**) on its own had no effect on growth (**Figure 4B**). Interestingly, deletion of DUF domain from the C-terminal fragment (C-terminal-ΔDUF, **Figure 4A**) restored normal yeast growth (**Figure 4B**; compare C-terminus vs. C-terminal-ΔDUF). Taken together, these results imply that DUF is essential, but not sufficient, for the severe growth phenotype.

We then examined the actin cytoskeleton in yeast cells expressing the different Cpn0572 variants. The GFP-N-terminal segment of the fusion protein colocalized with actin structures comparable to those induced by the full-length protein (**Figure 4C**). Interestingly, cells expressing the GFP-C-terminal segment showed a very different actin pattern, characterized by complete colocalization of the fusion protein with long, thick actin cables and little cytosolic GFP-C-terminus staining (**Figure 4C**). In contrast, cells expressing the GFP-C-terminal-ΔDUF segment showed typical actin cables and patches found in wild-type cells and a diffused distribution of the fusion protein comparable to that of cells expressing GFP alone, indicating that the lack of toxicity and actin remodeling is due to the absence of the DUF domain (**Figure 4C**). As expected, cells expressing the GFP-ΔDUF construct showed diffuse GFP staining in the cytosol, and their actin cytoskeleton was unaffected (**Figure 4C**). Finally, GFP-DUF itself was found to stain distinctive, unusually shaped and mostly cortically localized actin cables against a strong and diffuse background of the protein in the cytosol (**Figure 4C**). These data indicate that the DUF region of CPn0572 is crucial for the association of CPn0572 with F-actin (**Figure 4C**). The differences in the localization of the different GFP-CPn0572 segments are unlikely to be due to major alterations in protein expression levels (Figure S3A). Taken together, these observations strongly suggest that DUF is required for the association of CPn0572 with F-actin in yeast cells, while other elements further modulate the actin phenotype, which then impairs yeast cell growth.

Next we tested these findings in human cells. As shown above, GFP-CPn0572 was found to localize to complex actin structures, and all CPn0572-expressing cells showed the fusion protein filaments colocalizing with some, but not all actin fibers (**Figure 5**, upper panel, Z: 29; compare arrow and

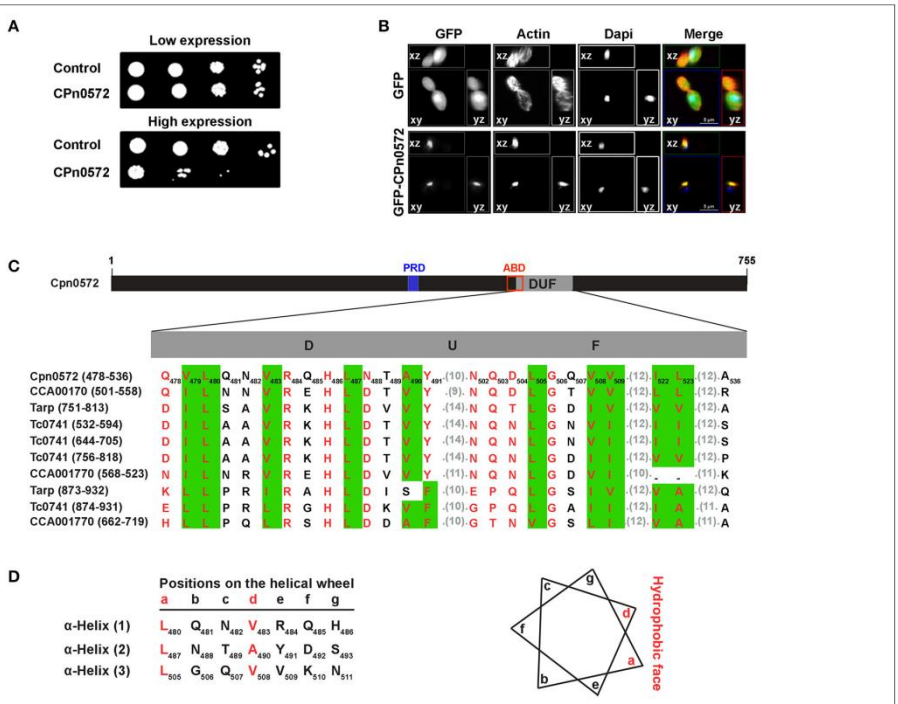

FIGURE 3 | Expression of CPn0572 in *S. cerevisiae* inhibits growth and disrupts the actin cytoskeleton. **(A)** Serial-dilution patch tests of cells bearing either the empty plasmid (control), the repressed (low expression) or the induced (high expression) CPn0572 plasmid. **(B)** Cells expressing GFP (green, upper panel) or GFP-CPn0572 (green, lower panel) were stained for F-actin (red) and nuclei (blue). Data are shown as MIP images. **(C)** Schematic representation of CPn0572. The proline-rich domain (PRD, blue box) associated with the oligomerization capacity of Tarp and the potential actin-binding domain (ABD, red box; identified by Jewett et al., 2006, 2010) and the DUF domain are indicated. The conserved hydrophobic amino acids in DUF are predicted to form three α-helices. Multiple sequence alignment of DUF domains from CPn0572 and its chlamydial orthologs (*C. pneumoniae* Cpn0572, *C. trachomatis* Tarp, *C. muridarum* TC0741 and *C. caviae* CCA00170) as shown by MultAlin. The first and last amino acids of each DUF are indicated on the left. The number of each amino acid residue within the CPn0572 sequence is shown by the subscripts. Conserved amino acids are boxed in green. Hydrophobic amino acids are shown in red. Aligned residues are shown and the numbers of intervening unaligned residues in each sequence are given in parentheses. **(D)** Schematic representation of the disposition of the residues organized into α-helices (as indicated by the lower case letters) as depicted by the helical wheel projection prediction program. The amino acids at positions a and d (in red) represent the hydrophobic face of the wheel as shown on the right.

arrowhead in Z: 16). In contrast, in more than 80% of transfected cells, most GFP-ΔDUF did not colocalize with actin fibers (**Figure 5**, lower panels; see arrow in Z: 16), although this variant was occasionally associated with F-actin aggregates (**Figure 5**, lower panels, MIP and Z: 29). Strikingly, however, the vast majority of GFP-ΔDUF was found in the form of filamentous structures that did not contain actin (**Figure 5**, lower panel). The phenotypic differences seen for GFP-CPn0572 and GFP-ΔDUF are likely not due to differences in protein expression (Figure S3B). These results confirm that DUF is required for the association of CPn0572 with F-actin in human cells. Moreover, CPn0572 has a DUF-independent ability to generate or interact with other filamentous structures.

CPn0572 Stabilizes F-actin by Inhibiting Its Depolymerization

Ectopic expression of CPn0572 in eukaryotic cells induces aggregation of F-actin into thick cables, which resemble analogous structures observed in yeast and human cells under conditions in which actin polymerization is favored over F-actin depolymerization (Ayscough, 2000; Lázaro-Diéguez et al., 2008). In part this can be explained by CPn0572's known ability to nucleate and promote the polymerization of F-actin *in vitro* (Jewett et al., 2010). However, the fact that in human cells CPn0572 exhibits continuous colocalization with distinct actin fibers suggested that CPn0572 might also stabilize F-actin against the action of actin-depolymerizing agents. To test this hypothesis, yeast cells expressing GFP alone or GFP-CPn0572

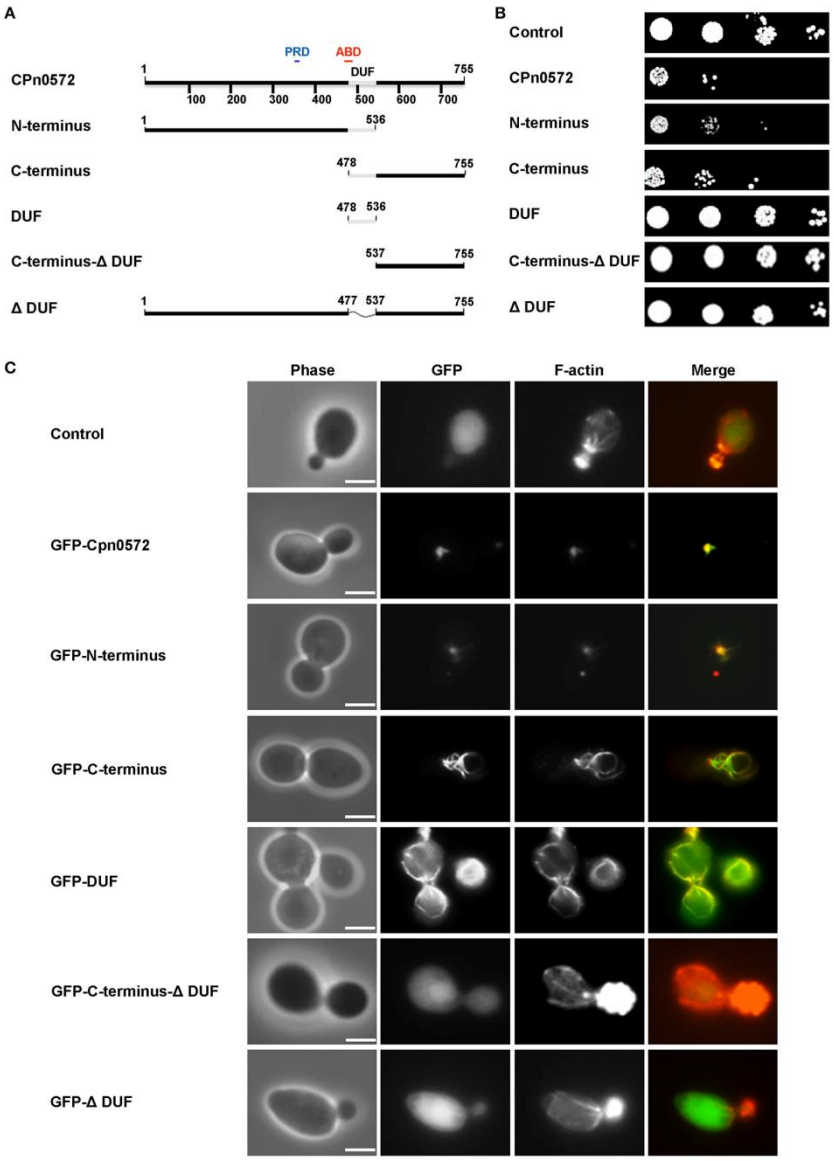

FIGURE 4 | Effects of CPn0572 derivatives on growth rates and F-actin organization in yeast. **(A)** Schematic representation of the CPn0572 variants tested. The functional dissection of CPn0572 was based on the study of the DUF domain in combination with an N- or C-terminal segment of the protein (N-terminus and C-terminus, respectively), the C-terminus lacking DUF (C-terminus-DUF), the DUF domain alone (DUF) or the full-length protein deleted of DUF only (ΔDUF). The positions of these protein variants within the full-length protein are indicated by amino acid numbers. **(B)** Serial-dilution patch tests of yeast cells expressing full-length CPn0572 or the deletion variants indicated in **(A)**. **(C)** Actin organization in yeast cells expressing GFP fused to the full-length CPn0572 or its deletion variants indicated in **(A)**. Bar = 3 μm.

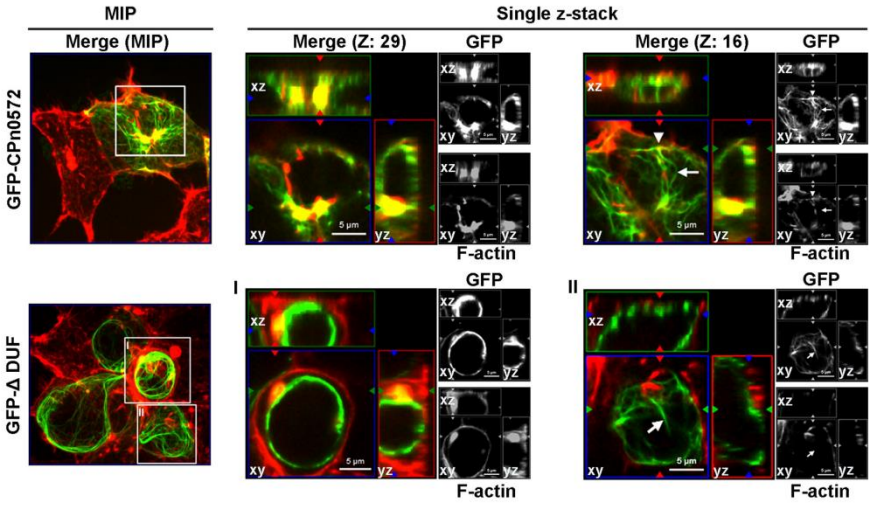

FIGURE 5 | GFP-ΔDUF associates with both actin and non-actin filaments. The actin cytoskeleton (red) in HEK293T cells expressing GFP-CPn0572 (green, upper row) or GFP-ΔDUF (green, bottom row) is shown as MIP images (from stacks of 40 sections) **(left)** and selected single z-stacks **(right)**, as indicated. The enlarged images of single z-sections correspond to the boxes in the MIP images (one box from GFPCPn0572: sections Z: 29 and Z: 16; boxes I and II from GFP-ΔDUF). GFP-CPn0572 cables made up of F-actin are indicated by arrowheads, while GFP-CPn0572- or GFP-DUF-bound cables not containing F-actin fibers are marked by arrows.

were exposed to Latrunculin A (Lat-A), which binds actin monomers, thus preventing their polymerization and effectively promoting depolymerization (Coué et al., 1987; Ayscough et al., 1997; Belmont and Drubin, 1998; Okada et al., 2006). Control cells expressing GFP alone were devoid of actin cables after treatment with Lat-A for 5 min, while some cortical actin patches were still visible after 1 h of exposure to Lat-A (**Figure 6A**). In contrast, the massive actin structures induced by GFP-CPn0572 were still detectable even after exposure to Lat-A for 1 h. Similarly, yeast cells expressing the GFP-C-terminus or GFP-DUF retained actin cables; however, in the presence of Lat-A, the GFP-C-terminus associated with more distinctively defined (compared to the GFP-DUF construct) cables and patches which were also phalloidin-positive (**Figure 6B**). Thus, CPn0572 stabilizes F-actin in yeast by inhibiting depolymerization *in vivo*.

CPn0572 Displaces Cofilin from F-actin Structures

ADF/cofilins are key regulatory proteins that bind to and sever F-actin *in vitro* and *in vivo* (Elam et al., 2013). We therefore tested the hypothesis that CPn0572 might alter F-actin dynamics by interfering with cofilin function. We determined the localization of cofilin in yeast by expressing $CPn0572_{6His}$ in an *aip1*Δ strain, in which both actin patches and cables are enriched for cofilin, and cofilin can be visualized on all actin structures (Okada et al., 2006). In *aip1*Δ cells carrying the empty vector, cofilin was detected in structures interpreted to represent actin cables and patches, as previously documented (**Figure 6C**, upper panel). Remarkably, in $CPn0572_{6His}$-expressing cells, this clear localization of cofilin was completely abolished, and only a diffuse cytosolic staining pattern was detectable (**Figure 6C**, lower panel; $CPn0572_{6His}$-expressing cells marked by arrowheads), while in the same micrograph, yeast cells with little or no $CPn0572_{6His}$ expression retained actin cables and patches (**Figure 6C**, lower panel; cells marked by arrows). Similarly, $CPn0572_{6His}$ also altered cofilin localization in a wild-type yeast strain (Figure S4). These results strongly suggest that CPn0572 inhibits F-actin depolymerization in yeast by displacing cofilin from F-actin.

Next we used *in vitro* assays with recombinant proteins to test whether the displacement of cofilin from filamentous actin by CPn0572 was a direct or indirect effect of the latter. Pre-assembled mammalian F-actin was mixed with recombinant human cofilin in the absence or presence of an equivalent amount of GST-CPn0572, and the mixture was subjected to ultracentrifugation. When F-actin was mixed with cofilin alone, 100% of the cofilin was found in the pellet, as expected given its ability to bind to F-actin (**Figure 7A**). However, when recombinant GST-CPn0572 was present in the mixture, cofilin was now found exclusively in the supernatant, and the fusion protein was found in the pellet with F-actin. Thus, these results show that CPn0572 binds F-actin and competes with cofilin for, and/or displaces it from, F-actin. Further analysis revealed that the GST-C-terminus displaced about 90% of the cofilin into the supernatant. Finally, the GST-DUF domain was able to displace only about 20% of the cofilin into the supernatant and a 2-fold excess of DUF was necessary to bring about 80% of the cofilin

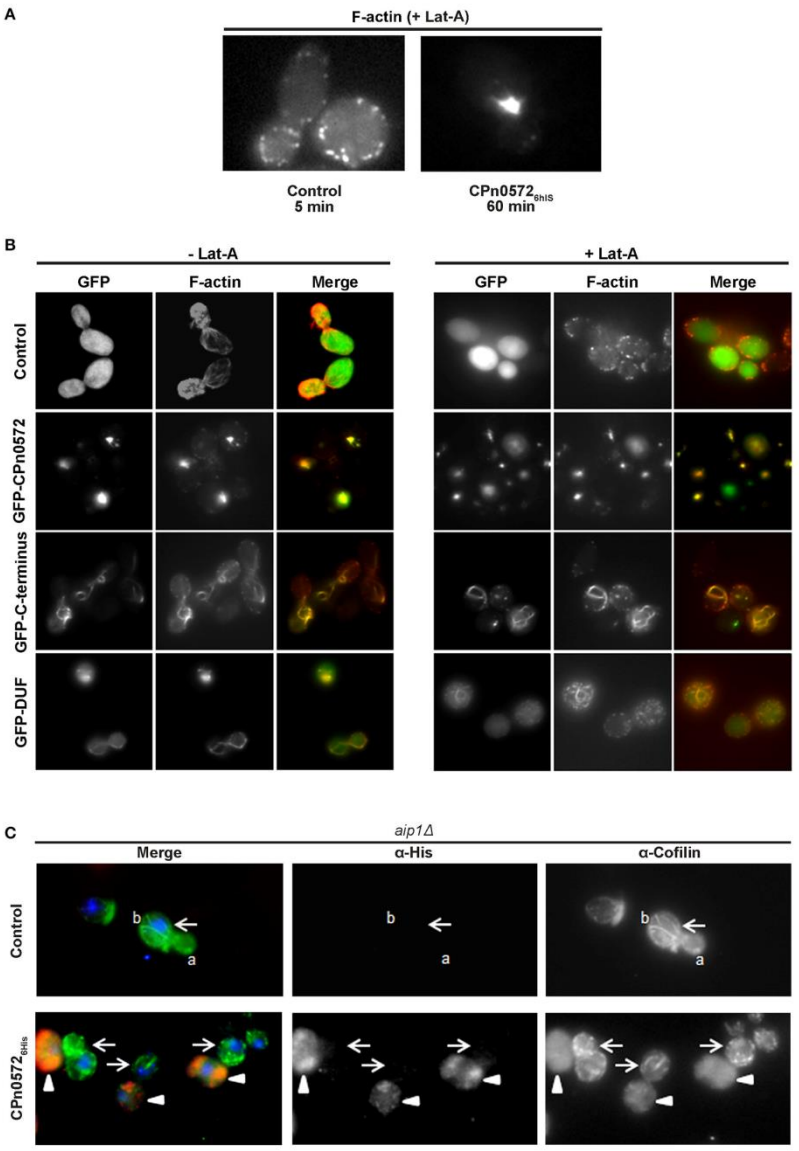

FIGURE 6 | CPn0572 and its C-terminal segment stabilize F-actin and displace cofilin from F-actin in yeast *in vivo*. **(A)** GFP- (control) or GFP-CPn0572-expressing cells were treated with Lat-A (+ Lat-A) for the indicated times, and stained for F-actin. **(B)** Actin cytoskeleton patterns in yeast cells expressing full-length CPn0572 or its deletion variants before and after treatment with Lat-A. Yeast cells expressing GFP (control), GFP-CPn0572, GFP-C-terminus or GFP-DUF were first grown to mid-log phase in inducing medium, exposed to DMSO alone (– Lat-A) or Lat-A (final concentration 2.5 μM) in DMSO (+ Lat-A) for 1 h, then fixed and stained with rhodamine-phalloidin to visualize F-actin, and examined using an Axiovert 200 microscope (Carl Zeiss). **(C)** In *aip1*Δ yeast cells carrying the empty vector (control), cofilin (green) localizes to actin patches and cables (marked by a and b, respectively). In cells expressing $CPn0572_{6H\text{-}His}$ (red), cofilin is diffusely distributed (arrowheads), while non-expressing cells retain distinct cofilin patches and cables (arrows). See also Figure S4.

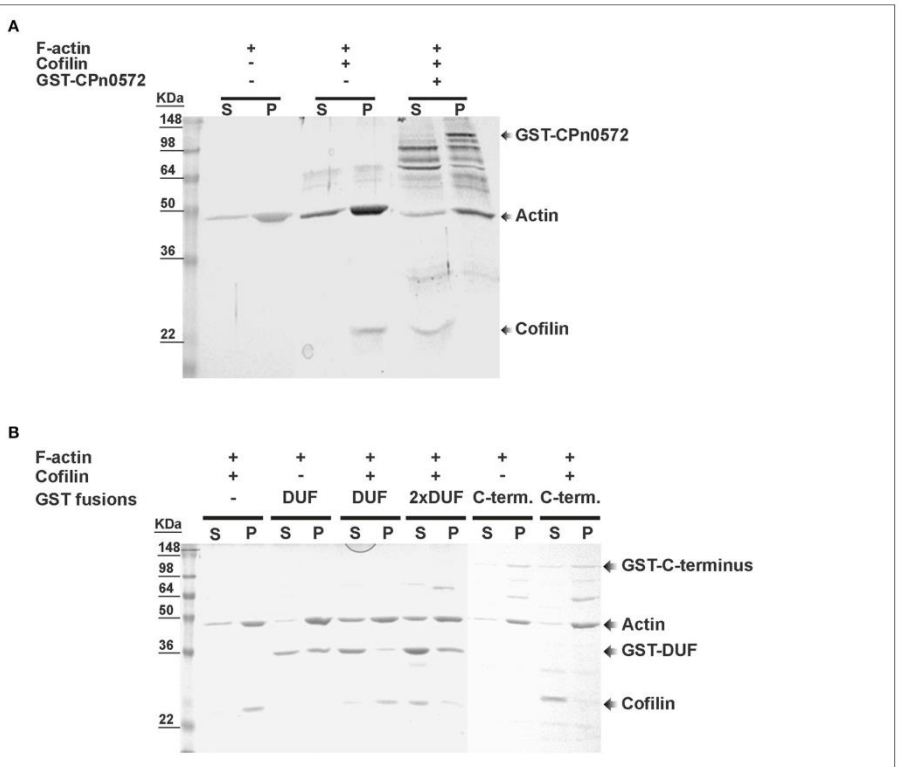

FIGURE 7 | Displacement of mammalian cofilin from preassembled mammalian F-actin by GST–CPn0572 and GST-coupled domains of CPn0572 *in vitro*. **(A)** Binding of GST-CPn0572 and cofilin to pre-assembled F-actin was analyzed using a co-sedimentation assay. Supernatant (s) and pellet (p) fractions were analyzed by SDS-PAGE and stained with Coomassie blue. The presence (+) or absence (–) of each protein in the reaction mix is indicated. The corresponding protein band is marked. **(B)** The experiment was performed as described in **(A)**, using 2 μM GST, GST-DUF (DUF) or GST-C-terminus (C-term.) or 4 μM GST-DUF (2x DUF). Supernatant (s) and pellet (p) fractions were analyzed by SDS-PAGE and stained with Coomassie blue. The presence or absence of each protein is indicated. The corresponding protein band is marked. A full-scale image of the original blot is presented in Figure S5.

into solution *in vitro* (**Figure 7B**). These results are consistent with our finding that DUF displays less colocalization with F-actin, and is a less potent stabilizer of F-actin in the presence of Lat-A. Thus, the ability of CPn0572 to prevent binding of cofilin to F-actin largely resides in its C-terminal segment.

We also probed the ability of CPn0572 to stabilize F-actin in human cells. When we destabilized F-actin by incubating HEK293T cells with cytochalasin D (CD), which inhibits actin filament dynamics in cells via multiple mechanisms, GFP-expressing control cells showed depolymerized F-actin with some dispersed cortical actin remaining intact (**Figure 8**, upper and lower panels). In contrast, CD had little effect on actin structures and fibers in HEK293T cells expressing GFP-CPn0572 in comparison to untreated cells (**Figure 8**, upper and lower panels). Interestingly, the actin aggregates induced by the *C. trachomatis* Tarp were also resistant to CD (**Figure 8**). Most interestingly however, treatment of HEK293T cells expressing a GFP-ΔDUF fusion with CD resulted in the complete loss of F-actin structures. Moreover, no colocalization of the remaining cortical actin with GFP-ΔDUF was observed, supporting our contention that the DUF domain is crucial for stabilization of F-actin by CPn0572 (**Figure 8**). Overall, these data show that CPn0572 and Tarp stabilize F-actin against depolymerizing and severing factors present in human cells.

DISCUSSION

The actin cytoskeleton is regarded as an important target for reorganization during *Chlamydia* uptake. Previous studies indicated that the *C. trachomatis* Tarp protein binds G-actin and nucleates its polymerization *in vitro* (Clifton et al., 2004; Jewett et al., 2006). However, previous work had also suggested that the *C. pneumoniae* Tarp ortholog might be functionally distinct in

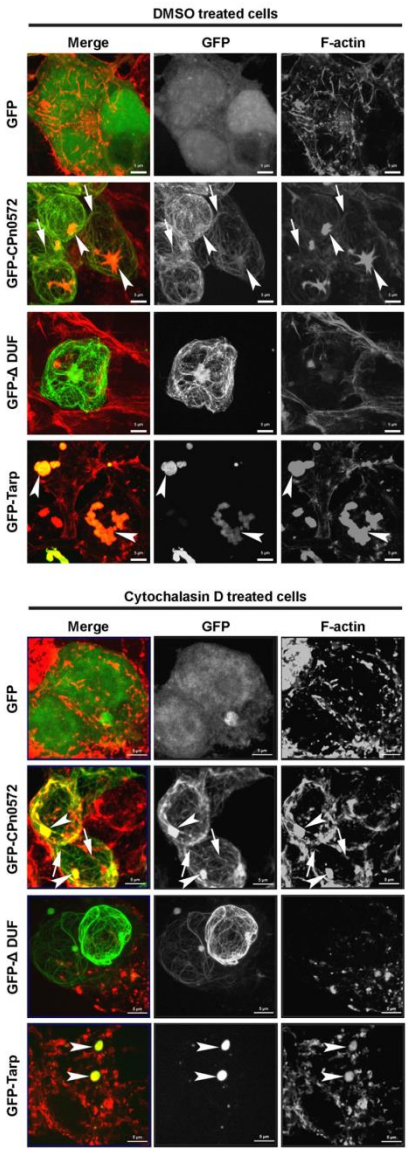

FIGURE 8 | Both CPn0572 and Tarp stabilize the actin cytoskeleton in HEK293T cells. F-actin staining of GFP-, GFP-CPn0572-, GFP-CPn0572-ΔDUF- or GFP-Tarp-expressing HEK293T cells exposed to the solvent DMSO **(upper)** or after treatment with cytochalasin D **(lower)**. The actin cytoskeleton is shown in red and GFP signals in green. GFP-CPn0572 cables associated with F-actin are indicated by arrows, while GFP-CPn0572 and GFP-Tarp associated actin aggregates are marked by arrows. Data are shown as MIP images.

some respects from other Tarp proteins (see Introduction). In this work, we show that the *C. pneumoniae* ortholog of Tarp, CPn0572 (previously classified as "hypothetical"), is expressed in EBs (**Figure 1A**) and secreted into HEp-2 cells early during infection (**Figure 1B**). During infection secretion of CPn0572 is detectable as early as 15 min after EB attachment. Thus, CPn0572 and Tarp are both translocated into the host cell, and are available at the site of bacteria entry. The fact that we could not observe CPn0572 signals at time point zero (**Figure 1B**) is consistent with the results obtained previously for Tarp (Clifton et al., 2004). Very likely, the antibody does not reach the bacterial cytoplasm during immunostaining.

After infection, secretion of CPn0572 continues for at least the first 60 min p.i. and the protein becomes associated with actin patches within 15 min after EB attachment. The *in vitro* data indicate that CPn0572 binds directly to F-actin (**Figure 7A**). This corroborates and extends biochemical data which demonstrated that CPn0572 is capable of binding G-actin and nucleating F-actin formation *in vitro* (Jewett et al., 2010). Thus, CPn0572 and Tarp share the same actin nucleation activity *in vitro* and show the same actin-recruiting activity early in infection *in vivo*; both functions are most probably essential for entry of the respective chlamydial species into their target cells (Clifton et al., 2004; Jewett et al., 2010).

Expression of CPn0572 in yeast has a very detrimental effect on growth, and converts the typical yeast actin cytoskeleton into a large aggregate very like that induced by the Tarp expressed by *C. trachomatis* serovar L2 (Sisko et al., 2006). The growth defect indeed results from the disruption of the actin cytoskeleton, since removal of the actin-binding domain DUF (aa 478 to aa 536) from CPn0572 restores both wild-type actin organization and growth rate. Conversely, CPn0572 binds actin *in vitro* via its DUF domain (**Figure 7B**). Moreover, it may well oligomerize via a proline-rich domain within its N-terminal segment (aa 349 to aa 371) as shown for the prototypic *C. trachomatis* Tarp (Jewett et al., 2006). Indeed, expression of a CPn0572 truncation mutant that lacks only the segment C-terminal to the DUF domain in yeast induces an actin phenotype almost identical to that induced by the full-length protein (**Figure 4B**). In contrast, the CPn0572 C-terminal segment including DUF does not form actin aggregates, but colocalizes with extra-long and thickened actin cables in yeast and also reduces growth rate, suggesting that the C-terminus also harbors actin-modulating capacities. Recently, two F-actin-binding domains (FAB1 and FAB2) have been described in the C-terminus of the *C. trachomatis* Tarp, the latter overlapping with a vinculin-binding site (VBS3) in the *C. caviae* GPIC Tarp (Jiwani et al., 2013; Thwaites et al., 2015). It is worth noting that FAB and VBS-like sequences have been found in Tarp orthologs from various chlamydial species, but not in CPn0572, which once again points to functional differences between Tarp proteins and CPn0572 (Jiwani et al., 2013; Thwaites et al., 2015). Interestingly, when the CPn0572 DUF domain alone (aa 478 to aa 536) is fused to GFP, the fusion protein colocalizes with actin patches and distinctly thickened and extended actin cables, indicating that the 59-aa DUF domain is sufficient for binding and bundling of F-actin. This is compatible with the *in vitro* actin-binding activity previously reported for a longer actin-binding segment (aa 440

to aa 540) of the protein (Jewett et al., 2010). In fact, the action of the CPn0572 DUF domain on F-actin in yeast is reminiscent of the actin phenotype induced by the *Salmonella* F-actin stabilizing protein SipA (Lesser and Miller, 2001).

As in yeast, ectopic expression of either CPn0572 or *C. trachomatis* Tarp in human cells induces an actin aggregation phenotype; however, only the former shows a continuous colocalization with distinct actin fibers (**Figure 2B**). Not only that, Cpn0572 was often seen to form filamentous structures that are apparently devoid of actin (e.g., **Figure 5**). The nature of these CPn0572-positive fibers and their relationship to other cellular structures are unknown at present.

Interestingly, the CPn0572-induced actin structures found upon expression of the protein in yeast and human cells are resistant to the action of the actin-depolymerizing drugs Lat-A and CD (**Figures 6**, **8**), which suggests that CPn0572 might stabilize F-actin against depolymerization. This phenotype is comparable to those described previously for yeast cells exposed to the actin-nucleating and stabilizing toxin jasplakinolide (Jpk), which inhibits actin depolymerization both *in vitro* and *in vivo* (Bubb et al., 1994; Ayscough, 2000; Vallotton et al., 2004; Lázaro-Diéguez et al., 2008). Jpk-induced F-actin fibers are resistant to the actin-depolymerizing drug Lat-A in yeast and to Lat-B in human cells (Ayscough, 2000; Lázaro-Diéguez et al., 2008).

Cofilin plays a central role in promoting actin turnover by severing/depolymerizing F-actin in all eukaryotic cells, and we therefore tested its potential role in CPn0572-induced actin stabilization (Elam et al., 2013). Indeed, upon CPn0572 expression in yeast, cofilin is excluded from the CPn0572-induced actin aggregates *in vivo* (**Figure 6C**). Thus, CPn0572 likely stabilizes F-actin via a mechanism that involves displacement of cofilin from F-actin. That Cpn0572 is indeed capable of displacing cofilin was confirmed biochemically using purified mammalian F-actin, recombinant human cofilin and recombinant CPn0572 *in vitro* (**Figure 7A**). Remarkably, the DUF domain suffices to displace cofilin from pre-assembled F-actin (**Figure 7B**). Interestingly, α-helix 3 of cofilin binds in the hydrophobic cleft located between subdomains 1 and 3 of actin (reviewed in Dominguez, 2004), and the α-helical structure found in DUF is compatible with the hypothesis that CPn0572 and cofilin compete for binding to the same cleft in actin. The ability of CPn0572 and Tarp to render actin aggregates and filaments resistant to CD in transfected HEK293T cells provides evidence that both proteins can stabilize F-actin not only against the action of cofilin but against other, perhaps even all, actin-depolymerizing and severing factors.

F-actin recruitment and stabilization by CPn0572 is very likely integrated with other entry-related processes. Adhesion of *C. pneumoniae* EBs to human cells occurs via the Pmp proteins, which bind and activate the EGF receptor, and signaling by the EGFR via Erk1/2 and the LIM kinase may lead to phosphorylation of cofilin, thereby inhibiting its actin-binding, filament-severing and depolymerizing activities, all of which may contribute to cytoskeletal changes during endocytosis of EBs.

ADF/cofilin is the central F-actin severing factor in human cells, and thus it is not surprising that modulation of its activity is also exploited for host-cell invasion by other intracellular bacteria and by viruses (Zheng et al., 2016). For example, *Listeria* activates the LIM kinase, which disables cofilin via phosphorylation by an unknown factor, thus preventing excessive depolymerization of the F-actin network upon entry of *Listeria* (Bierne et al., 2001). In *Salmonella*, SipA stabilizes F-actin by inhibiting the severing and depolymerizing activities of ADF/cofilin and gelsolin (McGhie et al., 2004), while a second effector, SipC, induces actin polymerization (Hayward and Koronakis, 1999). SipA appears to augment the activity of SipC (McGhie et al., 2004). Thus, F-actin nucleation and F-actin stabilization by displacement of cofilin are induced by two different *Salmonella* effectors, while in *Chlamydiae* the two functions have been co-opted into one protein. Actin assembly requires a flux of G-actin, which is normally provided by active actin depolymerization elsewhere in the cell. Cofilin displacement by CPn0572 should therefore enhance depolymerization of F-actin structures not associated with CPn0572, thus increasing the flux of G-actin required for actin nucleation by CPn0572. F-actin stabilization by cofilin displacement and the nucleation/polymerization activity of CPn0572/Tarp together would therefore be expected to significantly promote formation of highly polymerized and stable F-actin at sites of EB entry. That both functions reside in the CPn0572 protein is unprecedented and may represent an example of the concentration of functional units during genome reduction (Nunes and Gomes, 2014).

In conclusion, our data reveal that the important human pathogen *C. pneumoniae* has evolved an essential effector protein, which (i) re-models the actin cytoskeleton, and (ii) stabilizes F-actin by excluding cofilin. Further studies are required to fully decipher the CPn0572-mediated crosstalk between *C. pneumoniae* and actin dynamics.

AUTHOR CONTRIBUTIONS

RZ and JHH designed the experiments. RZ conducted the experiments and collected the data. CB performed additional transfection experiments of human cells and did Westernblot analyses of human HEK293 cells expressing GFP-CPn0572 fusion proteins. RZ prepared all figures except Figure S3B which was prepared by CB. RZ and JHH analyzed the data and wrote the manuscript.

ACKNOWLEDGMENTS

We thank Dr. Frederik Wuppermann for support in the early phase of the project and Irina Volfson for technical help. We are grateful to Dr. Bruce Goode and Dr. Guangming Zhong for the anti-cofilin and anti-MOMP antibodies respectively, and Dr. Scott Grieshaber for the mCherry-actin-expressing plasmid. This work was supported by the Deutsche Forschungsgemeinschaft, SFB 590, project No. C5 and project # 275334639.

SUPPLEMENTARY MATERIAL

The Supplementary Material for this article can be found online at: https://www.frontiersin.org/articles/10.3389/fcimb.2017.00511/full#supplementary-material

REFERENCES

Ayscough, K. R. (2000). Endocytosis and the development of cell polarity in yeast require a dynamic F-actin cytoskeleton. *Curr. Biol.* 10, 1587–1590. doi: 10.1016/S0960-9822(00)00859-9

Ayscough, K. R., Stryker, J., Pokala, N., Sanders, M., Crews, P., and Drubin, D. G. (1997). High rates of actin filament turnover in budding yeast and roles for actin in establishment and maintenance of cell polarity revealed using the actin inhibitor latrunculin-A. *J. Cell Biol.* 137, 399–416. doi: 10.1083/jcb.137.2.399

Belland, R., Ojcius, D. M., and Byrne, G. I. (2004). Chlamydia. *Nat. Rev. Microbiol.* 2, 530–531. doi: 10.1038/nrmicro931

Belmont, L. D., and Drubin, D. G. (1998). The yeast V159N actin mutant reveals roles for actin dynamics *in vivo*. *J. Cell Biol.* 142, 1289–1299. doi: 10.1083/jcb.142.5.1289

Bierne, H., Gouin, E., Roux, P., Caroni, P., Yin, H. L., and Cossart, P. (2001). A role for cofilin and LIM kinase in Listeria-induced phagocytosis. *J. Cell Biol.* 155, 101–112. doi: 10.1083/jcb.200104037

Brinkworth, A. J., Malcolm, D. S., Pedrosa, A. T., Roguska, K., Shahbazian, S., Graham, J. E., et al. (2011). *Chlamydia trachomatis* Slc1 is a type III secretion chaperone that enhances the translocation of its invasion effector substrate TARP. *Mol. Microbiol.* 82, 131–144. doi: 10.1111/j.1365-2958.2011.07802.x

Bubb, M. R., Senderowicz, A. M., Sausville, E. A., Duncan, K. L., and Korn, E. D. (1994). Jasplakinolide, a cytotoxic natural product, induces actin polymerization and competitively inhibits the binding of phalloidin to F-actin. *J. Biol. Chem.* 269, 14869–14871.

Clifton, D. R., Dooley, C. A., Grieshaber, S. S., Carabeo, R. A., Fields, K. A., and Hackstadt, T. (2005). Tyrosine phosphorylation of the chlamydial effector protein Tarp is species specific and not required for recruitment of actin. *Infect. Immun.* 73, 3860–3868. doi: 10.1128/IAI.73.7.3860-3868.2005

Clifton, D. R., Fields, K. A., Grieshaber, S. S., Dooley, C. A., Fischer, E. R., Mead, D. J., et al. (2004). A chlamydial type III translocated protein is tyrosine-phosphorylated at the site of entry and associated with recruitment of actin. *Proc. Natl. Acad. Sci. U.S.A.* 101, 10166–10171. doi: 10.1073/pnas.0402829101

Coué, M., Brenner, S. L., Spector, I., and Korn, E. D. (1987). Inhibition of actin polymerization by latrunculin A. *FEBS Lett.* 213, 316–318. doi: 10.1016/0014-5793(87)81513-2

Dominguez, R. (2004). Actin-binding proteins–a unifying hypothesis. *Trends Biochem. Sci.* 29, 572–578. doi: 10.1016/j.tibs.2004.09.004

Elam, W. A., Kang, H., and De la Cruz, E. M. (2013). Biophysics of actin filament severing by cofilin. *FEBS Lett.* 587, 1215–1219. doi: 10.1016/j.febslet.2013.01.062

Fechtner, T., Galle, J. N., and Hegemann, J. H. (2016). The novel chlamydial adhesin CPn0473 mediates the lipid raft-dependent uptake of *Chlamydia pneumoniae*. *Cell. Microbiol.* 18, 1094–1105. doi: 10.1111/cmi.12569

Hayward, R. D., and Koronakis, V. (1999). Direct nucleation and bundling of actin by the SipC protein of invasive Salmonella. *EMBO J.* 18, 4926–4934. doi: 10.1093/emboj/18.18.4926

Hegemann, J. H., and Moelleken, K. (2012). "Chlamydial adhesion and adhesins," in *Intracellular Pathogens I: Chlamydiales,* eds M. Tan, and P. Bavoil (Washington, DC: ASM Press).

Hower, S., Wolf, K., and Fields, K. A. (2009). Evidence that CT694 is a novel *Chlamydia trachomatis* T3S substrate capable of functioning during invasion or early cycle development. *Mol. Microbiol.* 72, 1423–1437. doi: 10.1111/j.1365-2958.2009.06732.x

Jantos, C. A., Heck, S., Roggendorf, R., Sen-Gupta, M., and Hegemann, J. H. (1997). Antigenic and molecular analyses of different *Chlamydia pneumoniae* strains. *J. Clin. Microbiol.* 35, 620–623.

Jewett, T. J., Dooley, C. A., Mead, D. J., and Hackstadt, T. (2008). *Chlamydia trachomatis* tarp is phosphorylated by src family tyrosine kinases. *Biochem. Biophys. Res. Commun.* 371, 339–344. doi: 10.1016/j.bbrc.2008.04.089

Jewett, T. J., Fischer, E. R., Mead, D. J., and Hackstadt, T. (2006). Chlamydial TARP is a bacterial nucleator of actin. *Proc. Natl. Acad. Sci. U.S.A.* 103, 15599–15604. doi: 10.1073/pnas.0603044103

Jewett, T. J., Miller, N. J., Dooley, C. A., and Hackstadt, T. (2010). The conserved Tarp actin binding domain is important for chlamydial invasion. *PLoS Pathog.* 6:e1000997. doi: 10.1371/journal.ppat.1000997

Jiwani, S., Alvarado, S., Ohr, R. J., Romero, A., Nguyen, B., and Jewett, T. J. (2013). *Chlamydia trachomatis* Tarp harbors distinct G and F actin binding domains that bundle actin filaments. *J. Bacteriol.* 195, 708–716. doi: 10.1128/JB.01768-12

Lane, B. J., Mutchler, C., Al Khodor, S., Grieshaber, S. S., and Carabeo, R. A. (2008). Chlamydial entry involves TARP binding of guanine nucleotide exchange factors. *PLoS Pathog.* 4:e1000014. doi: 10.1371/journal.ppat.1000014

Lázaro-Diéguez, F., Aguado, C., Mato, E., Sánchez-Ruíz, Y., Esteban, I., Alberch, J., et al. (2008). Dynamics of an F-actin aggresome generated by the actin-stabilizing toxin jasplakinolide. *J. Cell Sci.* 121, 1415–1425. doi: 10.1242/jcs.017665

Lesser, C. F., and Miller, S. I. (2001). Expression of microbial virulence proteins in *Saccharomyces cerevisiae* models mammalian infection. *EMBO J.* 20, 1840–1849. doi: 10.1093/emboj/20.8.1840

McGhie, E. J., Hayward, R. D., and Koronakis, V. (2004). Control of actin turnover by a salmonella invasion protein. *Mol. Cell* 13, 497–510. doi: 10.1016/S1097-2765(04)00053-X

Mehlitz, A., Banhart, S., Hess, S., Selbach, M., and Meyer, T. F. (2008). Complex kinase requirements for *Chlamydia trachomatis* Tarp phosphorylation. *FEMS Microbiol. Lett.* 289, 233–240. doi: 10.1111/j.1574-6968.2008.01390.x

Mölleken, K., Becker, E., and Hegemann, J. H. (2013). The *Chlamydia pneumoniae* invasin protein Pmp21 recruits the EGF receptor for host cell entry. *PLoS Pathog.* 9:e1003325. doi: 10.1371/journal.ppat.1003325

Mumberg, D., Müller, R., and Funk, M. (1994). Regulatable promoters of *Saccharomyces cerevisiae*: comparison of transcriptional activity and their use for heterologous expression. *Nucleic Acids Res.* 22, 5767–5768. doi: 10.1093/nar/22.25.5767

Nunes, A., and Gomes, J. P. (2014). Evolution, phylogeny, and molecular epidemiology of Chlamydia. *Infect. Genet. Evol.* 23, 49–64. doi: 10.1016/j.meegid.2014.01.029

Okada, K., Ravi, H., Smith, E. M., and Goode, B. L. (2006). Aip1 and cofilin promote rapid turnover of yeast actin patches and cables: a coordinated mechanism for severing and capping filaments. *Mol. Biol. Cell* 17, 2855–2868. doi: 10.1091/mbc.E06-02-0135

Parrett, C. J., Lenoci, R. V., Nguyen, B., Russell, L., and Jewett, T. J. (2016). Targeted disruption of *Chlamydia trachomatis* invasion by in trans expression of dominant negative tarp effectors. *Front. Cell. Infect. Microbiol.* 6:84. doi: 10.3389/fcimb.2016.00084

Pizarro-Cerdá, J., and Cossart, P. (2006). Bacterial adhesion and entry into host cells. *Cell* 124, 715–727. doi: 10.1016/j.cell.2006.02.012

Pringle, J. R., Adams, A. E., Drubin, D. G., and Haarer, B. K. (1991). Immunofluorescence methods for yeast. *Meth. Enzymol.* 194, 565–602. doi: 10.1016/0076-6879(91)94043-C

Schachter, J. (1999). "Infection and Disease Epidemiology," in *Chlamydia: Intracellular Biology, Pathogenesis, and Immunity,* ed R. S. Stephens (Washington, DC: ASM Press), 139–169.

Schramm, N., Bagnell, C. R., and Wyrick, P. B. (1996). Vesicles containing *Chlamydia trachomatis* serovar L2 remain above pH 6 within HEC-1B cells. *Infect. Immun.* 64, 1208–1214.

Sherman, F. (1991). Getting started with yeast. *Meth. Enzymol.* 194, 3–21. doi: 10.1016/0076-6879(91)94004-V

Siggers, K. A., and Lesser, C. F. (2008). The yeast *Saccharomyces cerevisiae*: a versatile model system for the identification and characterization of bacterial virulence proteins. *Cell Host Microbe* 4, 8–15. doi: 10.1016/j.chom.2008.06.004

Sisko, J. L., Spaeth, K., Kumar, Y., and Valdivia, R. H. (2006). Multifunctional analysis of Chlamydia-specific genes in a yeast expression system. *Mol. Microbiol.* 60, 51–66. doi: 10.1111/j.1365-2958.2006.05074.x

Thwaites, T., Nogueira, A. T., Campeotto, I., Silva, A. P., Grieshaber, S. S., and Carabeo, R. A. (2014). The Chlamydia effector TarP mimics the mammalian leucine-aspartic acid motif of paxillin to subvert the focal adhesion kinase during invasion. *J. Biol. Chem.* 289, 30426–30442. doi: 10.1074/jbc.M114.604876

Thwaites, T. R., Pedrosa, A. T., Peacock, T. P., and Carabeo, R. A. (2015). Vinculin interacts with the Chlamydia effector TarP via a tripartite vinculin binding domain to mediate actin recruitment and assembly at the plasma membrane. *Front. Cell. Infect. Microbiol.* 5:88. doi: 10.3389/fcimb.2015.00088

Valdivia, R. H. (2004). Modeling the function of bacterial virulence factors in *Saccharomyces cerevisiae*. *Eukaryotic Cell* 3, 827–834. doi: 10.1128/EC.3.4.827-834.2004

Vallotton, P., Gupton, S. L., Waterman-Storer, C. M., and Danuser, G. (2004). Simultaneous mapping of filamentous actin flow and turnover in migrating cells by quantitative fluorescent speckle microscopy. *Proc. Natl. Acad. Sci. U.S.A.* 101, 9660–9665. doi: 10.1073/pnas.0300552101

Wuppermann, F. N., Mölleken, K., Julien, M., Jantos, C. A., and Hegemann, J. H. (2008). Chlamydia pneumoniae GroEL1 protein is cell surface associated and required for infection of HEp-2 cells. *J. Bacteriol.* 190, 3757–3767. doi: 10.1128/JB.01638-07

Zheng, K., Kitazato, K., Wang, Y., and He, Z. (2016). Pathogenic microbes manipulate cofilin activity to subvert actin cytoskeleton. *Crit. Rev. Microbiol.* 42, 677–695. doi: 10.3109/1040841X.2015.1010139

Zrieq, R., Sana, T. G., Vergin, S., Garvis, S., Volfson, I., Bleves, S., et al. (2015). Genome-wide screen of *Pseudomonas aeruginosa* in *Saccharomyces cerevisiae* identifies new virulence factors. *Front. Cell. Infect. Microbiol.* 5:81. doi: 10.3389/fcimb.2015.00081

Conflict of Interest Statement: The authors declare that the research was conducted in the absence of any commercial or financial relationships that could be construed as a potential conflict of interest.

2.2.2 Manuscript II

CPn0572, the *C. pneumoniae* ortholog of TarP, reorganizes the actin cytoskeleton via a newly identified F-actin binding domain and recruitment of vinculin

Corinna Braun, Abel R. Alcázar-Román, Alexandra Laska, Katja Mölleken, Ursula Fleig and Johannes H. Hegemann

First author

Contribution: 55 %

Corinna Braun planned, performed, evaluated and quantified big parts of the experiments of this manuscript. Additionally, did she perform the following experiments and generated the corresponding figures (Fig1; Fig3; Fig4; Fig5 (50 %); Fig6; Fig7; Fig8; FigS2; FigS3; FigS4), wrote figure legends and parts of the material methods section. Furthermore, was she involved in correcting the manuscript and the submission/review process.

Published in: PLOS ONE, January 2019, doi: 10.1371/journal.pone.0210403. eCollection 2019.

Impact factor: 2.7 (2018)

PLOS ONE

RESEARCH ARTICLE

CPn0572, the *C. pneumoniae* ortholog of TarP, reorganizes the actin cytoskeleton via a newly identified F-actin binding domain and recruitment of vinculin

Corinna Braun[1], Abel R. Alcázar-Román[2], Alexandra Laska[1], Katja Mölleken[1], Ursula Fleig[2‡], Johannes H. Hegemann[1‡*]

1 Institute of Functional Microbial Genomics, Heinrich-Heine-University, Düsseldorf, Germany, **2** Eukaryotic microbiology, Institute of Functional Microbial Genomics, Heinrich-Heine-University, Düsseldorf, Germany

‡ These authors are joint senior authors on this work.
* johannes.hegemann@hhu.de

Citation: Braun C, Alcázar-Román AR, Laska A, Mölleken K, Fleig U, Hegemann JH (2019) CPn0572, the *C. pneumoniae* ortholog of TarP, reorganizes the actin cytoskeleton via a newly identified F-actin binding domain and recruitment of vinculin. PLoS ONE 14(1): e0210403. https://doi.org/10.1371/journal.pone.0210403

Editor: David M. Ojcius, University of the Pacific, UNITED STATES

Received: October 10, 2018

Accepted: December 21, 2018

Published: January 10, 2019

Data Availability Statement: All relevant data are within the manuscript and its Supporting Information files.

Funding: This study was supported by the Deutsche Forschungsgemeinschaft research grants FL 168/5-1 (UF) and HE 1383/13-1 (JHH) http://www.dfg.de. The funders had no role in study design, data collection and analysis, decision to publish, or preparation of the manuscript.

Abstract

Chlamydia pneumoniae is one of the two major species of the *Chlamydiaceae* family that have a profound effect on human health. *C. pneumoniae* is linked to a number of severe acute and chronic diseases of the upper and lower respiratory tract including pneumonia, asthma, bronchitis and infection by the pathogen might play a role in lung cancer. Following adhesion, *Chlamydiae* secrete effector proteins into the host cytoplasm that modulate the actin cytoskeleton facilitating internalization and infection. Members of the conserved TarP protein family comprise such effector proteins that polymerize actin, and in the case of the *C. trachomatis* TarP protein, has been shown to play a critical role in pathogenesis. In a previous study, we demonstrated that, upon bacterial invasion, the *C. pneumoniae* TarP family member CPn0572 is secreted into the host cytoplasm and recruits and associates with actin via an actin-binding domain conserved in TarP proteins. We have now extended our analysis of CPn0572 and found that the CPn0572 actin binding and modulating capability is more complex. With the help of the fission yeast system, a second actin modulating domain was identified independent of the actin binding domain. Microscopic analysis of HEp-2 cells expressing different CPn0572 deletion variants mapped this domain to the C-terminal part of the protein as CPn0572$^{536\text{-}755}$ binds F-actin *in vitro* and colocalizes with aberrantly thickened actin cables *in vivo*. Finally, microscopic and bioinformatic analysis revealed the existence of a vinculin binding sequence in CPn0572. Our findings contribute to the understanding of the function of the TarP family and underscore the existence of several actin binding domains and a vinculin binding site for host actin modulation.

Introduction

Chlamydia pneumoniae, an obligate intracellular Gram-negative bacterium, is the most prevalent intracellular bacterial pathogen worldwide [1]. It is commonly implicated in respiratory tract infections as well as atherosclerosis, cardiovascular illnesses, and diseases of the central nervous system

Competing interests: The authors have declared that no competing interests exist.

[2–6]. Like other *Chlamydiae*, *C. pneumoniae* displays a biphasic developmental cycle consisting of two metabolically and morphologically distinct developmental forms [7]. The extracellular form, referred to as an elementary body (EB), is metabolically dormant, infectious and fully capable of cellular invasion [8]. Within the confinements of a host-derived parasitophorous vacuole called an inclusion [9], EBs differentiate into reticulate bodies (RBs), which are metabolically active and non-infectious. RBs undergo several rounds of replication in a growing inclusion and eventually differentiate to infectious EBs prior to release from the host cell to initiate new rounds of infections [9]. Entry to the protective membrane-bound intracellular niche is essential to survival of *Chlamydiae* and thus represents an attractive target for disease treatment and prevention. The precise mechanism underlying chlamydial host cell invasion is still ill defined; however, it requires remodeling of the actin cytoskeleton at sites of attachment [10, 11]. The reorganization of the host actin cytoskeleton is mediated by the secretion of an actin modulating effector protein named chlamydial translocated actin recruiting phosphoprotein (TarP) through a type III secretion system [12].

Members of the TarP protein family have been identified in all sequenced *Chlamydia* species. These proteins display a number of conserved domains; however, the amino acid sequence identity is highly variable between 40 and 94% when comparing *C. trachomatis* L2 TarP to other TarP orthologs [11, 13, 14]. All TarP orthologs studied contain a proline-rich domain that mediates TarP oligomerization, a property required for the actin nucleation activity of *C. trachomatis* TarP and likely crucial for chlamydial infection [15, 16]. Furthermore all TarP family members harbor at least one and some up to three actin binding domains (ABDs) able to nucleate actin [14]. When the function of the single *C. trachomatis* L2 TarP ABD is obstructed during bacterial entry either through the expression of a dominant negative form of TarP that inhibits the actin nucleation ability of the wild-type TarP protein or by microinjection of anti-ABD-antibodies into the host cell, chlamydial entry is strongly inhibited [14, 17]. Thus, TarP family members play a pivotal role in actin-remodeling during chlamydial pathogenesis. Although TarP family members have a number of common characteristics required for actin modulation, an N-terminal tyrosine rich domain is only present in *C. trachomatis* TarP. This tyrosine rich domain becomes phosphorylated upon translocation to the host cell cytosol [12], which results in the binding of Rac GEFs, activation of Rac GTPases and ultimately Arp2/3-mediated actin remodeling [11, 18, 19]. Furthermore, focal adhesion kinase (FAK) binding motifs, vinculin binding sequences (VBSs) and ABD-independent F-actin binding domains (FABs) have to date only been identified in *C. trachomatis*, *C. muridarum* and *C. caviae* [13, 20–22].

The *C. pneumoniae* TarP ortholog CPn0572 is secreted into the host cytoplasm and associates with actin upon bacterial invasion through its single ABD region [23]. CPn0572 does not harbor the consensus TarP family FAK binding motif [20] and neither FABs nor VBSs had been identified bioinformatically [13, 21]. Thus, the possibility remained that CPn0572 actin modulating ability was solely dependent on its ABD domain. However, in this study, we show that CPn0572 harbors a second actin binding domain apart from the ABD as well as a VBS. Both domains have a profound effect on the host actin cytoskeleton. Intriguingly, the N-terminal part of CPn0572 appears to contain a domain that inhibits the ability of the ABD to colocalize with actin. Thus, the actin modulating activity of CPn0572 is driven by several domains that might affect the host actin cytoskeleton at different stages of the infection process.

Results

C. pneumoniae CPn0572 disrupts cytoskeleton function independently from its ABD-C domain

We have previously found that the strong actin modulatory potential of the *C. pneumoniae* CPn0572 protein requires the ABD-containing domain contained within amino acids 478–

536 (hereinafter referred to as ABD-C for the purposes of this this manuscript) [23]. However, we now present further analysis of CPn0572 variants expressed in the model yeast *Schizosaccharomyces pombe* that pointed to the existence of additional actin modulating domains. *S. pombe* represents an excellent model system for the study of actin function, as cell shape, cell growth and cell division require an intact actin cytoskeleton [24–26].

We generated plasmid-bearing *S. pombe* strains expressing two CPn0572 variants (Fig 1A) under the control of the *S. pombe nmt1*$^+$ promoter, which is repressed in the presence of thiamine, resulting in low expression, and de-repressed in the absence of thiamine, resulting in high expression (Fig 1B and S1D Fig) [27, 28]. Throughout the text we refer to repressed as "low expression," and de-repressed as "high expression". Low expression of all CPn0572 variants had no effect on the growth of cells as shown via a serial dilution patch test analysis (Fig 1C). However, high expression of untagged and mCherry-tagged versions of full length CPn0572 had a drastic effect on *S. pombe* cell viability (Fig 1C, left panels), consistent with our previous results in the budding yeast *S. cerevisiae* [23]. The growth defect was dependent on the presence of the ABD-C domain as yeast cells expressing CPn0572ΔABD-C deletion constructs grew at a comparable rate to transformants harboring a control vector (Fig 1C, left panels).

Chemogenetic profiling has been used extensively in yeasts to determine genetic interactions between genes. Genes are defined as interacting genetically if the double mutant has a massively reduced fitness compared to the single mutant strains [29]. Similarly, genetic interaction is also scored if the presence of a specific chemical leads to reduced fitness of the mutant but not the wild-type strain. Thus, we next tested the viability of the transformants in the presence of the actin-depolymerizing drug Latrunculin B (LatB) at 1 μM and 2 μM, concentrations at which the actin cytoskeleton is slightly compromised but wild-type cells are able to grow normally [30, 31]. Again, high-level expression of full-length versions of CPn0572 remained a

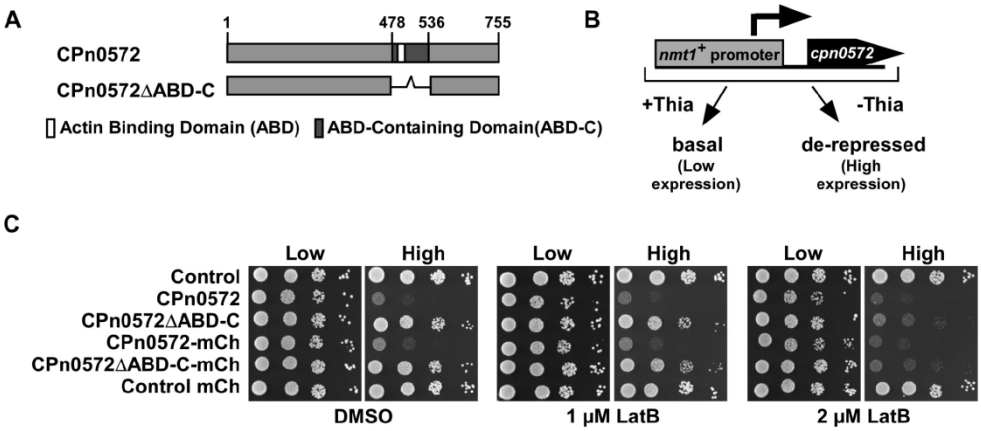

Fig 1. CPn0572 influences actin function in *S. pombe* independently of the ABD-C. (A) Diagrammatic representation of CPn0572 and CPn0572ΔABD-C with the location of the ABD-C (black) and ABD (white) domain. Numbers indicate amino acid positions. **(B)** Schematic representation of CPn0572 expression under control of the *nmt1*$^+$ promoter. This promoter is repressed in the presence of thiamine (Low expression) where it shows basal expression and is de-repressed in the absence of thiamine (High expression). **(C)** Serial dilution patch test (10^4–10^1 cells) of a wild-type yeast strain transformed with the indicated plasmids and grown for 5 days at 30˚C on plasmid selective minimal medium leading to either low expression (Low) or high expression (High) of constructs in the presence of Latrunculin B (LatB) or DMSO solvent control. Reproduced in n = 5 transformants tested per condition.

https://doi.org/10.1371/journal.pone.0210403.g001

burden to cell growth in comparison to vector only controls (Fig 1C, middle panels). Low-level expression of full-length CPn0572 constructs resulted in a slight growth defect at 2 μM LatB (Fig 1C, right panels "Low"). Interestingly, high-level expression of CPn0572ΔABD-C variants resulted in a severe growth defect in the presence of LatB (Fig 1C, right panels "High"). This finding shows that high expression of CPn0572ΔABD-C has a profound negative effect on growth of the yeast colonies in the presence of LatB. We conclude that CPn0572 ABD-C compromises actin function in fission yeast independently of the ABD-C domain revealing the existence of a further actin regulatory domain or binding site.

We next analyzed the fission yeast actin cytoskeleton in the presence of CPn0572 variants. CPn0572-mCherry or CPn0572ΔABD-C-mCherry expressing plasmids were transformed into a yeast strain containing a chromosomal copy of a gene encoding the actin probe lifeact fused to GFP, which decorates F-actin in living cells [32, 33]. This probe allowed us to visualize the three yeast actin structures: actin patches, actin cables, and the contractile ring. Cellular actin localization is cell cycle dependent (Fig 2A): in interphase, actin patches/cables are associated with one or both cell ends of the cylindrical fission yeast cell, representing monopolar or bipolar growth, respectively. After mitosis, cytokinesis requires the actin contractile ring in the cell middle for septum formation. It is also at these sites of actin-dependent cell growth that cell wall deposition takes place [34]. At low expression levels of CPn0572-mCherry 4.6% of cells showed abnormal actin localization phenotypes. The majority of these cells presented one or two slightly enlarged abnormal actin structures that differed in size to the normal actin patches that coexisted within these cells (Fig 2B, left panels 2 and 3). Interestingly, these aberrant actin structures colocalized with CPn0572-mCherry suggesting that CPn0572 presence was the cause of the abnormal actin cytoskeleton. Among cells expressing low levels of mCherry or CPn0572ΔABD-C-mCherry, less than 0.5% showed scorable defects in the yeast actin cytoskeleton (Fig 2B, left top and bottom panels, respectively).

High-level expression of CPn0572-mCherry resulted in an increased number of aberrant actin structures. Most prominently were very large actin structures that colocalized with the mCherry fluorescence signal (Fig 2B, right panels 2 and 3). 30% of cells showed an array of abnormal actin localization phenotypes including abnormal size of actin patches, diffused cytoplasmic actin or increased accumulation of actin at the contractile ring (Fig 2B, right panels 2 and 3; quantified in Fig 2D, sketched in Fig 2C). Interestingly, CPn0572-mCherry was only able to completely colocalize with actin when cells displayed very large aberrant structures (Fig 2B, right panel 3), and did not colocalize to all actin patches or septa when the cell cytoskeleton retained its classical structures (Fig 2B, right panel 3, Cell 5). Additionally, 11% of cells visualized exhibited abnormal cell morphology such as spherical, multiseptated, or deformed cells (Fig 2D, S1A Fig; sketched in Fig 2C), which are cell phenotypes associated with defects in actin cytoskeleton organization [26].

High-level expression of CPn0572ΔABD-C-mCherry resulted in a diffuse cytoplasmic distribution (Fig 2B, right bottom panels). Interestingly, even though these cells presented apparently normal actin localization without the large abnormal actin structures observed in CPn0572-mCherry expressing cells, 11.4% displayed abnormal cell morphology, including loss of polarized growth and irregular septa, consistent with the presence of a defective actin cytoskeleton (Fig 2B, right bottom panels; quantified in Fig 2D, sketched in Fig 2C). Importantly, the stronger phenotypes observed in cells expressing full length CPn0572 compared to cells expressing CPn0572ΔABD-C are not due to higher expression levels of the full length construct, as protein levels of CPn0572ΔABD-C were found to be higher (S1D Fig).

The actin cytoskeleton plays an essential part in the deposition of cell wall material [34]. To examine if CPn0572 expression has an impact in cell wall integrity, we examined the areas in which new cell wall deposition occurs by staining cells with the fluorescent dye Calcofluor

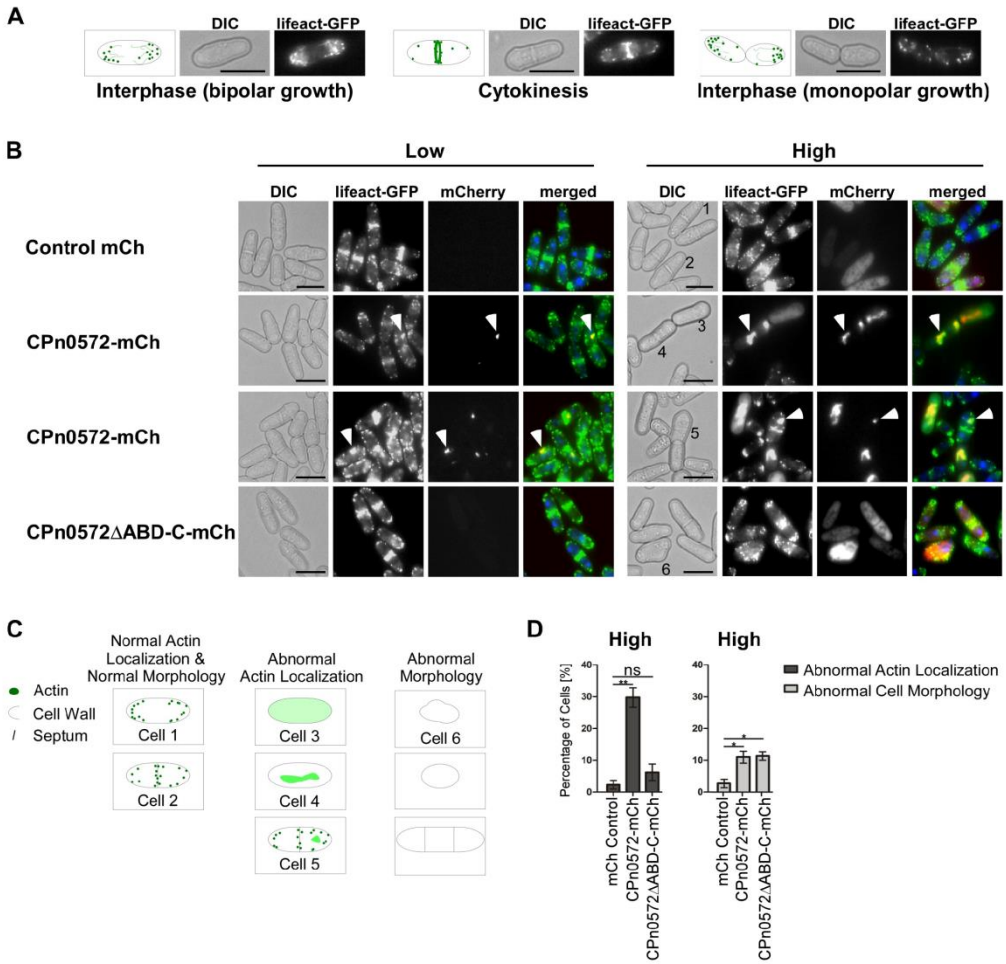

Fig 2. CPn0572 expression influences actin localization and morphology in *S. pombe*. **(A)** Actin localization during the cell cycle. Schematic representation of the Differential Interference Contrast microscopy (DIC) and lifeact-GFP images showing actin patches (green dots) and cables (green lines) localized to one or both cell ends (bipolar and monopolar growth respectively). During cytokinesis actin re-localizes to the cell middle. Bar, 5 μm **(B)** Live cell images of representative lifeact-GFP-expressing cells (F-actin is green in merged images) expressing the indicated mCherry protein variants (red in merged images). Cells were stained with Hoechst to visualize DNA (blue in merged images). Transformants were grown for 22 h under plasmid selective conditions leading to either low expression (Low) or high expression (High). White arrow heads point to selected aberrant actin structures within cells. Bars, 5 μm. **(C)** Diagrammatic representation of cells phenotypes used for quantification in D with examples labeled 1–6 shown in 2B (right panels). Normal actin localization and cell shape: Cell 1 (bipolar polarized actin localization) and Cell 2 (cytokinetic localization). Abnormal actin localization: Cell 3 (diffused actin), Cell 4 (aberrant actin structures without regular actin patches) and Cell 5 (aberrant actin structures with regular actin patches). Representative cell displaying aberrant cell morphology as depicted in schematic representation: Cell 6 (swollen cell morphology). **(D)** Quantification of cells grown under high expression of CPn0572 variants that present abnormal actin localization and abnormal cell morphology similar to the examples shown in B and S1 Fig A. n = 3 samples each representing 40–80 cells. Error bars denote standard error of the mean. Student's t-test was used to determine statistical significance. $p < 0.005$ (**), $p < 0.05$ (*), and not significant (ns).

https://doi.org/10.1371/journal.pone.0210403.g002

white. Control cells exhibited the typical staining at the cell periphery, with slight increase at the tip of cells undergoing bipolar growth and strong staining at the septa, where new cell wall is deposited during cytokinesis (S1B Fig, top panels). Interestingly, in cells expressing CPn0572-mCherry, a dramatic buildup of cell wall material was detected at the cell middle in 24.6% of cells (S1B Fig, bottom panels; quantified in S1C Fig), consistent with an altered actin cytoskeleton.

Together our analysis of CPn0572 function in *S. pombe* demonstrated that the yeast actin cytoskeleton was modulated by the chlamydial protein leading to increased sensitivity to LatB and massive defects in cell morphogenesis and septum formation. Similar results, albeit with a less severe phenotype in actin morphology, resulted from CPn0572ΔABD-C expression in yeast. Thus, actin modulation is not solely dependent on the ABD-C domain of CPn0572. We therefore generated a large number of different CPn0572 variants to identify new actin binding domains.

The C-terminus of CPn0572 mediates localization to the human actin cytoskeleton independently from the ABD-C

We have previously described a drastic reorganization of the actin cytoskeleton in mammalian cells expressing CPn0572 [23]. This strong change in the actin cytoskeleton was observed 24 h post transfection, a time at which standard plasmid expression is high [35]. To visualize early events in the actin cytoskeleton modifications due to CPn0572 expression and thus to identify more subtle actin-related phenotypes, a time-course experiment was carried out in HEp-2 cells transfected with GFP-CPn0572. The GFP signal from control cells was distributed evenly throughout the cell and did not colocalize with phalloidin-stained actin (Fig 3A, top panels). In contrast, GFP-CPn0572 was localized to < 200 nm-thick cable-like actin structures (referred to as "cables" in this study) in all cells observed as early as 12 h post transfection (Fig 3A, panel 2). At this early time point, no abnormal actin structure could be identified. However, 14 h post transfection, and progressively thereafter, 5% of cells expressing GFP-CPn0572 displayed GFP signal in actin positive patches and > 200 nm-thick cable structures (referred to as "thick cables" in this study) (Fig 3A, panel 3; quantified in Fig 3C), structures not found in control cells. At 24 h post transfection, nearly half of the cells displayed this phenotype (Fig 3A, panel 4; quantified in Fig 3C). Thus, CPn0572 binding to actin stimulates the generation of thick actin cables and eventually patches, potentially through direct binding and bundling of actin cables [14] in a time-dependent manner.

In order to test if the formation of these structures was dependent on the ABD-C domain only, we repeated the time-course experiment with the GFP-CPn0572ΔABD-C construct. Compared to full-length CPn0572, which colocalized with actin cables in 100% of cells observed 12 h post transfection, 83% of GFP-CPn0572ΔABD-C transfected cells displayed actin cable colocalization at this time point (Fig 3B, top panels; quantified in Fig 3C). At later time points, GFP-CPn0572ΔABD-C localized exclusively to a variety of abnormal actin structures including patches and thick cables (Fig 3B; panels 2 and 3; quantified in Fig 3C). These results show an ABD-C-independent abnormal actin phenotype triggered by CPn0572ΔABD-C expression, consistent with the phenotype observed in CPn0572ΔABD-C expressing yeast cells. Thus, we conclude that a further actin modulating domain exist in CPn0572 apart from the ABD-C domain.

To identify the region of CPn0572 harboring such domain, we generated a battery of plasmids encoding recombinant GFP-fusions of CPn0572 truncations missing either the N-terminus (encoded by amino acids 1–478), the ABD-C domain (encoded by amino acids 478–535), the C-terminus (encoded by amino acids 536–755), or a combination thereof (Fig 4A and S3

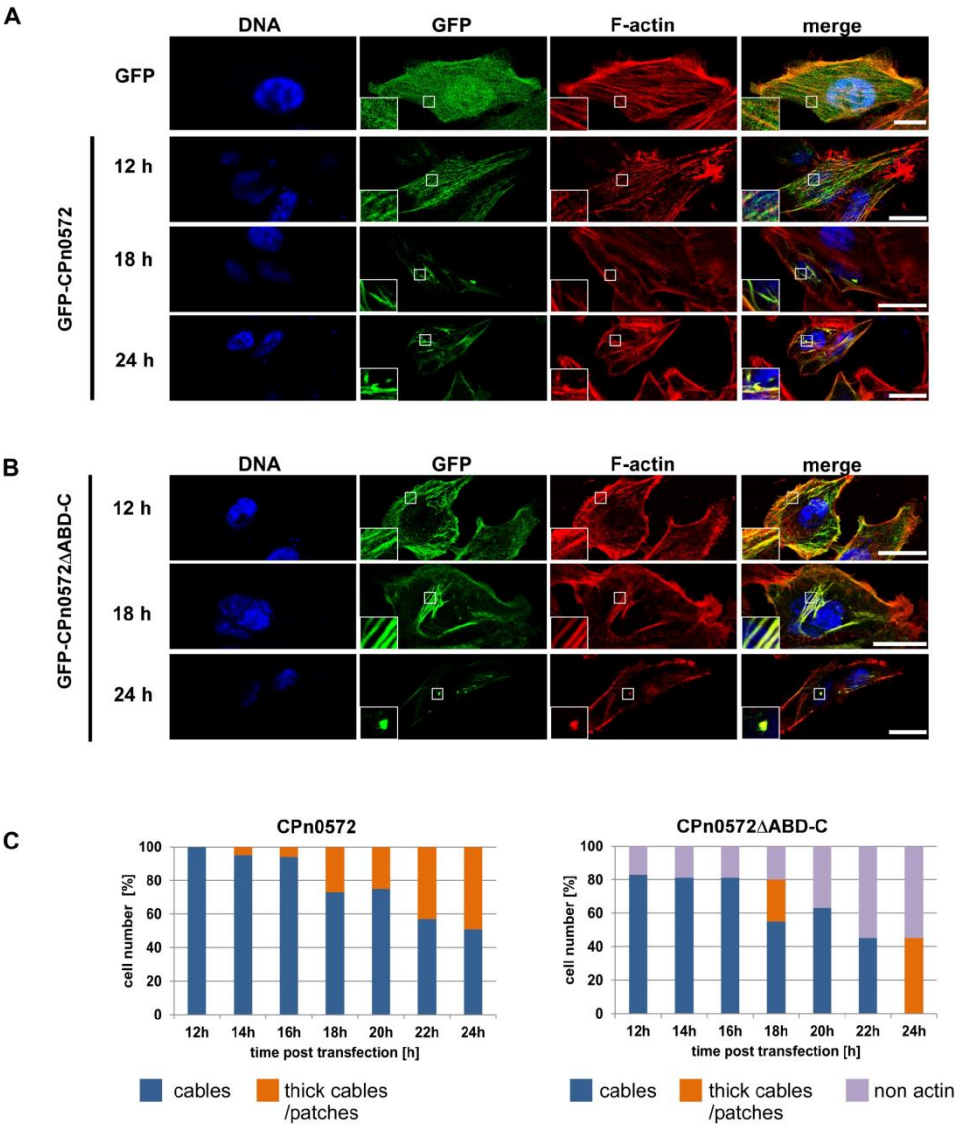

Fig 3. CPn0572ΔABD-C colocalizes with actin in mammalian cells. Confocal images of cells transfected with plasmids encoding GFP or GFP-CPn0572 **(A)** or GFP-CPn0572ΔABD-C **(B)**. HEp-2 cells were transfected with indicated plasmids for 12, 18, or 24 h and F-actin was visualized with phalloidin (red) and DNA with DAPI (blue). Scale bar: 10 μm. Boxed regions show 3-fold enlargement. **(C)** Quantification of GFP-CPn0572 and GFP-CPn0572ΔABD-C-derived phenotypes after transfection, monitored every 2 h (range: 12 to 24 h). n ≥ 100 cells per time point and per transfected plasmid. All quantifications were reproducible and analyzed from triplicates.

https://doi.org/10.1371/journal.pone.0210403.g003

Fig), and observed the localization of GFP tagged protein in transfected HEp-2 cells at 18 h post transfection (Fig 4B; quantified in Fig 4C). GFP-CPn0572 and GFP-CPn0572ΔABD-C colocalized with actin structures (Fig 4B, panels 2 and 3), but the localization of the N-terminal GFP-CPn0572$^{1-478}$ variant was cytoplasmic (Fig 4B, panel 4) supporting the notion that the N-terminus did not contain actin binding properties. Importantly, the ABD-C domain of CPn0572 (amino acids 478–536) was sufficient for actin colocalization (Fig 4B, panel 5), demonstrating that this domain is able to interact with actin without the aid of any additional CPn0572-derived domains, reminiscent of the ABD-C actin localization in budding yeast [23]. Surprisingly, when the ABD-C domain of CPn0572 is expressed fused to the N-terminus, the resulting protein GFP-CPn0572$^{1-536}$ did not colocalize with actin, but rather displayed a cytoplasmic distribution (Fig 4B, panel 6). This finding proposes that the N-terminal region (amino acid 1–478) inhibited the ability of the ABD-C domain to bind to actin structures. Interestingly, the C-terminal CPn0572 variants with or without the ABD-C, CPn0572$^{478-755}$ and CPn0572$^{536-755}$ respectively, both colocalized with actin structures (Fig 4B, panels 7 and 8). Thus, an actin binding domain exists downstream of the ABD-C domain. Collectively, our data show that CPn0572$^{536-755}$ harbors an additional actin-binding domain able to modulate the actin cytoskeleton in both yeast and mammalian cells.

CPn0572$^{536-755}$ binds directly to F-actin

In order to further examine the actin binding capacity of the newly identified actin modulatory domain within CPn0572$^{536-755}$, we used bacterially expressed recombinant proteins and tested them in an actin co-sedimentation assay. In short, pre-assembled F-actin was incubated with recombinant GST control or GST-CPn0572$^{536-755}$ (Fig 5A) followed by ultracentrifugation. The ultracentrifugation step generated an F-actin pellet that was analyzed for proteins co-sedimenting along with F-actin. In the absence of actin filaments, both proteins remained exclusively in the soluble fraction (Fig 5B). However, when F-actin was present, a proportion of GST-CPn0572$^{536-755}$ was found to co-sediment with F-actin (Fig 5C). This *in vitro* actin binding analysis shows that a second actin-modulating domain exists within the C-terminus of CPn0572 (amino acids 536–755) that can bind F-actin directly.

CPn0572$^{536-755}$ harbors actin and vinculin-binding domains

To better define the actin modulating domain in CPn0572$^{536-755}$ we performed a secondary-structure prediction analysis and identified candidate alpha-helical structures that could bind actin. A large number of actin binding proteins utilize an alpha-helix to interact within the hydrophobic cleft on the surface of actin, which represents a binding-hot spot for actin modulating proteins [36]. In fact, L2-TarP contains three alpha-helices that allow it to interact with either G-actin or F-actin [37]. Secondary structure elements as calculated by SOPMA [38] revealed two regions predicted to form alpha helices, amino acids 572–581 (Helix 1, referred to as H1 in this study) and amino acids 711–736 (Helix 2, referred to as H2) (S2A Fig). We then tested if protein variants containing these alpha helices would colocalize with actin in HEp-2 cells. Plasmids encoding N-terminal GFP-fusions of CPn0572$^{536-755}$, CPn0572$^{536-595}$, CPn0572$^{595-659}$, CPn0572$^{660-755}$ or CPn0572$^{695-755}$ (Fig 6A and S3 Fig) were expressed in HEp-2-cells, which were fixed and subsequently stained with rhodamine-phalloidin. As shown previously the majority of GFP-CPn0572$^{536-755}$ expressing cells displayed localization of the fusion protein to thick actin cables (Fig 6B, panel 2; quantified in Fig 6C). Interestingly, in 89% of the cells expressing CPn0572$^{536-595}$, which contains H1, the fusion protein localized to actin structures such as actin cables and actin-positive structures at the cell periphery (Fig 6B, panel 3; quantified in Fig 6C), demonstrating that this domain possesses actin-binding properties. In

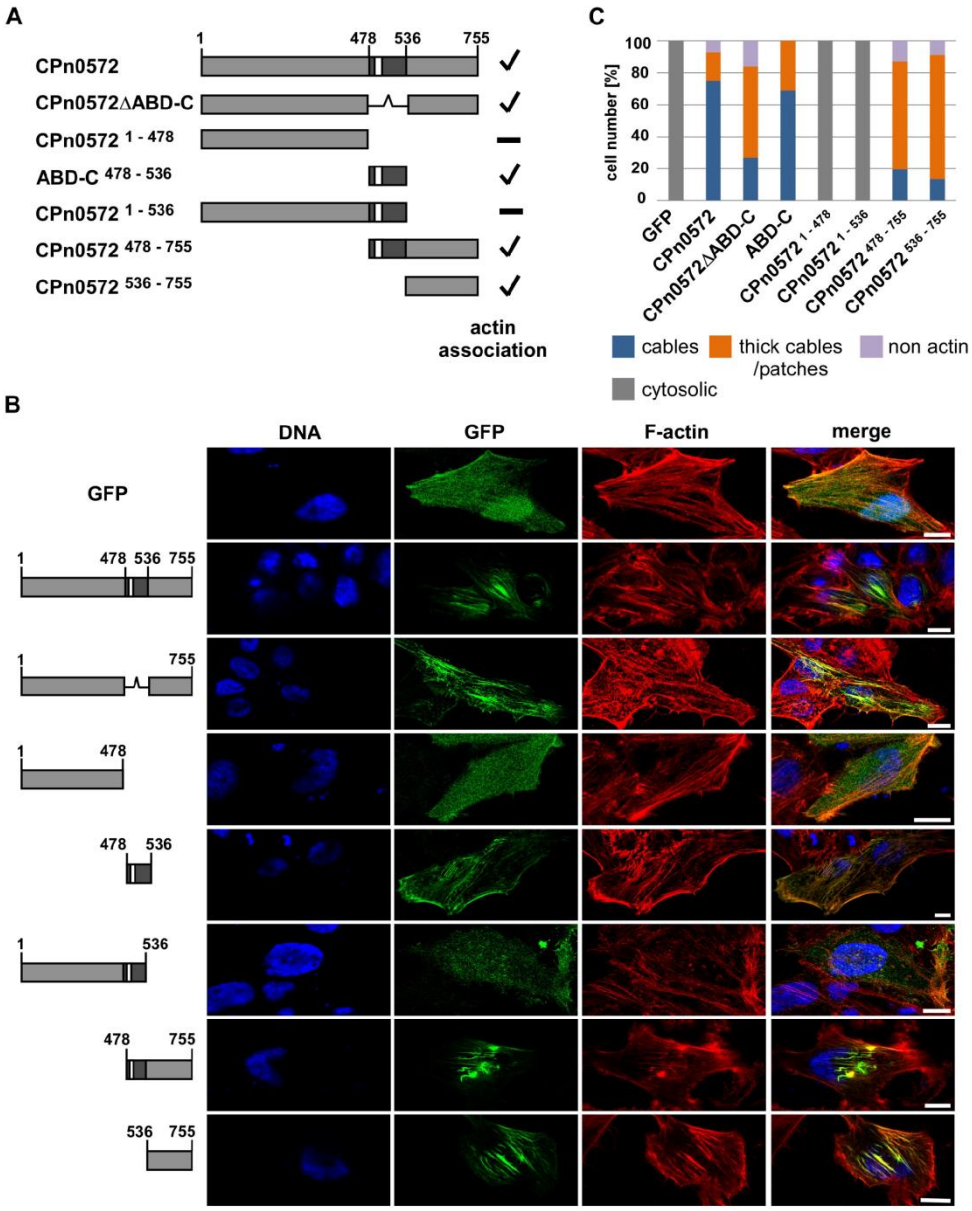

Fig 4. The N-terminus of CPn0572 inhibits actin association of the ABD-C domain while the C-terminus associates with actin in the absence of ABD-C domain. (A) Schematic representation of CPn0572 and deletion variants thereof. ABD-C, black box; ABD, white box. Numbers indicate amino

acid positions. Positive actin association is indicated by a checkmark and non-association with a minus on the right margin of the drawings. **(B)** Confocal images of HEp-2 cells transfected for 18 h with the indicated CPn0572 variants fused to GFP at the N-terminus. F-actin was visualized with phalloidin (red) and DNA with DAPI (blue). Bar: 10 μm. **(C)** Quantification of intracellular localization of GFP-CPn0572 and variants shown in **(B)**. n ≥ 90 cells per transfected plasmid. All quantifications were reproducible and analyzed from triplicates.

https://doi.org/10.1371/journal.pone.0210403.g004

contrast, CPn0572$^{595–659}$, which does not contain either H1 or H2, localized exclusively to the cytoplasm (Fig 6B, panel 4; quantified in Fig 6C). Surprisingly, CPn0572$^{660–755}$ and CPn0572$^{695–755}$, both of which contain the H2 motif, did not localize to actin cables. Instead these fusion proteins were present at tip-like structures at the cell periphery, often at the end of long actin cables (Fig 6B, panels 5 and 6; quantified in Fig 6C). This type of localization is reminiscent of vinculin staining at focal adhesions [39].

Some TarP orthologs have been shown to contain VBSs, which mediate the recruitment of vinculin through direct protein-protein interactions [13, 20, 22]. However, no VBS had been identified for CPn0572 thus far. Our results suggested that CPn0572 might contain a vinculin-binding site present between amino acids 695–755. Indeed, visual analysis of the primary sequence in this region of CPn0572 revealed a predicted VBS at amino acids 717–735 similar to the consensus LxxAAxxVAxxVxxLIxxA [40] (S2B Fig).

To assess the ability of CPn0572 to colocalize with vinculin, HEp-2 cells were co-transfected with plasmids encoding CPn0572$^{536-755}$, CPn0572$^{660-755}$ or CPn0572$^{695-755}$ fused to GFP at the

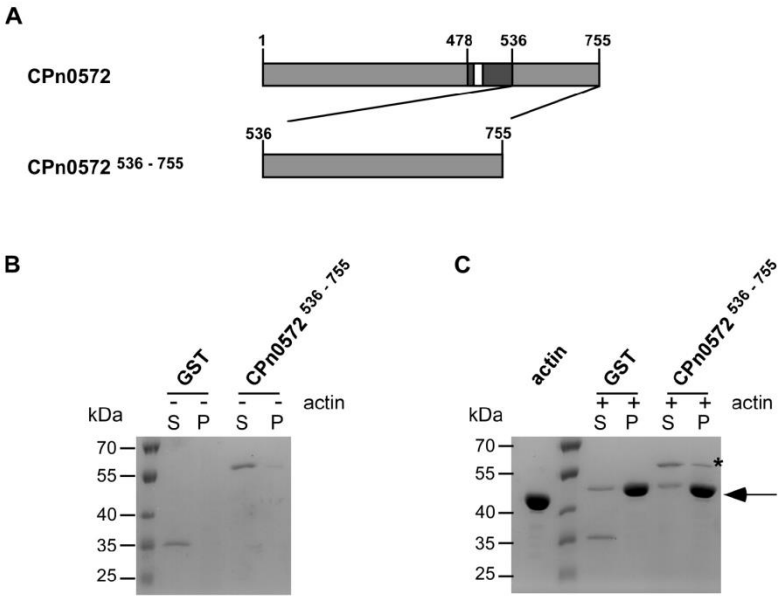

Fig 5. The C-terminus of CPn0572 binds F-actin *in vitro*. **(A)** Schematic representation of CPn0572 and CPn0572$^{536-755}$ variants. ABD-C, black box; ABD, white box; Numbers indicate amino acid positions. **(B)** and **(C)** F-actin binding of CPn0572$^{536-755}$ was analyzed using an actin co-sedimentation assay. Experiments were performed in the absence (-) or in the presence (+) of 40 μg of pre-assembled F-actin (B and C, respectively). Supernatant (S) and pellet (P) fractions were analyzed by SDS-PAGE and visualized with Coomassie blue. Actin is marked with an arrow and GST-CPn0572$^{536-755}$ in the pellet fraction is marked with a (*). n = 2.

https://doi.org/10.1371/journal.pone.0210403.g005

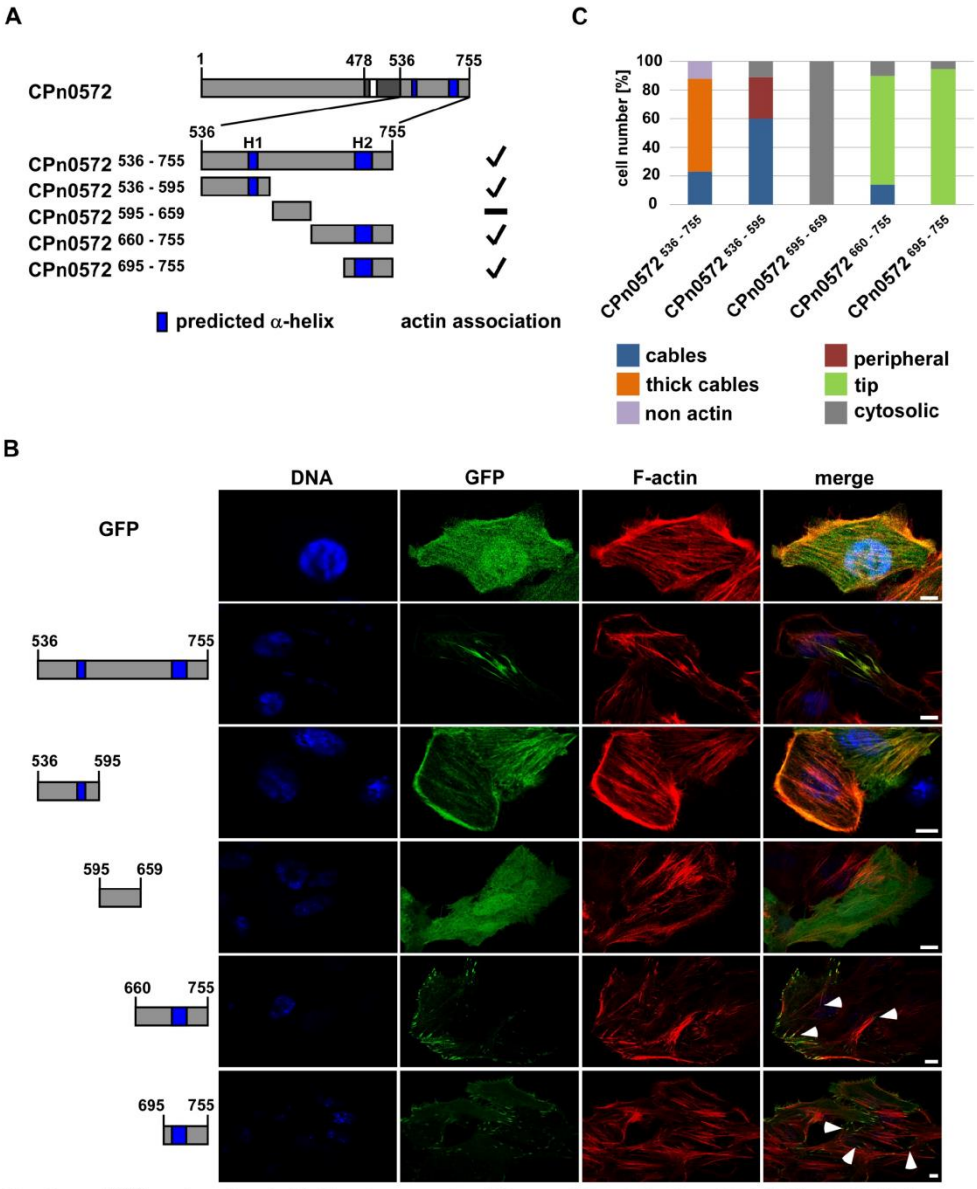

Fig 6. CPn0572$^{536-595}$ associates with actin. (A) Schematic representation of CPn0572 and C-terminal variants. ABD-C, black box; ABD, white box; predicted α-helices, dark blue boxes (labeled H1 and H2). Numbers indicate amino acid positions. Positive actin association is indicated by a checkmark and non-actin association with a minus on the right margin of the drawings. **(B)** Confocal fluorescence microscopy analysis of transfected cells expressing

GFP or GFP-CPn0572 variants. HEp-2 cells were transfected for 18 h before fixation. F-actin was visualized with phalloidin (red) and DNA with DAPI (blue). Tips of actin cables are marked by white arrow heads. Bar: 10 μm. **(C)** Quantification of localization phenotypes of GFP-CPn0572 and variants shown in **(B)**: CPn0572$^{536\text{-}755}$ (n = 572), CPn0572$^{536\text{-}595}$ (n = 313), CPn0572$^{595\text{-}659}$ (n = 380), CPn0572$^{660\text{-}755}$ (n = 347) and CPn0572$^{695\text{-}755}$ (n = 563). All quantifications were reproducible and analyzed from triplicates.

https://doi.org/10.1371/journal.pone.0210403.g006

N-terminus (Fig 7A and S3 Fig) and a plasmid encoding SNAP-tagged vinculin. Cells were labeled with the fluorescent SNAP-Cell SiR substrate and co-stained with phalloidin (Fig 7B; quantified in Fig 7C). In contrast to GFP-expressing control cells, where vinculin was concentrated in puncta at the tip of actin cables near the cell periphery, cells expressing GFP-CPn0572$^{536\text{-}755}$ mislocalized vinculin throughout the length of GFP-positive actin cables (Fig 7B, panels 1 and 2). Moreover, vinculin was no longer detected at the cell periphery, suggesting that CPn0572 was able to recruit it to abnormal actin structures. Interestingly, GFP-tagged CPn0572 proteins containing H2, namely GFP-CPn0572$^{660\text{-}755}$ and GFP-CPn0572$^{695\text{-}755}$, localized to typical vinculin structures, displayed as puncta at the cell periphery, and showed no disruption of the actin cytoskeleton (Fig 7B, panels 3 and 4; quantified in Fig 7C).

To determine if the predicted VBS of CPn0572 is required for vinculin association, we generated a plasmid encoding GFP-CPn0572$^{595\text{–}755\Delta H2}$, in which the VBS within H2 was deleted (Fig 8A) and transfected HEp-2 cells (S3A and S3C Fig). Compared to GFP-CPn0572$^{660\text{-}755}$ and GFP-CPn0572$^{695\text{-}755}$, the colocalization of GFP-CPn0572$^{595\text{-}755\Delta H2}$ and vinculin was reduced (Fig 8B, bottom panels; quantified in Fig 8D), demonstrating that H2 is important for vinculin-binding. However, a weak GFP-CPn0572$^{595\text{-}755\Delta H2}$ signal could still be detected colocalizing with vinculin staining. Further visual analysis of the amino acid sequence in CPn0572$^{595\text{–}755}$ revealed the presence of a second sequence upstream of the H2, with a lower homology to the consensus VBS and the CPn0572 VBS, at amino acids 682–700 (S2C Fig). The residual vinculin colocalization observed for GFP-CPn0572$^{595\text{–}755\Delta H2}$ could be a result of the presence of this second VBS-like sequence.

Taken together, our data have led to the identification of a new CPn0572 actin-binding domain at the proximal end of the C-terminal domain (amino acids 536–595) and a vinculin-binding domain at the end of the C-terminus (amino acids 717–736). Thus, we propose that the reorganization of the actin cytoskeleton by the *C. pneumoniae* TarP family member is driven by a combination of the ABD-C domain, the F-actin binding domain and the vinculin binding domain.

Discussion

In this study we have used the fission yeast *S. pombe* to confirm that the ABD-C domain of CPn0572 has strong actin cytoskeleton remodeling capacity. Moreover, the yeast analysis revealed that CPn0572 must contain an ABD-C independent actin modulatory domain. We recapitulated these findings in human epithelial HEp-2 cells and mapped an additional actin modulatory domain to amino acids 536–595 of CPn0572. Indeed, the C-terminus of CPn0572 bound F-actin directly *in vitro*, thus revealing it to harbor an FAB domain. Moreover, we demonstrated that the N-terminus of CPn0572 is able to inhibit the ability of the ABD-C domain to aggregate actin in HEp-2 cells. Finally, our results also identify a VBS in CPn0572, which enables it to colocalize with vinculin and recruit it to actin cables decorated with CPn0572.

An attractive advantage of utilizing fission yeast in the study of chlamydial effectors is the simplicity of the system. For instance, fission and budding yeast do not have many of the signaling pathways involved in *Chlamydia* entry, nor do they encode proteins involved in focal adhesion like vinculin. As a result, we can observe the impact of TarP on actin reorganization without the complexity of other pathways regulating its function. As a result, fission yeast represents an excellent tool for exploring domain structure-function relationships.

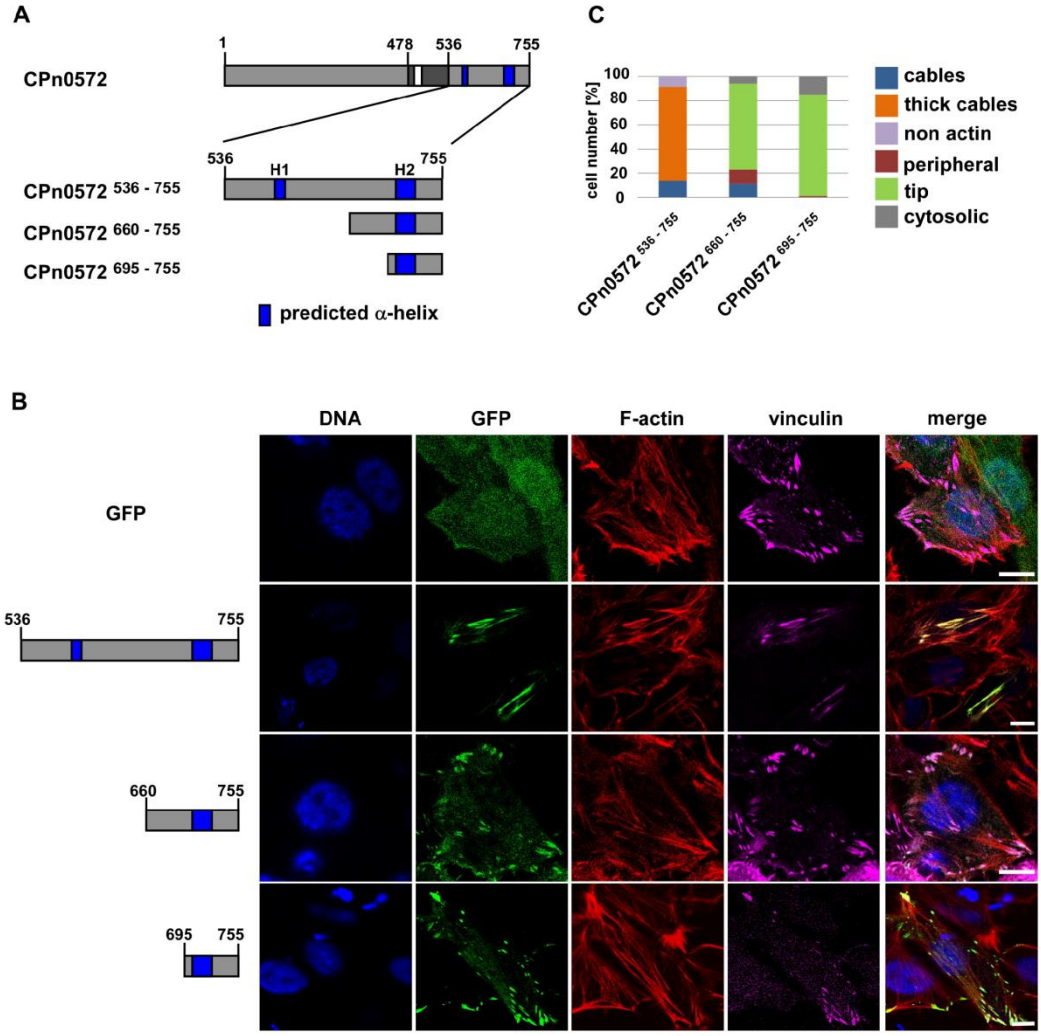

Fig 7. The C-terminus of CPn0572 contains a vinculin-binding domain. (A) Schematic representation of CPn0572 with its C-terminal variants. ABD-C, black box; ABD, white box; predicted α-helices, dark blue boxes (labeled H1 and H2). Numbers indicate amino acid positions. **(B)** Confocal fluorescence microscopy analysis of transfected cells expressing GFP or GFP-CPn0572 and vinculin fused to SNAP. HEp-2 cells were transfected for 18 h before fixation. F-actin was visualized with phalloidin (red), vinculin with SNAP-cell SiR647 (magenta) and DNA with DAPI (blue). Bars: 10 μm. **(C)** Quantification of localization phenotypes of GFP-CPn0572 variants shown in **(B).** n ≥ 90 cells per transfected plasmid. All quantifications were reproducible and analyzed from triplicates.

https://doi.org/10.1371/journal.pone.0210403.g007

In *Chlamydia* species the TarP family has been established as a master regulator of actin dynamics during bacterial invasion. Members of this family have the ability to bind actin directly through a number of actin binding sequences and the capacity to interact with a

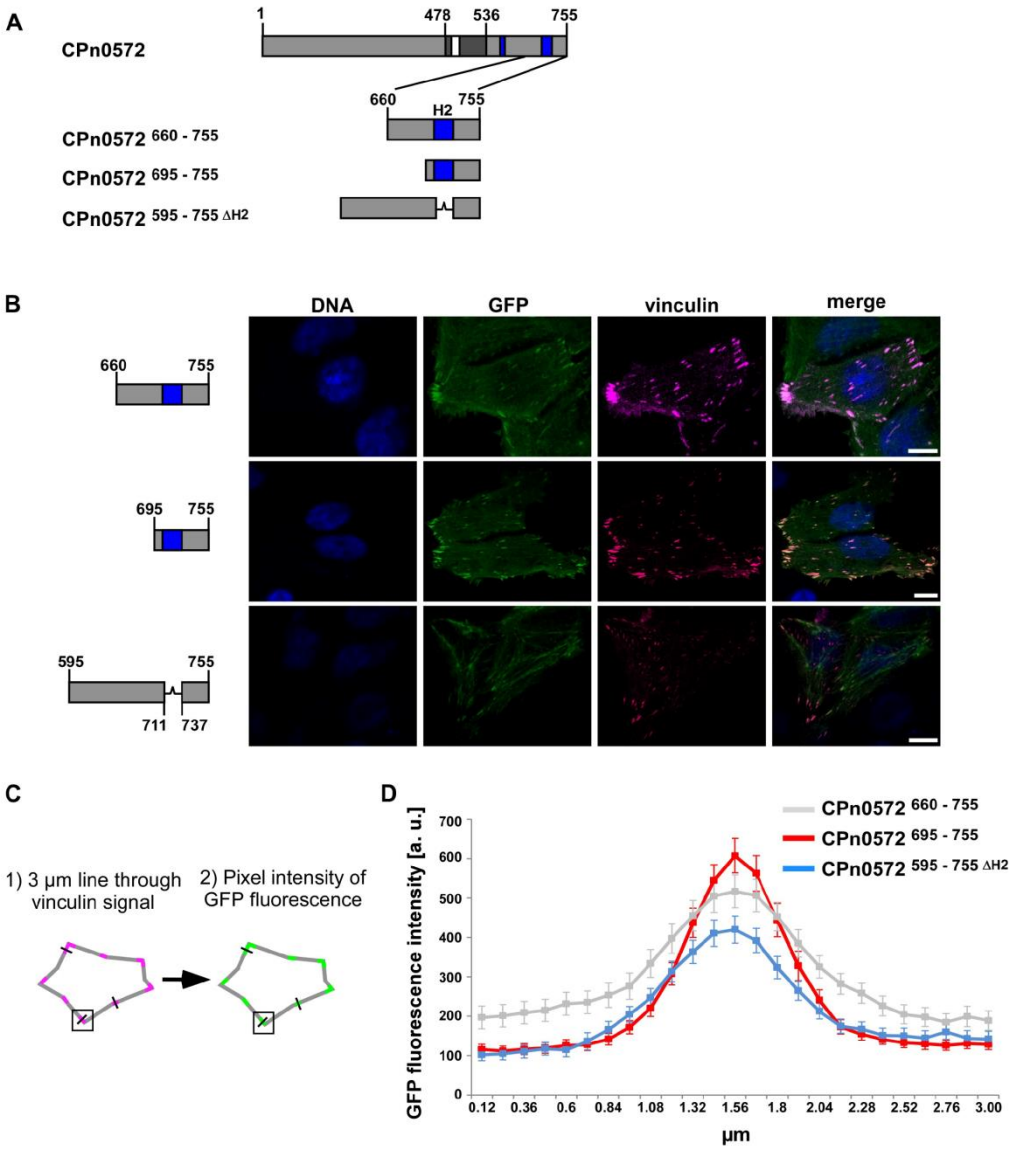

Fig 8. Helix 2 of CPn0572 plays a role in vinculin association. **(A)** Schematic representation of CPn0572 and variants thereof. **(B)** Confocal fluorescence microscopy analysis of transfected cells expressing CPn0572 variants fused to GFP and vinculin fused to SNAP. HEp-2 cells were transfected for 18 h before fixation. Vinculin was visualized with SNAP-cell SiR647 (magenta) and DNA with DAPI (blue). Bars: 10 µm. **(C)** Schematic representation of the methodology used for the quantification of GFP fluorescence intensity colocalized with vinculin. **(D)** GFP fluorescence intensity of GFP-CPn0572 variants that colocalize with vinculin puncta. arbitrary units (a.u.). n = 90 independent measurements for each construct analyzed from triplicates.

https://doi.org/10.1371/journal.pone.0210403.g008

number of cellular host factors that mediate cell signaling and participate in actin reorganization [13–16, 20, 21, 23, 37] (domains identified thus far in *C. trachomatis* TarP and *C. pneumoniae* CPn0572 are summarized in S4 Fig). In this study, we show that expression of full length CPn0572 in fission yeast or in mammalian cells results in a strong reorganization of the actin cytoskeleton; a phenotype that intensifies the longer CPn0572 is expressed. We and others have previously shown that *C. pneumoniae* CPn0572 possesses a single ABD motif able to bind actin [14, 23]. For this assay, Jewett et al. utilized a 100-amino acid-long region of CPn0572, which includes a 12 amino acid-long motif with high sequence identity to TarP family ABDs, embedded in an 19 amino acid-long alpha helix [14], which is proposed to be the G-actin-binding motif of TarP [37]. Interestingly however, we now show that expression of an ABD deletion version of CPn0572 (CPn0527ΔABD-C) exhibits a clear impact on the actin cytoskeleton in both yeast and human model systems, which suggested the presence of additional actin modulatory regions fully capable of altering the actin cytoskeleton in both systems. Subsequently, we found that the C-terminus of CPn0572 (amino acids 536–755) can by itself remodel the actin cytoskeleton and harbors an FAB domain.

Members of the TarP family can have up to three functional ABDs [14]. In addition to the ABDs, two FABs were identified experimentally in *C. trachomatis* L2 TarP. Sequence comparisons identified FABs in other *C. trachomatis* serovars and potential FABs in TarP orthologs from different chlamydial species; however, such domains were not identified in the *C. pneumoniae* TarP ortholog [21]. Our study demonstrated that CPn0572 contains at least one ABD and one FAB, consistent with the notion that TarP family members depend on ABDs and FABs to mediate the cytoskeletal changes to facilitate chlamydial invasion. The interplay between these domains during chlamydial entry is as yet unknown, but likely requires spatio-temporal regulation of the various actin modulatory domains present in the same molecule. However, it is possible that these domains have roles in separate steps of the chlamydial infection cycle.

Interestingly, the N-terminus of CPn0572, like the TarP orthologs of *C. caviae*, *C. abortus*, *C. felis* and *C. muridarum*, does not contain the tyrosine-rich repeats identified in *C. trachomatis* [13] and, as of yet, no function has been attributed to N-terminus of these orthologs. We now present preliminary evidence that the N-terminal domain of CPn0572 (amino acids 1–478) inhibits the actin-recruiting capacity of the ABD-C domain. The ABD-C of CPn0572 clearly localizes to actin structures in mammalian cells and budding yeast [23]. Addition of the CPn0572 N-terminus to the ABD-C abrogates actin localization in mammalian cells but not in budding yeast [23]. This suggests that the regulation of the ABD-C by the N-terminus may require mammalian host factors. The inhibitory effect of the N-terminus appeared to be specific for the ABD-C, as the C-terminal construct, amino acid 536–755, localized to actin in the presence of the N-terminus. Furthermore, the N-terminus in the context of full-length CPn0572 does not inhibit the protein from localizing to actin structures, uncovering an essential role for the C-terminus (amino acids 536–755) this process. It is likely that the ability of the N-terminus to regulate the ABD-C is itself regulated during infection. Interestingly, a *C. trachomatis* TarP construct containing the N-terminus but missing the C-terminal ABD and FAB domains still localizes to puncta, albeit without actin colocalization [16] whereas a similar CPn0572 construct localizes throughout the cytoplasm. This observation suggests that there are important functional differences in how the N-terminus of these proteins contributes to the localization of *C. trachomatis* TarP and CPn0572, possilby due to the presence of the tyrosine-rich domain in *C. trachomatis* TarP that is missing in CPn0572.

Importantly, we also identify a vinculin-binding domain (VBD) in the C-terminus of CPn0572 containing a 19-residue-long motif characteristic of a VBS. Multiple VBSs have been identified in the *Shigella* protein IpaA and the *Rickettsia* protein Sca4 [41], and both effector

proteins are thought to activate vinculin to mediate localized actin remodeling. In *Chlamydia*, RNA interference screens identified the necessity of vinculin during *C. trachomatis* L2 infection in culture cells [42, 43]. Additionally, vinculin was found to be recruited to sites of *C. caviae* entry while infection efficiency was reduced in vinculin KO cells, revealing that vinculin plays a role during invasion of *C. caviae* [13]. The precise role of vinculin during *Chlamydia* infection and whether it cooperates with the ABDs and FABs of the TarP family during invasion remains unknown at present. However, the VBD in CPn0572 is likely to be implicated in the recruitment of actin or the remodeling of the actin cytoskeleton. In mammalian cells, CPn0572 C-terminus containing both the FAB and the VBS localizes mostly to thick actin cables whereas a CPn0572 C-terminus construct containing only the FAB localizes to thin actin cables and the cell periphery. Vinculin recruitment to CPn0572 could enhance formation of thick actin cables through vinculin's actin and Arp2/3 binding domains [44]. Additionally, the lack of actin localization of CPn0527ΔABD-C in fission yeast pointed to additional mammalian-specific factors that stabilize the FAB domain interaction with actin. Vinculin could be one such factor. Fission yeast does not possess a vinculin homologue. Thus, the CPn0572 VBS could not aid in the formation of actin structures in this organism. These observations are consistent with recent findings in which the VBD of *C. caviae* TarP was sufficient for the recruitment of actin, but this ability was abrogated in vinculin KO cells [13]. Interestingly, as opposed to the VBD of *C. caviae* TarP, the VBD of CPn0572 was not sufficient to mediate recruitment of actin.

The data presented here demonstrate that the TarP family member CPn0572 has potential cytoskeletal remodeling functions at its C-terminal through vinculin and actin binding and recruitment. The N-terminal domain has a negative impact on the ABD actin binding. Further work will be necessary to elucidate the timing and specific roles of these domains during *C. pneumoniae* infection.

Material and methods

Cloning procedures, vector constructs and antibodies

Full length CPn0572 and variants were amplified by PCR from pre-existing vectors with custom synthesized oligonucleotide primers (Sigma Aldrich). Plasmids were generated by amplification of DNA fragments that were subsequently cloned into pJR1-3XU with or without mCherry (C-terminal mCherry) for yeast expression, pAE67 (CMVp N-terminal GFP) for mammalian expression vector or pKM36 (GST-Tag) for expression in *E. coli*. All constructs were generated by homologues recombination in *S. cerevisiae*. The SNAP-tag fusion plasmid vinculin-23 was a gift from Michael Davidson (Addgene plasmid #58198). Antibodies against mCherry (Abcam), GFP (chromotek) and γ-tubulin (Sigma) as well as secondary antibodies anti-rabbit (Promega) and anti-mouse (Sigma) were used for western blots.

Yeast strains and media

Wild-type, (UFY605: *his3-D1*, *ade6-M210*, *leu1-32*, *ura4-D18*, h^-) a gift from K. Gould, Vanderbilt University, USA, or lifeact-GFP, (UFY2999: *Pact1-LAGFP*::$leu1^+$, *ura4-D18*, *leu1-32* h^-) a gift of M. Balasubramanian, Warwick Medical School, UK, were used to obtained transformants by introducing plasmids in cells grown in YE5S and later maintained in minimal media with supplements as described [45]. To repress or derepress expression, cells bearing $nmt1^+$ promoter plasmids were grown in minimal medium plus 5 μg/ml thiamine for at least 48 h, washed twice with thiamine-less medium and finally resuspended in either media with thiamine or thiamine-less medium for 22 h at 30˚C and either utilized for serial-dilution patch tests, live-cell microscopy or preparation of protein extracts. For patch test analysis,

transformants were spotted in 10-fold serial dilutions in plates containing 1 μM or 2 μM Latrunculin B (Merck Chemicals, Germany), or DMSO. For western blots, 100 OD_{600} units of cells were used to prepare protein extracts, as described previously [46].

Live cell microscopy of fission yeast

For imaging of living *S. pombe* cells, cells were pre-grown in minimal plasmid-selection medium at 30˚C to an OD_{600} of 0.5 and stained with either Hoechst 33342 for 30 minutes or calcofluor white for 5 minutes. Cells were directly processed for microscopy by mounting them on slides. Images of live cells were acquired with a Zeiss Axiovert 200 fluorescence microscope (Carl Zeiss) using a 63x objective with a charge-coupled-device (CCD) camera (IEEE1394-Based Digital Camera Orca-ER 1394; Hamamatsu, Herrsching, Germany) and image editing and analysis was done with ImageJ 1.47v (National Institutes of Health). GFP and mCherry signals were exposed the same amount of time and processed equally for all strains in a given experimental condition.

Maintenance, transfection and staining of mammalian cells

HEp-2 cell were cultured in DMEM medium supplemented with 10% fetal calf serum (FCS), MEM vitamins (Thermo Fisher Scientific) and non-essential amino acids (Thermo Fisher Scientific) and incubated at 37˚C and 6% CO_2. A 40% confluent HEp-2 cell monolayer was grown on cover slips in 24 well plates (Sarstedt). For transfections, cells in fresh medium without FCS were transfected for 18 h using TurboFect (Thermo Fisher Scientific). Transfected HEp-2 cells were fixed with 3% paraformaldehyde in PBS for 10 min, washed three times with HBSS and permeabilized with 2% saponin (Sigma Aldrich) in PBS for 20 min at 30˚C. Staining of actin in human cells with rhodamine-phalloidin was performed as recommended by the manufacturer (Thermo Fischer Scientific). DAPI was used to visualize DNA and the far-red fluorescent substrate SNAP-Cell 647-SiR (New England Biolabs) to visualize SNAP-tagged Vinculin.

Microscopy of mammalian cells and image processing

Images were acquired using an inverse Nikon TiE Live Cell Confocal C2plus with 100 x TIRF objective and a C2 SH C2 Scanner. Analysis of images and measurements were generated with Nikon Element software. The thickness threshold under which long fibrous phalloidin-positive actin structures were identified as "cables" and above which long fibrous actin structures were identified as "thick cables" was set at 200 nm. Images for analysis of actin cable thickness was done using ImageJ 1.47v (National Institutes of Health). Quantification of CPn0572-derived phenotypes after transfection in HEp-2 cells was done by classifying individual cells in described phenotypic groups utilizing the GFP signal.

Quantification of GFP fluorescence intensity that colocalizes with vinculin fluorescence signal

For quantification of fluorescence intensity of GFP-CPn0572 variants at sites of vinculin localization, we transfected HEp-2 cells with SNAP-tagged vinculin and the relevant GFP constructs, stained cells with far-red fluorescent substrate SNAP-Cell 647-SiR, and captured images by confocal microscopy. GFP and vinculin signals were acquired with identical microscope settings. Quantification was done with ImageJ 1.47v (National Institutes of Health) as follows: For each cell analyzed, three 3 μm lines were drawn through individual vinculin puncta. The middle of the line was kept at the center of each vinculin signal. The line was used

to measure the pixel intensity of the GFP fluorescence every 0.12 μm for a total of 25 measuring points per line. For each of the constructs the background signal was determined by drawing 8 lines in areas without cells. The signal intensity for the background was homogenous and accounted for less than 0.2% of the fluorescence intensity measured in the lines drawn through GFP-CPn0572 expressing cells. The average background signal was subtracted from each of the data points. A total of 90 lines representing 30 cells were analyzed for each GFP construct.

Protein purification

GST-tagged proteins were expressed in *E. coli* BL21 and purified under native conditions from bacterial cell lysate by affinity chromatography using columns with Pierce Glutathione agarose (Thermo Fisher Scientific) and performed as recommended by the manufacturer. Proteins were eluted with reduced glutathione (Roth). Protein concentration was calculated by Bradford assay (Bio Rad) and verified using SDS/PAGE coupled with coomassie staining.

F-actin co-sedimentation assay

F-actin was assembled *in vitro* as recommended by the supplier (Cytoskeleton Inc.). 40 μl of 1 μg/μl assembled F-actin was incubated with 5 μg of bacterially purified recombinant GST-tagged protein or GST control in PBS 20% glycerol w/v and incubated for 30 minutes at room temperature. Samples were then spun at 100.000 x g for 1hr. Supernatants were separated from the pellet fraction and analyzed by SDS-gel electrophoresis followed by coomassie staining.

Bioinformatic analysis

Secondary structure prediction of CPn0572 variants was carried out with SOPMA (https://npsa-prabi.ibcp.fr/cgi-bin/npsa_automat.pl?page=/NPSA/npsa_sopma.html).

Accesssion numbers

Chlamydia trachomatis L2: NC_010287.1
Chlamydia pneumoniae GiD: LN847009.1

Supporting information

S1 Fig. Expression of CPn0572 in *S. pombe* results in aberrant cell morphology and cytokinesis defects. Examples of lifeact-GFP-expressing cells harboring an mCherry control plasmid or CPn0572-mCherry plasmid grown for 22 h under plasmid selective conditions without thiamine (high expression of CPn0572). In control cells, actin is present in actin patches at cell tips (arrow heads), the contractile ring in the center of dividing cells (*) and actin cables (arrows). Examples of normal (cells 1 and 2) and abnormal (cells 3–5) cell morphology used for quantification in Fig 1C. Cells were stained with Hoechst to visualize DNA. Bars, 5 μm. **(B)** Live cell images of lifeact-GFP-expressing strains to visualize F-actin (green in merged images) harboring indicated mCherry plasmids (red in merged images) grown for 22 h under plasmid selective conditions without thiamine (high expression of CPn0572). Cells were stained with calcofluor white to observe growth zones (blue in merged images). Abnormal accumulation of cell wall material in puncta (white arrow in calcofluor panels, repeated in lifeact-GFP and merged images), abnormal deposition of cell wall material at the cell middle (arrow head in calcofluor panels, repeated in lifeact-GFP and merged images. Bars, 5 μm. **(C)** Quantification of aberrant cell wall deposition at the cell middle as shown in **(B)**. n = 4 samples each representing 20–70 cells. Error bars denote standard error of the mean. Student's t-test was used to reveal statistical significance. $p < 0.005$ (**), $p < 0.05$ (*), and not significant (ns). **(D)**

Expression of mCherrry, CPn0572-mCherry and CPn0572ΔABD-C-mCherry in transformed yeast cells grown for 22 h under plasmid selective conditions leading to either low expression (Low) or high expression (High). Western blot was probed with anti-mCherry or anti- γ-tubulin antibodies. mCherrry containing-proteins are marked with (*). As mCherry-tagged proteins were expressed at low levels in the presence of thiamine, we loaded 6x times more protein to detect a signal.
(TIF)

S2 Fig. Secondary structure prediction of the CPn0572 C-terminus reveals potential α-helical structures and a vinculin-binding motif. (A) Secondary structure prediction carried out with SOPMA. The predicted α-helices are shown as a sequence of blue *h* letters below the amino acid sequence or as dark blue boxes in the schematic representation of CPn0572 and CPn0572 C-terminus ($CPn0572^{536-755}$). Letter *e* stands for extended strand, *c* stands for random coil and *t* for beta turn. **(B)** and **(C)** Schematic representation of $CPn0572^{536-755}$. Predicted α-helices are shown in dark blue. The amino acid sequence of the second predicted α-helix is shown in dark blue and the vinculin-binding motif is highlighted in green. H2 amino acids with identity or high similarity to the vinculin-binding motif sequence are depicted in bold. **(C)** A second possible vinculin-binding motif is underlined in the amino acids sequence. Amino acids in this sequence with identity or high similarity to the vinculin-binding motif sequence are depicted in bold.
(TIF)

S3 Fig. Expression of CPn0572 variants. (A-B) Schematic representation of the CPn0572 variants analyzed in **(C)** and **(D). (C-D)** Western blot analysis of GFP-CPn0572 and variants. After 18 h transfection GFP and GFP-tagged proteins were analyzed on SDS-PAGE and visualized with an anti-GFP antibody. γ-tubulin was used as a loading control. n = 3 independent transfections per construct.
(TIF)

S4 Fig. CPn0572 has a similar domain distribution to *C. trachomatis* TarP. Schematic representation of *C. trachomatis* TarP L2 and *C. pneumoniae* CPn0572. The N-terminal tyrosine (Y)-rich repeat region of *C.trachomatis* TarP is not present in CPn0572. For CPn0572, the newly identified FAB domain is depicted in purple and VBS in green. Matching domains in TarP L2 are displayed.
(TIF)

Acknowledgments

We thank K. Balasubramanian (Warwick Medical School, UK) and Kathleen L. Gould (Vanderbilt University, Nashville, TN, USA) for strains, Michael Davidson (National High Magnetic Field Laboratory, Tallahassee, FL, USA) for the vinculin-23 plasmid and Mona Hendlinger (Heinrich-Heine-University, Düsseldorf, Germany) for her help with plasmids utilized in Fig 6.

Author Contributions

Conceptualization: Corinna Braun, Abel R. Alcázar-Román, Alexandra Laska, Katja Mölleken, Ursula Fleig, Johannes H. Hegemann.

Data curation: Corinna Braun, Abel R. Alcázar-Román.

Formal analysis: Corinna Braun, Abel R. Alcázar-Román.

Funding acquisition: Ursula Fleig, Johannes H. Hegemann.

Investigation: Corinna Braun, Abel R. Alcázar-Román, Alexandra Laska.

Methodology: Corinna Braun, Abel R. Alcázar-Román, Katja Mölleken, Ursula Fleig, Johannes H. Hegemann.

Project administration: Ursula Fleig, Johannes H. Hegemann.

Resources: Johannes H. Hegemann.

Supervision: Ursula Fleig, Johannes H. Hegemann.

Validation: Corinna Braun, Abel R. Alcázar-Román, Alexandra Laska.

Visualization: Corinna Braun, Abel R. Alcázar-Román.

Writing – original draft: Abel R. Alcázar-Román.

Writing – review & editing: Corinna Braun, Abel R. Alcázar-Román, Ursula Fleig, Johannes H. Hegemann.

References

1. Blasi F, Tarsia P, Arosio C, Fagetti L, Allegra L. Epidemiology of Chlamydia pneumoniae. Clin Microbiol Infect. 1998; 4 Suppl 4:S1–S6.
2. Blasi F. Clinical features of Chlamydia pneumoniae acute respiratory infection. Clin Microbiol Infect. 1996; 1 Suppl 1:S14–S8.
3. Grayston JT, Campbell LA, Kuo CC, Mordhorst CH, Saikku P, Thom DH, et al. A new respiratory tract pathogen: Chlamydia pneumoniae strain TWAR. J Infect Dis. 1990; 161(4):618–25. PMID: 2181028
4. Belland RJ, Ouellette SP, Gieffers J, Byrne GI. Chlamydia pneumoniae and atherosclerosis. Cell Microbiol. 2004; 6(2):117–27. PMID: 14706098
5. Dahlen GH, Boman J, Birgander LS, Lindblom B. Lp(a) lipoprotein, IgG, IgA and IgM antibodies to Chlamydia pneumoniae and HLA class II genotype in early coronary artery disease. Atherosclerosis. 1995; 114(2):165–74. PMID: 7605385
6. Sriram S, Stratton CW, Yao S, Tharp A, Ding L, Bannan JD, et al. Chlamydia pneumoniae infection of the central nervous system in multiple sclerosis. Ann Neurol. 1999; 46(1):6–14. PMID: 10401775
7. Abdelrahman YM, Belland RJ. The chlamydial developmental cycle. FEMS Microbiol Rev. 2005; 29 (5):949–59. https://doi.org/10.1016/j.femsre.2005.03.002 PMID: 16043254
8. Elwell C, Mirrashidi K, Engel J. Chlamydia cell biology and pathogenesis. Nat Rev Microbiol. 2016; 14 (6):385–400. https://doi.org/10.1038/nrmicro.2016.30 PMID: 27108705
9. Cocchiaro JL, Valdivia RH. New insights into Chlamydia intracellular survival mechanisms. Cell Microbiol. 2009; 11(11):1571–8. https://doi.org/10.1111/j.1462-5822.2009.01364.x PMID: 19673891
10. Carabeo RA, Grieshaber SS, Fischer E, Hackstadt T. Chlamydia trachomatis induces remodeling of the actin cytoskeleton during attachment and entry into HeLa cells. Infect Immun. 2002; 70(7):3793–803. https://doi.org/10.1128/IAI.70.7.3793-3803.2002 PMID: 12065523
11. Clifton DR, Dooley CA, Grieshaber SS, Carabeo RA, Fields KA, Hackstadt T. Tyrosine phosphorylation of the chlamydial effector protein Tarp is species specific and not required for recruitment of actin. Infect Immun. 2005; 73(7):3860–8. https://doi.org/10.1128/IAI.73.7.3860-3868.2005 PMID: 15972471
12. Clifton DR, Fields KA, Grieshaber SS, Dooley CA, Fischer ER, Mead DJ, et al. A chlamydial type III translocated protein is tyrosine-phosphorylated at the site of entry and associated with recruitment of actin. Proc Natl Acad Sci U S A. 2004; 101(27):10166–71. https://doi.org/10.1073/pnas.0402829101 PMID: 15199184
13. Thwaites TR, Pedrosa AT, Peacock TP, Carabeo RA. Vinculin Interacts with the Chlamydia Effector TarP Via a Tripartite Vinculin Binding Domain to Mediate Actin Recruitment and Assembly at the Plasma Membrane. Front Cell Infect Microbiol. 2015; 5:88. https://doi.org/10.3389/fcimb.2015.00088 PMID: 26649283
14. Jewett TJ, Miller NJ, Dooley CA, Hackstadt T. The conserved Tarp actin binding domain is important for chlamydial invasion. PLoS Pathog. 2010; 6(7):e1000997. https://doi.org/10.1371/journal.ppat.1000997 PMID: 20657821

15. Jewett TJ, Fischer ER, Mead DJ, Hackstadt T. Chlamydial TARP is a bacterial nucleator of actin. Proc Natl Acad Sci U S A. 2006; 103(42):15599–604. https://doi.org/10.1073/pnas.0603044103 PMID: 17028176

16. Jiwani S, Ohr RJ, Fischer ER, Hackstadt T, Alvarado S, Romero A, et al. Chlamydia trachomatis Tarp cooperates with the Arp2/3 complex to increase the rate of actin polymerization. Biochem Biophys Res Commun. 2012; 420(4):816–21. https://doi.org/10.1016/j.bbrc.2012.03.080 PMID: 22465117

17. Parrett CJ, Lenoci RV, Nguyen B, Russell L, Jewett TJ. Targeted Disruption of Chlamydia trachomatis Invasion by in Trans Expression of Dominant Negative Tarp Effectors. Front Cell Infect Microbiol. 2016; 6:84. https://doi.org/10.3389/fcimb.2016.00084 PMID: 27602332

18. Carabeo RA, Grieshaber SS, Hasenkrug A, Dooley C, Hackstadt T. Requirement for the Rac GTPase in Chlamydia trachomatis invasion of non-phagocytic cells. Traffic. 2004; 5(6):418–25. https://doi.org/10.1111/j.1398-9219.2004.00184.x PMID: 15117316

19. Carabeo RA, Dooley CA, Grieshaber SS, Hackstadt T. Rac interacts with Abi-1 and WAVE2 to promote an Arp2/3-dependent actin recruitment during chlamydial invasion. Cell Microbiol. 2007; 9(9):2278–88. https://doi.org/10.1111/j.1462-5822.2007.00958.x PMID: 17501982

20. Thwaites T, Nogueira AT, Campeotto I, Silva AP, Grieshaber SS, Carabeo RA. The Chlamydia effector TarP mimics the mammalian leucine-aspartic acid motif of paxillin to subvert the focal adhesion kinase during invasion. J Biol Chem. 2014; 289(44):30426–42. https://doi.org/10.1074/jbc.M114.604876 PMID: 25193659

21. Jiwani S, Alvarado S, Ohr RJ, Romero A, Nguyen B, Jewett TJ. Chlamydia trachomatis Tarp harbors distinct G and F actin binding domains that bundle actin filaments. J Bacteriol. 2013; 195(4):708–16. https://doi.org/10.1128/JB.01768-12 PMID: 23204471

22. Whitewood AJ, Singh AK, Brown DG, Goult BT. Chlamydial virulence factor TarP mimics talin to disrupt the talin-vinculin complex. FEBS Lett. 2018; 592(10):1751–60. https://doi.org/10.1002/1873-3468.13074 PMID: 29710402

23. Zrieq R, Braun C, Hegemann JH. The Chlamydia pneumoniae Tarp Ortholog CPn0572 Stabilizes Host F-Actin by Displacement of Cofilin. Front Cell Infect Microbiol. 2017; 7:511. https://doi.org/10.3389/fcimb.2017.00511 PMID: 29376031

24. Kovar DR, Sirotkin V, Lord M. Three's company: the fission yeast actin cytoskeleton. Trends Cell Biol. 2011; 21(3):177–87. https://doi.org/10.1016/j.tcb.2010.11.001 PMID: 21145239

25. Chang F. Forces that shape fission yeast cells. Mol Biol Cell. 2017; 28(14):1819–24. https://doi.org/10.1091/mbc.E16-09-0671 PMID: 28684607

26. Hayles J, Wood V, Jeffery L, Hoe KL, Kim DU, Park HO, et al. A genome-wide resource of cell cycle and cell shape genes of fission yeast. Open Biol. 2013; 3(5):130053. https://doi.org/10.1098/rsob.130053 PMID: 23697806

27. Moreno MB, Duran A, Ribas JC. A family of multifunctional thiamine-repressible expression vectors for fission yeast. Yeast. 2000; 16(9):861–72. https://doi.org/10.1002/1097-0061(20000630)16:9<861::AID-YEA577>3.0.CO;2-9 PMID: 10861909

28. Zilio N, Wehrkamp-Richter S, Boddy MN. A new versatile system for rapid control of gene expression in the fission yeast Schizosaccharomyces pombe. Yeast. 2012; 29(10):425–34. https://doi.org/10.1002/yea.2920 PMID: 22968950

29. O'Neil NJ, Bailey ML, Hieter P. Synthetic lethality and cancer. Nat Rev Genet. 2017; 18(10):613–23. https://doi.org/10.1038/nrg.2017.47 PMID: 28649135

30. Asadi F, Michalski D, Karagiannis J. A Genetic Screen for Fission Yeast Gene Deletion Mutants Exhibiting Hypersensitivity to Latrunculin A. G3 (Bethesda). 2016; 6(10):3399–408.

31. Gachet Y, Tournier S, Millar JB, Hyams JS. A MAP kinase-dependent actin checkpoint ensures proper spindle orientation in fission yeast. Nature. 2001; 412(6844):352–5. https://doi.org/10.1038/35085604 PMID: 11460168

32. Huang J, Huang Y, Yu H, Subramanian D, Padmanabhan A, Thadani R, et al. Nonmedially assembled F-actin cables incorporate into the actomyosin ring in fission yeast. J Cell Biol. 2012; 199(5):831–47. https://doi.org/10.1083/jcb.201209044 PMID: 23185032

33. Riedl J, Crevenna AH, Kessenbrock K, Yu JH, Neukirchen D, Bista M, et al. Lifeact: a versatile marker to visualize F-actin. Nat Methods. 2008; 5(7):605–7. https://doi.org/10.1038/nmeth.1220 PMID: 18536722

34. Marks J, Hagan IM, Hyams JS. Growth polarity and cytokinesis in fission yeast: the role of the cytoskeleton. J Cell Sci Suppl. 1986; 5:229–41. PMID: 3477553

35. Leonhardt C, Schwake G, Stogbauer TR, Rappl S, Kuhr JT, Ligon TS, et al. Single-cell mRNA transfection studies: delivery, kinetics and statistics by numbers. Nanomedicine. 2014; 10(4):679–88. https://doi.org/10.1016/j.nano.2013.11.008 PMID: 24333584

36. Dominguez R. Actin-binding proteins—a unifying hypothesis. Trends Biochem Sci. 2004; 29(11):572–8. https://doi.org/10.1016/j.tibs.2004.09.004 PMID: 15501675

37. Tolchard J, Walpole SJ, Miles AJ, Maytum R, Eaglen LA, Hackstadt T, et al. The intrinsically disordered Tarp protein from chlamydia binds actin with a partially preformed helix. Sci Rep. 2018; 8(1):1960. https://doi.org/10.1038/s41598-018-20290-8 PMID: 29386631

38. Sapay N, Guermeur Y, Deleage G. Prediction of amphipathic in-plane membrane anchors in monotopic proteins using a SVM classifier. BMC Bioinformatics. 2006; 7:255. https://doi.org/10.1186/1471-2105-7-255 PMID: 16704727

39. Johnson RP, Craig SW. F-actin binding site masked by the intramolecular association of vinculin head and tail domains. Nature. 1995; 373(6511):261–4. https://doi.org/10.1038/373261a0 PMID: 7816144

40. Gingras AR, Ziegler WH, Frank R, Barsukov IL, Roberts GC, Critchley DR, et al. Mapping and consensus sequence identification for multiple vinculin binding sites within the talin rod. J Biol Chem. 2005; 280 (44):37217–24. https://doi.org/10.1074/jbc.M508060200 PMID: 16135522

41. Lamason RL, Bastounis E, Kafai NM, Serrano R, Del Alamo JC, Theriot JA, et al. Rickettsia Sca4 Reduces Vinculin-Mediated Intercellular Tension to Promote Spread. Cell. 2016; 167(3):670–83 e10. https://doi.org/10.1016/j.cell.2016.09.023 PMID: 27768890

42. Elwell CA, Ceesay A, Kim JH, Kalman D, Engel JN. RNA interference screen identifies Abl kinase and PDGFR signaling in Chlamydia trachomatis entry. PLoS Pathog. 2008; 4(3):e1000021. https://doi.org/10.1371/journal.ppat.1000021 PMID: 18369471

43. Gurumurthy RK, Maurer AP, Machuy N, Hess S, Pleissner KP, Schuchhardt J, et al. A loss-of-function screen reveals Ras- and Raf-independent MEK-ERK signaling during Chlamydia trachomatis infection. Sci Signal. 2010; 3(113):ra21. https://doi.org/10.1126/scisignal.2000651 PMID: 20234004

44. DeMali KA, Barlow CA, Burridge K. Recruitment of the Arp2/3 complex to vinculin: coupling membrane protrusion to matrix adhesion. J Cell Biol. 2002; 159(5):881–91. https://doi.org/10.1083/jcb.200206043 PMID: 12473693

45. Moreno S, Klar A, Nurse P. Molecular genetic analysis of fission yeast Schizosaccharomyces pombe. Methods Enzymol. 1991; 194:795–823. PMID: 2005825

46. Pohlmann J, Risse C, Seidel C, Pohlmann T, Jakopec V, Walla E, et al. The Vip1 inositol polyphosphate kinase family regulates polarized growth and modulates the microtubule cytoskeleton in fungi. PLoS Genet. 2014; 10(9):e1004586. https://doi.org/10.1371/journal.pgen.1004586 PMID: 25254656

2.2.3 Manuscript III

A novel set of Rab-GTPase-related *Chlamydia* effector proteins involved in the early phase of infection

Corinna Braun, Johannes H. Hegemann and Katja Mölleken

First author

Contribution: 75 %

Corinna Braun planned, performed, evaluated and quantified the experiments of this manuscript. Additionally, did she generate all the figures and wrote the first draft. Furthermore, was she involved in correction of the manuscript and submission process.

Submitted to: mBio (American Society for Microbiology); 13.03.2019

Dear Ms. Braun

On March 13, 2019, we received your manuscript "A novel set of Rab GTPase-related *Chlamydia* effector proteins involved in the early phase of infection" by Corinna Braun, Johannes Hegemann, and Katja Mölleken.
The manuscript has been assigned the control number mBio00655-19.

Regards,
Miriam Day
Peer Review Coordinator, mBio

Impact factor: 6.6 (2017/2018)

A novel set of Rab GTPase-related *Chlamydia* effector proteins involved in the early phase of infection

Running title: Cluster of early *Chlamydia* effector proteins

Corinna Braun[1], Johannes H. Hegemann[1‡] and Katja Mölleken[1‡*]

[1] Institute of Functional Microbial Genomics, Heinrich Heine University, Düsseldorf, Germany

*** Corresponding author**

‡ These authors are joint senior authors on this work

E-Mail: katja.moelleken@hhu.de

Abstract

Chlamydia pneumoniae is an obligate intracellular pathogen, which infects host cells by inducing endocytosis and converting the early endosome into an 'inclusion body'. Here we describe a novel *C. pneumoniae*-specific cluster of 13 genes (termed *cee1-13*) which encode early chlamydial effector proteins that share 32.6% overall identity. Eight of these carry one or both of the domains of unknown function DUF575 and DUF562, together with one or more of the G-box motifs found in the GTP-binding domain of the Ras superfamily. The DUF575-harboring Cee1 binds in a G1-box-dependent manner to the early endosomal marker PtdIns(3)P and the late-recycling-endosome markers Rab11 and Rab14. Within 5 min of infection, Cee1 and Cee4 become associated with the inclusion membrane. Both interact in a DUF575-dependent manner specifically with phosphatidylserine and PtdIns(4)P. Our data suggest that Cee proteins function as molecular mimics of Rab proteins during early infection.

Importance

Chlamydia pneumoniae infects the upper and lower respiratory tract, causing pharyngitis, sinusitis, bronchitis and pneumonia. Furthermore, *C. pneumoniae* is associated with a number of chronic diseases including asthma, atherosclerosis and Alzheimer's disease, and the infection has also been linked to lung cancer. How *C. pneumoniae* establishes its intracellular niche is not well understood. Using a bioinformatics approach, we discovered a *C. pneumoniae*-specific gene cluster encoding early effector proteins. Many of these proteins have significant identity to each other, and show structural and sequence similarity to Rab proteins. Indeed, in ectopic expression studies they associated with markers specific for either early or recycling endosomes, which have been shown to be important for infection. During infection, cluster proteins are found on invading chlamydial cells. Our data suggest that the cluster proteins may serve as molecular mimics of Rab proteins to promote the establishment of infection.

Introduction

Chlamydia pneumoniae is one of the two major pathogenic species of the Gram-negative *Chlamydiaceae* family of bacteria that infect humans, and is responsible for a variety of acute and chronic diseases of the upper and lower respiratory tract, such as pneumonia, asthma and bronchitis (Hahn, Dodge, and Golubjatnikov 1991). All *Chlamydiae* are obligate intracellular parasites with a unique biphasic life cycle consisting of the alternation of two morphological forms: the infectious, metabolically inactive elementary body (EB), and the metabolically active reticulate body (RB) which replicates in the host cell (Chi, Kuo, and Grayston 1987; Miyashita, Kanamoto, and Matsumoto 1993; Wolf, Fischer, and Hackstadt 2000). Adhesion of EBs to their target cells is the first essential step in the infection process. This is followed by internalization of EBs into a membrane-bound compartment, termed the inclusion, in which EBs develop into replicative RBs. Initial contact between the *C. pneumoniae* EB and the host cell occurs by binding of the conserved adhesin OmcB to heparan-sulfate-like proteoglycans (GAG), followed by binding of Pmp21 (which acts as both an adhesin and invasin) to the epidermal growth factor receptor (EGFR) (Moelleken and Hegemann 2008; Mölleken, Becker, and Hegemann 2013). The latter interaction promotes internalization of the EB by activating the EGFR, and the developing inclusion at first remains associated with the activated receptor (Mölleken, Becker, and Hegemann 2013). Normally, internalized cell receptors are delivered to the early or sorting endosomal compartment, so that they can be recycled back to the plasma membrane (PM) or delivered to the lysosome for degradation, respectively (Madshus and Stang 2009). However, *C. pneumoniae* disrupts these pathways to avoid both EGFR-triggered degradation and immediate recycling to the PM.

Endocytic trafficking pathways play an important role in recycling or degrading receptors and eliminating ingested microbes. The fate of internalized vesicles is determined by their acquisition of specific Rab GTPases, which are the master regulators of vesicular transport (Jovic et al. 2010; Jean and Kiger 2012; Di Fiore and von Zastrow 2014). Rab proteins act by attaching to membranes via C-terminal lipidation in a GTP-bound form and detaching upon hydrolysis of GTP to GDP.

Recently, it was shown that the early *Chlamydia* inclusion acquires a specific endosomal membrane identity by recruiting the recycling GTPases Rab11 and Rab14 and the late endosomal Rab7 (Molleken and Hegemann 2017). Rab11 and Rab14 are both retained, while Rab7 is subsequently lost. These markers allow *C. pneumoniae* to disguise the developing inclusion as a recycling endosome (RE), thus enabling it to evade degradation in the lysosomal compartment (Molleken and Hegemann 2017). However, it is not known which chlamydial proteins are involved in these processes.

In order to identify early chlamydial effector proteins, we used a bioinformatic approach, and screened all hypothetical *C. pneumoniae* proteins against known effector proteins of obligate intracellular pathogens and against the human proteome. In this report, we characterize the hypothetical protein GiD_A_04840, which was identified on the basis of its moderate and localized homology to the human Rab36 GTPase. We demonstrate that GiD_A_04840 is part of a novel set of *C. pneumoniae*-specific proteins, encoded by a gene cluster, which is also conserved in the phylogenetically basal koala *C. pneumoniae* isolate LPCoLN. These proteins displayed different localization patterns after transfection of expression plasmids into human epithelial cells. Strikingly, 04840 showed an association with early endosomes (EE) and EGFR-positive vesicles. Furthermore, we demonstrate that other products of the cluster are expressed during middle and late stages of the infection cycle, are associated with EBs both in the late inclusion and within the first minutes post infection, and bind to membranes with different phospholipid identity. Thus, we propose that they function as effector proteins involved in establishing the endosomal identity of the pathogen's intracellular niche.

Results

The novel *GiD_A_04840-04720* gene cluster is specific for *C. pneumoniae*

To identify chlamydial proteins with similarities to proteins involved in endocytic processes, we performed a bioinformatic screen of all 423 hypothetical proteins encoded by the genome of the *C. pneumoniae* GiD isolate (Weinmaier et al. 2015; Jantos et al. 1997) against the human genome, and sequences of effector proteins from various obligate intracellular bacterial pathogens. In this screen, the hypothetical protein GiD_A_04840 was identified, based on its 27.9% overall identity to the human GTPase Rab36, which is known to be involved in regulating vesicle traffic between the lysosome and the perinuclear region (Fig. S3A) (Chen et al. 2010).

Subsequent detailed bioinformatic analysis of the *04840* gene revealed that it belongs to a gene cluster consisting of 13 hypothetical genes, which code for proteins that display up to 59% pairwise sequence identity and which we termed "Cluster of Early Effectors 1-13" (Cee1-13) (Figs. 1A, B; 2A). The sizes of the genes within the cluster differ significantly, with three genes being less than 123 bp long, while the others range from 345 to 2088 bp in length. In our experimental subsequent studies, we focused on the products of the latter group.

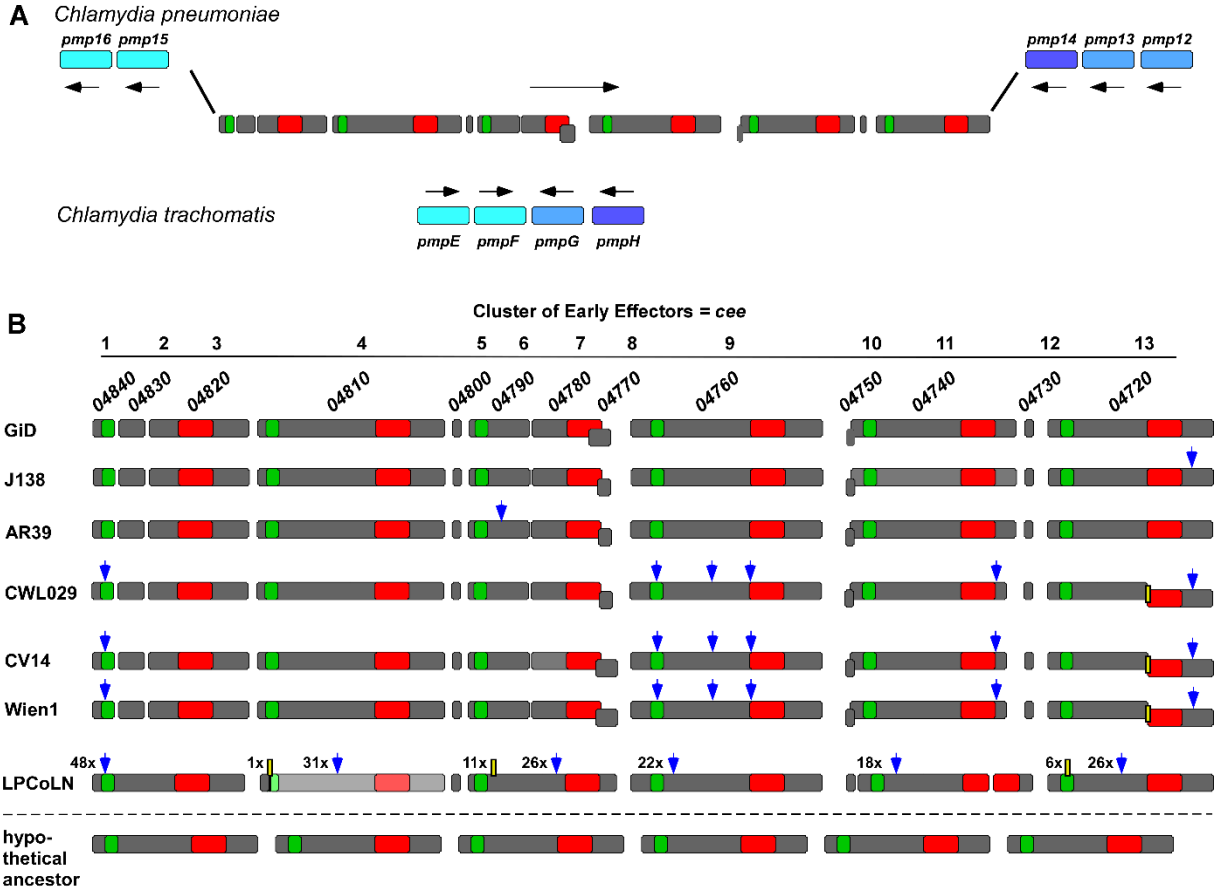

Fig. 1: The *GiD_A_cee1-cee13* gene cluster is specific for *Chlamydia pneumoniae*.

(A) Genomic context of the *C. pn* GiD *cee1-cee13* gene cluster located between *pmp15* (*C. tr. pmpE/F*) and *pmp14* (*C. tr. pmpH*) in comparison to the configuration of the corresponding genomic locus in *C. trachomatis*. Each dark grey box symbolizes one gene, and the arrows indicate their orientations in the genome. The distribution of the two predicted DUF domains, DUF575 (green box) and DUF562 (red box) is indicated. (**B)** Comparison of the GiD *cee1-cee13* gene cluster with its counterparts from six different *C. pneumoniae* isolates from humans, the chlamydial strain LPCoLN recovered from the koala (*Phascolarctos cinereus*), which is regarded as ancestral to them, and a hypothetical ancestor. The scheme shows the given (*04840-04720*) and termed ("Cluster of Early Effectors" (*cee1-13*) names and all detected sequence variations between the genes in different isolates relative to GiD. Blue arrow: bp exchange; yellow box: deletions (the digits give the number of exchanges or deletions). A gene in the LPCoLN isolate is most likely non-functional, because of a stop codon after codon 44 (light grey). The analysis detected three additional small genes *cee5*, *cee10*, and *cee12* increasing the total number to 13 genes.

The gene cluster is located between the adhesion genes *pmp15* (*C. trachomatis pmpE*) and *pmp14* (*C. trachomatis pmpH*), and is oriented in the opposite direction to these. Interestingly, two of the small genes, *cee8* and *cee10*, are in a different reading frame from the others in the cluster. The 13 proteins encoded by the GiD gene cluster show an overall identity of up to 58.5% (Cee4/Cee7) and an average identity of 32.6%. Moreover, eight of them harbor either or both of the domains of unknown function DUF575 and DUF562 (Figs.1B, 2A). The DUF575 domain, with approximately 100 amino acids (aa) length, is highly conserved within the predicted products of the cluster, with pairwise identities ranging

between 40.2% (Cee6/Cee1) and 59.8% (Cee11/Cee9) (Fig. 2B). Sequence alignments of DUF562, a domain of approximately 140 aa, show it to be more variable (Fig. 2C), with pairwise comparisons yielding identity scores of between 24.6% (Cee9/Cee3) and 66.2% (Cee7/Cee4). Secondary-structure predictions showed that all DUF575 domains consist of several α-helices and a single β-sheet, while all DUF562 domains carry alternating α-helices and β-sheets. Thus, DUF575 and DUF562 exhibit comparable secondary structures, which are in turn akin to that predicted for Rab36 (Figs. 2B, C; S3B).

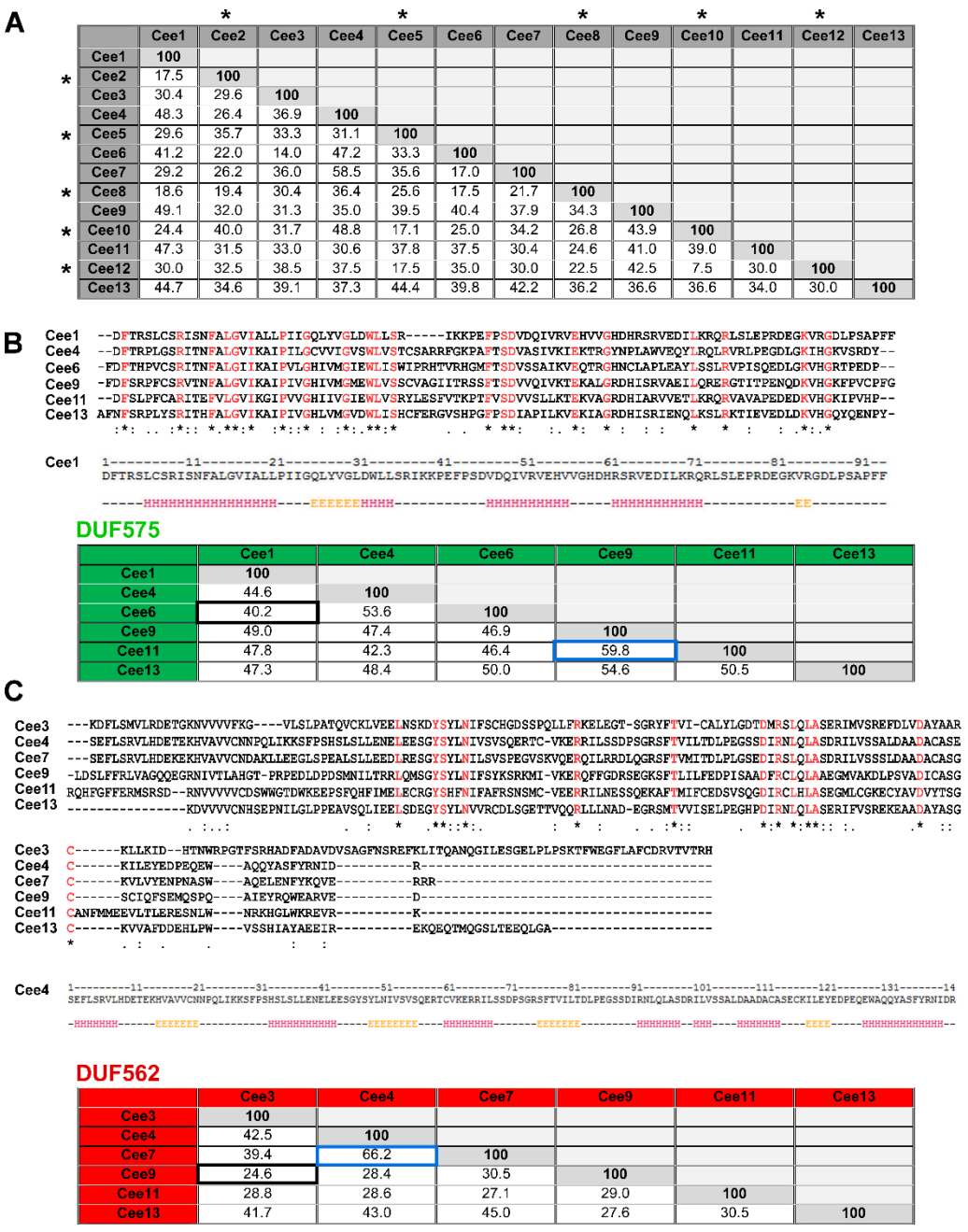

A

	Cee1	Cee2	Cee3	Cee4	Cee5	Cee6	Cee7	Cee8	Cee9	Cee10	Cee11	Cee12	Cee13
Cee1	100												
* Cee2	17.5	100											
Cee3	30.4	29.6	100										
Cee4	48.3	26.4	36.9	100									
* Cee5	29.6	35.7	33.3	31.1	100								
Cee6	41.2	22.0	14.0	47.2	33.3	100							
Cee7	29.2	26.2	36.0	58.5	35.6	17.0	100						
* Cee8	18.6	19.4	30.4	36.4	25.6	17.5	21.7	100					
Cee9	49.1	32.0	31.3	35.0	39.5	40.4	37.9	34.3	100				
* Cee10	24.4	40.0	31.7	48.8	17.1	25.0	34.2	26.8	43.9	100			
Cee11	47.3	31.5	33.0	30.6	37.8	37.5	30.4	24.6	41.0	39.0	100		
* Cee12	30.0	32.5	38.5	37.5	17.5	35.0	30.0	22.5	42.5	7.5	30.0	100	
Cee13	44.7	34.6	39.1	37.3	44.4	39.8	42.2	36.2	36.6	36.6	34.0	30.0	100

B

	Cee1	Cee4	Cee6	Cee9	Cee11	Cee13
Cee1	100					
Cee4	44.6	100				
Cee6	40.2	53.6	100			
Cee9	49.0	47.4	46.9	100		
Cee11	47.8	42.3	46.4	59.8	100	
Cee13	47.3	48.4	50.0	54.6	50.5	100

C

	Cee3	Cee4	Cee7	Cee9	Cee11	Cee13
Cee3	100					
Cee4	42.5	100				
Cee7	39.4	66.2	100			
Cee9	24.6	28.4	30.5	100		
Cee11	28.8	28.6	27.1	29.0	100	
Cee13	41.7	43.0	45.0	27.6	30.5	100

Fig. 2: The proteins of the cluster share significant levels of overall identity.

(A-C) Sequence comparison of predicted products of the GiD *cee1-cee13* gene cluster carried out with MUSCLE. https://www.ebi.ac.uk/Tools/msa/muscle/ The results are listed as % identity. **(A)** This table presents the pairwise overall identity among the proteins of the Cee1-Cee13 cluster. Asterisks (*) mark the proteins without either DUF

domain, which show the lowest overall identity to the other proteins. **(B)** Alignment of DUF575 sequences (top). Sequence identities are marked in red. Results of the alignment are listed in the table (bottom). The blue box marks the highest and the black box the lowest level of pairwise identity found. Secondary-sequence prediction was carried out with Jpred 4 and is exemplified by Cee1 (H, helical; E, extended). **(C)** Alignment of DUF562 sequences (top) with amino-acid identities marked in red. Results of the alignment are shown below (bottom). The blue box marks the highest and the black box the lowest level of pairwise identity found. Secondary-sequence prediction was carried out with Jpred 4 and is exemplified by Cee4.

Sequence comparisons with the genomes of other *Chlamydiae* species showed that the gene cluster is present only in human *C. pneumoniae* strains and in the related, phylogenetically basal isolate LPCoLN from the koala (Fig. 1A, B). Interestingly, detailed comparison of the GiD genes with those of five other human *C. pneumoniae* isolates and the ancestral koala isolate LPCoLN revealed significant differences (Fig. 1B). As a reference strain for sequence comparisons, we used our GiD isolate. Compared to GiD, the LPCoLN gene cluster harbors only 6 (larger) genes each carrying an N-terminal DUF575 and a C-terminal DUF562, plus only 3 smaller genes, thus in total only 9 genes. This suggests that, in the hypothetical common ancestor of koala and human strains, the cluster may have comprised 6 genes containing both DUF domains and that the koala isolate exhibits the first signs of gene fragmentation (Fig. 1B). In the younger human isolates, even more genes are found to be split, leading to the 13 ORFs seen today. Interestingly, the disposition and sizes of the two DUF domains are conserved among all species analyzed (Figs. 1B, S1B).

Besides gene fusions (relative to the GiD strain), the gene cluster from LPCoLN also shows a large number of single nucleotide polymorphisms (SNPs), one 6-base-pair (bp) insertion (CPK0969), and two deletions [CPK0947 (11 bp) and CPK0977 (2 bp)]. (Fig. 1B; Fig. S1A). Furthermore, the LPCoLN version of the *cee4* gene has a stop codon after codon 44, and is therefore likely to be non-functional (Figs. 1B, S1B). Moreover, one gene, the *cee11* gene in LPCoLN is actually split within the DUF562.

The variations revealed in the comparison of the human isolates involve both SNPs as well as deletions or insertions (Figs. 1B, S1A). One of the most interesting examples is a 1-bp deletion in the *cee13* homologs in the strains CWL029, CV14 and Wien1, which results in a premature stop codon and a new downstream start codon. Thus, each of these isolates harbors two short genes in this region, instead of the longer one found in the GiD isolate (Fig. 1B). When we compared the patterns of SNPs, deletions and insertions between GiD and the other respiratory (CWL029, AR39, J138) and vascular isolates (CV14, Wien1), we found that the coding sequences in GiD were virtually identical to those in AR39 and J138, with only one missense SNP distinguishing the three. Surprisingly, in this comparison the gene cluster from CWL029, as a respiratory isolate, showed the same pattern of substitutions as that observed in the two vascular isolates (Fig. 1B).

Taken together, this bioinformatic analysis characterizes a novel *C. pneumoniae*-specific gene cluster, which is conserved in the ancestral *C. pneumoniae* isolate from the koala. The distribution of mutations within human strains is (with the exception of CWL029) specific for respiratory and vascular strains, and probably represents an adaptation to the host and/or tissue.

Ectopically expressed Cee1 colocalizes with early endosomal vesicles and endocytosed EGFR

As we identified Cee1 based on its localized homology to a human Rab protein, we hypothesized that the cluster might encode a set of chlamydial effector proteins. To further test this hypothesis and to determine their subcellular localization, we constructed GFP fusion proteins of all 10 large cluster proteins and expressed each of them in human epithelial cells. We used the well characterized EGF receptor (EGFR) as a marker for the plasma membrane (PM) and for endocytotic vesicles (Fig. 3A). For four proteins (Cee8, Cee7, Cee3, Cee2) we observed a similar localization as for the GFP control, an ER-like localization for one protein (Cee11) and a vesicle-like distribution for five proteins (Cee11, Cee9, Cee6, Cee4, Cee1) (Figs. 3A, S2). Ectopic expression of Cee13 was not possible. Cee1-GFP, Cee9-GFP and Cee6-GFP also localized to the PM of transfected cells (Figs. 3A, S2). Strikingly, we found that endogenous, endocytosed EGFR colocalizes with Cee1-GFP and Cee9-GFP at the PM and also (in the case of Cee9-GFP only in part) on intracellular vesicles (Fig. 3A). Additionally, we detected a redistribution of EGFR to the ER in cells that expressed either Cee11 or Cee6 (Figs. 3A, S2).

Since Cee1 (which contains DUF575) and Cee4 (harboring both DUF575 and DUF562) are both found in association with vesicular structures, but only Cee1 colocalizes with the endocytosed EGFR, we further investigated the nature of these vesicles by performing co-localizing studies with mCherry-2xFYVE, a biosensor for the phosphoinositide PtdIns(3)P, which marks the early endosome (EE) (Fig. 3B). Indeed, while Cee1 nicely colocalizes with EGFR- and PtdIns(3)P-positive EE vesicles (Fig. 3B), the Cee4-labeled vesicles do not, although both contain the DUF575 (Fig. 3B). Thus, fusion proteins harboring DUF575 stain vesicle-like structures and show a mainly membrane association (Figs. 1A, 3A; S2). Notably Cee1 shows almost complete colocalization with EE and the PM (Fig. 3A, B).

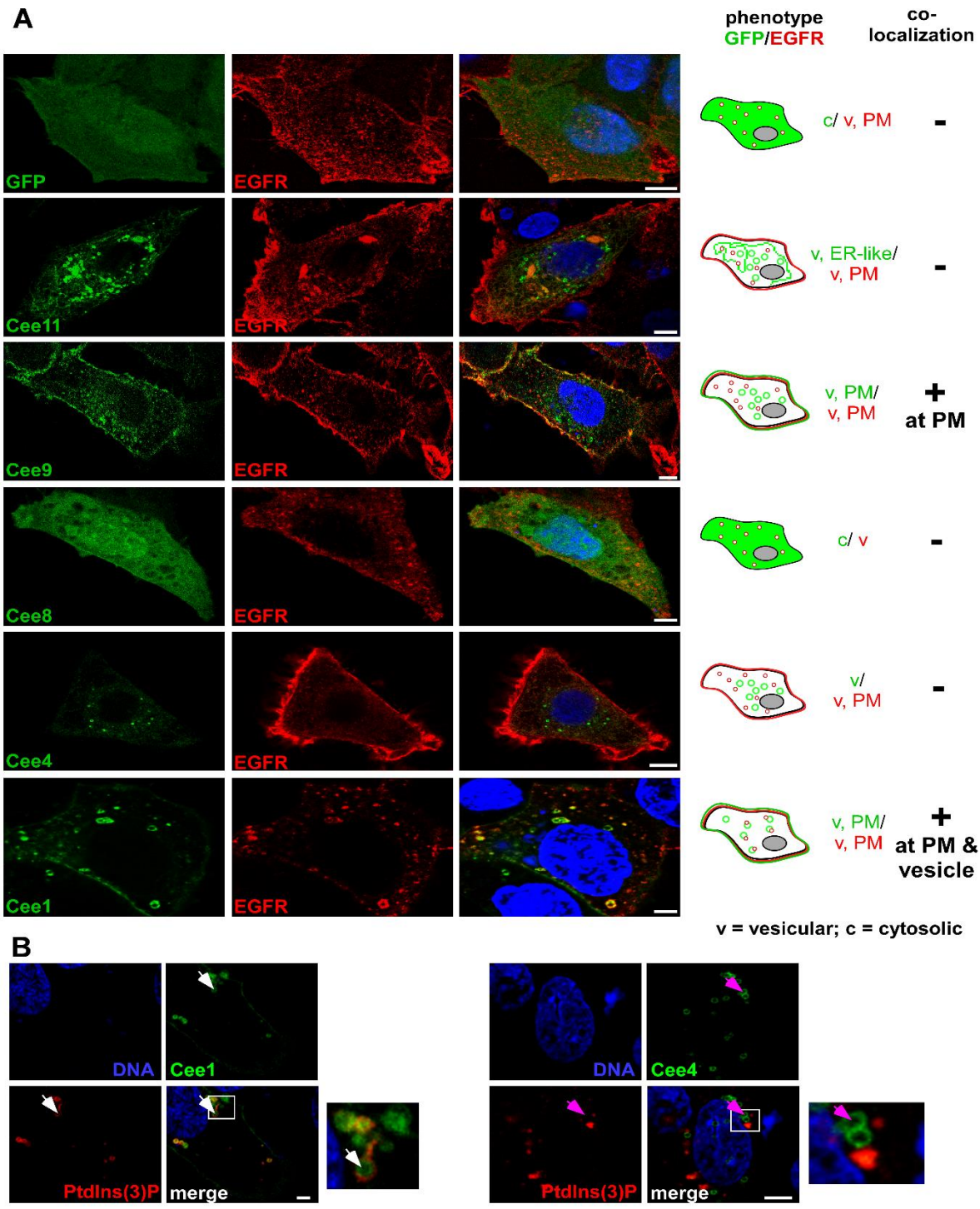

Fig. 3: In transfection experiments the proteins of the cluster show different patterns of localization, and Cee1 colocalizes with PtdIns(3)P and endocytosed EGFR.

(A) Confocal images of human epithelial cells transfected with five predicted products of the GiD gene cluster *cee1-cee13*, each fused to GFP. HEp-2 cells were transfected with the indicated GFP fusion proteins for 18 h, fixed with 3 % PFA and permeabilized with 100 % methanol. Endogenous EGFR was visualized with an anti-EGFR antibody in combination with anti-rabbit Alexa594. The DNA was stained with DAPI (blue). Bar: 10 µm. The right panel schematically depicts the localization phenotype of the GFP fusion proteins (green) and endocytosed EGFR (red). **(B)** Confocal images of Cee1 and Cee4 fused to GFP and the PtdIns(3)P membrane marker mCherry-2xFYVE (PtdIns(3)P). The white arrows indicate association of the GFP fusion protein with PtdIns(3)P; pink arrows point to instances of lack of association. Bar: 10 µm. (n =3).

A conserved sequence in Cee1 is essential for its binding to the early endosome

The EE localization of transiently expressed Cee1 prompted us to explore the role of its Rab36-like motif in this interaction (Figs. 3B, S3). A closer look revealed not only comparable secondary structures for Cee1 and Rab36, but also showed that, within the region of the highest identity between the two (aa 131 to aa 165 in Rab36), a perfect G1 box motif GXXXXGK[T/S] can be found in Rab36, while the motif present in Cee1 lacks the last two amino acids (Fig. S3A-C). The G1-box motif together with four other G box GDP/GTP-binding motif elements (G2 to G5) form the G domain, which is shared by members of the Ras superfamily of GTPases and is involved in guanine nucleotide binding (Wennerberg, Rossman, and Der 2005; Muller and Goody 2018; NCBI cited Dec 2018). In other cluster proteins harboring either or both DUF domains, up to three copies of the G1-like motif could be identified (Fig. S3D). Moreover, in six cluster proteins, up to four copies of the Rab36-like G3 motif (DXXG or DXXXG)) are also found. Finally, the proteins Cee3 and Cee4 display a single G5 motif ([C/S]A[K/L/T]) each (Fig. S3D) (NCBI, cited Dec 2018). Thus, all eight Cee proteins harboring one or both DUF domains carry one or more copies of G1, G3 or G5, but only Cee4 and Cee3 have all three.

Next, we tested whether the single G1 box motif found in Cee1 is functionally important for colocalization of the protein with a specific endosomal structure. We generated a Cee1 mutant with three of the conserved G1-box amino acids changed to alanine (Rab36: GDL**YVG**KT; Cee1: GQL**YVG**LD; Cee1mut: GQL**AAA**LD) (Fig. S3C). After transfection into human cells, Cee1mut associated with vesicular structures like the wild-type protein did; however, its specificity for particular membrane markers had changed. Approximately 40% of intracellular Cee1wt vesicles colocalized with PtdIns(3)P-positive EE vesicles; in the mutant this was reduced to around 30% (Fig. 4A, B). The recycling-specific Rab11-positive vesicles showed approximately 70% colocalization with Cee1wt, which was significantly reduced to 40% for Cee1mut (Fig. 4C, D). Similarly, Cee1wt vesicles showed 60% colocalization with the recycling-specific Rab14 protein, the mutant version only 27% (Fig. 4E, F). In contrast, both Cee1wt and Cee1mut showed the same level of colocalization with Rab7-positive, late endosomal vesicles 43% and 40%, respectively (Fig. 4G, F).

Together, these findings suggest that the conserved G1 motif in Cee1 plays an important role in directing the association of Cee1 with vesicles that display an EE or recycling endosome (RE) but not a late endosome (LE) identity.

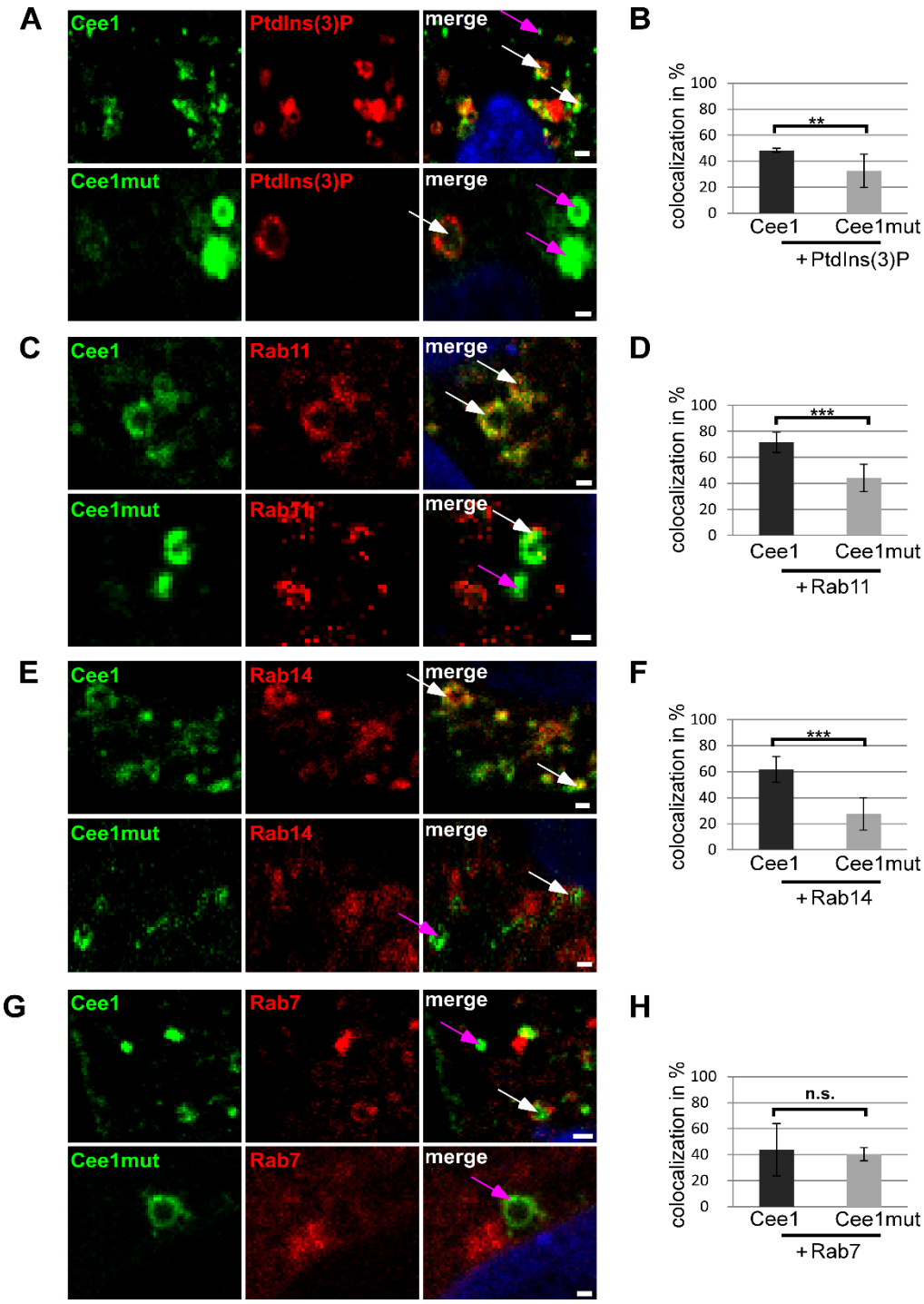

Fig. 4: The Cee1 point mutant (mut) shows reduced association with PtdIns(3)P, Rab11 and Rab14.
(A-F) Confocal images of colocalization studies with wild-type (Cee1) and mutant (Cee1mut) Cee1 proteins fused to GFP and 2xFYVE (PtdIns(3)P). The G1-box motif is intact (GQL**YVG**LD) in Cee1wt, but not in Cee1mut (GQL**AAA**LD), **(A,B),** Rab11 **(C,D)**, Rab14 **(E,F)** and Rab7 **(G,H)** fused to mCherry. Both plasmids were transfected for 18 h. White arrows indicate colocalization, pink arrows indicate instances of absence of colocalization of the protein pairs (lipids) tested. Bar: 1 µm. **(B,D,F)** Quantification of colocalization of GFP and mCherry signals counted in 20 individual transfected cells (n=3). *** *P* value ≤0.001, ** *P* value ≤0.01, n.s. *P* value ≤0.05.

Cee1 and Cee4 are associated with EBs during adhesion

Early chlamydial effector proteins are expressed at mid-to-late stages of the preceding infection cycle, and stored in the EB in preparation for secretion early in the next infection. Therefore, we analyzed the localization of Cee1 harboring DUF575 and Cee4 carrying DUF575 and DUF562 during infection. Specific antibodies against Cee1 and Cee4 confirmed that both proteins colocalized with DnaK, an RB-specific marker, during mid-infection [24 h post infection (hpi)] (Fig. 5A). Similarly, late in infection (72 hpi), Cee4 and Cee1 remain associated with DnaK-positive RBs (Fig. 5A). Additionally, we observed Cee1 and Cee4 signals associated with condensed DNA signals, which probably originate from re-differentiated EBs. We then tested whether the proteins could be detected in association with EBs early in infection. We infected HEp-2 cells, fixed them at early time points, and found Cee4 and Cee1 to be associated with adhering EBs at 0 and 5 min post infection (Fig. 5B). These results show that both proteins are associated with EBs during the adhesion step.

Next we used a solubilization assay to probe the subcellular localization of Cee4 in infectious EBs. To do so, purified *C. pneumoniae* EBs were treated with either PBS or various mild or harsh detergents. MOMP, a member of the outer membrane complex, can only be released from the EB by a combination of NP-40 and DTT, whereas the intrachlamydial protein S1 can only be partially solubilized by strong detergents, such as Sarkosyl (Fig. 5C). Both the adhesin CPn0473 and CPn0572, which is secreted by a type III secretion system (T3SS), were detectable in supernatants after mild detergent extraction with Triton X-100. The Cee4 protein shows a solubility pattern resembling those of the adhesin CPn0473 and CPn0572, implying a surface localization or a pre-loaded state in preparation for T3SS-mediated secretion (Fig. 5C).

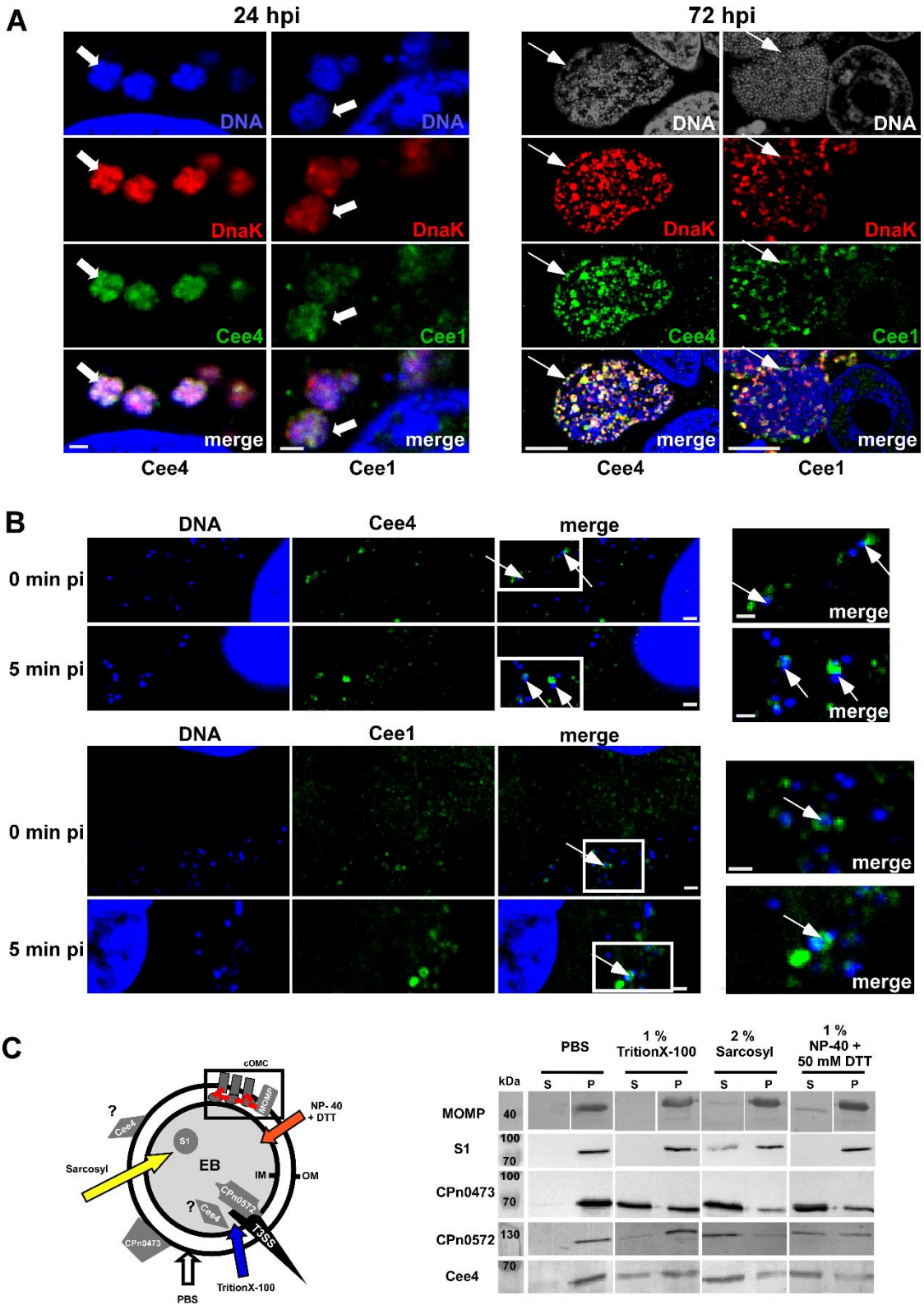

Fig. 5: Cee4 and Cee1 are expressed mid-/late in the infection cycle, associate with adhering EBs and show a solubilization pattern similar to adhesins and type III secreted proteins.

(A) Confocal images of mid-to-late *C. pneumoniae* inclusions stained with DAPI (24 hpi; 72 hpi) and for antibodies specific for Cee4, Cee1 and DnaK, visualized with anti-rabbit Alexa488/anti-mouse Alexa594 antibodies. Bold white arrows indicate colocalization of Cee4/Cee1 with DnaK. Small arrows indicate more circumscribed but stronger DNA signals (probably condensed EBs) and larger and fainter DNA signals (most likely RBs) associated with Cee4/Cee1 and DnaK. Bar: 10 µm. **(B)** Confocal images of *C. pneumoniae* EBs (stained with DAPI) attaching

to HEp-2 cells (0 min pi and 5 min pi). Endogenous Cee4 and Cee1 were visualized with specific antibodies against Cee4/Cee1 and anti-rabbit Alexa488. Boxed areas from the merged images are shown enlarged in the panel on the right. Association of EBs and Cee4/Cee1 is marked by white arrows. Bar: 1 µm. **(C)** Pattern of solubilization of the indicated proteins from purified *C. pneumoniae* EBs following exposure to PBS, 1 % Triton X-100, 2% Sarkosyl and 1 % NP40 + 50 mM DTT for 1 h at 37 °C. The panel on the left shows a model of the *C. pn* EB indicating the localization of the different proteins (grey) tested in the assay. The type III secretion needle (T3SS) is shown in black and the outer (OM) and inner (IM) membranes are represented by black circles. The chlamydial outer membrane complex (cOMC) is shown schematically within the black box. Disulfide bonds are depicted in red. The arrows in different colors indicate the detergents used in the assay. The panel on the right shows an immunoblot analysis of *C. pneumoniae* EBs treated with PBS alone or in combination with different detergents. Samples were divided into pellet (P) and supernatant (S) fractions by centrifugation and analyzed by SDS/PAGE using specific antibodies against the analyzed protein. (n=2).

Proteins of the cluster can bind to membranes of different phosphoinositide identity

The fact that proteins encoded in the cluster associate with membranes, e.g. the PM and early endosomal membranes (Fig. 3), suggests that they may bind to membranes directly. In order to test this, we performed adhesion studies with selected recombinant versions of proteins encoded by the cluster (Fig. 6A). As the positive control we used the adhesin CPn0473 (Fechtner, Galle, and Hegemann 2016), as a negative control GST (Fig. 6A). Interestingly, Cee4 and Cee1, both of which carry DUF575, bind to HEp-2 cells (Fig. 6A). In contrast, Cee3, which contains only DUF562, and Cee2 (which has neither DUF) did not bind to these cells (Fig. 6A). Furthermore, the DUF575 domain is essential for adhesion, as Cee4$^{121\text{-}672}$, a DUF575 deletion derivative of Cee4, showed strongly reduced adhesion to HEp-2 (Fig. 6A). These data indicate that DUF575 plays a critical role in the ability of Cee4 to bind to the PM of epithelial cells.

Next, we tested whether the binding of the DUF575-containing proteins to the host cell PM is relevant for the initial phase of infection. Cells were pre-incubated with the recombinant protein (in order to saturate potential binding sites on HEp-2), prior to exposure to *C. pneumoniae* EBs, and infection levels were compared to that of cells pre-incubated with PBS buffer; BSA served as a negative control. The positive control heparin blocks OmcB-mediated adhesion, reducing the infection rate by 96% (Fig. 6C). In contrast, pre-incubation with Cee1, Cee4 or Cee4$^{121\text{-}672}$ (all of which showed some capacity to bind to human cells) had very little (Cee1) or no influence on the subsequent *C. pneumoniae* infection (Fig. 6C). These data indicate that some cluster proteins have the ability to bind to the human PM but do not play a role in the EB adhesion process.

We then asked whether proteins encoded by the cluster act as monomers or oligomers, using Blue Native PAGE (BN/PAGE) to assess complex formation (Fig. 6B). All proteins carrying either one or both DUF domains formed high-molecular-weight homomeric oligomers with more than 10 molecules per complex. In contrast, Cee8 which lacks both DUF

domains formed smaller, tetrameric complexes (Fig. 6B). These results indicate the cluster proteins oligomerize and that both DUF domains contribute to the formation of large oligomers.

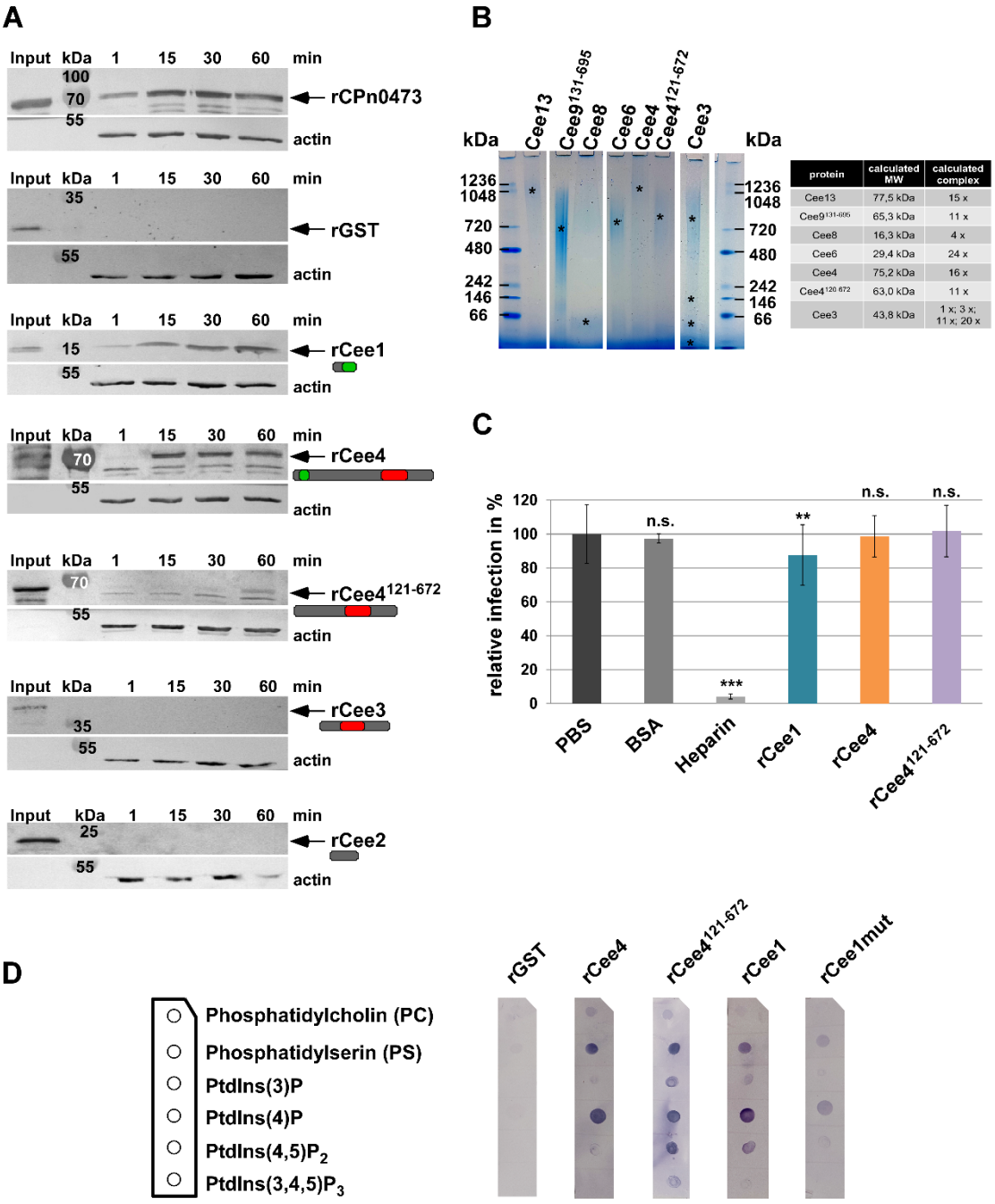

Fig. 6: Proteins encoded by the *cee1-cee13* gene cluster in *C. pn* adhere to the plasma membrane and bind to different PtdIns, but have no influence on infectivity.

(A) Adhesion of His-tagged recombinant proteins to HEp-2 cells. HEp-2 cells were incubated with the indicated recombinant proteins for the times specified points. Unbound protein was washed away and the amount of protein bound to the PM was analyzed on immunoblots with an anti-His antibody and secondary anti-mouse antibody and compared to the input level. The arrows indicate the respective protein bands. The positions of molecular-weight markers are also indicated. **(B)** Portions of non-denaturing Blue Native-PA gels that had been loaded with 1 µg of the indicated renatured recombinant protein per lane, and stained with Coomassie blue. Asterisks mark the

centers of each band distribution. The numbers of molecules in each high-molecular-weight complex (marked by the asterisks) was calculated based on the theoretical MW of the respective protein (shown in the Table). **(C)** Results of infection blocking assays using 100 µg/ml of each indicated blocking agent. BSA and heparin were used as controls (grey). Relative infectivity was determined by comparing the number of inclusions per human cell and is expressed as a percentage of the number of inclusions determined for the PBS-treated control sample (dark grey). Data shown are means. *** *P* value ≤0.001, ** *P* value ≤0.01, n.s. *P* value ≤0.05. (n=6). **(D)** Membrane lipid strip assay with recombinant protein variants of the cluster. Scheme of the membrane lipid strip is shown on the left side. Membrane lipid strips were incubated with 1 µg/ml His-tagged rGST, rCee4, rCee4$^{121-672}$, rCee1 and rCee1mut and analyzed with anti-His antibody (n=2).

Given that these proteins have the ability to bind to the PM of human cells and to EEs, we tested for binding to phospholipids and phosphoinositides (PtdIns). The control, rGST, did not bind to any of the lipids displayed on the membrane strips used (Fig. 6D). In contrast, Cee1 showed significant binding to PS and PtdIns(4)P, both predominantly located in the inner leaflet of the PM. Moreover, weak binding to PtdIns(3)P (which is enriched in the EE envelope) and PtdIns(4,5)P_2 was observed (Fig. 6D). Interestingly, Cee1mut showed a significantly reduced binding (Fig. 6D). Cee4 also showed binding to PS and PtdIns(4)P_2 and very weak binding to PC, which is the major phospholipid in the PM (Fig. 6D). Strikingly, the Cee4 variant without DUF575 bound to all phospholipids and PtdIns on the membrane, with weaker binding to PC, PtdIns(3)P and PtdIns(3,4,5)P_3, suggesting that DUF575 mediates binding specificity to membranes with specific PtdIns identity (Fig. 6D).
Taken together, these results show that the proteins of the cluster bind to membranes with different PtdIns identity, which seems to be mediated in part by the DUF575.

Discussion

As an obligate intracellular pathogen, *C. pneumoniae* must first gain entry to the host cell in order to set up a productive infection. After internalization, *Chlamydia* reside in a membrane-bound compartment called an inclusion. The early inclusion retains the GTPases Rab11 and Rab14 that it acquired during the preceding infection cycle. These markers designate the inclusion as a slowly recycling endosome that is protected from degradation, thus enabling a further chlamydial replication cycle to proceed (Molleken and Hegemann 2017). How *Chlamydiae* subvert membrane traffic to avoid transport to degradative intracellular compartments is not understood. Here we provide evidence that *C. pneumoniae* secretes early effector proteins that exhibit certain Rab characteristics, which have the capacity to bind to host-cell membranes, associate with EE and RE markers in transfection experiments, and which are found in infectious EBs.

The novel *C. pneumoniae*-specific gene cluster that codes for these effector proteins was identified based on a 27.9% overall identity of one of its predicted products (Cee1) to the human GTPase Rab36. Rab36 is one the lesser-known Rab family members; however, available data indicate a possible regulatory role in the spatial distribution of LE and lysosomes (Chen et al. 2010). The chromosomal *cee13-cee1* DNA segment is inserted within one of the *pmp* gene clusters between *pmp15* and *pmp14*. In the related *C. pneumoniae* strain LPCoLN isolated from the koala, which is regarded as the ancestor of all human strains, several of the genes found in the GiD strain are fused, resulting in a nine-gene cluster. This finding is similar what has been found for the *pmp* gene family. In that case, it has been shown that the LPCoLN isolate encodes the largest number of full-length *pmps* of all *C. pneumoniae* strains examined (Myers et al. 2009; Van Lent et al. 2016). Thus, both the *pmp* and the *cee* gene cluster show similar patterns of adaptation from the koala to the human isolates, and therefore, the pattern of split and fused *pmp* and *cee* genes can possibly be used to differentiate between animal and human *C. pneumoniae* isolates (Mitchell et al. 2010). Moreover, we speculate that the hypothetical ancestor of both the koala and the modern human isolates carried only six fused genes containing both DUF domains. Thus, during adaptation to the koala host the first gene splits took place and the subsequent zoonotic events, followed by further adaptation in humans, are responsible for the gene structure found in the modern human isolates (Fig. 1B).

Moreover, comparison of our gene cluster from the respiratory GiD isolate with those from other *C. pneumoniae* isolates from humans revealed significant differences between respiratory and vascular isolates. Interestingly, the respiratory isolate CWL029 shows the same SNPs and the 1-bp deletion in the *cee* gene cluster as those found in the vascular isolates, in accordance with a SNP-based phylogenetic tree of various *C. pneumoniae* isolates, in which the CWL029 isolate is closer to CV14 and Wien1 than to the respiratory

isolates (Weinmaier et al. 2015). Thus very likely, the observed differences in the gene cluster of respiratory and vascular isolates represent an adaptation to the initial site of infection (tissue) and even the host.

The first member of the cluster identified, the Cee1 protein, was detected on the basis of its homology to Rab36, which reaches its maximum (35.5%) within a 31-aa domain (orange box; Fig. S3A). Every known Rab protein harbors a G domain with five G-box motifs (G1 to G5) which is responsible for guanine nucleotide binding (Muller and Goody 2018). Rab36 has a complete G1 motif (GXXXXGK[T/S]) (black box) within the domain of high identity, while the G1-box motif in Cee1 lacks the last two aa at its C-terminus. Surprisingly, this incomplete G1-box motif (GXXXXG) is found at least once in each DUF575 domain. Moreover, five out of six DUF562 domains carry at least one G3-box motif, and two of them harbor in addition a single G5-box motif. Importantly, none of the cluster proteins harbors detectable G2- or G4-box motifs. Moreover, with an incomplete G1 box motif and no G2- or G4-box motifs, it is unlikely that any of these proteins is able to bind guanine nucleotides. Thus, the role(s) of the G1, G3 and G5 boxes in the cluster proteins remain(s) enigmatic. However, all cluster proteins exhibit some secondary structure similarity with Rab36. Thus, it is tempting to speculate that the cluster proteins may mimic some structural and possibly also functional aspects of human Rab proteins, specifically Rab36. A role for Rab36 during infection by *C. pneumoniae* has not been described so far. Other intracellular pathogens have been shown to manipulate Rab-controlled vesicular transport to ensure their own survival (for reviews see: (Stein, Muller, and Wandinger-Ness 2012; Muller and Goody 2018). *Salmonella* and *Legionella pneumophila* secrete the effector proteins SopB and VipD respectively, both of which interact with the early endosomal Rab5 protein to prevent binding to downstream effectors in order to modulate the surface of the pathogen-containing vacuole (Spano and Galan 2018; Gaspar and Machner 2014; Ku et al. 2012). Moreover, both pathogens also inject additional effector proteins, DrrA and SopE respectively, into the host cytosol and use their guanine nucleotide exchange factor (GEF) activities to recruit and mislocalize Rab1 and Rab5 respectively (Murata et al. 2006; Schoebel et al. 2009; Mukherjee et al. 2001). *Salmonella* Typhimurium also secrets its SopD2 effector, which possesses GAP activity toward Rab32 (Spano et al. 2016). As expected, the Cee proteins, with their distinct similarities to Rab proteins, show no similarity to these known Rab-interacting bacterial effector proteins.

Interestingly, ectopic expression of individual members of the Cee1-13 cluster in epithelial human cells revealed a 100% correlation (5 out of 5; Cee13 could not be ectopically expressed) between the presence of DUF575 and a vesicular and membrane localization phenotype. Furthermore, Cee1 itself showed a significant association with EGFR-, PtdIns(3)P-, Rab11-, Rab14- and Rab7-positive EEs, which are known markers of the early

C. pneumoniae inclusion (Molleken and Hegemann 2017). Point mutation of the conserved G1-box motif in the DUF575 of Cee1 revealed a specific and essential role of its G1 box motif in mediating its association with EEs and REs. Moreover, recombinant rCee1 and rCee4 bind to the PM of epithelial cells in a DUF575-dependent manner, and bind specifically to phospholipids of the inner leaflet of the PM, e.g. phosphatidylserine and PtdIns(4)P, presumably post-infection. These data strongly suggest a DUF575-dependent interaction of this protein family with specific membranes; however, how the proteins are recruited to these membranes is unknown at present. Intriguingly, both Cee4 and Cee1 were found to be associated with invading EBs by 5 min pi., strongly suggesting a role of these proteins on the immature inclusion membrane. None of them carries a C-terminal cysteine residue, thus Cee4 and Cee1 cannot localize to internal membranes by post-translational prenylation, which is a prerequisite for membrane localization and function of Rab proteins. Thus, it is likely that Cee4 and Cee1 are secreted – possibly by a T3SS (as they do not contain an identifiable secretion signal for Sec-dependent transport across the chlamydial PM) – into the host cytosol early in infection, where they may interact with the endosomal membrane by binding to specific phospholipids and/or unknown membrane-associated human or chlamydial proteins. Active Rab proteins (in their GTP-bound form) are recruited to specific membranes, where they regulate different steps in vesicular trafficking, and fuse with, or tether target membranes together (Muller and Goody 2018). The cluster proteins may mimic aspects of Rab protein function by interacting with Rab-specific effector proteins. The two DUF562-harboring cluster proteins Cee3 und Cee7 showed a cytosolic localization after transfection, and the recombinant Cee3 protein did not bind the PM. However, DUF562- as well as DUF575-harboring proteins are able to form homomeric structures. The similarities between the proteins encoded by the cluster suggest that, during infection, even heteromeric complex formation might be possible, which would allow recruitment of all cluster proteins to (different) endosomal membranes.

In conclusion, we would like to speculate that the cluster proteins may function during early infection as molecular mimetics of Rab proteins. They may be recruited by specific human Rab-interacting proteins located at specific endosomal membranes and thus block their interaction with Rab proteins. Alternatively, the cluster proteins may bind directly to membranes and themselves recruit specific Rab-interacting proteins. This could result in local depletion of specific Rab effector proteins and thus inactivate the corresponding Rab proteins at the inclusion membrane, or alternatively, the recruited Rab effector proteins are activated to promote maturation of the inclusion. Thus this set of effector proteins may act via a novel mechanism to manipulate Rab proteins for the maturation process of the chlamydial inclusion compartment.

Materials and Methods

Antibodies

Primary antibodies against DnaK were kindly provided by S. Birkelund (Birkelund, Lundemose, and Christiansen 1990). Antibodies directed against recombinant Cee4 and Cee1 were produced by Eurogentec (Seraing, Belgium) and purified for this study. Anti-CPn0572, -CPn0473, -CPn0147 and -MOMP antibodies were generated in our lab. The anti-GST antibody was purchased from Cell Signaling Technology (Frankfurt am Main, Germany), the anti-His antibody from Qiagen (Hilden, Germany), the anti-EGFR antibody from Thermo-Fisher Scientific (Waltham, Massachusetts, USA) and the anti-β-actin antibody from Merck Millipore (Darmstadt, Germany). Secondary anti-rabbit/mouse antibodies coupled to Alexa 488 and 594 for immunofluorescence were purchased from Thermo-Fisher Scientific. Secondary anti-rabbit/mouse antibodies coupled to AP conjugate for immunoblot analysis were obtained from Promega (Fitchburg, Wisconsin, USA).

Cloning procedures and vector constructs

The genes *cee1* to *cee13* were amplified from *C. pneumoniae* GiD DNA by PCR and integrated into pKM55 (C-terminal GFP) or pSL4 (C-terminal 10x His-Tag). Coding sequences for Rab7, Rab11-a and Rab14 were amplified from pGreenLanternRab7, pEGFP-C2-Rab11a, and pEGFP-C1-Rab14, respectively, and for 2xFYVE from pGFP-FYVE(2x), and each cDNA was integrated into pAE66 (N-terminal mCherry). All constructs were generated by homologous recombination in *S. cerevisiae* and verified by sequencing.

Growth of *Chlamydia* and human cell lines

HEp-2 cells were cultured in DMEM medium supplemented with 10% fetal calf serum (FCS), MEM vitamins and non-essential amino acids (Thermo Fisher Scientific). *C. pneumoniae* GiD EBs were propagated in HEp-2 cells (ATCC: CCL-23). Elementary bodies (EBs) were purified using a 30% gastrografin solution (Bayer; Leverkusen, Germany) and stored in SPG buffer (220 mM sucrose, 3.8 mM KH_2PO_4, 10.8 mM Na_2HPO_4, 4.9 mM L-glutamine).

Infection experiments

HEp-2 cells were exposed to *C. pneumoniae* GiD EBs (MOI 1) by centrifugation at 2900 rpm (Rotanda, Hettich) for 20 min (early infection time points 0, 5 and 15 min) or 60 min (mid-/ late infection time points 24 h and 72 h) at 25 °C. After centrifugation, cells were shifted to 37

°C to initiate infection, and grown under 6% CO_2 for periods ranging from 0 min to 72 h prior to fixation with 3% paraformaldehyde in PBS (PFA) for 10 min at RT.

Transfection experiments

HEp-2 cells were grown in 24-well plates (Sarstedt; Nümbrecht, Germany) on coverslips for 24 h in complete medium with FCS. For transfection, fresh medium without FCS was added and cells were transfected for 18 h using TurboFect (Thermo-Fisher Scientific). The cells were then fixed with 3% paraformaldehyde and analyzed by confocal microscopy (Nikon Confocal C2plus).

Solubilization assay

C. pneumoniae EBs (1×10^7) were centrifuged for 30 min at 4 °C and 15,000 x g. The pellet was resuspended in PBS (sonification bath) and incubated with PBS (control), 1 % Triton-X 100, 2% Sarkosyl or 1% NP-40 + 50 mM DTT at 37 °C for 1 h with a short burst of sonification every 10 min, then centrifuged for 1 h at 4 °C and 100,000 x g. The supernatant was recovered and the pellet resuspended in PBS. Samples of pellet and supernatant fractions were subjected to SDS/PAGE and analyzed with specific antibodies after Western blotting.

Adhesion assay

Confluent monolayers of HEp-2 cells were grown in 24-well plates (Sarstedt). The spent medium was removed and replaced with fresh DMEM (250 µl) containing recombinant His-tagged protein (100 µg/ml) and incubated at 37 °C in the presence of 6% CO_2. The medium was removed after 1 min, 15 min, 30 min and 60 min and the unbound protein washed away with HBSS. The cells were then detached with cell dissociation solution (Merck Millipore). The suspension was transferred to a new reaction tube and centrifuged for 5 min at 1000 x g. Supernatant was discarded and the pellet resuspended in PBS. The sample was analyzed by SDS/PAGE and the proteins detected with a specific anti-His antibody.

Infection blocking assay

HEp-2 cells were grown as described in the previous paragraph. DMEM medium was removed and 250 µl (100 µg/ml) of recombinant protein in DMEM medium was added to the cells and incubated at 37 °C and 6% CO_2 for 1 h. Unbound protein was washed away, the cells infected with *C. pneumoniae* GiD (MOI 1) and incubated for 2 h. EB solution was removed, replaced with fresh medium supplemented with cycloheximide (1.2 µg/ml) and incubated for 48 h. Cells were fixed with 3% PFA, permeabilized with 100% methanol and

the inclusion stained with anti-CPn0147 antibody. DNA was visualized with DAPI. The number of nuclei and inclusions was quantified by confocal imaging.

Protein purification

His-tagged proteins were expressed in *E. coli* BL21 and purified under denaturing conditions from cell lysates by affinity chromatography on Ni-NT agarose columns (Merck Millipore).

Blue Native PAGE

A precast Native PAGE 3-12% Bis Tris gel (Thermo Fisher Scientific) was placed in a XCell SureLock Mini Cell (Thermo Fisher Scientific) and the inner chamber filled with Native PAGE Light blue buffer (2.5 mM Bis Tris, 2.5 mM Tricine, 0,05 g Coomassie G-250; pH 6.8; cathode buffer). Two µg protein was prepared in native PAGE sample buffer (4x; 50 mM Bis Tris, 6 N HCl, 50 mM NaCl, 10% glycerol, 0.001% Ponceau S; pH 7.2) and loaded in the wells. NativeMark Protein Std (Thermo Fisher Scientific; LC0725) was loaded in one well and the outer chamber filled with native PAGE running buffer (2.5 mM Bis Tris, 2.5 mM Tricine; pH 6.8; anode buffer). Electrophoresis was performed at 4 °C at 150 V (8-10 mA) for 60 min and then at 250 V (2-4 mM) for 45 min. Proteins were visualized by Coomassie staining.

Lipid strip assay

Aliquots (1.5 µg) of test lipids were spotted on a PDVF membrane (Merck Millipore) and left to dry at RT for 1 h. The membrane was then exposed to a blocking solution (3% BSA (fatty acid free, Serva; Heidelberg, Germany) + 0.1% Tween (w/v)) and incubated overnight at 4 °C with 2 µg/ml of the test protein. After washing with PBS-T (1x PBS pH 7.4 + 0.1% Tween), binding of the protein was analyzed with the appropriate anti-His antibody.

Immunofluorescence staining

Transfected and infected HEp-2 cells were fixed at the indicated time points with 3% paraformaldehyde in PBS (PFA) for 10 min, then washed three times with HBSS and permeabilized with either 100% methanol for 10 min at room temperature or with 2% saponin (Merck) in PBS for 20 min at 30 °C. Cells were analyzed for the subcellular localization of proteins from the 04840-04720 cluster by confocal microscopy (Nikon Confocal C2plus). Primary antibodies were diluted in PBS or 0.5% saponin solution, applied to the cells, and incubated at 30 °C for 30 min. Cells were washed three times with PBS with or without 0.5% saponin, and then incubated with secondary antibody anti-rabbit/mouse Alexa488/Alexa594 at 30 °C for 30 min. DAPI was used to visualize DNA.

Microscopy and image processing

Immunofluorescence microscopy was performed on an inverse Nikon TiE Live Cell Confocal C2plus equipped with a 100x TIRF objective and a C2 SH C2 Scanner. All images and image-related measurements were generated with Nikon Element software.

Bioinformatic analysis

Sequence comparisons of proteins of the *C. pneumoniae* GiD cluster (Cee1-Cee13) were carried out with MUSCLE: https://www.ebi.ac.uk/Tools/msa/muscle/. The identity between the proteins was determined by using the Clustal W output of the MUSCLE alignment tool. Secondary-structure predictions were carried out with Jpred 4: http://www.compbio.dundee.ac.uk/jpred/.

Statistical analysis

The data represent the means (±SD) of *n* experiments. A Student's *t*-test was chosen for simple paired analysis between two groups. *** *P* value ≤0.001, ** *P* value ≤0.01. A *P* value of ≤0.05 was considered non-significant (n.s.).

Accession numbers

Homo sapiens Epidermal growth factor receptor (EGFR): NM_005228.3

Canis lupus Rab7a: NM_001003316.1

Homo sapiens Rab11a: AF000231.1

Homo sapiens Rab14: NM_016322.3

Chlamydia pneumoniae GiD: LN847009.1

Chlamydia pneumoniae J138: NC_002491.1

Chlamydia pneumoniae AR39: NC_002180.1

Chlamydia pneumoniae CWL029: NC_000922.1

Chlamydia pneumoniae CV14: NZ_LN846996.1

Chlamydia pneumoniae Wien1: NZ_LN846980.1

Chlamydia pneumoniae LPCoLN: NC_017285.1

Acknowledgements

For funding, we thank the Strategischer Forschungsfonds SFF-F2014_730-8 Mölleken. The funders had no role in study design, data collection and interpretation, or the decision to submit the work for publication. We thank Dr. Elisabeth Becker for help with the MOMP solubilization assay in Fig. 5 and Mona Höhler for adhesion assay of Cee2 in Fig.6.

References

1. Hahn DL, Dodge RW, Golubjatnikov R. Association of Chlamydia pneumoniae (strain TWAR) infection with wheezing, asthmatic bronchitis, and adult-onset asthma [see comments]. Jama. 1991;266(2):225-30.
2. Chi EY, Kuo CC, Grayston JT. Unique ultrastructure in the elementary body of Chlamydia sp. strain TWAR. J Bacteriol. 1987;169(8):3757-63.
3. Miyashita N, Kanamoto Y, Matsumoto A. The morphology of Chlamydia pneumoniae. J Med Microbiol. 1993;38(6):418-25.
4. Wolf K, Fischer E, Hackstadt T. Ultrastructural analysis of developmental events in Chlamydia pneumoniae-infected cells. Infect Immun. 2000;68(4):2379-85.
5. Moelleken K, Hegemann JH. The Chlamydia outer membrane protein OmcB is required for adhesion and exhibits biovar-specific differences in glycosaminoglycan binding. Mol Microbiol. 2008;67(2):403-19.
6. Mölleken K, Becker E, Hegemann JH. The Chlamydia pneumoniae invasin protein Pmp21 recruits the EGF receptor for host cell entry. PLoS Pathog. 2013;9(4):e1003325.
7. Madshus IH, Stang E. Internalization and intracellular sorting of the EGF receptor: a model for understanding the mechanisms of receptor trafficking. J Cell Sci. 2009;122(Pt 19):3433-9.
8. Jovic M, Sharma M, Rahajeng J, Caplan S. The early endosome: a busy sorting station for proteins at the crossroads. Histology and histopathology. 2010;25(1):99-112.
9. Jean S, Kiger AA. Coordination between RAB GTPase and phosphoinositide regulation and functions. Nat Rev Mol Cell Biol. 2012;13(7):463-70.
10. Di Fiore PP, von Zastrow M. Endocytosis, signaling, and beyond. Cold Spring Harbor perspectives in biology. 2014;6(8).
11. Molleken K, Hegemann JH. Acquisition of Rab11 and Rab11-Fip2-A novel strategy for Chlamydia pneumoniae early survival. PLoS Pathog. 2017;13(8):e1006556.
12. Weinmaier T, Hoser J, Eck S, Kaufhold I, Shima K, Strom TM, et al. Genomic factors related to tissue tropism in Chlamydia pneumoniae infection. BMC Genomics. 2015;16:268.
13. Jantos CA, Heck S, Roggendorf R, Sen-Gupta M, Hegemann JH. Antigenic and molecular analyses of different Chlamydia pneumoniae strains. J Clin Microbiol. 1997;35:620-3.
14. Chen L, Hu J, Yun Y, Wang T. Rab36 regulates the spatial distribution of late endosomes and lysosomes through a similar mechanism to Rab34. Molecular membrane biology. 2010;27(1):23-30.
15. Wennerberg K, Rossman KL, Der CJ. The Ras superfamily at a glance. J Cell Sci. 2005;118(Pt 5):843-6.

16. Muller MP, Goody RS. Molecular control of Rab activity by GEFs, GAPs and GDI. Small GTPases. 2018;9(1-2):5-21.
17. NCBI NNCfBI. National Library of Medicine (US). National Center for Biotechnology Information; [1988]. cited Dec 2018.
18. Fechtner T, Galle JN, Hegemann JH. The novel chlamydial adhesin CPn0473 mediates the lipid raft-dependent uptake of Chlamydia pneumoniae. Cell Microbiol. 2016;18(8):1094-105.
19. Myers GS, Mathews SA, Eppinger M, Mitchell C, O'Brien KK, White OR, et al. Evidence that human Chlamydia pneumoniae was zoonotically acquired. J Bacteriol. 2009;191(23):7225-33.
20. Van Lent S, Creasy HH, Myers GS, Vanrompay D. The Number, Organization, and Size of Polymorphic Membrane Protein Coding Sequences as well as the Most Conserved Pmp Protein Differ within and across Chlamydia Species. J Mol Microbiol Biotechnol. 2016;26(5):333-44.
21. Mitchell CM, Hovis KM, Bavoil PM, Myers GS, Carrasco JA, Timms P. Comparison of koala LPCoLN and human strains of Chlamydia pneumoniae highlights extended genetic diversity in the species. BMC Genomics. 2010;11:442.
22. Stein MP, Muller MP, Wandinger-Ness A. Bacterial pathogens commandeer Rab GTPases to establish intracellular niches. Traffic. 2012;13(12):1565-88.
23. Spano S, Galan JE. Taking control: Hijacking of Rab GTPases by intracellular bacterial pathogens. Small GTPases. 2018;9(1-2):182-91.
24. Gaspar AH, Machner MP. VipD is a Rab5-activated phospholipase A1 that protects Legionella pneumophila from endosomal fusion. Proc Natl Acad Sci U S A. 2014;111(12):4560-5.
25. Ku B, Lee KH, Park WS, Yang CS, Ge J, Lee SG, et al. VipD of Legionella pneumophila targets activated Rab5 and Rab22 to interfere with endosomal trafficking in macrophages. PLoS Pathog. 2012;8(12):e1003082.
26. Murata T, Delprato A, Ingmundson A, Toomre DK, Lambright DG, Roy CR. The Legionella pneumophila effector protein DrrA is a Rab1 guanine nucleotide-exchange factor. Nature cell biology. 2006;8(9):971-7.
27. Schoebel S, Oesterlin LK, Blankenfeldt W, Goody RS, Itzen A. RabGDI displacement by DrrA from Legionella is a consequence of its guanine nucleotide exchange activity. Molecular cell. 2009;36(6):1060-72.
28. Mukherjee K, Parashuraman S, Raje M, Mukhopadhyay A. SopE acts as an Rab5-specific nucleotide exchange factor and recruits non-prenylated Rab5 on Salmonella-containing phagosomes to promote fusion with early endosomes. J Biol Chem. 2001;276(26):23607-15.
29. Spano S, Gao X, Hannemann S, Lara-Tejero M, Galan JE. A Bacterial Pathogen Targets a Host Rab-Family GTPase Defense Pathway with a GAP. Cell Host Microbe. 2016;19(2):216-26.
30. Birkelund S, Lundemose AG, Christiansen G. The 75-kilodalton cytoplasmic Chlamydia trachomatis L2 polypeptide is a DnaK-like protein. Infect Immun. 1990;58(7):2098-104.

Supplement information

A

GiD respiratory; Gießen, Germany	AR39 respiratory pharynx; Seattle, USA		J138 respiratory pharynx; Japan		CWL029 respiratory throat; Atlanta,USA		CV14 vascular coronary artery; Mainz, Germany		Wien1 vascular carotid artery; Vienna, Austria		LPCoLN respiratory nasal swab (koala); Australia	
gene name	**gene name**	**number of SNP's**	**gene name**	**number of SNP's**	**gene name**	**number of SNP's**	**gene name**	**number of SNP's**	**gene name**	**number of SNP's**	**gene name**	**number of SNP's**
Cee13	CP0297	0	CPj0456	1	CPn0455	1	A04700	1	A04670	1	CPK0969	6 bp deletion s 26 SNP
					CPn0456	1 (bp deletion)	A04710	1 (bp deletion)	A04680	1 (bp deletion)		
Cee11	CP0295	0	CPj0457	0	CPn0457	0	A04730	1	A04700	1	CPK0971	18; shorter C-terminu s
Cee9	CP0294	0	CPj0458	0	CPn0458	3	A04750	3	A04720	3	CPK0973	22
Cee8	CP0293	0	CPj0459	0	CPn0459	0	A04760	0	A04730	0	CPK0974	11 bp deletion s 6 SNP
Cee7	CP0292	0	CPj0460	0	CPn0460	0	A04770	0	A04740	0	CPK0974	9
Cee6	CP0291	1	CPj0461	0	CPn0461	0	A04780	0	A04750	0	CPK0974	11
Cee4	CP0290	0	CPj0462	0	CPn0462	0	A04800	0	A04770	0	CPK0977 no protein	1 deletion 31 SNP
Cee3	CP0289	0	CPj0463	0	CPn0463	0	A04810	0	A04780	0	CPK0979	24
Cee2	CP0288	0	CPj0464	0	CPn0464	0	A04820	0	A04790	0	CPK0979	15
Cee1	CP0287	0	CPj0465	0	CPn0465	1	A04830	1	A04800	1	CPK0979	9

B

GiD respiratory; Gießen, Germany		CWL029 respiratory throat; Atlanta,USA		LPCoLN respiratory nasal swab (koala); Australia	
gene name	**aa**	**gene name**	**aa**	**gene name**	**aa**
Cee13	protein: 1 – 692 DUF575: 19 – 118 DUF562: 411 - 556	CPn0455	protein: 1 – 297 DUF562: 1 - 146	CPK0969	protein: 1 – 690 DUF575: 19 – 119 DUF562: 397 - 541
		CPn0456	protein: 1 – 403 DUF575: 18 – 101		
Cee11	protein: 1 – 629 DUF575: 21 – 117 DUF562: 405 - 553	CPn0457	protein: 1 – 582 DUF575: 21 – 117 DUF562: 405 - 553	CPK0970	protein: 1 – 179 DUF562: 1 - 57
				CPK0971	protein: 1 – 486 DUF575: 19 – 119 DUF562: 404 - 486
Cee9	protein: 1 – 695 DUF575: 21 – 120 DUF562: 411 - 553	CPn0458	protein: 1 – 695 DUF575: 21 – 120 DUF562: 411 - 553	CPK0973	protein: 1 – 684 DUF575: 20 – 120 DUF562: 411 - 555
Cee8	protein: 1 – 143	CPn0459	protein: 1 – 129	CPK0974	protein: 1 – 677 DUF575: 20 – 120 DUF562: 403 - 549
Cee7	protein: 1 – 283 DUF562: 139 - 283	CPn0460	protein: 1 – 283 DUF562: 139 - 283		
Cee6	protein: 1 – 265 DUF575: 21 – 118	CPn0461	protein: 1 – 265 DUF575: 21 – 118		
Cee4	protein: 1 – 672 DUF575: 21 – 117 DUF562: 415 - 556	CPn0462	protein: 1 – 672 DUF575: 21 – 117 DUF562: 415 - 556	CPK0977	none
Cee3	protein: 1 – 389 DUF562: 103 - 289	CPn0463	protein: 1 – 389 DUF562: 103 - 289	CPK0979	protein: 1 – 677 DUF575: 19 – 114 DUF562: 387 - 529
Cee2	protein: 1 – 159	CPn0464	protein: 1 – 159		
Cee1	protein: 1 – 114 DUF575: 21 – 114	CPn0465	protein: 1 – 114 DUF575: 21 – 114		

Fig. S1: Variation in the *cee1-cee13* gene cluster in the isolates GiD, CWL029 and the koala-derived *C. pn.* strain LPCoLN.

(A) Comparisons of SNP distribution and deletions within the ten large genes of the cluster in six different *C. pneumoniae* isolates including the koala isolate LPCoLN from which all human strains are thought to derive, relative to the reference isolate GiD. **(B)** Size and localization of DUF575/DUF562 domains of cluster proteins in GiD, CWL029 and koala strain LPCoLN. DUF575 and DUF562 residues are indicated in green and red, respectively.

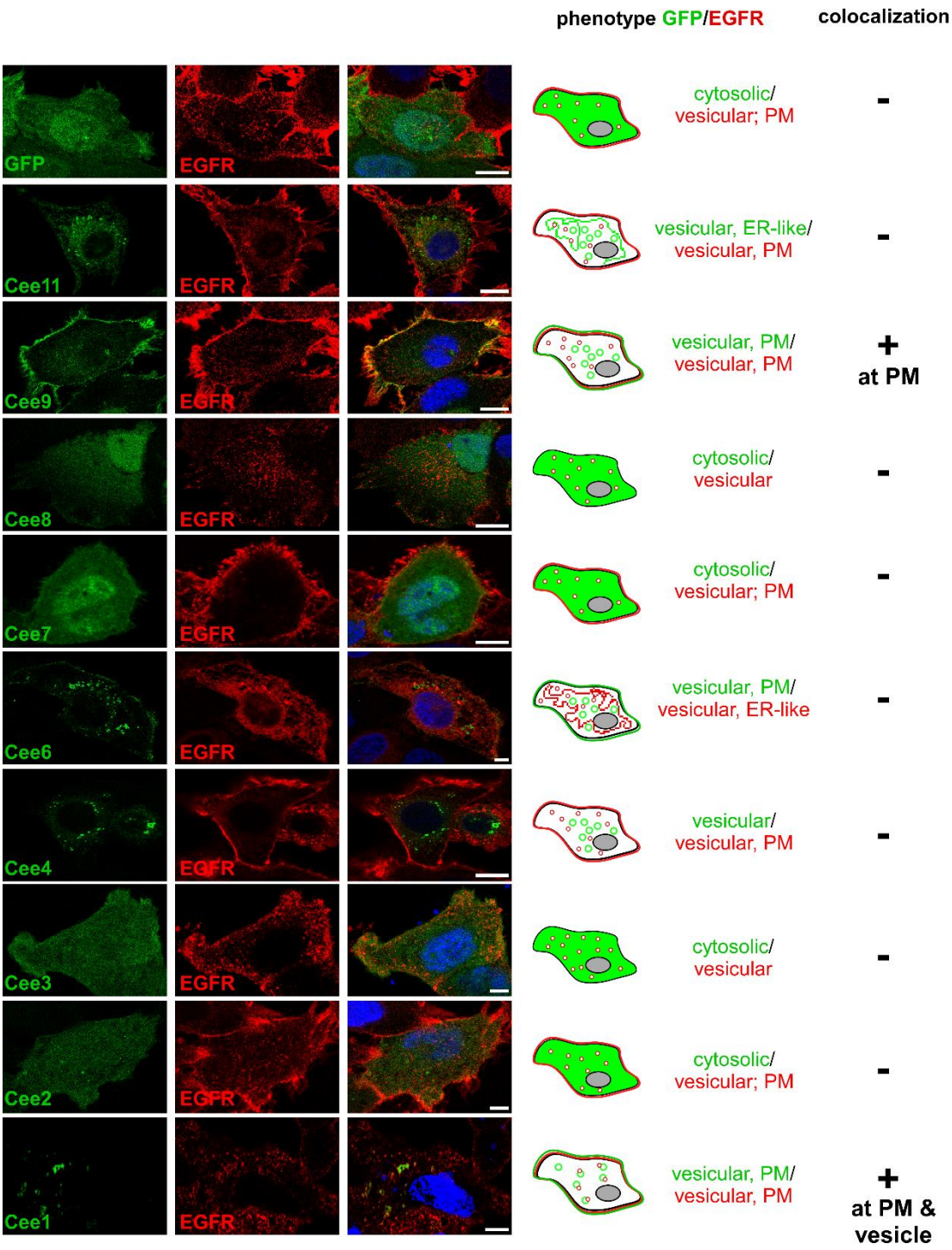

Fig. S2 Fig: Transfection experiments show different phenotypes for the proteins of the Cee1-Cee13 cluster.

Confocal images of human epithelial cells transfected with nine proteins of the GiD Cee1-Cee13 cluster each fused to GFP. HEp-2 cells were transfected for 18 h, fixed with 3 % PFA and permeabilized with 100 % methanol. Endogenous EGFR was visualized with an anti-EGFR antibody in combination with anti-rabbit Alexa594. The DNA was stained with DAPI (blue). Bar: 10 µm. The right panel depicts the schematically localization phenotype of the GFP-fusion proteins (green) and endogenous and endocytosed EGFR (red).

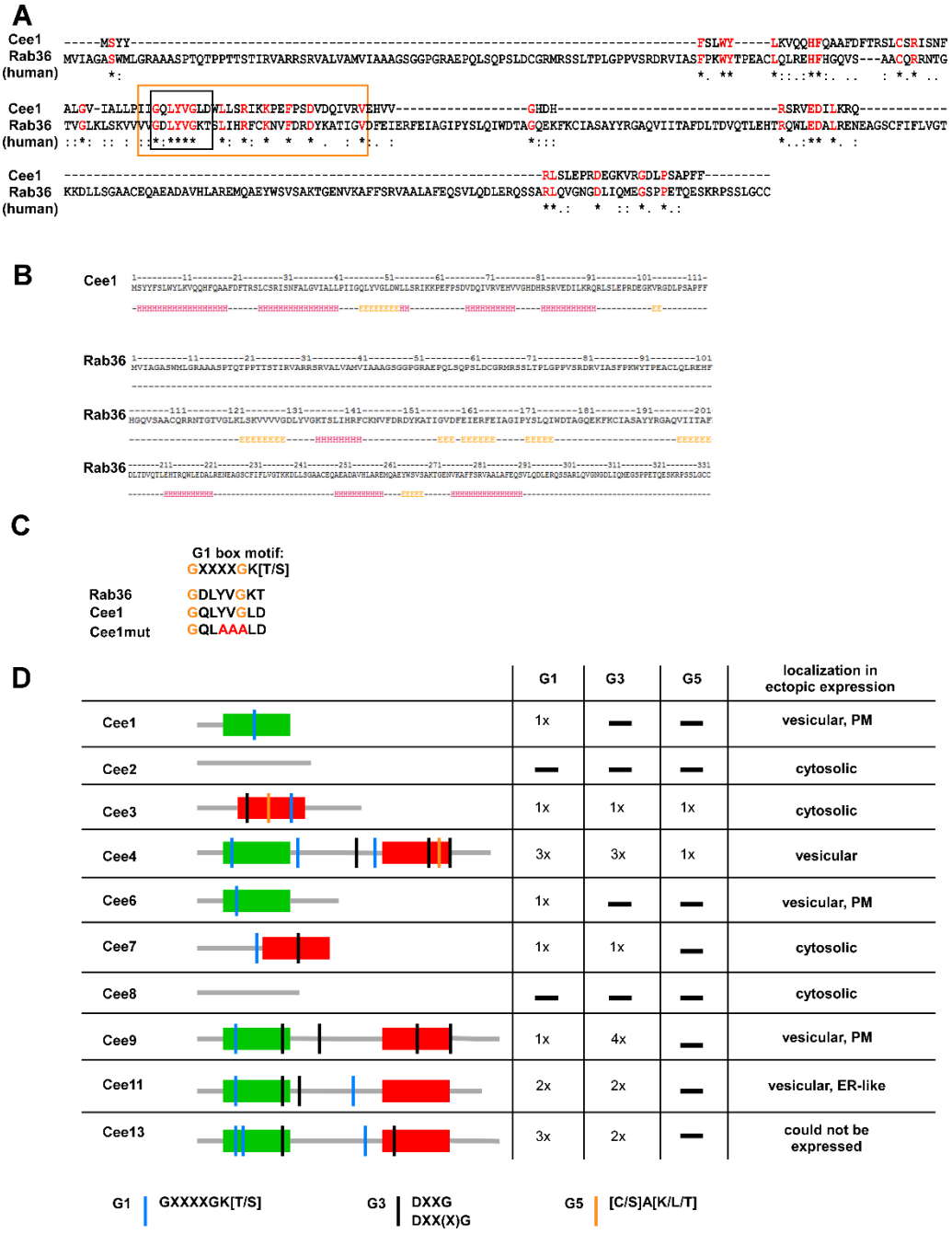

Fig. S3: Cee1 shows identity to the human Rab36 GTPase.

(A) Sequence comparison of the hypothetical *C. pn.* GiD Cee1 protein with the human Rab36 GTPase by MUSCLE https://www.ebi.ac.uk/Tools/msa/muscle/. The region with the highest similarity is marked by the orange box. The G1 box motif (G1 box motif: GXXXXGK[T/S]) is highlighted by the black box. **(B)** Secondary structure prediction of Cee1 and the human Rab36 GTPase were carried out by Jpred 4 (http://www.compbio.dundee.ac.uk/jpred/) (H, helical; E, extended). **(C)** Consensus sequence of the G1 box motif of proteins of the Ras superfamily. The G1 box motif of Rab36 is shown in comparison to the motif found in Cee1. The conserved amino acids are shown in orange. Three aa in Cee1 were changed to alanine (marked red). **(D)** Table of members of the Cee1-Cee13 cluster with DUF575 (green) and DUF562 (red). The localization of identified G box motifs in cluster proteins are shown in blue (G1), black (G3) and orange (G5). The middle panel shows the number of G box motifs identified in each protein. The localization of the depicted cluster proteins in transfected HEp-2 cells is indicated in the right panel. Plasma membrane (PM) and ER (endoplasmic reticulum).

2.3 Unpublished results for the characterization of the *GiD_A_04840-04720* gene cluster

2.3.1 Introduction

C. pneumoniae, like all *Chlamydia* is a Gram-negative, obligate intracellular pathogen and as such has to first gain entry into the host cell and establish its own niche to complete its intracellular life cycle. All intracellular pathogens have evolved highly efficient mechanisms to enter the host cell, subvert host defense mechanisms and engage host organelles to establish their unique intracellular niches, in case of *C. pneumoniae* the inclusion. Up to date not a lot is known about the early events of the chlamydial infection and which chlamydial and host proteins might be involved. Recently, it was shown that the early *Chlamydia* inclusion acquires early membrane identity and specific Rab proteins, like recycling Rab11, Rab14 and late endosomal Rab 7 are recruited to it (Molleken and Hegemann 2017). In a bioinformatic screen against the human and other intracellular bacteria genomes, GiD_A_04840 was identified, because of a 27.9 % identity to the human Rab 36 GTPase. A more detailed bioinformatic analysis of *04840* revealed that the gene belongs to a gene cluster, *04840-04720*, consisting of thirteen genes harboring up to two different DUF (domain of unknown function) domains, DUF575 and DUF562. The cluster is specific for *C. pneumoniae* and conserved in the ancestral koala *C. pneumoniae* isolate (Fig6A+B; taken from (Braun, Hegemann, and Mölleken 2019, submitted)).

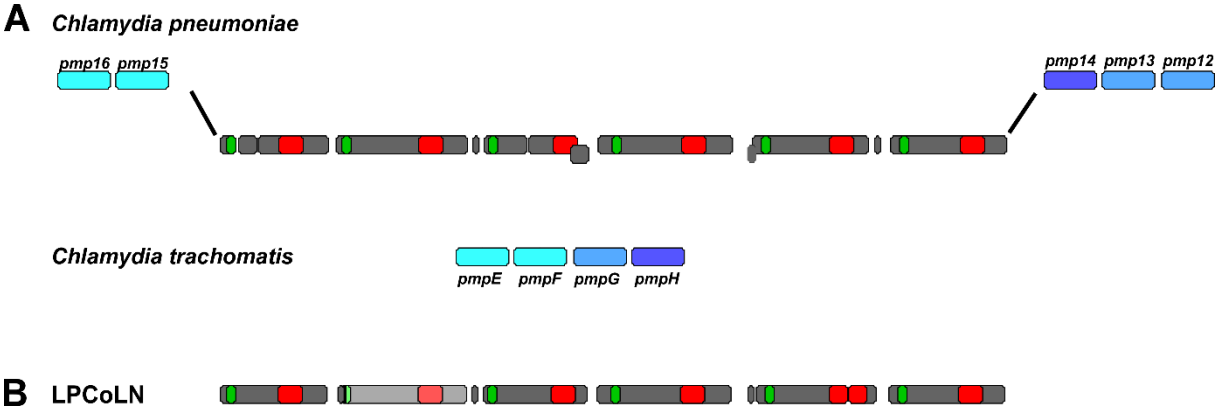

Fig6: The *GiD_A_04840-04720* gene cluster in its genomic context.

(A) Scheme of the genomic context of the *C. pneumoniae* GiD *04840-04720* gene cluster located between *pmp15* (*C. trachomatis pmpF*) and *pmp14* (*C. trachomatis. pmpG*) in comparison to the respective genomic locus of *C. trachomatis*. **(B)** The GiD *04840-04720* cluster in the koala *C. pneumoniae* LPCoLN strain. **(A+B)** Each dark grey box symbolizes one ORF and shows the distribution of the two predicted DUF domains, DUF575 (green box) and DUF562 (red box) (taken and modified from Fig1 from MSIII).

Ectopic expression studies revealed that all proteins harboring the DUF575 showed vesicle-like structures and membrane association. 04840 specifically shows a co-localization with the early endosome (EE), endocytosed EGFR and recycling Rabs, Rab11 and Rab14, which are recruited to the early inclusion, in a G1 box dependent manner (Molleken and Hegemann 2017; Braun, Hegemann, and Mölleken 2019, submitted). Furthermore, it was shown that the proteins of the cluster are present on invading EBs, which is known to be the case for early chlamydial effector proteins. Moreover, it could be shown that proteins of the cluster show the capacity to bind to membranes with different phosphoinositide identity, adhere to the plasma membrane of human epithelial cells, most likely depending on the DUF575, but do not influence the *C. pneumoniae* infection rate (Braun, Hegemann, and Mölleken 2019, submitted).

2.3.2 Objective of this work

In manuscript III it was shown that tested cluster proteins are able to form homomeric complexes, 04840 associates with EEs and internalized EBs and cluster proteins with a DUF575 domain show adhesive capacity to human cells and binding capacity to phospholipids/phosphosinositides.
In this part of the study the possibility to form heteromeric complexes was investigated via Far Western Dot-Blot assays. Furthermore, a possible colocalization of Rab36 and Rab34 with EEs and internalized EBs should be analyzed. Additionally, with the help of adhesion assays using giant unilammelar vesicle (GUV), the binding capacity of the 04840-04720 cluster proteins to specific phospholipids/phosphosinositides should be investigated in more depth.

2.3.3 Material and Methods

2.3.3.1 Antibodies and antibody purification

Table 1: Primary antibodies

Antibody	Reactivity	Origin	Dilution	Source
Anti-Actin	Human actin	Mouse	WB 1:2000	Sigma
Anti-GST	GST-Tag	Rabbit	WB 1:1000	Cell Signaling Technologies
Anti-His	6x and 10x Histidin	Mouse	WB 1:2500	Qiagen
Anti-IncA	Chlamydial IncA	Mouse	IF 1:50	
Anti-04840	Chlamydial 04840	Rabbit	IF 1:50	This work
Anti-04810	Chlamydial 04810	Rabbit	IF 1:25	This work

WB = Western blot IF = Immunofluorescence microscopy

Anti-04840 and anti-04810 sera were enriched in this work by using recombinant protein. 200 µg recombinant 04840 or 04810 was loaded on a SDS/PAGE and transferred on a PVDF membrane (Millipore). The membrane was blocked for 15 min with blocking solution (3 % BSA + 0,05 % Tween20) and then incubated with 04840/04810 sera (1:20) in 2 ml blocking solution ON at 4 °C. The supernatant was discarded, the antibody eluted with 5 times 1 ml 0.1 M Glycin pH 2.5 at RT and neutralized with 100 µl 1 M Tris pH 9. All elution fractions were analyzed in Western Blot assays against boiled samples of *C. pn*. infected HEp-2 cells and immunofluorescence microscopy against a monolayer of *C.pn*. infected HEp-2 cells (Nikon Confocal C2plus). Elution 1 and elution 2 of the anti-04810 antibody showed a good signal in immunofluorescence microscopy (dilution 1:50 to 1:10), but no signal in Western Blot experiments. Anti-04840 could not be used after enrichment. A second approach was to enrich the sera by again using SDS/PAGE, but in addition the proteins were renatured on the PVDF membrane before they were blocked and incubated with 04840/04810 sera. This approach did not result in any functioning antibody.

A third approach was the depletion of the 04840 and 04810 sera of human proteins by using HEp-2 cells. A confluent HEp-2 cell monolayer was grown in a 25 cm^2 cell culture flask, cells fixed with 3 % PFA and permeabilized with 100 % methanol. Afterwards, the cells were washed three times with PBS (137 mM NaCl, 2.7 mM KCl, 10 mM Na_2HPO_4, 1.8mM KH_2PO_4, pH7.4) for at least 30 min at RT, then the 04810 or 04840 sera (1:25) in blocking solution added and incubated ON at 4 °C. Antibody was harvested and analyzed in Western Blot studies and immunofluorescence microscopy. No signal could be detected for any tested dilution (1:1; 1:5, 1:10, 1:20) of anti-04840, whereas a 1:1 dilution resulted in a signal for anti-04810 in immunofluorescence microscopy.

Table 2: Secondary antibodies

Antibody	Reactivity	Origin	Dilution	Source
Anti-Mouse AP	Mouse	Rabbit	WB 1:7500	Promega
Anti-Rabbit AP	Rabbit	Goat	WB 1:7500	Promega
Alexa488 anti-rabbit	Rabbit	Goat	IF 1:200	Invitrogen
Alexa594 anti-mouse	Mouse	Goat	IF 1:200	Invitrogen

WB = Western blot IF = Immunofluorescence microscopy

2.3.3.2 Plasmids

Plasmids were generated as described in manuscript III. All constructs were generated by homologous recombination in *S. cerevisiae*, verified by sequencing and amplified in *E. coli*. Plasmid purification was performed following Qiagen Plasmid Midi Kit protocol.

2.3.3.3 Transfection and infection experiments

Transfection experiments were performed as described in manuscript III. To analyze if ectopically expressed Rab36 or Rab34 associate with EBs or if ectopically expressed 04840 and 04810 influence a subsequent *C. pneumoniae* infection; HEp-2 cells were first transfected for 18 h using TurboFect (Thermo Fisher), infected for 15, 30 min or 40 h, fixed with 3 % PFA and analyzed by immunofluorescence microscopy (Nikon Confocal C2plus). For the 40 h infection the inclusion membrane was visualized by specific anti-IncA antibody and secondary anti-mouse antibody coupled to Alexa 594 and DAPI was used to visualize DNA. All images and related measurements were generated with Nikon Element software.

2.3.3.4 Protein expression and purification

His-tagged cluster proteins were expressed in *E. coli* BL21 and purified under denatured conditions. *E. coli* pellets containing the heterologously expressed proteins were resuspended in 20 ml denaturing lysis buffer (6 M Guanidine-HCl, 20 mM Tris-HCl, 0,5 M NaCl, 1 mM β-Mercaptoethanol, pH 8) and incubated ON at 4 °C. The lysate was centrifuged at 24000 rpm for 1 h at RT (Beckman; rotor JA 25.50) and then incubated with Ni-NTA agarose (Roche) for 2 h at RT. A manual protein purification column with filter (Thermo Scientific) was filled with the supernatant/Ni-NTA agarose suspension, washed with 10 ml 20 mM imidazole (8 M Urea, 0.1 M NaH2PO4, 10 mM Tris-HCl; pH 8) and 10 ml 40 mM imidazole (8 M Urea, 0.1 M NaH2PO4, 10 mM Tris-HCl; pH 6.3). The His-tagged proteins were eluted with 500 mM imidazole (8 M Urea, 0.1 M NaH2PO4, 10 mM Tris-HCl; pH 6.3)

and dialyzed in PBS at 4 °C, except for the cluster proteins 04840, 04840 mutant and 04740, for which a Amicon Ultra-15 (Merck Millipore) was used with 200 mM arginine added to PBS.

2.3.3.5 Labeling of proteins

To label native cluster proteins with biotin, EZ-Link Sulfo-NHS-biotin (Thermo Scientific) was resuspended in PBS to a final concentration of 10 mM. A 20-fold molar excess of this biotin solution was added to the protein (total volume 250 µl) and incubated on ice for 2 h. The reaction was quenched with 1 M Tris pH 7.5 (final concentration of 50 mM) and the labeled proteins stored at 4 °C until used in Far Western Dot-Blot assays.
Native cluster proteins were also labeled with NHS-fluorescin (FITC) to perform adhesion and GUV assays. 1 mg NHS-fluorescin (Thermo Scientific) was dissolved in 1 ml DMSO and a 10-fold molar excess added to the native cluster protein (total volume 250 µl), incubated on ice for 2 h and the reaction quenched with 1 M Tris pH 8 (final concentration of 50 mM). The labeled proteins were stored at 4 °C.

2.3.3.6 Far Western Dot-Blot assay

To analyze if cluster proteins are able to interact with each other Far Western Dot-Blot assays were performed. Therefore, 1 µg denatured recombinant cluster protein (prey protein) was spotted on an activated PVDF membrane (Millipore), let enter via capillary forces at RT and then immobilized by incubation for 10 min in 8 % acetic acid. The membrane was washed with 1 x PBS and the prey proteins then slowly renatured with several buffers with a decreasing concentration of Guanidine-HCl (Serva):

Table 3: Buffer composition of a Far Western Blot assay

Guanidine-HCl [M]	**6**	**3**	**1**	**0,1**	**0**
Glycerin (ml)	5	5	5	5	5
5 M NaCl (ml)	1	1	1	1	1
1 M Tris pH7.5 (ml)	1	1	1	1	1
0.5 M EDTA (ml)	0.1	0.1	0.1	0.1	0.1
20 % Tween-20 (ml)	0.25	0.25	0.25	0.25	0.25
Milk powder (g)	1	1	1	1	2
1 M DTT(ml)	0.05	0.05	0.05	0.05	0.05
8 M Guanidine-HCl (ml)	37.5	18.6	6.3	0.6	0
H_2O (ml)	3.8	22.8	35	40.8	41.4

Final Volume (ml)	50	50	50	50	50
Minutes / T °C	30/RT	30/RT	30/RT	30/4 °C	ON/4 °C

Afterwards, the membrane was incubated with 2 µg/ml biotinylated native cluster proteins (bait protein) in blocking solution (5 % milk in PBS) for 2 h at 4 °C, washed three times with PBS and then incubated with AP-conjugated anti-streptavidin antibody (Sigma) for 1 h at RT. The protein-protein interaction was analyzed with NBT/BCIP added to detection buffer (0.1 M Tris/HCl pH 9.5, 0.1 M NaCl, 50 mM MgCl2).

2.3.3.7 Adhesion assay with FITC-labeled proteins

Adhesion assays were performed as described in manuscript III, with the exception that cluster proteins were labeled with FITC, before 100 µg/ml per well were used for the assay. The binding of FITC-labeled cluster proteins was analyzed by immunofluorescence microscopy, using Wheat germ agglutinin (WGA) to visualize the cell membrane to analyze if the FITC-labeled protein binds and on a SDS/PAGE by detecting them with a specific anti-His antibody.

2.3.3.8 Giant unilammelar vesicle assay

Giant unilammelar vesicles (GUVs) were prepared via electroformation as previously described in (Romer et al. 2007; Galle et al. 2019). The lipids were purchased from Avanti Polar Lipids, Inc, resuspended in chloroform and stored covered with argon gas at – 20 °C. The lipid-mix used for synthesis of GUVs was as followed: 5 mol % PtdIns, 0.25 % TexasRed (for the red fluorescence in immunofluorescence microscopy), 20 mol % cholesterol and 74.75 mol % phosphatidylcholine (PC). GUVs were formed by the use of an electric field and a 1 M sucrose solution. In more detail: 20 µl of lipid-mix was evenly spread on two ITO-coated glas slips (</= 10 Ohm/sq) (purchased from pgo; Präzisions Glas & Optik). The two cover slips were put together with the coated sites facing each other and a small gap was left in between via wax (VITREX), which was filled with 1 M sucrose solution and then also closed with wax. An electrical field (11 Hz; 02.0 Vp-p) was applied to the cover slips for 4 to 5 h, the wax seal broken, the sucrose solution containing the GUVs pipetted into a reaction tube and used immediately. Generated GUVs could be used until the next morning, but needed to be stored on ice and in the dark. To analyze protein binding to the GUVs via immunofluorescence microscopy, 15 µ slide Angiogenesis from Ibidi were used. Each well was coated with casein (2 mg/ml) and then washed with 50 µl PBS three times. 20 µl GUV solution was mixed with 10 µl protein (100 µg/ml) in each well, incubated for 20 min at RT,

fixed with 3 % PFA and washed with PBS once. The binding of 04840 and 04810 was visualized via specific antibodies and then analyzed via immunofluorescence microscopy.

2.3.3.9 Bioinformatic analysis

Protein sequence comparisons of the *C. pn.* GiD 04840 with Rab36 and Rab34 were carried out with MUSCLE multiple sequence alignment (Clustal W Output). https://www.ebi.ac.uk/Tools/msa/muscle/.

2.3.4 Results

2.3.4.1 Proteins of the 04840-04720 cluster can interact with each other

In manuscript III it was shown that individual proteins of the 04840-04720 cluster carrying either one or two DUF domains are able to form high molecular weight complexes (Braun, Hegemann, and Mölleken 2019, submitted). To analyze if these proteins are not only able to interact with themselves, but with each other, a Far Western Dot Blot experiment was performed in this part of the study. 1 µg denatured recombinant His- or GST-tagged protein or biotinylated protein was spotted on a membrane, renatured and then either incubated with α-His antibody/α-GST antibody (input control), α-streptavidin-AP (input control; to analyze successful biotinylation of the proteins) or 2 µg of the depicted biotinylated native recombinant cluster protein (Fig7A+B). In the α-His/α-GST control all proteins could be detected with different intensities, whereas the α-streptavidin-AP blot showed a very weak signal for 04770 and 04780, and 04830 and 04840 could not be biotinylated at all (Fig7B). Furthermore, the GST control showed no binding to any of the tested proteins (Fig7B). For all other tested proteins, except 04770 and $04810^{121\text{-}672}$, a strong binding to 04830 and 04840 could be observed (Fig7B+C). Additionally, a weak binding of 04720 to 04770, 04780, 04790, 04810, $04810^{121\text{-}672}$ and 04820 could be observed as well as weak binding of 04790 and 04810 to themselves respectively (Fig7B+C). This data show that proteins of the cluster do not only have the ability to form homomeric complexes, but are also capable to interact with each other, which seems to be independent of any DUF domain.

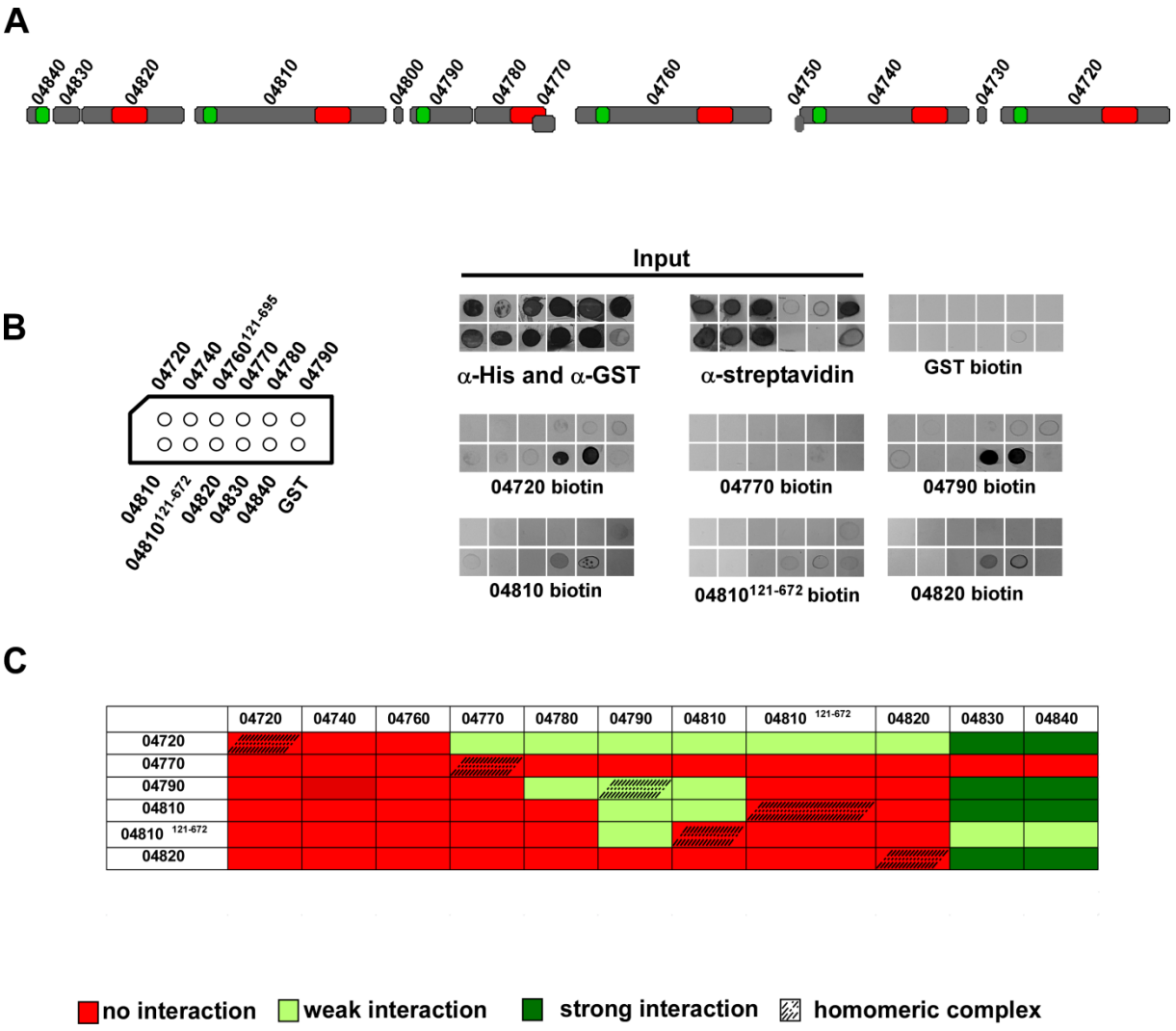

	04720	04740	04760	04770	04780	04790	04810	04810 121-672	04820	04830	04840
04720											
04770											
04790											
04810											
04810 121-672											
04820											

Fig7: Proteins of the 04840-04720 cluster are able to interact with each other.
(A) Schematic representation of the proteins from the *C. pn.* GiD 04720-04840 cluster. DUF575 is shown in green and DUF562 in red. **(B)** The left panel shows the scheme of how the proteins of the cluster were plotted on the membrane. The results of the Far Western Dot Blot assay are shown in the right panel. 1 µg denatured protein of each of the indicated proteins was spotted and then renatured on the membrane. 2 µg of native biotinylated protein was incubated with the membrane and bound protein detected via α-streptavidin. As controls the proteins were once detected with a α-His/α-GST antibody and the biotinylation of the recombinant cluster proteins verfied with α-streptavidin. GST was used as a control for the assay. **(C)** Table shows a summary of observed interactions between the proteins of the 04720-04840 cluster via a Dot Blot assay. Light green shows weak interaction, dark green strong interaction, red no interaction and shaded marks proteins that are able to form homomeric complexes (blue native gels; taken from manuscript III).

2.3.4.2 04840 associates with Rab36 and Rab34

As described before, 04840 was initially identified in a bioinformatic screen because of a 27.9 % identity to the human Rab GTPase 36. In a more detailed sequence comparison it could be shown that Rab36 harbors a perfect G1 box motif (GXXXXGK[T/S]) typical for all members of the Rab protein family, while the motif in 04840 lacks the last two amino acids (Braun, Hegemann, and Mölleken 2019, submitted). There is not a lot known about Rab36 and its function, except that it has a high homology to Rab34 (56 %), which is Golgi-associated and regulates lysosomal distribution. Rab36, like Rab34 regulates the distribution

of late endosomes and lysosomes (Wang and Hong 2002; Chen et al. 2010). As there is such a high homology of Rab36 to Rab34, and more is known about Rab34, Rab34 was also included in the next experiments. A sequence comparison of 04840 to Rab36 and Rab34 revealed one different amino acid (aa) in the G1 box motif of Rab34 in comparison to Rab36 and four different aa in comparison to 04840 (Fig8A-D).

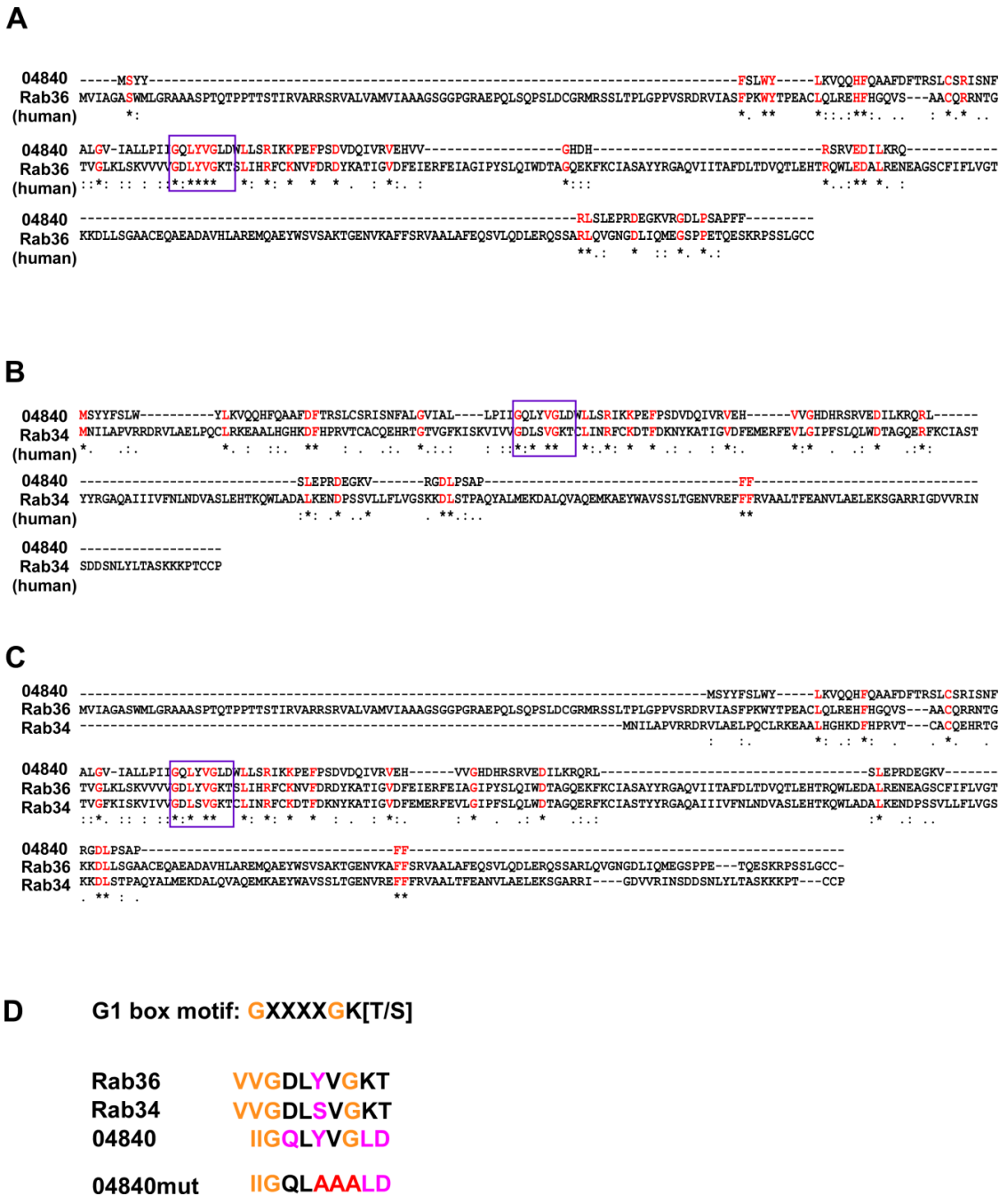

Fig8: Sequence comparison of 04840 with Rab36 and Rab34.
(A-C) Sequence comparison of the hypothetical *C. pneumoniae* GiD 04840 protein with the human Rab36 GTPase **(A)**, Rab34 GTPase **(B)** and comparison of all three **(C)** carried out with muscle https://www.ebi.ac.uk/Tools/msa/muscle/. The G1 box motif (G1 box motif: GXXXXGK[T/S]) is highlighted by the lila box. **(D)** Consensus sequence of the G1 box motif of proteins of the Ras superfamily. The G1 box motif of Rab36 and Rab34 is shown in comparison to the motif found in 04840. The conserved amino acids are shown in orange and the amino acids exchanged in the 04840mut in red. Different amino acids between Rab36/04840 and Rab34 are shown in pink.

Next, to analyze the localization of Rab36 and Rab34 in human epithelial cells and a possible association with 04840, ectopic expression studies with Rab36 and Rab34 were performed. The group from Mitsunori Fukuda has kindly provided us with the Rab36-GFP and Rab34-GFP constructs for the ectopic expression studies (Fukuda et al. 2008). In transfection experiments, Rab36-GFP and Rab34-GFP expressed alone showed vesicle-like structures, as has been published and are most likely associated with the Golgi apparatus (Fig9A) (Chen et al. 2010). 04840 fused to mCherry exhibits the same localization pattern than shown before. In co-transfection studies, all proteins still showed vesicle-like structures, and 04840 did co-localize with Rab36 and Rab34 (Fig9A, B).

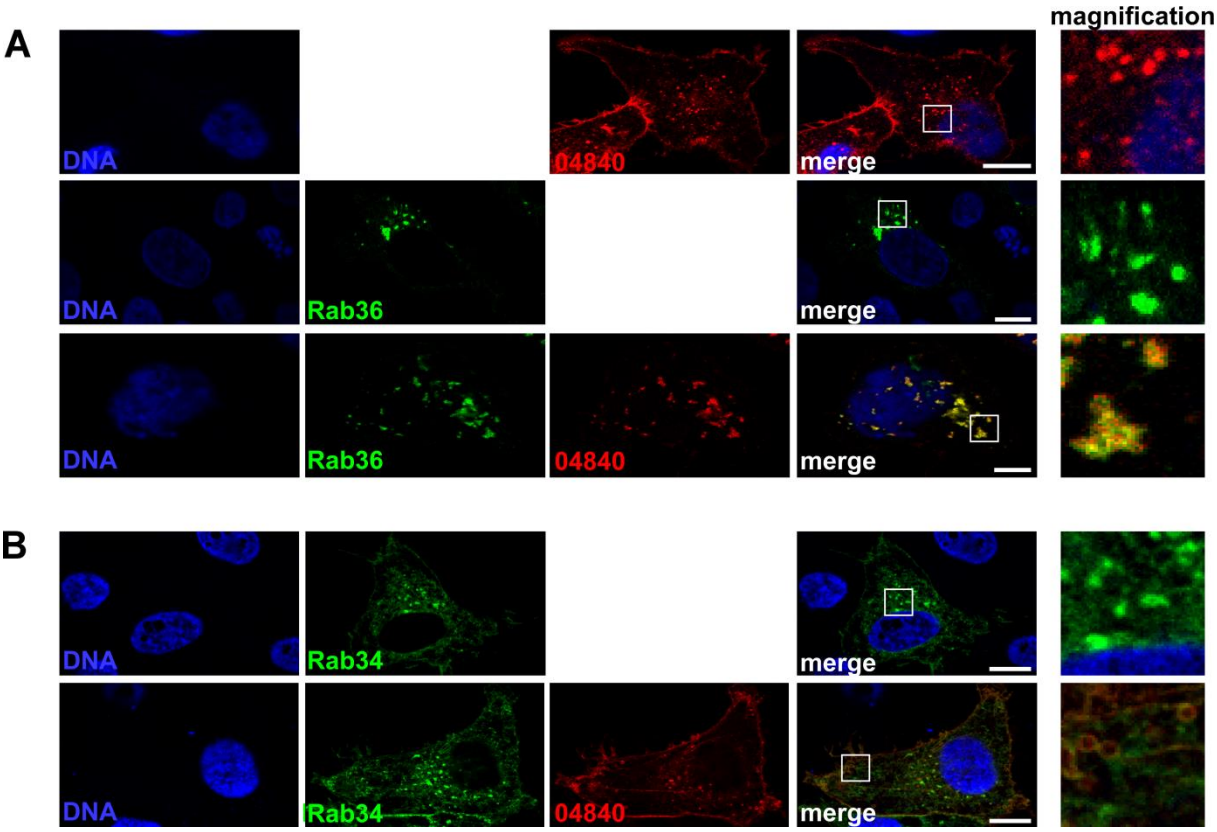

Fig9: 04840 co-localizes with Rab36 and Rab34 in transfection experiments.
(A+B) Confocal images of co-transfection studies with Rab36 **(A)** or Rab34 **(B)** fused to GFP (green) and 04840 fused to mCherry (red). The DNA was visualized with DAPI. A magnification of the white box is shown in the right panel. Magnification is 5 fold. Scale: 10 µm.

In previous experiments it has been shown that ectopically expressed 04840 associates with early endosomes and endogenous 04840 associates to EBs during the adhesion process. The association of 04840 to Rab34 and Rab36 lead to the question if Rab36 and Rab34 might also associate to early endosomes and invading EBs (Braun, Hegemann, and Mölleken 2019, submitted). HEp-2 cells were co-transfected with either Rab36-GFP or Rab34-GFP and 2xFYVE-mCherry (PtdIns(3)P) and afterwards infected with *C. pneumoniae* EBs for 15 or 30 min p. i. (Fig10). Interestingly, Rab36 associated with early endosomes and

EBs which show an early endosome identity 15 min and 30 min p. i., which could not be observed for Rab34 (Fig10A+B). Taken together this data shows that 04840 associates with Rab36 and Rab34 in transfection experiments, but only Rab36 associates with early endosomes and EBs, like it was previously observed for 04840.

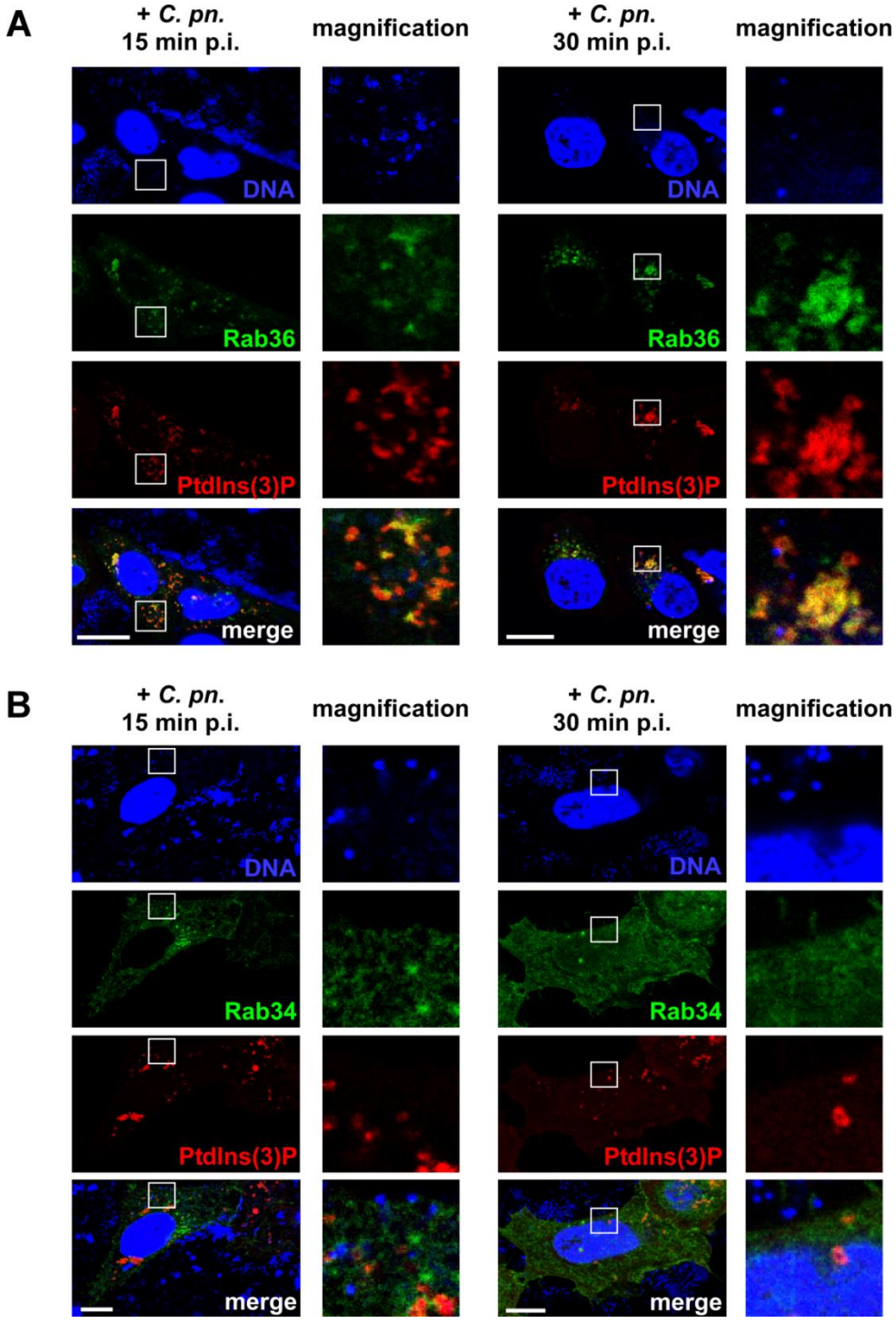

Fig10: Rab36 co-localized with early endosomes and EBs early in the infection.
(A+B) Confocal images of epithelial cells co-transfected with Rab36-GFP **(A)** or Rab34-GFP **(B)** and the PtdIns(3)P membrane marker 2xFYVE fused to mCherry. After 18 h transfection the cells were additionally infected with *C. pneumoniae* GiD (MOI 1) for 15 min and 30 min and then fixed with 3 % paraformaldehyde (PFA). The DNA was visualized with DAPI. A magnification of the white box is shown in the right panel. Magnification is 5 fold. Scale: 10 µm.

2.3.4.3 04840 associates with the late inclusion membrane

Next, a possible impact of the protein expression on the subsequent *C. pneumoniae* infection was analyzed. Incubating human cells previous to a *C. pneumoniae* infection with recombinant 04840 or 04810, did not show an impact on the number of inclusions (Braun, Hegemann, and Mölleken 2019, submitted). Therefore, we tested next, whether ectopic expression of cluster proteins might influence the subsequent infection. HEp-2 cells were transfected for 18 h with either 04840-GFP, 04810-GFP or GFP (control), afterwards infected with *C. pneumoniae* GiD for 40 h, fixed and the inclusion membrane visualized with an α-IncA antibody. To analyze a possible effect of protein expression on the infection, the area of every single inclusion (inclusion size) and number of inclusions per cell was analyzed (Fig11D). The GFP control showed an average of three inclusions per cell with around 20 μm^2. Comparable results could be obtained in the cells that expressed 04840 (Fig11D). Interestingly, in cells that expressed 04810 an average number of 2.5 inclusions could be counted, with an average size of approximately 14.8 μm^2, which is 5.2 μm^2 smaller than in the control or in 04840 expressing cells (Fig11D). These results lead to the conclusion that the expression of 04810 might have an impact on the *C: pneumoniae* infection. A closer look revealed that the cells expressing 04810 were smaller and more roundish than the control cells or cells expressing 04840. As a control, to see if the long protein expression has an impact on the cells and subsequently an influence on the infection, cells were transfected for 48 h, without infecting them. As a matter of fact, cells expressing 04810 were much smaller than cells expressing only GFP or 04840 (Fig11E). Deductively, it seems that the long expression of 04810 has a negative effect on the HEp-2 cells, which in turn could influence the infection, thus no definite conclusion can be made about 04810 influencing the infection.
Even though no influence on the infection could be observed, the localization of 04840-GFP was surprising. 04840 still showed the vesicle like phenotype, but also associated with the inclusion membrane 40 h p. i. (Fig11A), which was not the case for 04810-GFP or the GFP control (Fig11A+C). Taken together, the results show that 04840 associates to the late inclusion membrane, but ectopic expression does not influence the size or number of inclusions, whereas for the expression of 04810 no decisive conclusion could be made.

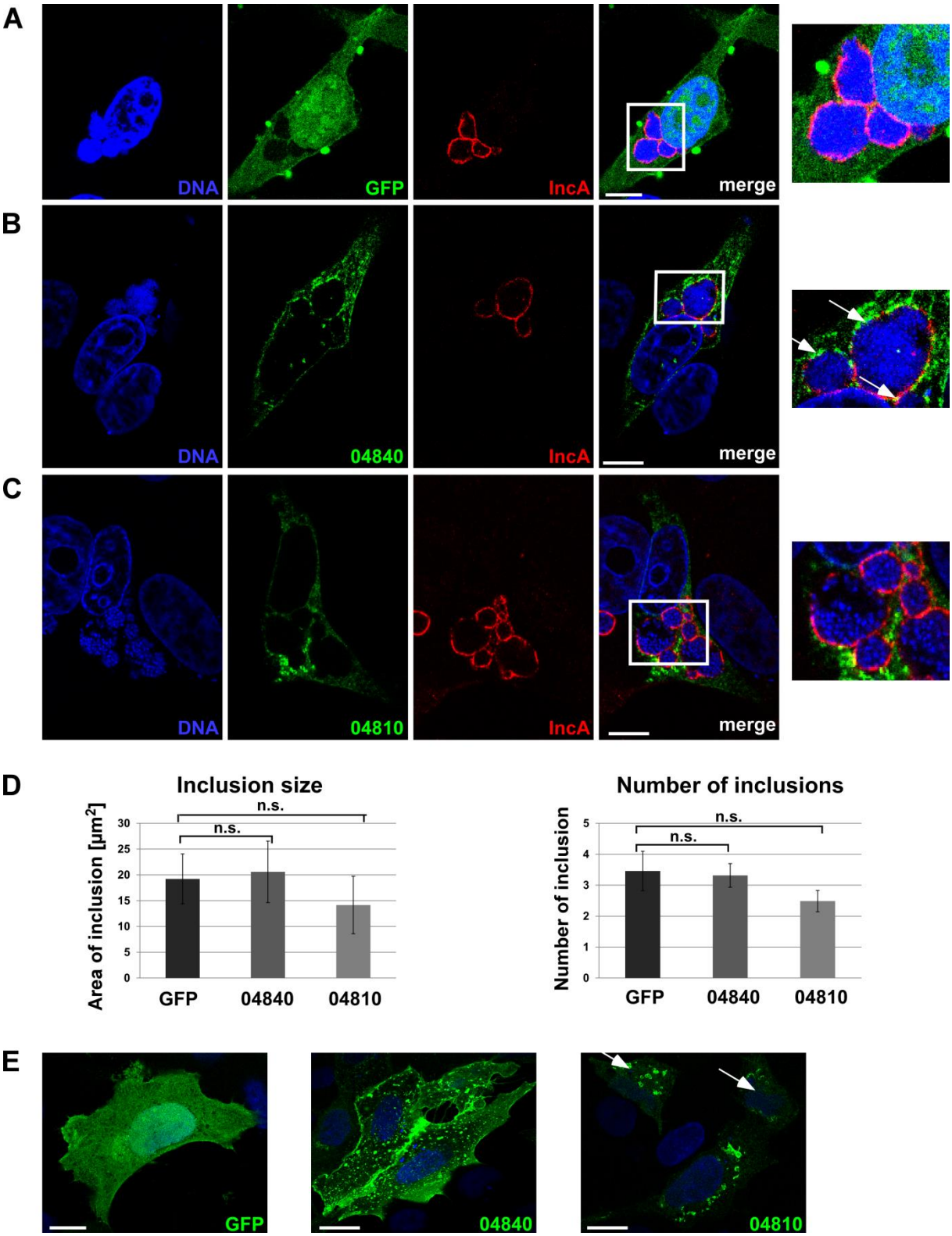

Fig11: 04840 associates to the late inclusion membrane.

(A-E) Transfection followed by an *C. pneumoniae* infection assay. **(A-D)** HEp-2 cells were transfected with GFP control **(A)**, 04840-GFP **(B)** or 04810-GFP **(C)** for 18 h, infected with *C. pneumoniae* for 40 h, fixed with 3 % PFA and analyzed via immunofluorescence microscopy. The inclusion membrane was visualized using specific primary antibody against IncA and secondary antibody anti-mouse Alexa594. Arrow indicates association of 04840 to the late inclusion membrane. Bar: 10 µm **(D)** Quantification of the cells from (**A-C)** of area and number of inclusion per cell. n=3 (37 cells were counted each *n*). **(E)** HEp-2 cell were transfected with GFP, 04840-GFP and 04810-GFP for 48 h, fixed with 3 % PFA and analyzed via immunofluorescence microscopy. White arrows mark more roundish HEp-2 cells. Bar: 10 µm.

2.3.4.4 Proteins of the cluster bind to membranes with different phosphoinositide and phospholipid identity

Formerly, it was shown that proteins of the 04840-04720 cluster have the ability to bind to human cells, in a DUF575 domain dependent manner, but do not show any influence on *C. pneumoniae* infection rate, like typical chlamydial adhesins usually do (Fechtner et al. 2013; Becker and Hegemann 2014; Braun, Hegemann, and Mölleken 2019, submitted). As the proteins did not behave like typical chlamydial adhesins, but can bind to the plasma membrane and EE (PtdIns(3)P) in transfection studies, the question was if the proteins can bind different lipids and that way possibly membranes in general. A self-made phospholipid and phosphoinositide membrane strip was used to test binding to specific lipids and especially binding to PtdIns(3)P, which is not included in commercial lipid strips. In this assay binding of 04840 to phosphatidylserine (PS), PtdIns(4,5)P_2, PtdIns(4)P_2 and PtdIns(3)P, could be shown. For 04810 binding to PS, phosphatidylcholine (PC) and PtdIns(4,5)P_2, could be observed (Fig12A; taken from (Braun, Hegemann, and Mölleken 2019, submitted)). Here, additional lipids were tested using a commercial PtdIns membrane strip (Fig12B). In this assay binding to PtdIns(4,5)P_2, which is mostly located in the inner leaflet of the plasma membrane and PtdIns(4)P_2, which is a precursor of PtdIns(4,5)P_2 and located at the Golgi, could be observed for 04840. Binding to PS, as shown before, could not be shown in this experiment (Fig12E). Due to the absence of PtdIns(3)P on the commercial lipid strip binding could not be tested. 04810 also showed binding to PtdIns(4,5)P_2, PtdIns(4)P_2 and additionally to PtdIns(3,4,5)P_2, which is mostly localized at the plasma membrane, but also no binding to PS or PC as shown before could be detected (Fig12D+E).

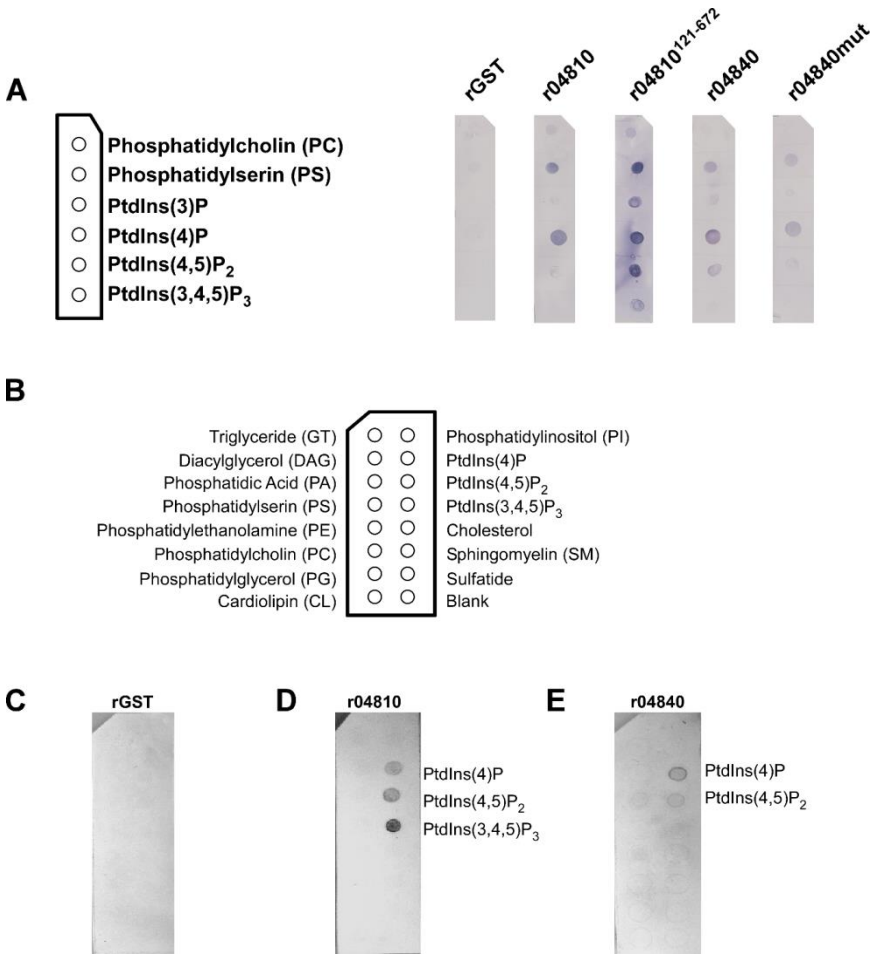

Fig12: 04840 and 04810 show binding to specific phosphatidylinositol phosphates.
(A) Self-made membrane lipid strip assay with depicted recombinant protein variants of the cluster. Scheme of the membrane lipid strip is shown on the left side. Membrane lipid strips were incubated with 1 µg/ml His-tagged rGST, r04810, r04810$^{121-672}$, r04840 and r04840mut and analyzed with anti-His antibody (n=2) (taken from (Braun, Hegemann, and Mölleken 2019, submitted)). **(B-E)** Commercial membrane lipid strip assay with recombinant 04810 and 04840. **(B)** Scheme of the membrane lipid strip (Echelon Biosciences Inc). **(C-E)** Membrane lipid strips were incubated with 0,5 µg/ml His-tagged rGST **(B),** r04810 **(C)** and r04840 **(D)** and analyzed with anti-His antibody. n=2

As the two lipid strip experiments showed different binding of cluster proteins to lipids, we next tested the binding in a different context by using artificial membranes. On the lipid strips, the lipids spotted on a membrane are randomly organized and no membrane context is analyzed, which could be important for the binding ability of proteins. To analyze the latter, giant unilammelar vesicles (GUVs) were used. In GUV binding assays the GUVs were created out of a lipid mix containing mainly PC and cholesterol. To test binding to different lipids PS, PtdIns(3)P, PtdIns(4)P_2, PtdIns(4,5)P_2 or PtdIns(3,4,5)P_2 were additionally incorporated to 5 mol %. 04840, 04810 and GST as a control were labeled with fluorescein isothiocyanate (FITC) and the respective GUVs incubated with the labeled protein. Surprisingly, no biding to any of the tested GUVs was observed (data not shown).

Thus, it was analyzed if the FITC-labeling might be inhibiting the binding site. Again recombinant 04840, 04810$^{121-672}$ (a version of 04810 without DUF575) and GST were labeled

with FITC and this time human epithelial cells incubated with 100 µg of the labeled protein (Fig13A-D). At different time points the unbound protein was washed away, the cells fixed with PFA and stained with wheat germ agglutinin (WGA) to visualize the cell membrane (Fig13B-D). The labelling of the protein with FITC was successful, but the efficiency varies, as can be seen in Fig13A. Surprisingly, no binding of 04810$^{121-672}$-FITC or 04840-FITC to the cells at 15 min or 60 min could be observed, even though in previous adhesion assays a binding of these proteins to human cells was shown as early as 1 min (Fig13C+D; Braun et al., 2019). To analyze these observations in more detail, further experiments were performed, where FITC labeled proteins from the 04840-04720 cluster were used for an adhesion assay. 04820, which did not bind to human cells before, did also not bind when labeled with FITC (Fig13E+G). Interestingly, 04840 showed significantly reduced binding to the plasma membrane of human epithelial cells, when labeled with FITC, and 04810$^{121-672}$, which showed a weak binding to human cells before, did not bind at all when labeled with FITC (Fig13E+G). Taken together, it seems that the proteins of the cluster that have the ability to bind to the human plasma membrane, lose the ability when labeled at their free primary amines (Fig13E+G).

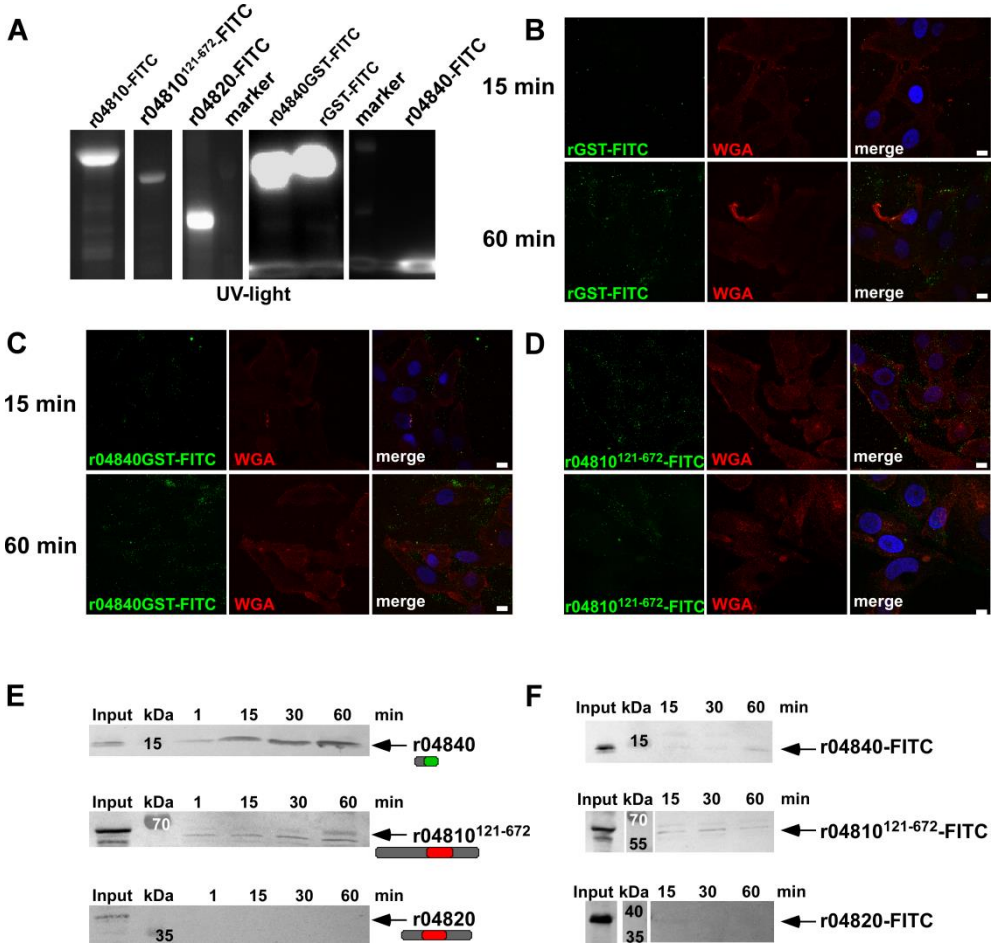

Fig13: FITC labeled proteins of the 04840-04720 cluster lose their ability to bind to human cells
(A) FITC-labeled proteins of the cluster and GST used in the adhesion assays **(B-G)** under UV-light. **(B-D)** Immunofluorescence microscopy of HEp-2 cells previously incubated with FITC-labeled GST **(B)**, 04840 **(C)** and

$04810^{121-672}$ **(C)** for 15 and 60 min, fixed with PFA and stained with WGA (red). DNA (blue) in merge. Bar: 10 µm. **(E)** Adhesion of unlabeled recombinant 04840, $04810^{121-672}$ and 04820 (modified from (Braun, Hegemann, and Mölleken 2019, submitted)). **(F)** Adhesion assay of FITC-labeled 04840, $04810^{121-672}$ and 04820 to HEp-2 cells. HEp-2 cells were incubated with recombinant protein as indicated for different time points. Unbound protein was washed away and bound protein was analyzed on immunoblots with an anti-His antibody and secondary anti-mouse antibody in comparison to the input protein. The arrow indicates the band of the protein.

To circumvent the labeling of proteins, examine the binding of the proteins to membranes and to investigate if GUV assays can also be performed with fixed GUVs, GUVs were incubated with unlabeled recombinant 04840 or 04810 for 20 min with the respective GUVs and then fixed with 3 % PFA. The cluster proteins were visualized with the corresponding primary antibody of the used recombinant protein and a secondary antibody labeled with Alexa488 and analyzed via immunofluorescence microscopy. As a control GUVs from each mix were stained with the antibodies without being previously incubated with recombinant protein. In this experiment the 04810 antibody alone showed a weak binding to PtdIns(3,4,5)P_2 GUVs and no specific binding of 04810 to any of the tested GUVs could be observed, except for a weak binding to PC (Fig14A). Surprisingly, the 04840 antibody alone showed binding to PS and PtdIns(4)P_2, wherefore the observed binding of 04840 to these lipids is inconclusive (Fig14C+D). The only binding that could be observed and fits to the observed lipid binding of the lipid strip assays, is binding of 04840 to PtdIns(4,5)P_2 and PtdIns(3,4,5)P_2 (Fig14B+D).

Taken together these results show that some proteins of the 04840-04720 cluster are able to bind to human cells and to different phospholipids and phosphoinositides, but the binding seems to be disturbed after protein labelling. The GUV binding assay is a good way to study binding of proteins to different membranes, but in the case of the 04840-04720 cluster new ways to visualize the proteins need to be found, to fully use this system to its possibilities.

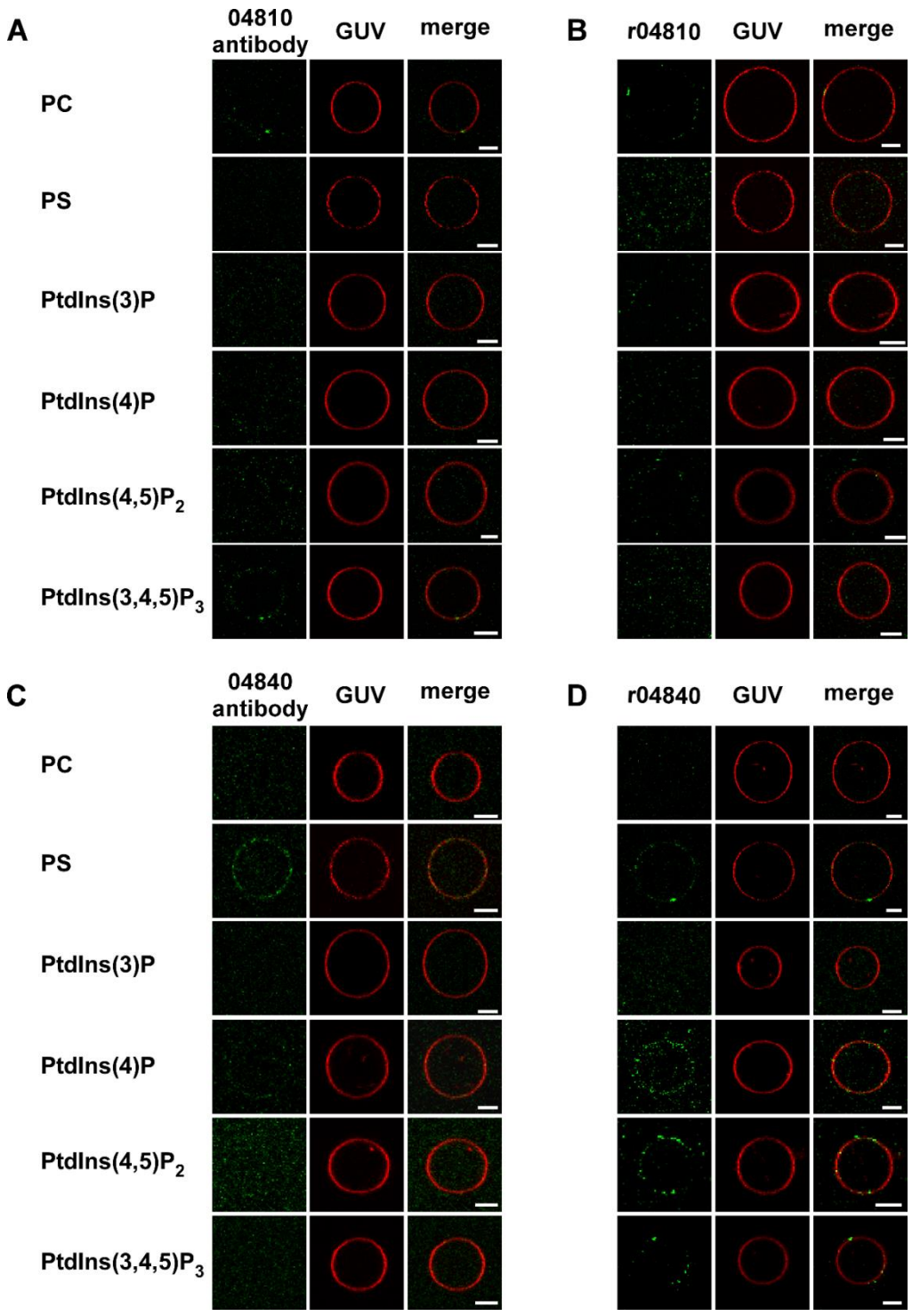

Fig14: 04840 binds to PtdIns(4,5)P_2 and PtdIns(3,4,5)P_2 positive GUVs.
(A-D) GUV binding assay with depicted PtdIns. GUVs were generated from a lipid mix of phosphatidylcholine (DOPC, 74,74 mol %), cholesterol (20 mol %), TexasRed (0,25 mol %) and the depicted PtdIns (5 mol %) and incubated with 1 µg recombinant 04810 **(B)** or 04840 **(D)** at RT for 30 min. GUVs were fixed with 3 % PFA and stained with specific primary antibody against 04810 **(A+B)** or 04840 **(C+D)** and secondary antibody anti rabbit Alexa488. The binding of the proteins/antibodies was analyzed via immunofluorescence microscopy. Bar 2.5 µm **(A+C)** GUVs were stained with the specific antibodies without previous incubation with recombinant protein.

2.3.5 Discussion

2.3.5.1 04840 shares a ectopic localization pattern with Rab36 and associates with Rab34

To identify chlamydial proteins with similarities to proteins involved in endocytic processes a bioinformatic screen was performed, were all hypothetical *C pneumoniae* proteins were compared to the human genome and other obligate intracellular pathogens. GiD_A_04840 was initially identified due to its localized identity to the human Rab36. Rab GTPases play an important role in membrane identity and vesicle transport. (Braun, Hegemann, and Mölleken 2019, submitted). The additional data of 04840 associating with Rab34 and Rab36 and Rab36 associating with PtdIns(3)P vesicles and invading EBs, further supports the previous hypothesis (manuscript III) of the cluster being involved with Rab GTPases or their effectors. Strikingly, these findings place Rab36 at the early inclusion. It was already shown for other intracellular pathogens that they manipulate Rab-controlled vesicular transport, by e.g. stopping recruitment of downstream effectors. One such example would be the bacterial effector SopD2, from *Salmonella typhimurium*, which interacts directly with Rab34 and modulates Rab34 cellular function (Teo et al. 2017). Furthermore, depletion of Rab34 leads to a delay in *Salmonella* containing vacuole maturation (Teo et al. 2017). Next to *Salmonella typhimurium* also for *Mycobacterium tuberculosis*, a role of Rab34 could be observed (Spano and Galan 2018). It was shown that Rab34 is upregulated in *Mycobacterium*-infected macrophages and survival or killing of *Mycobacterium* could be observed when Rab34 was silenced or overexpressed (Spano and Galan 2018). Even though the mechanism on how Rab34 is influencing *Mycobacterium* intracellular survival is not understood it is interesting to know that in infected cells the recruitment of RILP, also one of the effectors of the late endosomal Rab7, is inhibited, which is also an effector for Rab34 and Rab36 (Spano and Galan 2018; Khan and Menetrey 2013). A next step, to further understand early *Chlamydia* infection events, the possible involvement of Rab36 and Rab34 during the *C. pneumoniae* infection could be investigated by depletion of Rab34 or Rab36 in human cells with a subsequent *C. pneumoniae* infection. Additionally, transformation of single proteins of the cluster proteins into *C. trachomatis* or *C. pneumoniae*, the latter is possible since September 2018, could lead to more information about function, localization and expression of the cluster proteins during the infection cycle (Wang et al. 2011; Shima et al. 2018). Especially, the SNAP-tag, a general tool for labeling proteins, in combination with transformation in *C. pneumoniae* would be a favorable way to analyze localization of cluster proteins during the infection, as it can be used in life cell imaging. Even further, a double labeling would be possible. The SNAP-tag, which derives from the human O^6-alkylguanine-DNA alkyltransferase (AGT) is covalent labeled by using O^6-benzylguanine derivates bearing a

chemical probe. A mutation variant of the SNAP-tag, called CLIP-tag, reacts with O^2-benzylcytosine instead of O^6-benzylguanine, and allows the possibility of simultaneous and specific labeling of two different fusion proteins (Keppler et al. 2003; Gautier et al. 2008). Moreover, the TargeTron Gene Knockout System could be an option to gain more insight in function (Targetronics, LLC).
Moreover, even though it is unlikely that cluster proteins bind guanine nucleotides, as the G2 and G4 box motif are missing, enzymatic and binding assays with GTP, GDP or possibly also GMP or ATP/ADP, might give an answer to the question if cluster proteins could possibly bind nucleotides. A restriction for this assay might be the protein purification. Especially, 04840 and 04810 are quite difficult to obtain native in sufficiently high concentrations and buffer conditions for subsequent biochemical assays. Further experiments need to be done, like testing of additional dialysis buffers (different pH, added detergents, salts or nucleotides), purification via the Äkta protein purification system, under native and denatured conditions, column refolding or the use of better engineered bacterial strains for difficult to purify proteins, like membrane proteins.

2.3.5.2 Proteins of the 04840-04720 cluster bind to different membranes

Next to the association of 04840 to EE, Rab11 and Rab14 vesicles, the capability to bind to the human plasma membrane was observed for individual proteins of the 04840-04720 cluster. Additional experiments in the direction of typical chlamydial adhesins showed the proteins of the cluster do not influence a subsequent *C. pneumoniae* infection, like typical adhesins usually do, which further supports the hypothesis of the proteins being effectors (Braun, Hegemann, and Mölleken 2019, submitted).
One characteristic of Rab proteins is a C-terminal CAAX box that contains two cysteine residues where geranylgeranyl tails are attached, by which Rabs get bound to the membrane. No C-terminal cysteine could be found in any protein of the 04840-04720 cluster. To analyze the observed binding of individual proteins of the cluster to different lipids in more detail, phospholipids and phosphoinositide membrane strip assays, self-made and purchased, were performed and showed that 04840 and 04810 are able to bind to different PtdIns (Fig5, (Braun, Hegemann, and Mölleken 2019, submitted). Alongside others, binding to PS and PtdIns(4,5)P_2, both usually located at the inner leaflet of the plasma membrane and PtdIns(4)P, a precursor of PtdIns(4,5)P_2 and located at the plasma membrane and Golgi, were observed with this technique. The discrepancy in the observed binding properties of the cluster proteins between self-made and purchased lipid strip assays could be explained by the different concentrations and lipids used. For example, on the purchased strips (Echelon Bioscience Inc.) 100 pmol of each lipid were spotted, whereas on the self-made ones at least

1,53 nmol were spotted. Furthermore, the commercial strips used the 1,2-Dipalmitoyl-sn-glycerol-3 phosphocholin (PC) and the self-made strips 1,2-dioeoyl-sn-glycerol-3phosphocholin (PC).

In immunofluorescence microscopy analysis and adhesion studies with FITC-labeled recombinant protein no binding of any of the proteins, which showed binding before in their unlabeled form, could be observed (Fig13). FITC is a popular and widely used fluorescent probe to label proteins, antibodies or other molecules (Clark Brelje, Wessendorf, and Sorenson 2002). Stable binding of FITC mostly occurs with primary amine groups, modifying ε- and N-terminal amines in proteins, like the ones in lysine (Jobbagy and Kiraly 1966; Clark Brelje, Wessendorf, and Sorenson 2002). Up to 36 lysine could be found in proteins of the 04840-04720 cluster, which explains why the FITC-labeling was successful. A potential explanation might be that FITC blocks amino acids in the binding site which the proteins need to bind to membranes. The use of other fluorophores might be an option, but have to be carefully analyzed, as with increased wavelength the fluorophore does increase in size too, like Cy3B which is five times the size of tryptophan and more likely to disturb labeled protein function (Toseland 2013). Another important point is to use the right protein to fluorescein ratio. A ratio of approximately eight to ten fluorescein molecules per protein molecule are used, with an optimum of four to five (Clark Brelje, Wessendorf, and Sorenson 2002). The ratio is also important to predict the behavior of labeled proteins (Beutner 1971). In the case of FITC-labeled 04840 and 04810, a ratio of ten fluorescein molecules per protein molecule was used. To test a lower ratio might be a promising next step to generate labelled and functional proteins. Additionally, GUVs were used to analyze binding to different membranes. These artificial membranes allowed analyzing the binding in an artificial membrane context which might be important for protein binding. The specific antibodies against 04840 and 04810 showed unspecific binding to some of the GUVs. Therefore, binding to most of the tested lipids could not be evaluated. For the GUV assay the use of unlabeled protein with antibody staining afterwards is not the optimal and desired approach, but was used because of the reduced binding ability of FITC-labeled cluster proteins. Fixation and different washing steps lead to a high loss and deformation rate of the GUVs and precipitation of the proteins. In GUV assays, labeled protein would be preferable to use, as no fixation or staining would be needed and life imaging and even binding kinetics could be performed. This emphasizes the need to analyze the different FITC to protein molecule ratios and finding another way to label proteins. A possibility would be to use maleimide-fluorophore conjugates which are specific for the thiol group of cysteine, which can be introduced at specific sites of the respective protein and are often used for small molecules (Toseland 2013). Even though the FITC-labeling and GUV assays did not give conclusive results, it could be shown that proteins of the 04840-04720 cluster are able to bind to

membranes with different lipid compositions. Additionally, the ability of cluster proteins to not only form homomeric, but also heteromeric complexes could be an important feature, as proteins that are not able to bind to membranes could still be recruited to different membrane compartments via protein-protein interaction.

Alongside Rab GTPases, PtdIns are another important group involved in membrane identity and regulating vesicle transport and might be another opportunity for pathogens to target host cell proteins for their own benefit. For other intracellular bacteria it could be shown that they modulate and use the functions of the host PtdIns, even though most of the processes and signaling pathways are still poorly understood. One example is IpgD, a type III secreted protein of the genus *Shigella* spp., which is a PI 4- phosphatase that de-phosphorylates PtdIns(4,5)P_2 into PtdIns(5)P (Pizarro-Cerda, Kuhbacher, and Cossart 2015). PtdIns(5)P concentrates at bacterial entry sites, triggers PI 3-kinase/Akt pathway, which leads to phosphorylation of anti-apoptotic effectors. Additionally, PtdIns(5)P prevents EGFR degradation thus prolonging EGFR signaling and survival of *Shigella* inside the host cell (Pizarro-Cerda, Kuhbacher, and Cossart 2015). Further studies need to be done in this direction for *C. pneumoniae*.

All in all, these results facilitate the speculation that the proteins of the 04840-04720 cluster are effectors that interact with the endosomal membrane by binding specific phospholipids and with that are in close proximity to possibly mimic Rab GTPases, to favor the *C. pneumoniae* infection.

3. Discussion

C. pneumoniae, like all intracellular pathogens has to gain entry into a host cell to complete its intracellular life cycle. Adhesion via so-called adhesins, internalization and the establishment of the early inclusion are the first essential steps for a successful infection. Not a lot is known about the early events of the chlamydial infection and only TarP as an early secreted effector is well analyzed in *C. trachomatis*. Recent studies have shown that the early *C. pneumoniae* inclusion develops into an EE, which acquires specific Rab proteins, like recycling Rab11 and Rab14. These markers protect the inclusion from degradation, as the inclusion is marked as slowly recycling endosome (Molleken and Hegemann 2017). To further understand the early *C. pneumoniae* infection the identification of effector proteins is an important step.

In this thesis, the *C. pneumoniae* TarP ortholog, CPn0572, was analyzed and a gene cluster of new effector proteins potentially involved in the early phase of infection was identified and characterized.

After the reversible adhesion of OmcB to Heparan sulfate-like Glycosaminglycan (HS-like GAG), the stable adhesion takes place by Pmp21 binding to and activating the EGFR and CPn0473, which binds to a not yet identified receptor (Fig12). Furthermore, it was shown that CPn0473 might be incorporated into the plasma membrane, where it binds to and externalizes PS, which is usually located at the inner leaflet of the plasma membrane. The externalization of PS can further lead to the re-localization of human membrane-bound proteins, like Rac proteins, and membrane curvature, which supports the internalization of the EB. (Mölleken and Hegemann 2008; Mölleken, Schmidt, and Hegemann 2010; Mölleken, Becker, and Hegemann 2013; Fechtner, Galle, and Hegemann 2016; Galle 2017). As a consequence of the stable contact, the type III secretion system of the bacteria is activated and effector proteins are secreted into the host cell. One such protein is CPn0678, which interacts with SNX9. SNX9 can among others interact with Arp2/3 and N-WASP, which are actin binding proteins and plays in general an important role during endocytosis, which makes CPn0678 an important player during the internalization of EBs (Hänsch 2016). Another early secreted protein, which is important during internalization, is the in this thesis further analyzed CPn0572. CPn0572 binds and polymerizes actin at the bacterial invasion site and in turn promotes the internalization of the bacterium by the host cell (Clifton et al. 2004; Zrieq, Braun, and Hegemann 2017) (Fig15). Next to the already known actin binding domain, a second actin binding domain and a vinculin binding site could be identified in this thesis (Braun et al. 2019). Vinculin is a protein, which localizes to integrin-mediated cell-matrix adhesions and cadherin-mediated cell-cell junctions. It is an adapter protein with binding sites for more than 15 proteins, among them actin, talin and α-actinin (Carisey and

Ballestrem 2011). More actin binding domains and especially also a vinculin binding site can be found in the *C. trachomatis* ortholog TarP and RNA interference screens revealed the necessity of vinculin during *C. trachomatis* infection (Elwell et al. 2008; Gurumurthy et al. 2010). Moreover, in infection studies it was shown that vinculin gets recruited to the site of invasion and experiments with vinculin KO cells showed that the infection efficiency of *C. caviae* was reduced (Thwaites et al. 2015). A more in depth study of the vinculin binding site 1 of *C. trachomatis* TarP revealed that it has the capacity to uncouple vinculin-mediated cytoskeletal connections (Whitewood et al. 2018). The role of vinculin during the *Chlamydia* infection is ill-defined, but vinculin itself can bind to actin and it is possible that the binding of CPn0572 to vinculin further supports the recruitment of actin and subsequently the internalization of the EB.

After the internalization of the EB, the maturation of the inclusion is the next essential step of the chlamydial infection. At this point proteins of the 04840-04720 cluster might potentially have a function as molecular mimetic of Rab proteins (Fig15). During internalization, the membrane around the EB has a PtdIns(4,5)P_2, PtdIns(3,4,5)P_3 and PtdIns(3)P identity, which later changes to PtdIns(3)P alone and recruits specific Rabs, like recycling Rab11, Rab14 and late endosomal Rab7 (Molleken and Hegemann 2017). 04840 associates with the endogenous, endocytosed EGFR, which stays in the early inclusion, and with EE, Rab11 and Rab14 proteins, in a G1 box-dependent manner (Fig12) (Braun, Hegemann, and Mölleken 2019, submitted). Additionally, the ability to bind to PtdIns(3)P, PtdIns(4)P_2, PtdIns(3,4,5)P_3, PS and PC could be observed for tested cluster proteins. All these lipids are present during the steps of the maturation of the early inclusion (Fig12) (Molleken and Hegemann 2017). Furthermore, G1, G3 and G5 box motifs can be identified in all proteins with a DUF domain (NCBI cited Dec 2018; Braun, Hegemann, and Mölleken 2019, submitted). Cluster proteins might interact with early endosomal membranes by binding specific phospholipids or with unknown membrane associated human/chlamydial proteins and recruit specific Rab-interacting proteins. This could lead to a local depletion of Rab effectors unfavorable for the early infection or the recruitment of favorable Rab effectors. The inclusion is then transported to the peri-nuclear region, where it stays until the end of the life cycle (Fig15).

There is still a lot more to investigate and understand about the early *C. pneumoniae* infection and the proteins involved, but this thesis could already shed new light on some of these events, by analyzing the early secreted effector CPn0572 and showing its role during the internalization, by binding actin. Furthermore, a novel protein cluster could be identified, which is a promising candidate to play an important role during the early phase of infection by possibly being a molecular mimic of Rab proteins or recruiting specific Rab-interacting effectors.

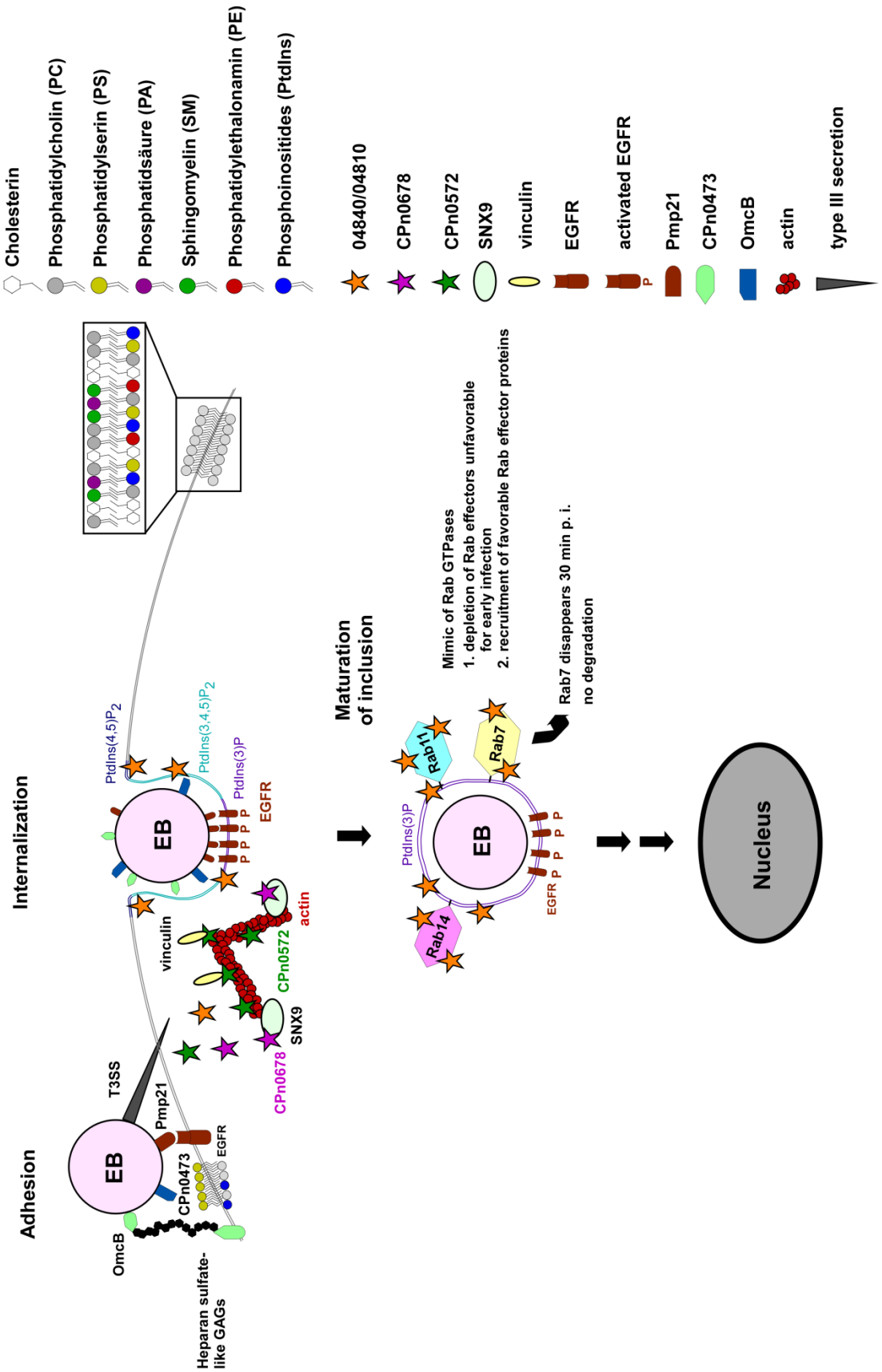

Figure 15: Model of the early *C. pneumoniae* infection
The model shows that the adhesion of *C. pneumoniae* EBs takes place by binding of adhesins like OmcB, Pmp21 and CPn0473 to specific human proteins and receptors like the EGFR. After the stable contact, type III secreted proteins like CPn0572 and possible the proteins of the GiD 04840-04720 cluster are secreted into the host cell.

CPn0572 polymerizes actin at the site of bacterial invasion and promotes internalization. After the internalization the early inclusion acquires a PtdIns(3)P identity and recruits recycling Rab GTPases Rab11 and Rab14 and the late endosomal Rab7. 04840 associates with endogenous EGFR, which stays associated with the inclusion membrane after internalization and PtdIns(3)P positive vesicle, which puts it at the early stages of the infection portrait in this model and supports the hypothesis that the proteins of the cluster are effectors with a role in the early *C. pneumoniae* infection.

4. Literature

Andersson, Jan O Andersson and Siv GE. 1999. 'Insights into the evolutionary process of genome degradation', *Current Opinion in Genetics & Development*.

Balla, T. 2013. 'Phosphoinositides: tiny lipids with giant impact on cell regulation', *Physiol Rev*, 93: 1019-137.

Bays, J. L., and K. A. DeMali. 2017. 'Vinculin in cell-cell and cell-matrix adhesions', *Cell Mol Life Sci*, 74: 2999-3009.

Beatty, W. L., G. I. Byrne, and R. P. Morrison. 1993. 'Morphologic and antigenic characterization of interferon gamma-mediated persistent Chlamydia trachomatis infection in vitro', *Proc Natl Acad Sci U S A*, 90: 3998-4002.

Becker, E., and J. H. Hegemann. 2014. 'All subtypes of the Pmp adhesin family are implicated in chlamydial virulence and show species-specific function', *Microbiologyopen*, 3: 544-56.

Beeckman, D. S., and D. C. Vanrompay. 2009. 'Zoonotic Chlamydophila psittaci infections from a clinical perspective', *Clin Microbiol Infect*, 15: 11-7.

Belland, R. J., S. P. Ouellette, J. Gieffers, and G. I. Byrne. 2004. 'Chlamydia pneumoniae and atherosclerosis', *Cell Microbiol*, 6: 117-27.

Beutner, E. H. 1971. 'Defined immunofluorescent staining: past progress, present status, and future prospects for defined conjugates', *Ann N Y Acad Sci*, 177: 506-26.

Birkelund, S., A. G. Lundemose, and G. Christiansen. 1990. 'The 75-kilodalton cytoplasmic Chlamydia trachomatis L2 polypeptide is a DnaK-like protein', *Infect Immun*, 58: 2098-104.

Blasi, F., P. Tarsia and S. Aliberti. 2009. 'Chlamydophila pneumoniae', *Clin Microbiol Infect*.

Braun, C., A. R. Alcazar-Roman, A. Laska, K. Molleken, U. Fleig, and J. H. Hegemann. 2019. 'CPn0572, the C. pneumoniae ortholog of TarP, reorganizes the actin cytoskeleton via a newly identified F-actin binding domain and recruitment of vinculin', *PLoS One*, 14: e0210403.

Braun, C., J.H. Hegemann, and K. Mölleken. 2019, submitted. 'A novel set of Rab GTPase-related Chlamydia effector proteins involved in the early phase of infection', *MBio*.

Brumell, J. H., and M. A. Scidmore. 2007. 'Manipulation of rab GTPase function by intracellular bacterial pathogens', *Microbiol Mol Biol Rev*, 71: 636-52.

Cain, R. J., R. D. Hayward, and V. Koronakis. 2008. 'Deciphering interplay between Salmonella invasion effectors', *PLoS Pathog*, 4: e1000037.

Carabeo, R. A., S. S. Grieshaber, A. Hasenkrug, C. Dooley, and T. Hackstadt. 2004. 'Requirement for the Rac GTPase in Chlamydia trachomatis invasion of non-phagocytic cells', *Traffic*, 5: 418-25.

Carisey, A., and C. Ballestrem. 2011. 'Vinculin, an adapter protein in control of cell adhesion signalling', *Eur J Cell Biol*, 90: 157-63.

Chen, H., B. W. Bernstein, and J. R. Bamburg. 2000. 'Regulating actin-filament dynamics in vivo', *Trends Biochem Sci*, 25: 19-23.

Chen, L., J. Hu, Y. Yun, and T. Wang. 2010. 'Rab36 regulates the spatial distribution of late endosomes and lysosomes through a similar mechanism to Rab34', *Mol Membr Biol*, 27: 23-30.

Chi, E. Y., C. C. Kuo, and J. T. Grayston. 1987. 'Unique ultrastructure in the elementary body of Chlamydia sp. strain TWAR', *J Bacteriol*, 169: 3757-63.

Chu, D. J., S. G. Guo, C. F. Pan, J. Wang, Y. Du, X. F. Lu, and Z. Y. Yu. 2012. 'An experimental model for induction of lung cancer in rats by Chlamydia pneumoniae', *Asian Pac J Cancer Prev*, 13: 2819-22.

Clark Brelje, T., Martin W. Wessendorf, and Robert L. Sorenson. 2002. 'Chapter 5 - Multicolor Laser Scanning Confocal Immunofluorescence Microscopy: Practical Application and Limitations.' in Brian Matsumoto (ed.), *Methods in Cell Biology* (Academic Press).

Clarke, I. N. 2011. 'Evolution of Chlamydia trachomatis', *Ann N Y Acad Sci*, 1230: E11-8.

Clausen, J. D., G. Christiansen, H. U. Holst, and S. Birkelund. 1997. 'Chlamydia trachomatis utilizes the host cell microtubule network during early events of infection', *Mol Microbiol*, 25: 441-9.

Clifton, D. R., C. A. Dooley, S. S. Grieshaber, R. A. Carabeo, K. A. Fields, and T. Hackstadt. 2005. 'Tyrosine phosphorylation of the chlamydial effector protein Tarp is species specific and not required for recruitment of actin', *Infect Immun*, 73: 3860-8.

Clifton, D. R., K. A. Fields, S. S. Grieshaber, C. A. Dooley, E. R. Fischer, D. J. Mead, R. A. Carabeo, and T. Hackstadt. 2004. 'A chlamydial type III translocated protein is tyrosine-phosphorylated at the site of entry and associated with recruitment of actin', *Proc Natl Acad Sci U S A*, 101: 10166-71.

Cooper, J. A., and T. D. Pollard. 1982. 'Methods to measure actin polymerization', *Methods Enzymol*, 85 Pt B: 182-210.

Cortes, C., K. A. Rzomp, A. Tvinnereim, M. A. Scidmore, and B. Wizel. 2007. 'Chlamydia pneumoniae inclusion membrane protein Cpn0585 interacts with multiple Rab GTPases', *Infect Immun*, 75: 5586-96.

Cossart, P., J. Pizarro-Cerda, and M. Lecuit. 2003. 'Invasion of mammalian cells by Listeria monocytogenes: functional mimicry to subvert cellular functions', *Trends Cell Biol*, 13: 23-31.

Damiani, M. T., J. Gambarte Tudela, and A. Capmany. 2014. 'Targeting eukaryotic Rab proteins: a smart strategy for chlamydial survival and replication', *Cell Microbiol*, 16: 1329-38.

DesMarais, V., M. Ghosh, R. Eddy, and J. Condeelis. 2005. 'Cofilin takes the lead', *J Cell Sci*, 118: 19-26.

Di Fiore, P. P., and M. von Zastrow. 2014. 'Endocytosis, signaling, and beyond', *Cold Spring Harb Perspect Biol*, 6.

Dominguez, R. 2004. 'Actin-binding proteins--a unifying hypothesis', *Trends Biochem Sci*, 29: 572-8.

Dramsi, S., and P. Cossart. 1998. 'Intracellular pathogens and the actin cytoskeleton', *Annu Rev Cell Dev Biol*, 14: 137-66.

Elwell, C. A., A. Ceesay, J. H. Kim, D. Kalman, and J. N. Engel. 2008. 'RNA interference screen identifies Abl kinase and PDGFR signaling in Chlamydia trachomatis entry', *PLoS Pathog*, 4: e1000021.

Elwell, C., K. Mirrashidi, and J. Engel. 2016. 'Chlamydia cell biology and pathogenesis', *Nat Rev Microbiol*, 14: 385-400.

Everett, K. D., R. M. Bush, and A. A. Andersen. 1999. 'Emended description of the order Chlamydiales, proposal of Parachlamydiaceae fam. nov. and Simkaniaceae fam. nov., each containing one monotypic genus, revised taxonomy of the family Chlamydiaceae, including a new genus and five new species, and standards for the identification of organisms', *Int J Syst Bacteriol*, 49 Pt 2: 415-40.

Fadel, S., and A. Eley. 2008. 'Is lipopolysaccharide a factor in infectivity of Chlamydia trachomatis?', *J Med Microbiol*, 57: 261-6.

Fechtner, T., J. N. Galle, and J. H. Hegemann. 2016. 'The novel chlamydial adhesin CPn0473 mediates the lipid raft-dependent uptake of Chlamydia pneumoniae', *Cell Microbiol*, 18: 1094-105.

Fechtner, T., S. Stallmann, K. Moelleken, K. L. Meyer, and J. H. Hegemann. 2013. 'Characterization of the interaction between the chlamydial adhesin OmcB and the human host cell', *J Bacteriol*, 195: 5323-33.

Fields, K. A., and T. Hackstadt. 2002. 'The chlamydial inclusion: escape from the endocytic pathway', *Annu Rev Cell Dev Biol*, 18: 221-45.

Fletcher, D. A., and R. D. Mullins. 2010. 'Cell mechanics and the cytoskeleton', *Nature*, 463: 485-92.

Fukuda, M., E. Kanno, K. Ishibashi, and T. Itoh. 2008. 'Large scale screening for novel rab effectors reveals unexpected broad Rab binding specificity', *Mol Cell Proteomics*, 7: 1031-42.

Galle, J. N., T. Fechtner, T. Eierhoff, W. Romer, and J. H. Hegemann. 2019. 'A Chlamydia pneumoniae adhesin induces phosphatidylserine exposure on host cells', *Nat Commun*, 10: 4644.

Galle, Jan. 2017. 'Die Rolle des LIPP Proteins in einer *Chlamydia pneumoniae* Infektion'.

Gaspar, A. H., and M. P. Machner. 2014. 'VipD is a Rab5-activated phospholipase A1 that protects Legionella pneumophila from endosomal fusion', *Proc Natl Acad Sci U S A*, 111: 4560-5.

Gautier, A., A. Juillerat, C. Heinis, I. R. Correa, Jr., M. Kindermann, F. Beaufils, and K. Johnsson. 2008. 'An engineered protein tag for multiprotein labeling in living cells', *Chem Biol*, 15: 128-36.

Gerard, H. C., U. Dreses-Werringloer, K. S. Wildt, S. Deka, C. Oszust, B. J. Balin, W. H. Frey, 2nd, E. Z. Bordayo, J. A. Whittum-Hudson, and A. P. Hudson. 2006. 'Chlamydophila (Chlamydia) pneumoniae in the Alzheimer's brain', *FEMS Immunol Med Microbiol*, 48: 355-66.

Grayston, J. T., M. B. Aldous, A. Easton, S. P. Wang, C. C. Kuo, L. A. Campbell, and J. Altman. 1993. 'Evidence that Chlamydia pneumoniae causes pneumonia and bronchitis', *J Infect Dis*, 168: 1231-5.

Greub, G. 2010. 'International Committee on Systematics of Prokaryotes. Subcommittee on the taxonomy of the Chlamydiae: minutes of the inaugural closed meeting, 21 March 2009, Little Rock, AR, USA', *Int J Syst Evol Microbiol*, 60: 2691-3.

Grieshaber, S. S., N. A. Grieshaber, and T. Hackstadt. 2003. 'Chlamydia trachomatis uses host cell dynein to traffic to the microtubule-organizing center in a p50 dynamitin-independent process', *J Cell Sci*, 116: 3793-802.

Grimwood, J., L. Olinger, and R. S. Stephens. 2001. 'Expression of Chlamydia pneumoniae polymorphic membrane protein family genes', *Infect Immun*, 69: 2383-9.

Grimwood, J., and R. S. Stephens. 1999. 'Computational analysis of the polymorphic membrane protein superfamily of Chlamydia trachomatis and Chlamydia pneumoniae', *Microb Comp Genomics*, 4: 187-201.

Gurumurthy, R. K., A. P. Maurer, N. Machuy, S. Hess, K. P. Pleissner, J. Schuchhardt, T. Rudel, and T. F. Meyer. 2010. 'A loss-of-function screen reveals Ras- and Raf-independent MEK-ERK signaling during Chlamydia trachomatis infection', *Sci Signal*, 3: ra21.

Hahn, D. L., R. W. Dodge, and R. Golubjatnikov. 1991. 'Association of Chlamydia pneumoniae (strain TWAR) infection with wheezing, asthmatic bronchitis, and adult-onset asthma [see comments]', *Jama*, 266: 225-30.

Hänsch, Sebastian. 2016. 'Analyse der neuen potentiellen Effektorproteine CPn0712, CPn0677 und CPn0678 von *Chlamydia pneumoniae*'.

Hayward, R. D., and V. Koronakis. 1999. 'Direct nucleation and bundling of actin by the SipC protein of invasive Salmonella', *EMBO J*, 18: 4926-34.

Holzer, M., K. Laroucau, H. H. Creasy, S. Ott, F. Vorimore, P. M. Bavoil, M. Marz, and K. Sachse. 2016. 'Whole-Genome Sequence of Chlamydia gallinacea Type Strain 08-1274/3', *Genome Announc*, 4.

Hutagalung, A. H., and P. J. Novick. 2011. 'Role of Rab GTPases in membrane traffic and cell physiology', *Physiol Rev*, 91: 119-49.

Jantos, C. A., S. Heck, R. Roggendorf, M. Sen-Gupta, and J. H. Hegemann. 1997. 'Antigenic and molecular analyses of different Chlamydia pneumoniae strains', *J. Clin. Microbiol.*, 35: 620-23.

Jean, S., and A. A. Kiger. 2012. 'Coordination between RAB GTPase and phosphoinositide regulation and functions', *Nat Rev Mol Cell Biol*, 13: 463-70.

Jeffrey, B. M., R. J. Suchland, K. L. Quinn, J. R. Davidson, W. E. Stamm, and D. D. Rockey. 2010. 'Genome sequencing of recent clinical Chlamydia trachomatis strains identifies loci associated with tissue tropism and regions of apparent recombination', *Infect Immun*, 78: 2544-53.

Jewett, T. J., E. R. Fischer, D. J. Mead, and T. Hackstadt. 2006. 'Chlamydial TARP is a bacterial nucleator of actin', *Proc Natl Acad Sci U S A*, 103: 15599-604.

Jewett, T. J., N. J. Miller, C. A. Dooley, and T. Hackstadt. 2010. 'The conserved Tarp actin binding domain is important for chlamydial invasion', *PLoS Pathog*, 6: e1000997.

Jiwani, S., S. Alvarado, R. J. Ohr, A. Romero, B. Nguyen, and T. J. Jewett. 2013. 'Chlamydia trachomatis Tarp harbors distinct G and F actin binding domains that bundle actin filaments', *J Bacteriol*, 195: 708-16.

Jiwani, S., R. J. Ohr, E. R. Fischer, T. Hackstadt, S. Alvarado, A. Romero, and T. J. Jewett. 2012. 'Chlamydia trachomatis Tarp cooperates with the Arp2/3 complex to increase the rate of actin polymerization', *Biochem Biophys Res Commun*, 420: 816-21.

Jobbagy, A., and K. Kiraly. 1966. 'Chemical characterization of fluorescein isothiocyanate-protein conjugates', *Biochim Biophys Acta*, 124: 166-75.

Jovic, M., M. Sharma, J. Rahajeng, and S. Caplan. 2010. 'The early endosome: a busy sorting station for proteins at the crossroads', *Histol Histopathol*, 25: 99-112.

Kabsch, W., and K. C. Holmes. 1995. 'The actin fold', *Faseb j*, 9: 167-74.

Kabsch, W., H. G. Mannherz, D. Suck, E. F. Pai, and K. C. Holmes. 1990. 'Atomic structure of the actin:DNase I complex', *Nature*, 347: 37-44.

Kalman, S., W. Mitchell, R. Marathe, C. Lammel, J. Fan, R. W. Hyman, L. Olinger, J. Grimwood, R. W. Davis, and R. S. Stephens. 1999. 'Comparative genomes of Chlamydia pneumoniae and C. trachomatis', *Nat Genet*, 21: 385-9.

Keppler, A., S. Gendreizig, T. Gronemeyer, H. Pick, H. Vogel, and K. Johnsson. 2003. 'A general method for the covalent labeling of fusion proteins with small molecules in vivo', *Nat Biotechnol*, 21: 86-9.

Khan, A. R., and J. Menetrey. 2013. 'Structural biology of Arf and Rab GTPases' effector recruitment and specificity', *Structure*, 21: 1284-97.

Ku, B., K. H. Lee, W. S. Park, C. S. Yang, J. Ge, S. G. Lee, S. S. Cha, F. Shao, W. D. Heo, J. U. Jung, and B. H. Oh. 2012. 'VipD of Legionella pneumophila targets activated Rab5 and Rab22 to interfere with endosomal trafficking in macrophages', *PLoS Pathog*, 8: e1003082.

Kumar, Y., and R. H. Valdivia. 2008. 'Actin and intermediate filaments stabilize the Chlamydia trachomatis vacuole by forming dynamic structural scaffolds', *Cell Host Microbe*, 4: 159-69.

Langemeyer, L., F. Frohlich, and C. Ungermann. 2018. 'Rab GTPase Function in Endosome and Lysosome Biogenesis', *Trends Cell Biol*, 28: 957-70.

Luczak, S. E., S. H. Smits, C. Decker, L. Nagel-Steger, L. Schmitt, and J. H. Hegemann. 2016. 'The Chlamydia pneumoniae Adhesin Pmp21 Forms Oligomers with Adhesive Properties', *J Biol Chem*, 291: 22806-18.

Madshus, I. H., and E. Stang. 2009. 'Internalization and intracellular sorting of the EGF receptor: a model for understanding the mechanisms of receptor trafficking', *J Cell Sci*, 122: 3433-9.

McGhie, E. J., R. D. Hayward, and V. Koronakis. 2004. 'Control of actin turnover by a salmonella invasion protein', *Mol Cell*, 13: 497-510.

Mitchell, C. M., K. M. Hovis, P. M. Bavoil, G. S. Myers, J. A. Carrasco, and P. Timms. 2010. 'Comparison of koala LPCoLN and human strains of Chlamydia pneumoniae highlights extended genetic diversity in the species', *BMC Genomics*, 11: 442.

Miyashita, N., Y. Kanamoto, and A. Matsumoto. 1993. 'The morphology of Chlamydia pneumoniae', *J Med Microbiol*, 38: 418-25.

Moelleken, K., and J. H. Hegemann. 2008. 'The Chlamydia outer membrane protein OmcB is required for adhesion and exhibits biovar-specific differences in glycosaminoglycan binding', *Mol Microbiol*, 67: 403-19.

Mojica, S., H. Huot Creasy, S. Daugherty, T. D. Read, T. Kim, B. Kaltenboeck, P. Bavoil, and G. S. Myers. 2011. 'Genome sequence of the obligate intracellular animal pathogen Chlamydia pecorum E58', *J Bacteriol*, 193: 3690.

Mölleken, K., E. Becker, and J. H. Hegemann. 2013. 'The Chlamydia pneumoniae invasin protein Pmp21 recruits the EGF receptor for host cell entry', *PLoS Pathog*, 9: e1003325.

Molleken, K., and J. H. Hegemann. 2017. 'Acquisition of Rab11 and Rab11-Fip2-A novel strategy for Chlamydia pneumoniae early survival', *PLoS Pathog*, 13: e1006556.

Mölleken, K., and J. H. Hegemann. 2008. 'The Chlamydia outer membrane protein OmcB is required for adhesion and exhibits biovar-specific differences in glycosaminoglycan binding', *Mol Microbiol*, 67: 403-19.

Mölleken, K., E. Schmidt, and J. H. Hegemann. 2010. 'Members of the Pmp protein family of Chlamydia pneumoniae mediate adhesion to human cells via short repetitive peptide motifs', *Mol Microbiol*, 78: 1004-17.

Moore, E. R., and S. P. Ouellette. 2014. 'Reconceptualizing the chlamydial inclusion as a pathogen-specified parasitic organelle: an expanded role for Inc proteins', *Front Cell Infect Microbiol*, 4: 157.

Moorhead, A. M., J. Y. Jung, A. Smirnov, S. Kaufer, and M. A. Scidmore. 2010. 'Multiple host proteins that function in phosphatidylinositol-4-phosphate metabolism are recruited to the chlamydial inclusion', *Infect Immun*, 78: 1990-2007.

Mukherjee, K., S. Parashuraman, M. Raje, and A. Mukhopadhyay. 2001. 'SopE acts as an Rab5-specific nucleotide exchange factor and recruits non-prenylated Rab5 on Salmonella-containing phagosomes to promote fusion with early endosomes', *J Biol Chem*, 276: 23607-15.

Muller, M. P., and R. S. Goody. 2018. 'Molecular control of Rab activity by GEFs, GAPs and GDI', *Small GTPases*, 9: 5-21.

Mullins, R. D., J. A. Heuser, and T. D. Pollard. 1998. 'The interaction of Arp2/3 complex with actin: nucleation, high affinity pointed end capping, and formation of branching networks of filaments', *Proc Natl Acad Sci U S A*, 95: 6181-6.

Murata, T., A. Delprato, A. Ingmundson, D. K. Toomre, D. G. Lambright, and C. R. Roy. 2006. 'The Legionella pneumophila effector protein DrrA is a Rab1 guanine nucleotide-exchange factor', *Nat Cell Biol*, 8: 971-7.

Myers, G. S., S. A. Mathews, M. Eppinger, C. Mitchell, K. K. O'Brien, O. R. White, F. Benahmed, R. C. Brunham, T. D. Read, J. Ravel, P. M. Bavoil, and P. Timms. 2009. 'Evidence that human Chlamydia pneumoniae was zoonotically acquired', *J Bacteriol*, 191: 7225-33.

NCBI, NCBI "National Center for Biotechnology Information. cited Dec 2018. 'National Library of Medicine (US)', *National Center for Biotechnology Information; [1988]*.

Neil A. Campbell, Jane B. Reece, Jürgen Markl (Hg.). 2006. 'Biologie', *Pearson Studium*, 6. aktualisierte Auflage.

Nunes, A., and J. P. Gomes. 2014. 'Evolution, phylogeny, and molecular epidemiology of Chlamydia', *Infect Genet Evol*, 23: 49-64.

Pak, C. W., K. C. Flynn, and J. R. Bamburg. 2008. 'Actin-binding proteins take the reins in growth cones', *Nat Rev Neurosci*, 9: 136-47.

Pan, X., S. Eathiraj, M. Munson, and D. G. Lambright. 2006. 'TBC-domain GAPs for Rab GTPases accelerate GTP hydrolysis by a dual-finger mechanism', *Nature*, 442: 303-6.

Pannekoek, Y., Q. Qi-Long, Y. Z. Zhang, and A. van der Ende. 2016. 'Genus delineation of Chlamydiales by analysis of the percentage of conserved proteins justifies the reunifying of the genera Chlamydia and Chlamydophila into one single genus Chlamydia', *Pathog Dis*, 74.

Parrett, C. J., R. V. Lenoci, B. Nguyen, L. Russell, and T. J. Jewett. 2016. 'Targeted Disruption of Chlamydia trachomatis Invasion by in Trans Expression of Dominant Negative Tarp Effectors', *Front Cell Infect Microbiol*, 6: 84.

Peeling, R. W., and R. C. Brunham. 1996. 'Chlamydiae as pathogens: new species and new issues', *Emerg Infect Dis*, 2: 307-19.

Pereira-Leal, J. B., and M. C. Seabra. 2000. 'The mammalian Rab family of small GTPases: definition of family and subfamily sequence motifs suggests a mechanism for functional specificity in the Ras superfamily', *J Mol Biol*, 301: 1077-87.

Pillonel, T., C. Bertelli, N. Salamin, and G. Greub. 2015. 'Taxogenomics of the order Chlamydiales', *Int J Syst Evol Microbiol*, 65: 1381-93.

Pizarro-Cerda, J., A. Kuhbacher, and P. Cossart. 2015. 'Phosphoinositides and host-pathogen interactions', *Biochim Biophys Acta*, 1851: 911-8.

Pospischil, A., R. Thoma, M. Hilbe, P. Grest, and J. O. Gebbers. 2002. 'Abortion in woman caused by caprine Chlamydophila abortus (Chlamydia psittaci serovar 1)', *Swiss Med Wkly*, 132: 64-6.

Pylypenko, O., H. Hammich, I. M. Yu, and A. Houdusse. 2018. 'Rab GTPases and their interacting protein partners: Structural insights into Rab functional diversity', *Small GTPases*, 9: 22-48.

Rafelski, S. M., and J. A. Theriot. 2004. 'Crawling toward a unified model of cell mobility: spatial and temporal regulation of actin dynamics', *Annu Rev Biochem*, 73: 209-39.

Rockey, D. D., J. Lenart, and R. S. Stephens. 2000. 'Genome sequencing and our understanding of chlamydiae', *Infect Immun*, 68: 5473-9.

Romer, W., L. Berland, V. Chambon, K. Gaus, B. Windschiegl, D. Tenza, M. R. Aly, V. Fraisier, J. C. Florent, D. Perrais, C. Lamaze, G. Raposo, C. Steinem, P. Sens, P. Bassereau, and L. Johannes. 2007. 'Shiga toxin induces tubular membrane invaginations for its uptake into cells', *Nature*, 450: 670-5.

Rzomp, K. A., L. D. Scholtes, B. J. Briggs, G. R. Whittaker, and M. A. Scidmore. 2003. 'Rab GTPases are recruited to chlamydial inclusions in both a species-dependent and species-independent manner', *Infect Immun*, 71: 5855-70.

Saka, H. A., and R. H. Valdivia. 2010. 'Acquisition of nutrients by Chlamydiae: unique challenges of living in an intracellular compartment', *Curr Opin Microbiol*, 13: 4-10.

Schink, K. O., K. W. Tan, and H. Stenmark. 2016. 'Phosphoinositides in Control of Membrane Dynamics', *Annu Rev Cell Dev Biol*, 32: 143-71.

Schoebel, S., L. K. Oesterlin, W. Blankenfeldt, R. S. Goody, and A. Itzen. 2009. 'RabGDI displacement by DrrA from Legionella is a consequence of its guanine nucleotide exchange activity', *Mol Cell*, 36: 1060-72.

Scidmore, M. A., E. R. Fischer, and T. Hackstadt. 2003. 'Restricted fusion of Chlamydia trachomatis vesicles with endocytic compartments during the initial stages of infection', *Infect Immun*, 71: 973-84.

Shima, K., M. Wanker, R. J. Skilton, L. T. Cutcliffe, C. Schnee, T. A. Kohl, S. Niemann, J. Geijo, M. Klinger, P. Timms, T. Rattei, K. Sachse, I. N. Clarke, and J. Rupp. 2018. 'The Genetic Transformation of Chlamydia pneumoniae', *mSphere*, 3.

Spano, S., and J. E. Galan. 2018. 'Taking control: Hijacking of Rab GTPases by intracellular bacterial pathogens', *Small GTPases*, 9: 182-91.

Spano, S., X. Gao, S. Hannemann, M. Lara-Tejero, and J. E. Galan. 2016. 'A Bacterial Pathogen Targets a Host Rab-Family GTPase Defense Pathway with a GAP', *Cell Host Microbe*, 19: 216-26.

Stein, M. P., M. P. Muller, and A. Wandinger-Ness. 2012. 'Bacterial pathogens commandeer Rab GTPases to establish intracellular niches', *Traffic*, 13: 1565-88.

Stephens, R. S., S. Kalman, C. Lammel, J. Fan, R. Marathe, L. Aravind, W. Mitchell, L. Olinger, R. L. Tatusov, Q. Zhao, E. V. Koonin, and R. W. Davis. 1998. 'Genome sequence of an obligate intracellular pathogen of humans: *chlamydia trachomatis*', *Science*, 282: 754-9.

Stephens, R. S., G. Myers, M. Eppinger, and P. M. Bavoil. 2009. 'Divergence without difference: phylogenetics and taxonomy of Chlamydia resolved', *FEMS Immunol Med Microbiol*, 55: 115-9.

Teo, W. X., Z. Yang, M. C. Kerr, L. Luo, Z. Guo, K. Alexandrov, J. L. Stow, and R. D. Teasdale. 2017. 'Salmonella effector SopD2 interferes with Rab34 function', *Cell Biol Int*, 41: 433-46.

Thwaites, T., A. T. Nogueira, I. Campeotto, A. P. Silva, S. S. Grieshaber, and R. A. Carabeo. 2014. 'The Chlamydia effector TarP mimics the mammalian leucine-aspartic acid motif of paxillin to subvert the focal adhesion kinase during invasion', *J Biol Chem*, 289: 30426-42.

Thwaites, T. R., A. T. Pedrosa, T. P. Peacock, and R. A. Carabeo. 2015. 'Vinculin Interacts with the Chlamydia Effector TarP Via a Tripartite Vinculin Binding Domain to Mediate Actin Recruitment and Assembly at the Plasma Membrane', *Front Cell Infect Microbiol*, 5: 88.

Toseland, C. P. 2013. 'Fluorescent labeling and modification of proteins', *J Chem Biol*, 6: 85-95.

Valdivia, R. H. 2008. 'Chlamydia effector proteins and new insights into chlamydial cellular microbiology', *Curr Opin Microbiol*, 11: 53-9.

Van Lent, S., H. H. Creasy, G. S. Myers, and D. Vanrompay. 2016. 'The Number, Organization, and Size of Polymorphic Membrane Protein Coding Sequences as well as the Most Conserved Pmp Protein Differ within and across Chlamydia Species', *J Mol Microbiol Biotechnol*, 26: 333-44.

Voigt, A., G. Schofl, and H. P. Saluz. 2012. 'The Chlamydia psittaci genome: a comparative analysis of intracellular pathogens', *PLoS One*, 7: e35097.

Volceanov, L., K. Herbst, M. Biniossek, O. Schilling, D. Haller, T. Nolke, P. Subbarayal, T. Rudel, B. Zieger, and G. Hacker. 2014. 'Septins arrange F-actin-containing fibers on the Chlamydia trachomatis inclusion and are required for normal release of the inclusion by extrusion', *MBio*, 5: e01802-14.

Wang, T., and W. Hong. 2002. 'Interorganellar regulation of lysosome positioning by the Golgi apparatus through Rab34 interaction with Rab-interacting lysosomal protein', *Mol Biol Cell*, 13: 4317-32.

Wang, Y., S. Kahane, L. T. Cutcliffe, R. J. Skilton, P. R. Lambden, and I. N. Clarke. 2011. 'Development of a transformation system for Chlamydia trachomatis: restoration of glycogen biosynthesis by acquisition of a plasmid shuttle vector', *PLoS Pathog*, 7: e1002258.

Weinmaier, T., J. Hoser, S. Eck, I. Kaufhold, K. Shima, T. M. Strom, T. Rattei, and J. Rupp. 2015. 'Genomic factors related to tissue tropism in Chlamydia pneumoniae infection', *BMC Genomics*, 16: 268.

Wennerberg, K., K. L. Rossman, and C. J. Der. 2005. 'The Ras superfamily at a glance', *J Cell Sci*, 118: 843-6.

Wesolowski, J., M. M. Weber, A. Nawrotek, C. A. Dooley, M. Calderon, C. M. St Croix, T. Hackstadt, J. Cherfils, and F. Paumet. 2017. 'Chlamydia Hijacks ARF GTPases To Coordinate Microtubule Posttranslational Modifications and Golgi Complex Positioning', *MBio*, 8.

Whitewood, A. J., A. K. Singh, D. G. Brown, and B. T. Goult. 2018. 'Chlamydial virulence factor TarP mimics talin to disrupt the talin-vinculin complex', *FEBS Lett*, 592: 1751-60.

Wolf, K., E. Fischer, and T. Hackstadt. 2000. 'Ultrastructural analysis of developmental events in Chlamydia pneumoniae-infected cells', *Infect Immun*, 68: 2379-85.

Wuppermann, F. N., K. Molleken, M. Julien, C. A. Jantos, and J. H. Hegemann. 2008. 'Chlamydia pneumoniae GroEL1 protein is cell surface associated and required for infection of HEp-2 cells', *J Bacteriol*, 190: 3757-67.

Zerial, M., and H. McBride. 2001. 'Rab proteins as membrane organizers', *Nat Rev Mol Cell Biol*, 2: 107-17.

Zhan, P., L. J. Suo, Q. Qian, X. K. Shen, L. X. Qiu, L. K. Yu, and Y. Song. 2011. 'Chlamydia pneumoniae infection and lung cancer risk: a meta-analysis', *Eur J Cancer*, 47: 742-7.

Zrieq, R., C. Braun, and J. H. Hegemann. 2017. 'The Chlamydia pneumoniae Tarp Ortholog CPn0572 Stabilizes Host F-Actin by Displacement of Cofilin', *Front Cell Infect Microbiol*, 7: 511.

Acknowledgments

At this point I want to thank everyone who supported me during the whole duration of my PhD thesis.

First of all, I would like to thank Prof. Dr. Johannes H. Hegemann for giving me the opportunity to work in his lab, his guidance and giving me the space to not only work with one, but two very interesting topics, which allowed me to not only learn a lot, but also helped me to evolve a scientific thinking. Furthermore, I want to thank him for giving me the opportunity to teach. The possibility to supervise students, helped me to learn a lot about myself and deepened my understanding about my own work.

I am grateful to Prof. Dr. Thomas Klein for accepting to co-supervise my thesis, always having time for me, his always useful advice, input and questions that often helped me to think outside of the box.

Thanks to Prof. Dr. Ursula Fleig for her helpful comments and discussions, not only about actin and microtubules, but also about how to write a paper and selling my work. Especially, for always having time to listen and advise on presentations. I learned a lot and will try to implement everything in my future.

Special thanks to Dr. Katja Mölleken for her support and always having my back. Thank you for always supporting and encouraging me, always listening to me and giving me great advice not only lab related, but also for the life out there. Thank you for all the great discussions and all the time you took out of your day to explain things or new techniques to me. Especially, thank you for always telling me everything will be ok and helping me to see a light at the end of the tunnel when the frustration about an experiment got really bad.

I also want to thank the whole new and old “Chlamydia” and “Pombe” lab for giving me a great, welcoming and friendly environment to work in. I met not only new colleagues but also new friends. Special thanks to Philipp, after the Master Module we participated in together, he came back and accompanied me through the Master and PhD. During that time, he not only became a friend, he also introduced me into the “Whiskey world”, showed me it is possible to have a life outside of the lab, always made me laugh and always had time to discuss experiments and finding solutions to almost impossible lab problems. Thanks to Sebastian for showing me the world of Computer gaming, which kept me sane (or maybe made me more insane) during really stressful times and always having nice and supporting words in times that I was not feeling very self-confident in the lab. Thanks to all my Bachelor and Master students (my kids) for always keeping me on my toes, helping me to learn a lot about myself and giving me a new and exciting way to experience the lab world. Jan, thank you for introducing me into the world of GUVs, protein purification and lipids, but most importantly ARK. Thank you for always having time when I had a question, especially thank you for your support during stressful times.

To Alison, Marina and Natascha thank you for everything. I came as the new Master student (I know I will always be “the Master student”) and you immediately welcomed me with open arms and took me under your wings. I experienced Germany and my life through new eyes, I grew stronger, more self-confident and finally started to accept myself. Thank you for always being there, listening to my ramblings, problems and obsessions. Also after you left Düsseldorf (Alison, Marina) you always had time to talk if I needed to and thank you Natascha for always trying to get me out into the world to try to relax in between stressful days. Alison, thank you for always listening to me and my weird obsessions and just being someone who gets me.

Der nächste Dank geht an meine Familie.

Meine Mutter, danke, dass du immer an mich geglaubt und nie an mir gezweifelt hast. Für deine dauerhafte und unermüdliche Unterstützung, die aufbauenden Worte und das du mich immer so akzeptiert hast wie ich bin. Du hattest immer ein offenes Ohr für mich und für alles was du für mich getan hast bin ich dir unendlich dankbar.

Danke an meine Schwester, die ebenfalls nie an mir gezweifelt hat und mich mit Bildern, Worten, Sprachnachrichten und häufiger mal besserwisserischen Bemerkungen aus der Ferne und bei spontanen Besuchen in Düsseldorf immer unterstützt und in stressigen Situationen abgelenkt hat.

An meine Oma, meine Tante Gitte und meine beiden Onkel Uwe und Bernd, vielen Dank für alles. Vielen Dank das ihr immer für mich da wart und mich auf unterschiedlichste Art immer unterstützt habt. Danke, dass ihr meinen Wegzug von zu Hause einfacher gemacht habt und ich immer einen Ort habe an den ich mich zurückziehen kann. Vor allem danke, dass etwas Abwechslung in meinen Speiseplan kam, ganz besonders in Zeiten, wenn ich vergessen hatte selber zu kochen.

Danke an meinen Vater, dass er mich während der ganzen Zeit unterstützt hat und da war, wenn ich etwas brauchte.

Danke an meine ganze Familie. Ohne euch wäre ich nicht da wo ich jetzt bin.

Eidesstattliche Erklärung

Hiermit versichere ich, dass ich die vorliegende Arbeit selbständig verfasst habe und außer den genannten Hilfsmitteln keine weiteren verwendet habe. Alle Stellen, die aus anderen Werken im Wortlaut oder Sinn entsprechend übernommen wurden, habe ich mit den Quellenangaben kenntlich gemacht.

Corinna Ursula Braun

(Düsseldorf, 2019)